이학석사학위논문

The Rational Design and Synthesis of novel PPARγ Phosphorylation Inhibiting Agonism-Free Ligands and The Library Construction of Small Molecule Autophagy Modulators

퍼옥시점 증식자 활성화 수용체 감마 전사활성화 비촉진 인산화 저해제의 합리적 설계 및 합성과 자가포식 조절 저분자 화합물 라이브러리의 구축

2015 년 8 월

서울대학교 대학원

화학부 유기화학 전공

Pavel Printsev (현수)

The Rational Design and Synthesis of novel PPAR gamma Phosphorylation Inhibiting Agonism-Free Ligands and The Library Construction of Small Molecule Autophagy Modulators

지도교수 박 승 범

이 논문을 이학석사 학위논문으로 제출함
2015년 8월

서울대학교 대학원
화학부 유기화학 전공
Pavel Printsev (현수)
Pavel Printsev (현수)의 석사학위논문을 인준함

2015년 6월

위 원 장 홍 순 혁 (인)

부 위 원 장 박 승 범 (인)

위 원 홍 경 인 (인)

Abstract

The Rational Design and Synthesis of novel PPARγ Phosphorylation Inhibiting Agonism-Free Ligands and The Library Construction of Small Molecule Autophagy Modulators

Pavel Printsev (현수)

Department of Chemistry, Organic Chemistry
The Graduate School
Seoul National University

Chapter 1: The transcription factors peroxisome proliferator-activated receptors (PPAR) are well known for their key roles in the regulation of glucose and lipid metabolism. Naturally, the PPAR family has become an attractive target for researchers seeking to create compounds that can interact with the receptors and in turn modulate their downstream gene expression levels to instigate a desired biological response. With over-activation of PPARγ being linked to a cascade of serious side effects and relatively recent developments attributing cyclin-dependent kinase 5 (CDK5)-mediated PPARγ phosphorylation inhibition to the dysregulation of several insulin sensitizing genes, a rationally designed set of isoxazole-based compounds which exhibit moderate to no agonism towards PPARγ while simultaneously inhibiting phosphorylation of PPARγ at Ser273 have been synthesized and will be presented in this thesis. The compound set has been split into 3 families (carbamate, urea and amide), each differing slightly from the last in terms of rigidity and their electronic environment adjacent to the isoxazole core. The compound set was designed around a convergence principle in which functional group modifications that generated desired biological outcomes in one family were then incorporated into the other family sets for more accurate cross-comparisons along with ‘converging’ our compound set into a smaller more active

subset comprising the most biologically active compounds of all three of the family sets. The compounds were all tested for their effectiveness in inhibiting CDK5-mediated phosphorylation through western blotting tests and select compounds also underwent transcriptional activity assays to determine the extent of their agonism towards PPARγ. Afterwards, docking studies were carried out to first, gain insight into what possible interactions between our ligand and PPARγ's binding pocket could be generating the observed bio-activity and second, provide us with some rationale regarding future functional group modifications. Of the 3 family sets, the urea set proved to be the most consistently active with regards to phosphorylation inhibition as well as having moderate to no agonism towards PPARγ, next was the carbamate set and last was the amide set.

In Chapter 2, the isoxazole-based ligand core from Chapter 1 was incorporated into the library construction of small molecule autophagy modulators. Autophagy is the major intercellular degradation system by which unnecessary or dysfunctional cytoplasmic material is delivered and degraded within the lysosome. Intra and extracellular Amyloid Beta (Aβ) plaque accumulation within the brain, a signature pathological biomarker for Alzheimer's disease, has been shown to leave neurons in an autophagy-dependent manner, and suggests that aggregation of intracellular Aβ plaque contributes to Alzheimer's pathology. With this in mind, a small molecule library based off of a hit compound (P41H06) from our previous image-based phenotypic HTS for autophagy modulation was constructed and tested for its relative effect on autophagy modulation. The goal of this compound set was to synthesize compounds that have a moderate autophagy inducing effect, such as to avoid the potential side effects that may be associated from autophagy over-activation.

Keywords: PPAR, rational design, phosphorylation inhibition, Ser-273, partial agonist, Amyloid Beta, autophagy modulation, small molecule modulator, SF-44
Student Number: 2013-22445

Contents

Chapter 1

The Rational Design and Synthesis of novel PPARγ Phosphorylation Inhibiting Agonism-Free Ligands

1.1.1. Introduction

Obesity, the second highest cause of preventative death after smoking in the US, which has been linked to heart disease, stroke, insulin resistance (type 2 diabetes) and certain types of cancers[1] has amassed an estimated annual medical cost in excess of $147 billion dollars[2]. With more than 34% of US adults and 17% of youth being classified as obese as of 2012[3], obesity is emerging as not only a serious health condition but also as a severe economic burden. While not everyone with type 2 diabetes is overweight, obesity is responsible for an overwhelming 90-95% of type 2 diabetes cases in the US, according to the CDC[4]. While the link between obesity and the development of type 2 diabetes is fairly clear, the exact role that obesity has on causing type 2 diabetes is not perfectly agreed upon yet. The general consensus is that obesity stresses the endoplasmic reticulum (ER), which then in turn causes the ER to suppress insulin receptor signals, eventually leading to diabetes[5].

With obesity commonly being characterized by an increase in the size and amount of adipocytes, and with peroxisome proliferator-activated receptors (PPARs) being primarily expressed in adipose tissues as well as being known as master regulators of adipogenesis, allows for PPARs to serve as lipid sensors and in turn makes PPARs attractive targets for treating obesity and thus type 2 diabetes. The peroxisome proliferator-activated receptors (PPARs) are a group of three nuclear receptors: PPARα, PPARβ/δ, and PPARγ who control gene expression by binding to specific PPAR response elements (PPREs) within the promoter regions of their target genes involved in fatty acid uptake and storage, inflammation and glucose homeostasis[6]. PPARs bind as permissive heterodimers with retinoid X receptor (RXR) and upon ligand activation undergo specific conformational changes that release bound corepressors (such as NcoR2/SMRT) and then allow for the recruitment of coactivators (such as SRC1/NCoA1, CBP/p300, PPAR co-activator-1)[6,7] Upon coactivator complexation, the rate of transcription initiation is increased as well as the elevated downstream gene expression of several lipid

metabolizing (e.g. LPL, ACAT1, PLA) and insulin sensitizing genes (e.g. adipocytokine adiponectin)[9]. The transcriptional activity of PPARγ is regulated by various post-translational modifications such as SUMOylation[10], unbiquitation[11] and most notably phosphorylation[12]. The latter of which, when inhibited, has been shown to have a direct effect on the observed increases in gene expression levels of various insulin sensitizing genes, rather than from ligand-induced activation, agonism[13] and will be heavily focused on in this thesis.

Thiazolidinediones (TZDs), some of the most well known synthetic PPARγ agonists (Rosiglitazone, Pioglitazone, Ciglitazone and Troglitazone) have been used in clinical practice (except for Ciglitazone) for treating type 2 diabetes by lowering plasma glucose levels in patients. Unfortunately, while the drugs were successful in reducing plasma glucose levels, they were found to cause several serious side effects. Ciglitazone (CIG), developed by Takeda Pharmaceuticals in the early 1980s, while not making it past clinical trials due to high hepatotoxicity, is often regarded as the prototypical TZD compound that initiated research and development of all the subsequent TZDs[14]. The first TZD to make it to the shelves was Troglitazone (TRO), which was immediately discontinued after reports of severe liver failure and death[14]. Shortly after came Rosiglitazone (ROSI) and Pioglitazone (PIO), both of which received approval by the Food and Drug Administration (FDA) in 1999, but were still found to be responsible for inducing heart attacks and liver failure in some patients, albeit not as severe and frequent as their predecessors[15]. The positive therapeutic effects of these drugs were long accredited to their agonism, however after the discovery of several partial and non-agonist compounds (such as MRL24 and SR1664 respectively) that also showed similar therapeutic effects to the full agonist TZDs, PPARγ agonism was no longer considered the key factor for enhancing cellular glucose uptake[16]. After extensive studies into the underlying causes of the mode of action between therapeutically active PPARγ agonists and non/partial agonists, it was found that both of these groups inhibited Cdk5-mediated phosphorylation of PPARγ at Ser-273 and restored a more normal, non-diabetic pattern of gene expression[13,16]. Additionally, throughout the course of these studies,

mice that were fed high fat, high sugar foods, after developing obesity, started to become insulin-resistant. This insulin-resistance was attributed to obesity-induced activation of the protein kinase Cdk5 in adipose tissue[13]. This activated Cdk5 is then able to phosphorylate PPARγ at Ser-273. The phosphorylation in of itself does not affect PPARγ's ability in adipogenesis, but it does lead to a dysregulation of a large number of genes whose expression is changed in obesity, such as the reduced expression of the insulin sensitizing adipokine[13]. Also, it is worth mentioning that the side effects commonly associated with the TZD family of drugs could be due to their increased transcriptional activity upon binding to an agonist, which as a result may affect which coactivators interact with PPARγ. While the exact connection between classical agonism and their side effects still remains a topic of debate, this may be an interesting area to investigate for further PPARγ-related research. Nevertheless, with all of these exciting developments, there is a lot of interest in developing a novel class of anti-diabetes medicine that is tailored towards inhibiting Cdk5-mediated phosphorylation of PPARγ while simultaneously being devoid of classical agonism. With this goal in mind, an isoxazole core-based library (Figure 1), stemming from our in-house discovered hit compound C06, which is a PPARγ partial agonist, has been designed, synthesized and tested in vivo for their effectiveness towards Cdk5-mediated phosphorylation inhibition at SER-273 and transcriptional activity. The results are presented in Chapter 1 of this thesis herein.

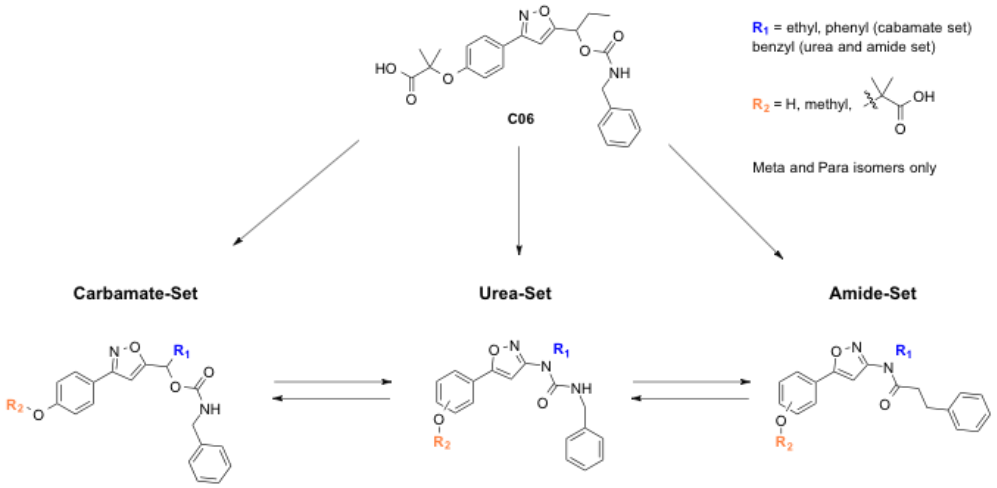

Figure 1. General overview of the structurally optimized isoxazole-based compound sets synthesized for targeting PPARγ.

1.1.2. Preceding Work on C06 Optimization (Activity Enhancement)

The first generation of C06-derived compounds, designed and synthesized by Dr. Minseob Koh from our group, focused on increasing C06's low activity towards PPARγ (Figure 2).

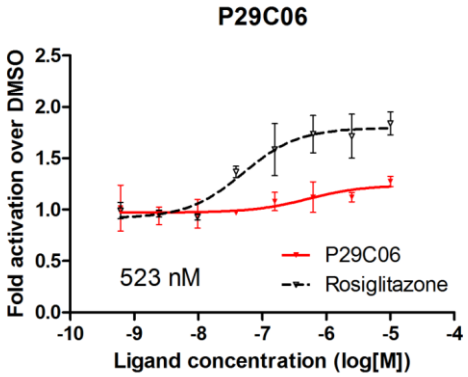

Figure 2. Transactivation activity profile of a PPARγ-derived reporter gene in 293T cells after treatment with rosiglitazone and C06 for 24h.

By recognizing PPARγ's distinct Y-shaped ligand binding domain (LBD), Dr. Koh focused on 'growing' C06, such that it extends outwards, occupying and potentially interacting with more of the LBD so that it could activate PPARγ more effectively. Throughout this, the carbamate functionality, carboxylic acid moiety, as well as its position on the benzene ring remained unchanged for all modifications. Rather, Dr. Koh focused on elongating the urea-bound benzyl substituent, functionalizing the secondary carbamate nitrogen with a benzyl or propyl benzyl group and then decorating them with various substituents designed to interact with amino acid residues within the LBD (Figure 3). Lastly, once narrowing in on his most active compounds, he then made their enantiomerically pure versions and compared their activity.

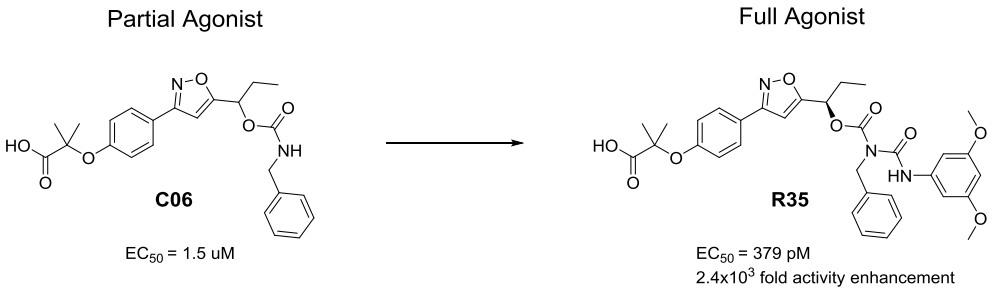

Figure 3. An example of one of Dr.Koh's fully optimized C06-based full PPARγ agonists, R35.

While the target and initial scaffold for which our structural modifications were carried out on remain the same, the desired response that we seek to generate from PPARγ is completely opposite.

1.2.1. Rational Design - C06 Optimization (Activity Suppression)

In order to rationally design ligands for PPARγ, particularly ligands that behave as non/partial agonists or full agonists towards PPARγ, an understanding of the structure-function relationship of ligand activation of each of these classes of

receptors was crucial. Structural insights into PPARγ activation have shown that interactions with the H11 and particularly H12 helixes of PPARγ within its LBD have often led to activation of PPARγ via the stabilization of recruited coactivators, such as with the steroid receptor coactivator (SRC)[17]. Crystal structure superposition data have further supported the notion that the majority of PPARγ agonists tend to form hydrogen bonding interactions with H12 while partial agonists or non-agonists do not (Figure 4)

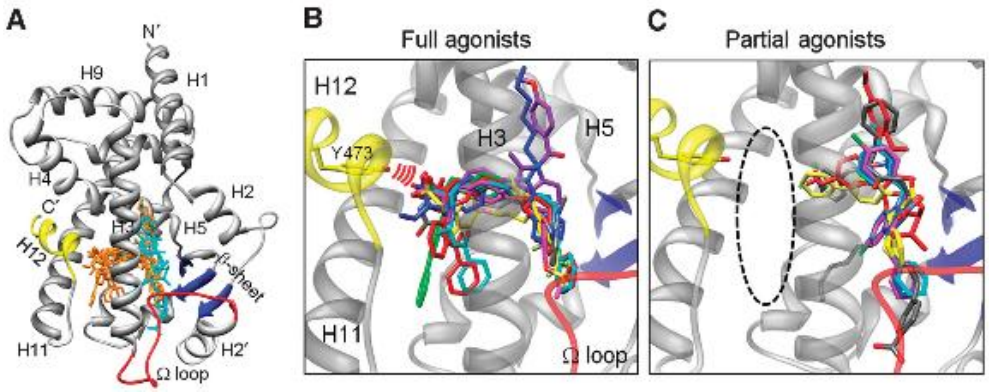

Figure 4. (Morikawa et al 2010) Configurations of indole acetate-containing ligands and known agonists in the PPARg LBD. (A) Superposition of known agonists in PPARg LBDs. Full agonists (orange) and partial ones (cyan) are shown within the apo-LBD (2ZK0; Waku et al, 2009a). (B) Close-up view of the full agoinsts. Red arcs indicate hydrogen bonds between full agonists and Tyr473. (C) Close-up view of the partial agonists. The area enclosed by the black dashed line is the AF-2 pocket.[17]

Binding with helix 3 generally does not result in any conformational changes in PPARγ and rarely generates any changes in biological responses. As such, this helix was used as an 'anchorage' point. The ligand's isoxazole heteroatom would attach itself to this helix via H-bonding, so as to stabilize itself while its extremities are free to interact with amino acid residues on the other helixes. Docking studies of C06 (Figure 5), as expected for a partial agonist, show an absence of interactions

with H11 and H12.

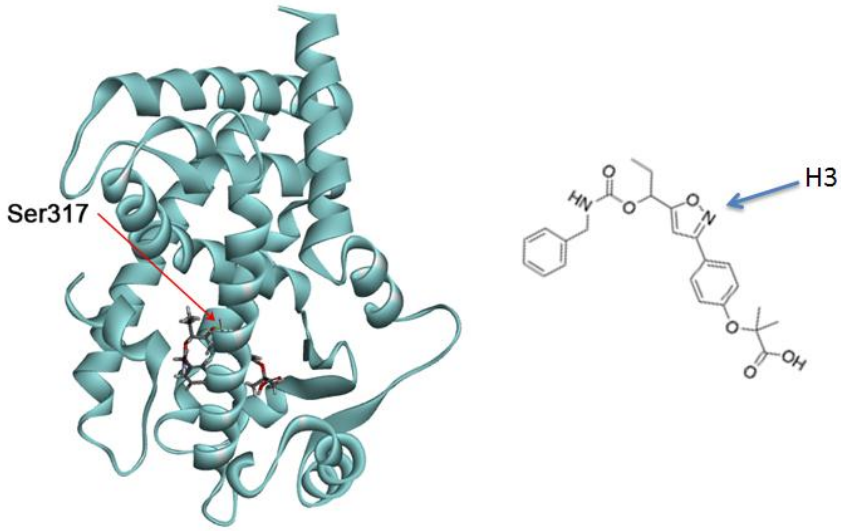

Figure 5. Docking simulation of C06 with the crystal structure of PPARγ's ligand binding domain (PDB ID: 2hfp, Discovery Studio 1.7, Accelrys was used). The Nitrogen of C06's isoxazole ring is hydrogen bonded to the Ser317 residue of H3. A two dimensional representation of C06's approximate orientation within the LBD is illustrated to the right of the docked image.

With this knowledge in hand, all subsequent modifications to C06 were designed in such a way to as to maintain the area around H11 and H12 vacant as it already is with C06. While the conditions necessary for preventing PPARγ activation, are relatively straight forward, inhibiting Cdk5-mediated phosphorylation has proven to be quite more challenging. As a result, the majority of the modifications to C06 have been targeted towards improving its effect on phosphorylation inhibition.

1.2.2. Rational Design – C06 Optimization (Phosphorylation Inhibition)

Obesity-linked phosphorylation of PPARγ by cyclin-dependent kinase 5 (Cdk5) occurs on the Serine 273 amino acid residue situated on the omega loop[13.]. Ligand-induced inhibition of this reaction is due to the conformational change that

the bound ligand evokes on PPARγ, which puts serine 273 in a sterically unfavorable position that hinders Cdk5-mediated phosphorylation. Once inside PPARγ's LBD, a ligand has access to several key areas (H11, H12, H3, H8, H2', B-sheet and omega loop), and with every H-bonding interaction acting similar to a puppeteer controlling the movements of his puppet by tugging on strings, a well designed ligand, at least for this project's purposes, should be able to selectively alter the conformation of only the desired area (the omega loop in this case) while having a minimal effect on the other areas. The discovery of the effect of Cdk5-mediated phosphorylation inhibition at SER273 was reported as recently as 2010 by Choi JH[13], however the details into how to rationally design a ligand that will predictably inhibit this phosphorylation reaction has yet to be discovered. With this task in mind, a strategy for creating a ligand that maintains a similar or diminished activity towards PPARγ as C06, while inducing conformational changes in the omega loop for inhibiting Cdk5-mediated phosphorylation has been devised, implemented and tested.

1.3.1. Results and Discussion – Carbamate Set: R_1 Modifications

With C06's isoxazole ring functioning as the ligand's anchor by securing itself to H3, identifying the effect that a modification to C06's ethyl group adjacent the isoxazole ring, would have on this interaction as well as on phosphorylation inhibition and agonism was chosen as the starting point for structural modification. Adding bulk to a ligand causes the ligand to 're-equilibrate' itself inside the LBD, positioning itself to be in an orientation with minimal steric interactions. One concern however, was that modifications neighboring the isoxazole ring could hamper its interaction with H3, preventing the ligand from remaining in the LBD. So to test whether or not the addition of significant bulk adjacent to the isoxazole ring would disrupt this important interaction, three large phenyl-based substituents ranging in size and electronic effects were synthesized and tested (Figure 6).

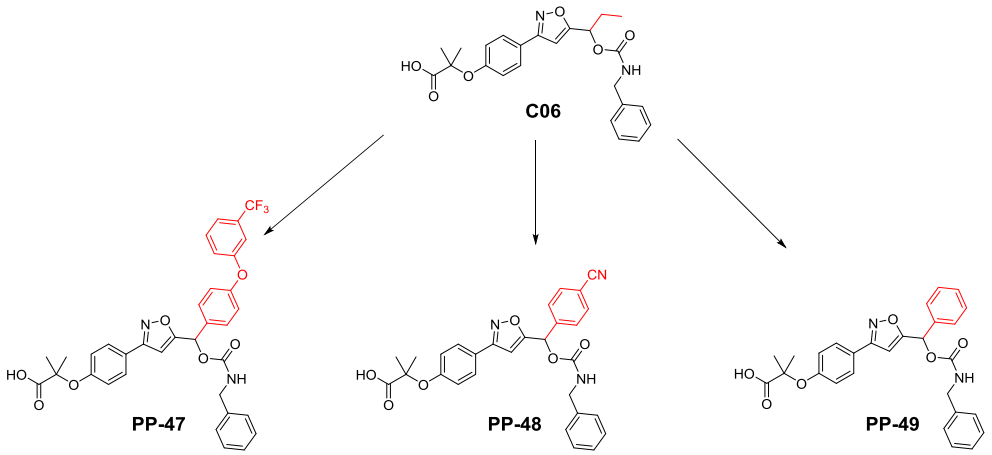

Figure 6. Structural modifications to the ethyl functionality adjacent the isoxazole ring in C06 depicted in red for compounds PP-47 through PP-49.

The incorporation of the phenyl ring in PP-49 was primarily for probing the effects of steric changes, while the para-cyano addition in PP-48 was to investigate if an H-bond acceptor was situated on the phenyl ring, whether or not it could further stabilize itself through an auxiliary interaction with either H3 or H8. Lastly the diphenyl ether moiety with the meta-trifluoromethyl substituent was chosen to explore the steric threshold for destabilizing the isoxazole H3 interaction as well as to allow for a greater area to be swept by the rotating trifluoromethylphenyl ring so that the CF_3 moiety could interact with nearby amino acid residues if present.

The synthesis of this compound set was achieved in 5 steps starting from 4-hydroxybenzaldehyde. The t-butyl protected carboxylic acid moiety **1** was synthesized via an S_N1 reaction under basic conditions with high yield. Subsequent addition of hydroxylamine in aqueous ethanol, generates the oxime **2**. Diversification of this compound set begins in this stage with the selection of the desired acetylene partner for the formation of isoxazole **3** via a [2+3] cycloaddition reaction. Next, the carbamate **4**, is achieved via nucleophilic attack of the isocyanate carbon atom by the hydroxyl oxygen. However, the nature of the electronic environment of R_1 was found to greatly affect the stability of the carbamate product

4. Incorporation of electron donating groups such as dimethylamine and diethylamine in the R_1 position resulted in carbamate **4** being cleaved at the ester C-O bond, re-generating alcohol **3**. Lastly, t-butyl deprotection was carried out under acidic conditions, yielding the carboxylic acid **5**. (Scheme 1)

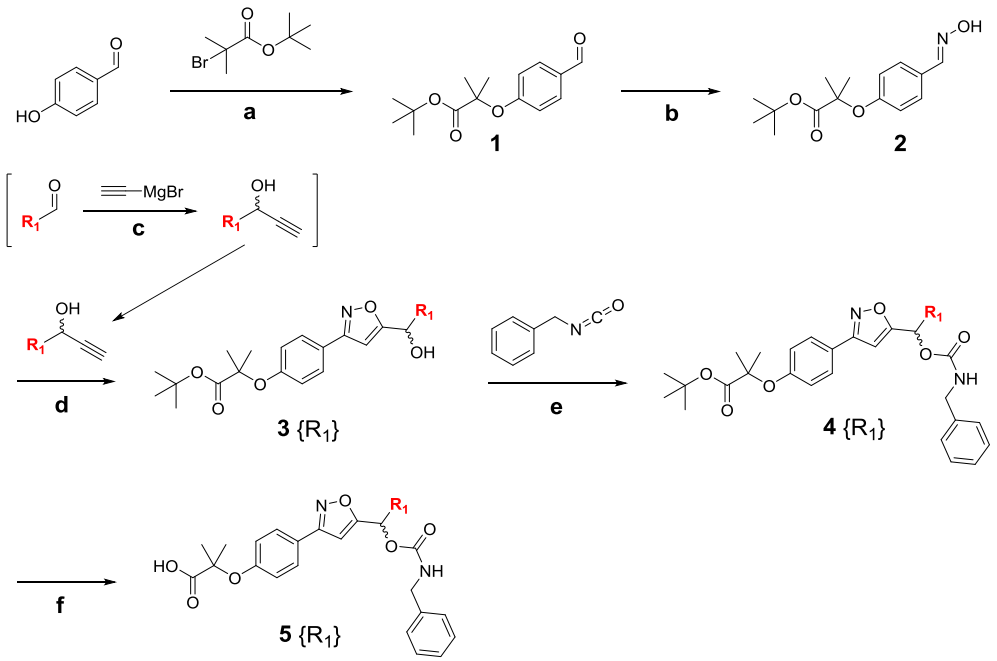

R$_1$: ethyl {E}, phenyl {P}, p-cyanophenyl {CN}, 3-trifluoromethyldiphenylether {CF3}

Scheme 1. Synthetic procedure for PPAR γ ligands C06 and PP-47 through PP-49. a) K_2CO_3, $MgSO_4$, DMF, 100 ^oC, 22h, 99%, b) hydroxyamine, Na_2CO_3, *aq*. ethanol, 65 ^oC, 12h, 85%, c) dry THF, -78 ^oC, 2h, 93-99% d) NCS, pyridine, then acetylene, TEA, THF, 60 ^oC, 2h, 67%, e) pyridine, CuCl, DCM, r.t., 2h, 99%, f) TFA, DCM, r.t., 6-12h, 80-93%

Transactivation assays performed on the compounds in Figure 6 showed that the modifications resulted in a slight reduction in PPARγ activation compared to C06 for compounds PP-47 and PP-48 (Figure 7A). However, due to an unclear readout for the fold activation curve for PP-49, the transactivation assay was re-run for PP-

49 separately. The new data showed PP-49 behaving as a partial agonist relative to Rosiglitazone, similar to C06 (Figure 7B).

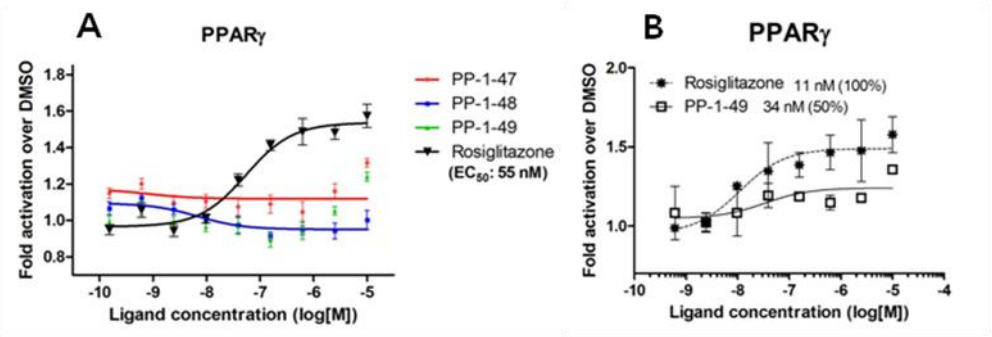

Figure 7. Transcriptional activity profile of a PPARγ-derived reporter gene in 293T cells after treatment with rosiglitazone and a) PP-47 through PP-49 for 24h. b) with PP-49 for 24h (repeated due to unclear readout from PP-49's fold activation curve in A)

The *in vitro* Cdk5 kinase assay data for compounds PP-47 through PP-49 reveal that among the three compounds, PP-49 with the phenyl for ethyl substitution, was the most effective in inhibiting Cdk5-mediated PPARγ phosphorylation, with inhibition appearing from the 1μM range (Figure 8).

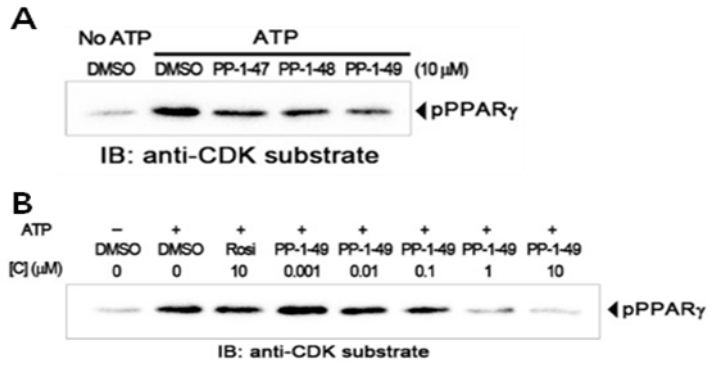

Figure 8. In vitro Cdk5 assay with a) PP-47, PP-48 and PP-49 with PPARγ substrates. b) Rosiglitazone and concentration dependent PP-49, ranging from 0.001 μM to 10 μM dosages. IB, immunoblot; pPPARγ, phosphorylated PPARγ.

Taking into account both the transactivation assay data and the Cdk5 kinase assay results, the phenyl substituent was chosen to be carried on into the urea and amide sets depicted in Figure 1.

1.3.2. Results and Discussion – Carbamate Set: R_2 Modifications

The carboxylic acid moiety, which seems to be a crucial component in all of Dr.Koh's C06-based full agonists was the focus of the next wave of modifications. The first task was to modify the carboxylic acid such to retain its structural integrity while removing its polar heteroatoms in order to disrupt any potential interactions that they may be participating in. To achieve this, the isobutyric acid was replaced with the structurally similar TBDMS-protected alcohol analog (Figure 8, PP-43). Due to C06 being a partial agonist, any drops in its transcriptional activity compared to in a full agonist would be less drastic, therefore this modification was also incorporated into the full agonist BP (Figure 9, PP-45). Additionally, partly due to synthetic simplicity, the TBDMS deprotected compounds (Figure 8, PP-44 and PP-46) were also synthesized to see if shortening the compound's backbone would cause any changes in activity.

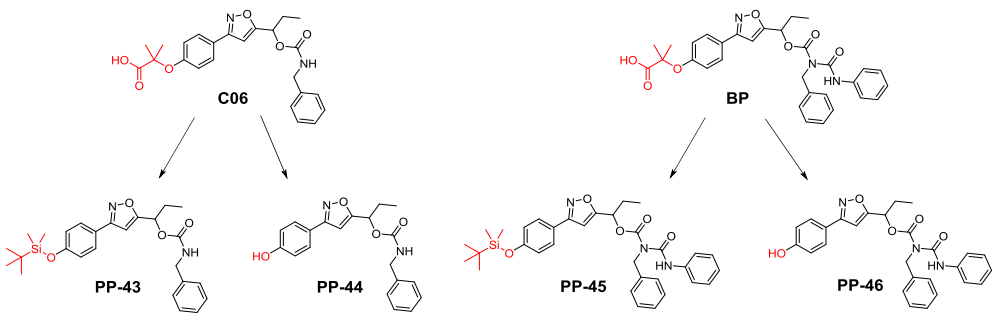

Figure 9. Structural modifications to the carboxylic acid moiety in C06 and BP depicted in red for compounds PP-43 through PP-46.

The synthesis of this compound set bears great similarity to the previous set introduced in Scheme 1 with only a few modifications. Starting with 4-

hydroxybenzaldehyde the alcohol group was protected with TBDMS under standard reaction conditions affording compound **6**. Subsequent addition of hydroxylamine in aqueous ethanol, generates the oxime **7**. Afterwards, introduction of the acetylene partner produces the isoxazole **8** via [2+3] cycloaddition. Nucleophilic addition to the benzyl isocyanate generates compound **PP-43**. From here one portion of the compound was deprotected, forming the alcohol **PP-44** and the other portion underwent a second isocyanate addition with phenyl isocyanate, generating **PP-45**. The base in this reaction had to be modified from pyridine to TEA, such as to follow standard carbamylation conditions. Without this adjustment, the ester bond in the newly formed carbamate PP-45, cleaves under pyridine and CuCl conditions re-generating our single urea compound PP-43. However, with amine as the base no such problem was encountered. Finally, TBAF-mediated deprotection of PP-45 yields the alcohol **PP-46** (Scheme 2).

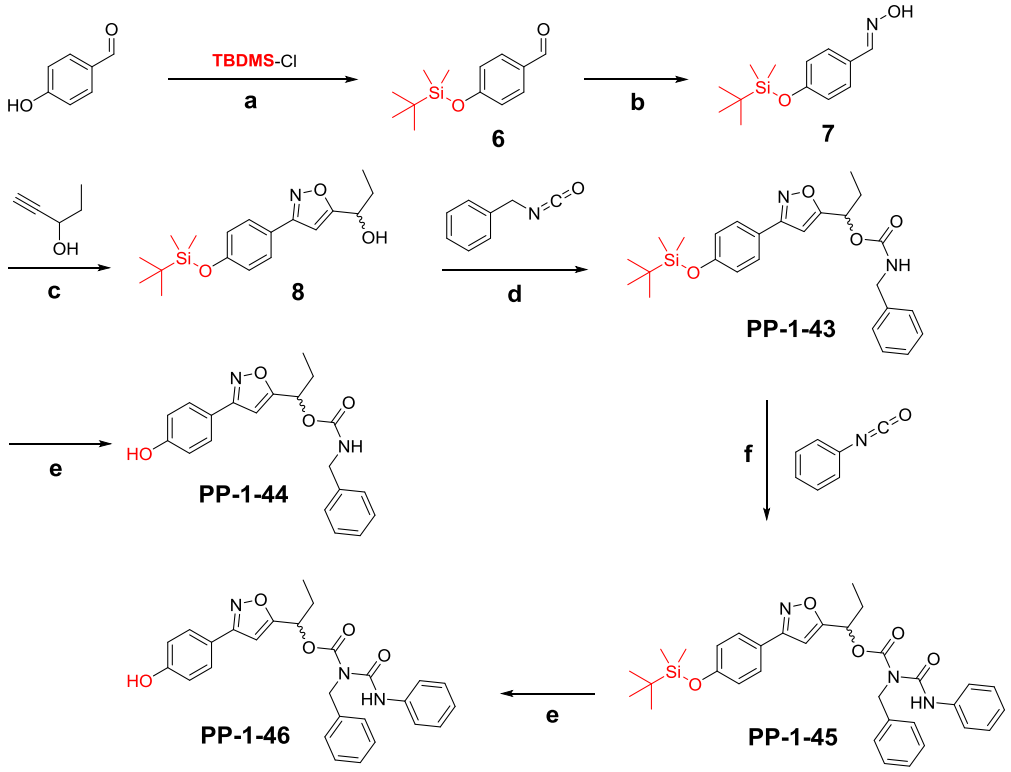

Scheme 2. Synthetic procedure for PPARγ ligands PP-43 through PP-46. a) imidazole, dry DMF, 0 ^{o}C, 1h, 94% b) hydroxyamine, Na_2CO_3, *aq*. ethanol, 65 ^{o}C, 12h, 85%, c) NCS, pyridine, then acetylene, TEA, THF, 60 ^{o}C, 2h, 67%, d) pyridine, CuCl, DCM, r.t., 2h, 99%, e) TBAF, THF, r.t., 1h, 86% f) TEA, CuCl, DCM, r.t., 2h, 93%

As expected, transactivation assay data confirmed the carboxylic acid's influence on PPARγ's transcriptional activity. For both C06 and BP carboxylic acid substituted derivates (PP-43, PP-44 and PP-45, PP-46 respectively), transcriptional activity dropped dramatically after the removal of the carboxylic acid moiety (Figure 10). PP-43 and PP-44 showed virtually no sign of any agonism towards PPARγ while PP-45 and PP-46 became reduced to partial agonists relative to the full agonist BP. However, comparing the partial agonist PP-46 to C06, it can be seen that C06 is roughly 7 times less active than PP-46. Functionalization of the carbamate nitrogen with the formation of a urea was originally carried out for increasing the transcriptional activity of C06. While these results did validate the hypothesis regarding the carboxylic acid's effect on transcriptional activity, due to the relatively high activity of the BP-based compounds, it was decided not to incorporate the urea functionalization into the future compound sets. Additionally, even though the TBDMS-protected compounds PP-43 and PP-45 exhibited desirable low activity towards PPARγ activation, because of poor *in vivo* solubility concerns, this modification was also chosen to be left behind. Lastly, the effect of replacing the carboxylic acid functionality with a hydroxyl group showed very promising results with PP-44 and PP-46, and as a result it was decided to incorporate this modification into the future compound sets.

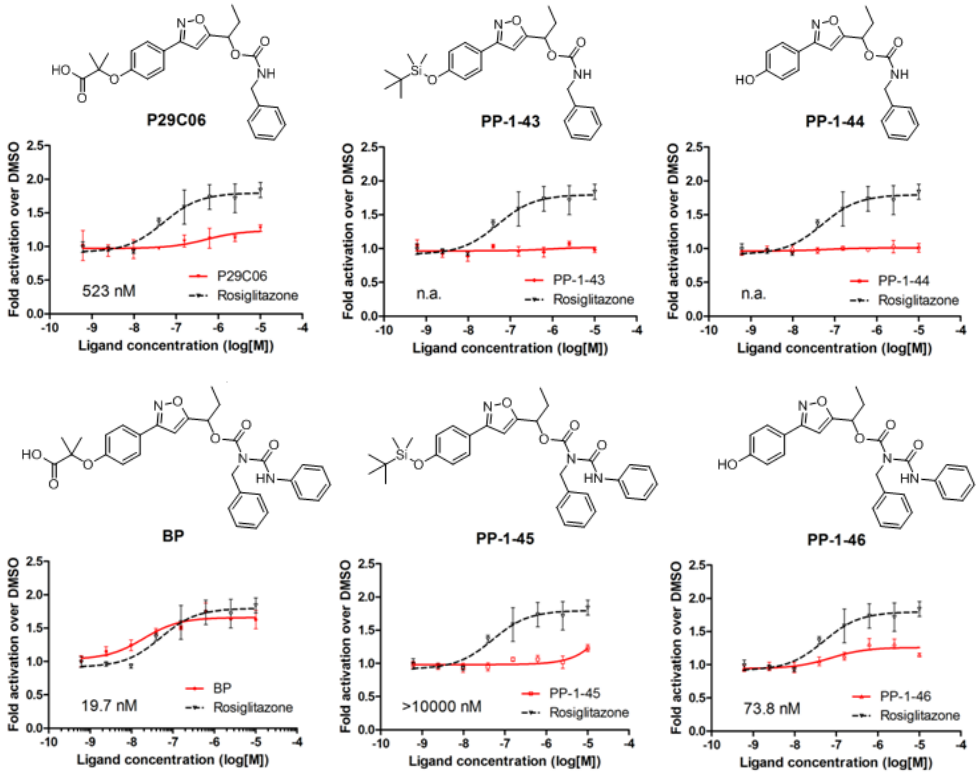

Figure 10. Transcriptional activity profile of a PPAR γ-derived reporter gene in 293T cells after treatment with rosiglitazone and C06, BP, and PP-43 through PP-46 for 24h.

The dramatic drop in transactivation activity with the incorporation of the TBDMS functionality, prompted us to explore an amide analog for isobutyric acid; the amide is more polar than TBDMS, such that it should resolve previous solubility issues, and less polar than the carboxylic acid so it will not interact with amino acid residues as strongly (Figure 11).

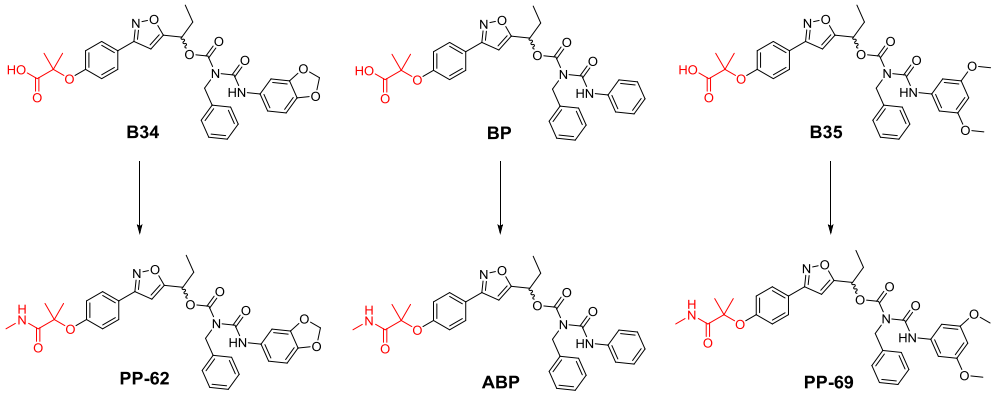

Figure 11. Structural modifications to the carboxylic acid moiety in B34, BP and B35 depicted in red, forming the respective amide analogs PP-62, ABP and PP-69.

Synthesis of the amide analogs follows an identical procedure to Scheme 1, where the addition of the urea moiety was performed under the same reaction conditions as step f in Scheme 2. The amide functionality was introduced via an amide coupling reaction with EDC and HOBt with TEA as base in 1,4-dioxane overnight at room temperature affording yields in the range of 70-78%.

Due to the high transactivational activity of the urea containing C06 derivates (B34, BP, B35, Figure 11), one may expect that by synthesizing the amide analogs of these compounds, provided the cause of this high activity is due to the carboxylic acid moiety as hypothesized, would generate the most easily detectable change in transactivational activity (such as the case with the BP to PP-45 and PP-46 modifications in Figure 10). However, what was found was that the transactivational activity of the amide analogs PP-62 and PP-69 was unchanged compared to their carboxylic acid partners (Figure 12).

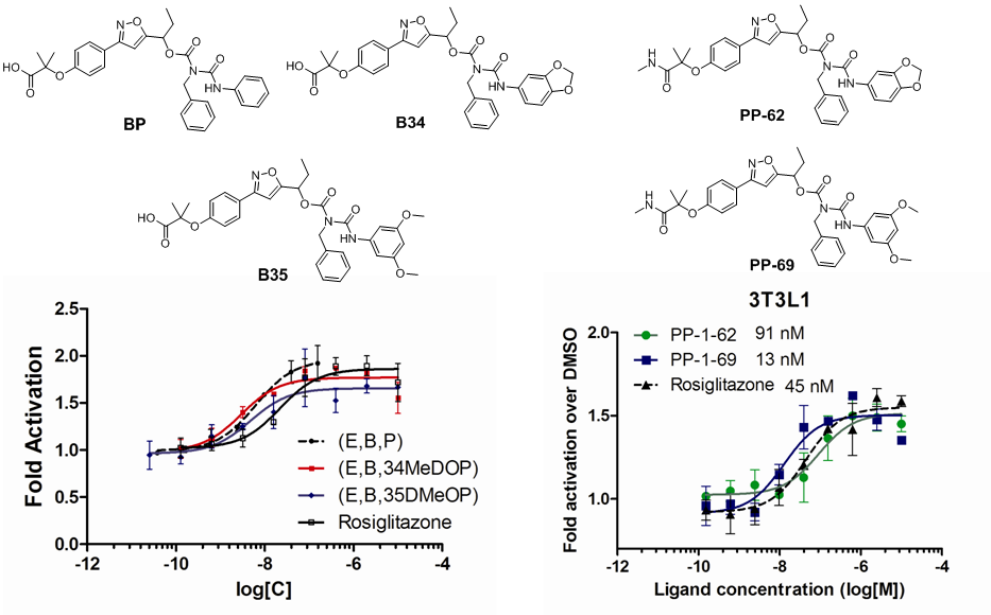

Figure 12. Transcriptional activity profile of a PPARγ-derived reporter gene in 293T cells after treatment with rosiglitazone and BP, B34, B35, PP-62 and PP-69 for 24.

To help better make sense of this result, PPARγ co-crystal structures of the enantiomers of B35 (named R35 and S35, Figure 13A and B) were analyzed. It can be seen that each enantiomer's orientation within the LBD is vastly different. The carboxylic acid of S35 is found to be hydrogen bonding with the omega loop, and R35's orientation turns out to be not only flipped relative to S35, but was also found to have its carboxylic acid hydrogen bonding with helix 12.

Because of these orientation differences, transcriptional activity of R35 and S35 as well as their phosphorylation inhibition efficacies are different from one another. R35 acts as a full agonist with moderate phosphorylation inhibition (0.1uM) and S35 as a partial agonist with poorer phosphorylation inhibition (1uM)[18]. As interesting as these results may be, it became clear that there is too much uncertainty associated with analyzing ligand-PPARγ interactions when the ligand exists in racemic form.

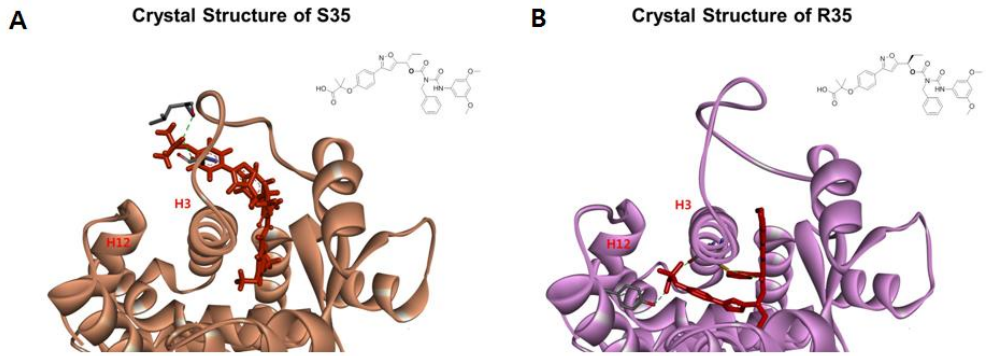

Figure 13. PPARγ co-crystal structures with a) S35 and b) R35

Keeping these concerns in mind, dramatic differences in transcriptional activity was observed between BP and ABP, where the amide modification in ABP resulted in complete eradication of transcriptional activity (Figure 14A). Docking analysis of these two compounds attributed these activity differences to ABP being incapable of hydrogen bonding with the omega loop, unlike BP (Figure 15).

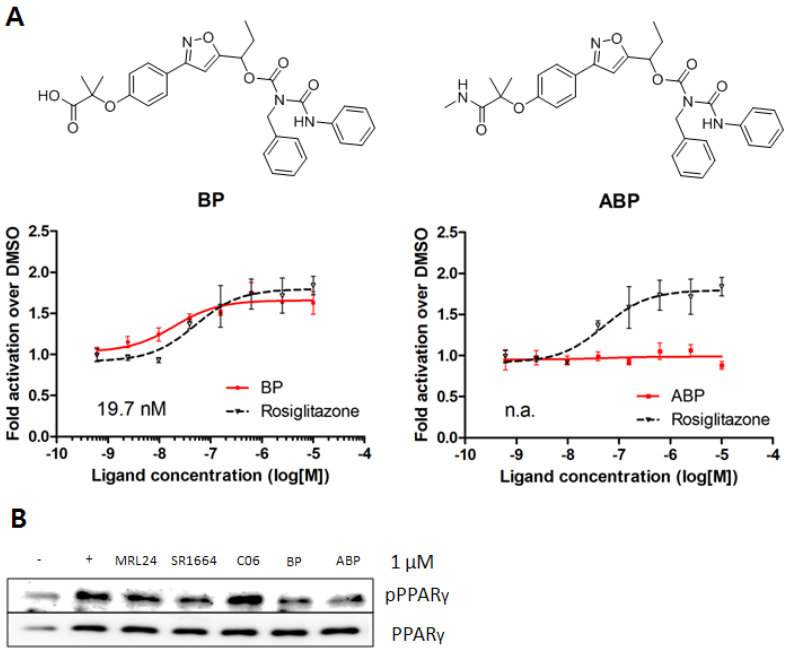

Figure 14. a) Transcriptional activity profile of a PPARγ-derived reporter gene in 293T cells after treatment with rosiglitazone and BP (left) and with rosiglitazone and ABP (right). b) In vitro Cdk5 assay with known partial agonist MRL24, non-agonist SR1664, partial agonist C06, BP and ABP with PPARγ substrates.

One might expect that a hydrogen bonding interaction with the omega loop, as can be seen in the docking simulation of BP (Figure 15), should likely result in inhibition of Cdk5-mediated phosphorylation of Ser273 due to serine 273 being situated there. However, whether that apparent interaction is there or not (BP vs ABP, Figure 15), has no effect on phosphorylation (Figure 14B). As was seen in the case of B35 and the relative binding of its enantiomers, a similar situation with BP and ABP where one enantiomer resides in the LBD preferentially to the other, resulting in conflicting effects on PPARγ could exist there too. Moreover, with PPARγ's LBD being so large, many conformations with similar docking scores can be generated, with some being in significantly different orientations. As such, with so many conformations existing, all with such similar docking scores, selecting the most appropriate conformation is difficult. Therefore, the docking simulations serve strictly as guides for visualizing the sorts of potential orientations that a ligand could adopt in the LBD as well as providing clues into identifying ligands that would unlikely remain in the LBD.

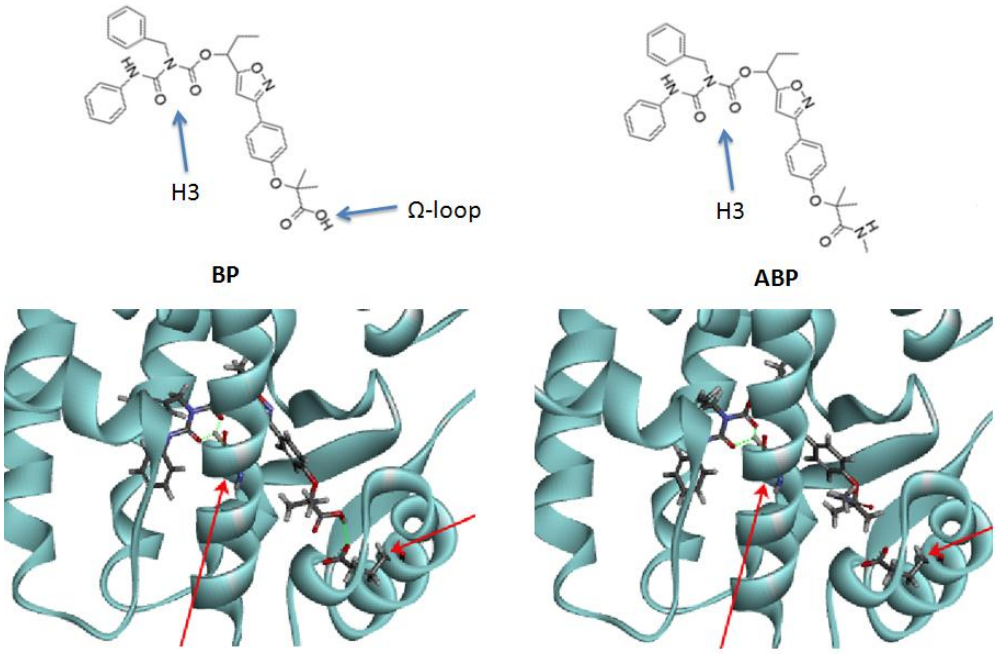

Figure 15. Docking simulation of BP (left) and ABP (right) with the crystal structure of PPARγ's ligand binding domain (PDB ID: 2hfp, Discovery Studio 1.7, Accelrys was used). Two dimensional representation of the ligands' approximate orientation within the LBD is illustrated above the respective docked image.

Also, it should be noted that when running a docking simulation for a racemic ligand, an enantiomer for that racemate is randomly selected and it is that enantiomer that is docked. Initially such drastic orientation differences in the LBD between a set of enantiomers was not anticipated, but after confirmation from crystal structure data of R35/S35 the future compound sets were adjusted to be enantiomerically pure.

1.4.1 Results and Discussion – Urea-Centered Set

After collecting all of the key concepts and revelations acquired from the carbamate set, they were then incorporated into the next ligand family, the urea set (Figure 16).

Due to the issues outlined in the previous section, the most significant modification to the carbamate set was replacing its chiral carbamate carbon with a nitrogen atom, generating a chiral-free urea.

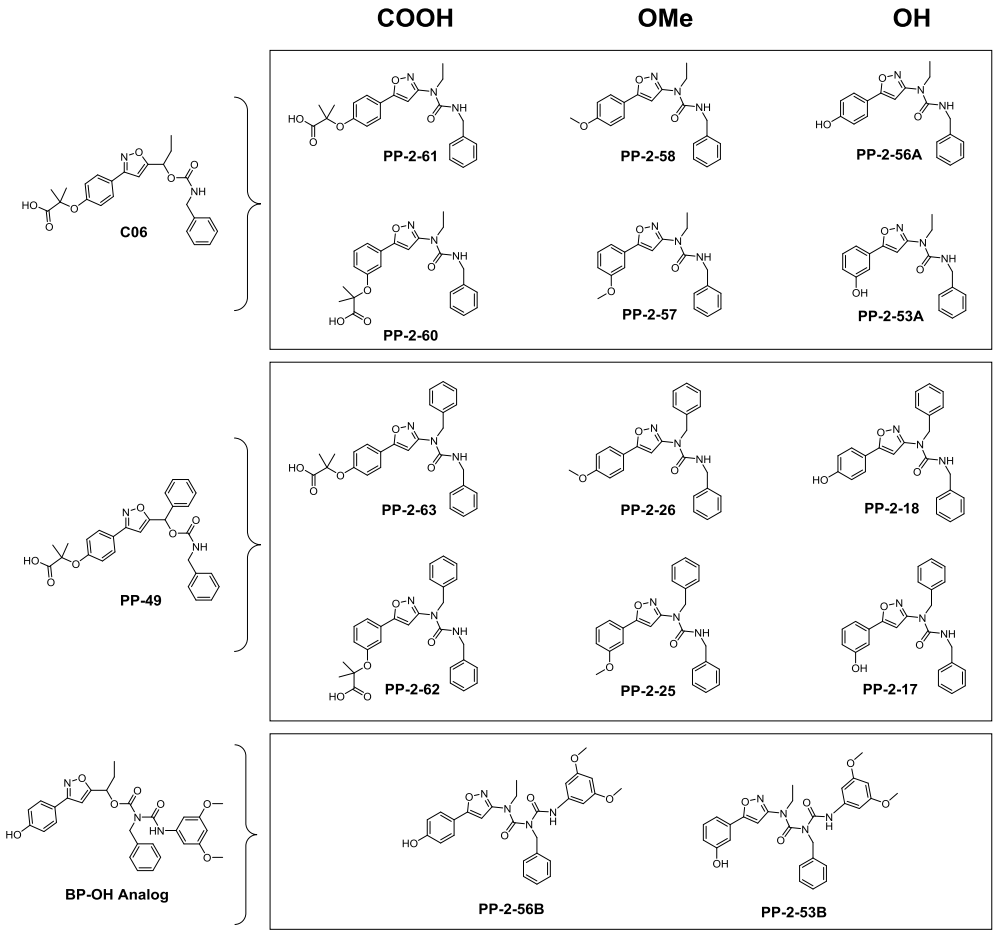

Figure 16. Urea-centered PPARγ ligand set. Derived from the carbamate set ligands C06 and PP-49 as well as the BP hydroxyl analog. Compounds further split into carboxylic acid, methoxy and hydroxyl functionalized groups as well as into their respective para and meta isomers.

Also, with all of the various orientations that some of the carbamate set ligands were found to adopt, a modification that would reduce the amount of these

conformations was required. One solution to this would be increasing the ligand's rigidity. Fortunately, the previous replacement of the carbamate carbon for nitrogen atom already provides this, so no further modifications in this area had to be performed.

Next, in order to allow for the possibility of greater interactions within the LBD, meta isomers were also synthesized (Scheme 4). The synthesis of the urea-centered set begins with the alpha-keto bromination of hydroxyl benzophenone with $CuBr_2$ followed by an S_N2 reaction with NaCN generating the ketonitrile **10**. For the formation of isoxazole **11** this reaction was found to be regioselective for where the hydroxylamine attacks **10**. Takase et al (1991)[19] attributed this phenomenon to nucleophilic attack of the ketonitrile **10** being possible at both the ketone and at the nitrile, leading to the formation of the two isomers following acid-mediated cyclization. When this reaction was performed at room temperature under mild basic conditions (pH ~8), the 3-aminoisoxazole was predominantly formed (~90% yield). However, at elevated temperatures (above 70 ^{o}C) with pH>8, the 5-aminoisoxazole was formed, albeit in much lower yield (~35%) (Figure 17).

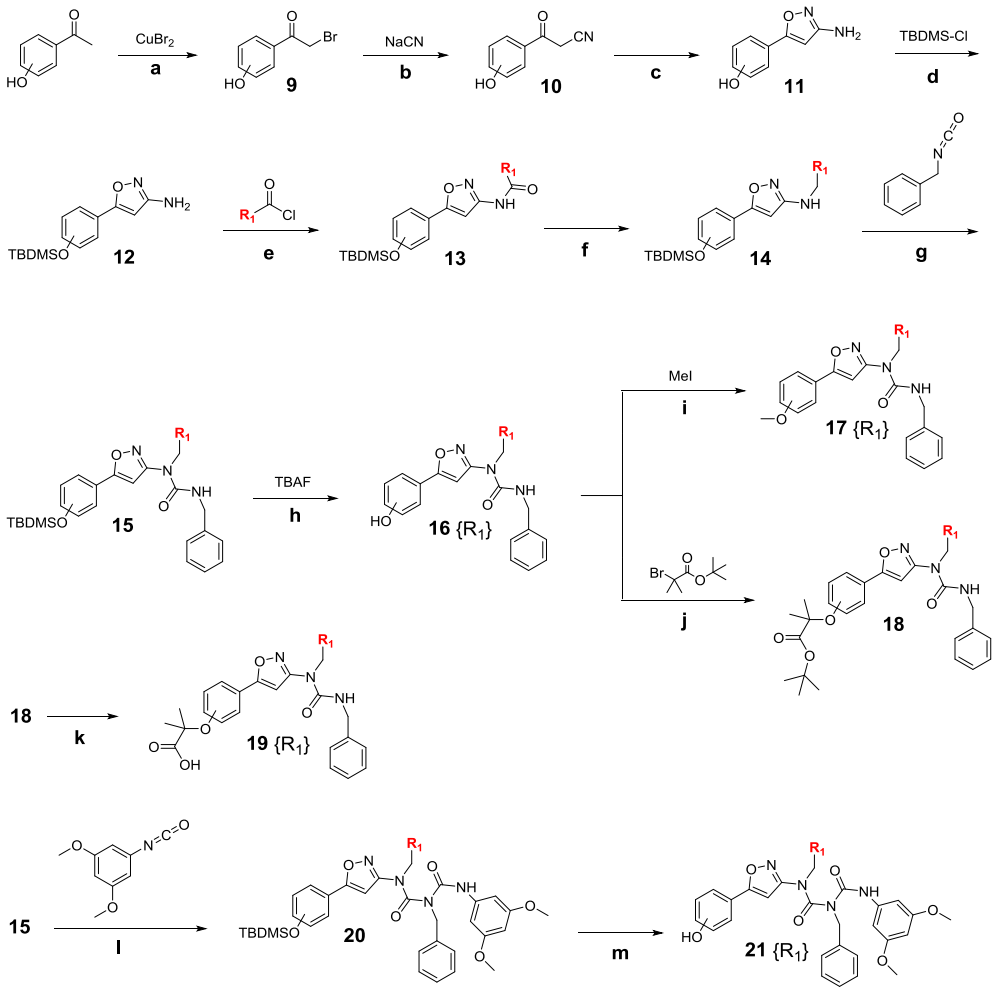

Scheme 4. General synthetic procedure for urea-centered PPARγ ligands. a) ethyl acetate, DCM, methanol; (5:5:1), r.t., 4h, 98%, b) EtOH:water; (3:1), 0 ^{o}C, 2h, 73%, c) NaOH, NH_2OH-HCl, (EtOH:water; 3:2), r.t., 24h, then HCl 2h, 93%, d) imidazole, dry DMF, 0 ^{o}C, 4h, 84%, e) pyridine, DCM, 0 ^{o}C, 24h, 90%, f) TMSCl, DCM, 0 ^{o}C, 1h, then $LiAlH_4$, 2h, 95%, g) pyridine, CuCl, DCM, r.t., 2h, 83%, h) DCM, r.t., 2h, 98%, i) K_2CO_3, acetone, reflux, 24h, 72%, j) K_2CO_3, $MgSO_4$, DMF, 50 ^{o}C, 24h, 41%, k) TFA, DCM, 8h, 98%, l) $SnCl_4$, DCM, r.t., 9h, 35%, m) HF-pyridine 5% in THF, r.t., 1h, 10%

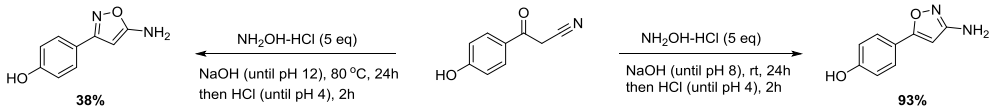

Figure 17. Reaction conditions that have shown to favor the formation of the 3-aminoisoxazole isomer (right) and 5-aminoisoxazole (left).

The addition-elimination equilibrium between **1** and **4** exists at under weakly basic conditions,[17] and attack of the hydroxylamine at the nitrile in **1** can proceed while this equilibrium exists (Figure 18). This irreversible addition of NH_2OH to the CN group of **1**, after treatment with HCl generates the 3-aminoisoxazole, **3**. Another factor found to influence NH_2OH attack at the CN group was the size of R[20]. The relatively bulky phenol group may have also contributed to the preferential formation of 3-amino-5-(4-hydroxy)phenylisoxazole over its isomer, even at elevated temperatures under basic conditions.

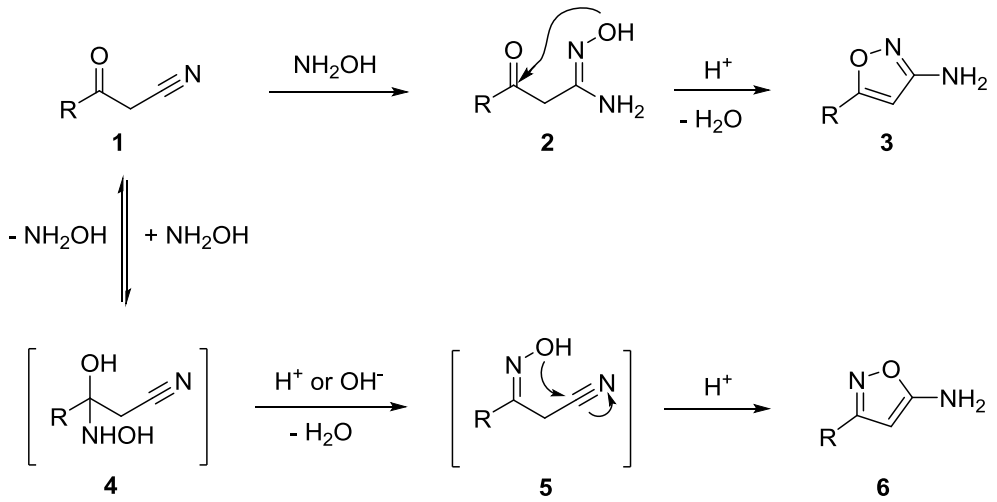

Figure 18. Proposed reaction pathways for the formation of the 3-aminoisoxazole (**3**) and 5-aminoisoxazole (**6**) isomers[19].

Since the isoxazole moiety functions as an anchor, latching itself onto the sturdy H3 backbone, whether the N,O positions within the isoxazole ring are switched or not is unlikely to affect the PPARγ conformation. So for this reason and the fact that a

much higher yield is achieved in the 3-aminoisoxazole pathway, the urea-set synthesis was carried on with this minor modification.

Next, after protecting the hydroxyl group with TBDMS under standard conditions generating **12**, we introduced the R_1 group via the Schotten-Baumann reaction, affording our amide **13**. Originally, our intention was to attach a phenyl ring as one of the R_1 groups in this urea-set, such as to bear close resemblance to PP-49. However, the deactivated amine, due to its nitrogen's electron lone pair being delocalized through resonance with the isoxazole nitrogen, made the amine a particularly poor nucleophile, thwarting various palladium-based cross coupling reaction attempts to introduce this functionality. So before moving on, thorough docking simulation analyses on the benzyl version ligands were conducted in order to see if whether the pursuit of the incorporation of this moiety may be a reasonable substitute for the phenyl group. The docking data showed no adverse docking scores or presence of any additional interactions that may interfere with the binding of these ligands with the LBD of PPARγ. Therefore, it was decided to continue the synthesis of the urea-set with the incorporation of the synthetically accessible benzyl moiety instead. At first, synthesizing the secondary amine from **12** to **14** directly was attempted, but all the attempts were unsuccessful (reductive ammination, imine formation, activating the benzaldehyde carbonyl group to make it more electrophilic, as well as various S_N2 pathways were all tested). With the amine being such a poor nucleophile, the only choice at this point was to react it with an extremely good electrophile, an acid chloride. Even though this reaction does not generate the desired product, a simple amide reduction should provide the secondary amine. While the amide formation reaction with benzoyl chloride, generating **13** worked wonderfully (90% yield), reducing it proved to be another challenge. Various reductants, including $LiAlH_4$ were ineffective in reducing the amide. Only after Lewis acid activation of the amide carbonyl group with TMS followed by subsequent addition of $LiAlH_4$ was the secondary amide **14** finally generated with 95% yield. Afterwards, treatment of **14** with benzyl isocyanate, pyridine and CuCl generates urea **15** to which TBDMS deprotection via TBAF

affords the hydroxyl ligands (PP-2-16, PP-2-17, PP-2-53A and PP-2-56A). Then subjecting **15** to S_N2 conditions with MeI, generates the methoxy set **17** (PP-2-25, PP-2-26, PP-2-57 and PP-2-58) and under S_N1 conditions with t-butyl-alpha-bromo-isobutyrate, gave **18**. Then simple treatment of **18** with TFA, produces the carboxylic acid set **19** (PP-2-60, PP-2-61, PP-2-62 and PP-2-63). Originally the plan was to only synthesize the single urea compounds mentioned thus far, however if the double ureas proved to be synthetically feasible, there was no reason not to include a few of them for extra data comparisons. The initial goal was to synthesize the carboxylic acid version of the double urea, but due to the instability resulting from the chain of nitrogens in the double urea compound, it readily decomposed even under mild basic or acid conditions. Therefore, the alcohol analog **21**, was as far as the stability of this compound would allow to go. Forming the double urea in **20** required using $SnCl_4$ to increase the electrophilicity of the isocyanate through chelation such that the deactivated urea nitrogen would be able to react with it. However, the reaction continuously failed to go to completion, always resulting in a mix of the starting material and product **20**. Due to similar polarity, column separation was not possible, so the mixture was deprotected together under HF-Pyridine conditions, generating the alcohol versions of both the single and double urea compounds. The polarity differences of the two were much more pronounced and were easily separable by flash column chromatography affording the double ureas **21** (PP-2-53B and PP-2-56B).

After evaluating the transactivational and phosphorylation inhibiting activity of the benzyl versions of the methoxy and hydroxyl compounds, it was pleasing to see that incorporating the benzyl moiety not only resulted in all compounds exhibiting no agonism relative to rosiglitazone but also showed consistent phosphorylation inhibition at the 10 μM mark (Figure 19).

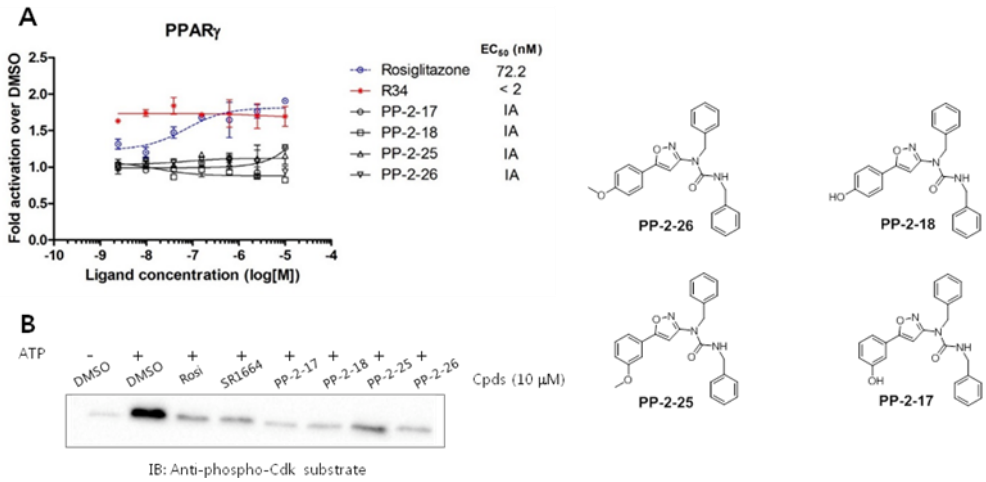

Figure 19. a) Transcriptional activity profile of a PPARγ-derived reporter gene in 293T cells after treatment with rosiglitazone, R34, PP-2-17, PP-2-18, PP-2-25 and PP-2-26. b) In vitro Cdk5 assay with Rosiglitazone, SR1664, PP-2-17, PP-2-18, PP-2-25 and PP-2-26 with PPARγ substrates.

To get a rough idea of how these ligands are behaving in the LBD, docking simulation data was used to shed some light on their possible interactions (Figure 20). It was found that none of the ligands had any interactions with H11 or H12, which was in accordance with their absent transcriptional activity (Figure 19A), as well each having two interactions on H3, which is what may have influenced conformational change on the omega loop, owing to the observed phosphorylation inhibition (Figure 19B).

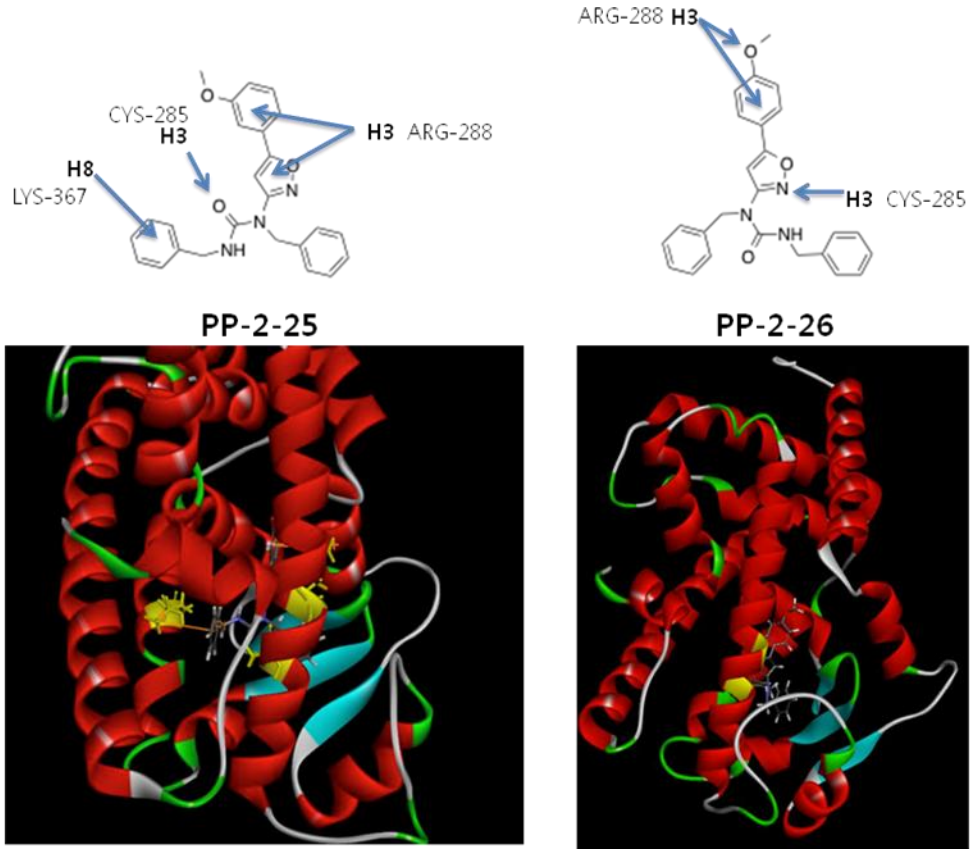

Figure 20. Docking simulation of PP-2-25 (left) and PP-2-26 (right) with the crystal structure of PPARγ's ligand binding domain (PDB ID: 2hfp, Discovery Studio 1.7, Accelrys was used). Two dimensional representations of the ligands' approximate orientation within the LBD along with identification of the amino acid residues they are interacting with (indicated in yellow in the docked image) are illustrated above the respective docked image.

In the case of the ethyl versions of the methoxy and hydroxyl compounds, their phosphorylation inhibition activity was analyzed first (Figure 21). While PP-2-56B showed some mild phosphorylation inhibition activity, the rest were ineffective. However, the carboxylic acid versions for both the ethyl and benzyl compounds all showed varying levels of phosphorylation inhibition, with the benzyl ligands being the most effective. Interestingly, docking simulation results predicted that the benzyl

version carboxylic acid ligands PP-2-62 and PP-2-63 latch on to H3 without utilizing the isoxazole ring (Figure 22). However, similar to the previous benzyl version ligands, these ligands too have been found to have multiple interactions with the H3 helix, which are in agreement with the phosphorylation inhibition activity that these interactions have been showing to instigate.

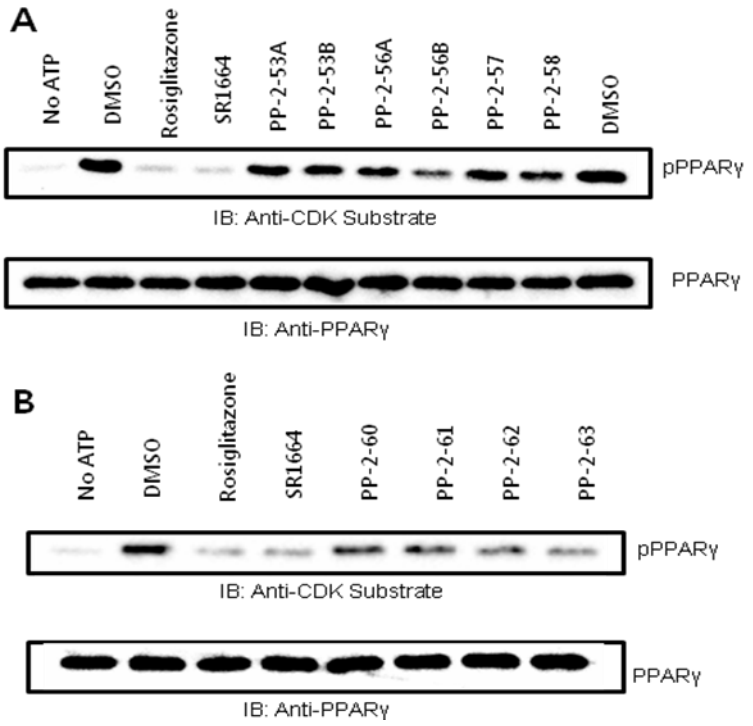

Figure 21. In vitro Cdk5 assay with a) Rosiglitazone, SR1664, PP-2-53A, PP-2-53B, PP-2-56A, PP-2-56B, PP-2-57 and PP-2-58 with PPARγ substrates. b) Rosiglitazone, SR1664, PP-2-60, PP-2-61, PP-2-62 and PP-2-63 with PPARγ substrates

Pending definitive confirmation from crystal structure data, if these interactions prove to be as depicted in Figure 22, without the inclusion of the isoxazole ring, this could allow for the development of other structurally similar ligands with other rings serving as substitutes for the isoxazole. Candidates could include cycloalkenes,

various triazoles, thiadiazoles, etc. One advantage to such a system would be the electronic environment around the primary amine in **12**, depending on the choice of ring, may not facilitate the resonance delocalization of the amine nitrogen's electrons, resulting in a more reactive nucleophilic amine which would allow for a greater choice of substrates that it can react with.

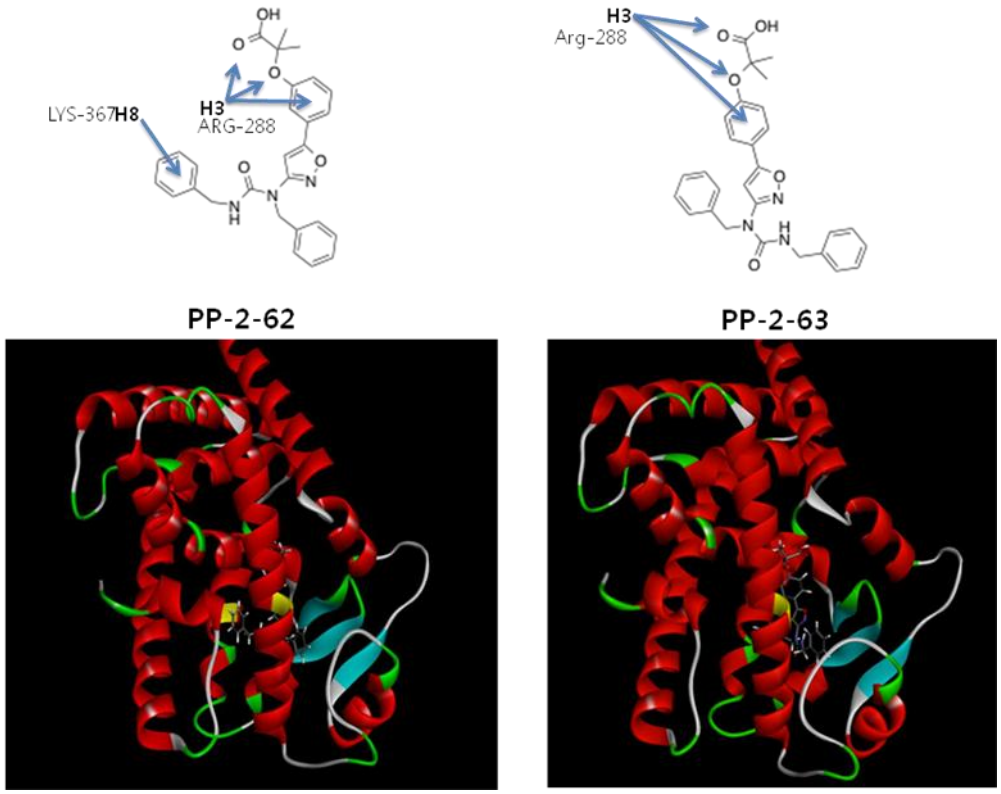

Figure 22. Docking simulation of PP-2-62 (left) and PP-2-63 (right) with the crystal structure of PPARγ's ligand binding domain (PDB ID: 2hfp, Discovery Studio 1.7, Accelrys was used). Two dimensional representations of the ligands' approximate orientation within the LBD along with identification of the amino acid residues they are interacting with (indicated in yellow in the docked image) are illustrated above the respective docked image.

1.5.1 Results and Discussion – Amide Set

After careful analysis of the various conformations adopted by the urea set ligands within PPARγ's LBD, it was found that not one had any interactions with the urea nitrogen furthest the isoxazole ring. This nitrogen's primary effect was rigidifying the benzyl arm that it was attached to. Replacing this nitrogen with a methylene bridge, forming the amide, would allow this arm to adopt a more preferred orientation within the binding cavity, opening up the possibility for interacting with neighboring helixes. Contingent on the amide ligand set's performance, the next step was to functionalize the mobile carbonyl bound arm with polar heteroatoms (such as replacing the benzene ring with pyridine) to not only aid in the compound's solubility for in vitro testing, but to also to strengthen its interactions with the help of a hydrogen bond acceptor. Before devising a synthetic scheme for the incorporation of the modified arm, the amide set, based on the successful compound groups from the carbamate and urea set were synthesized first (Figure 23).

Synthesizing the amide set follows an identical procedure to the urea set (Scheme 4) with only one alteration. After obtaining **14**, the amine was reacted with hydrocinnamoyl chloride, generating the amide in relatively high yield. From this step, obtaining the carboxylic acid, methoxy and hydroxyl ligands were carried out under the same conditions depicted in Scheme 4.

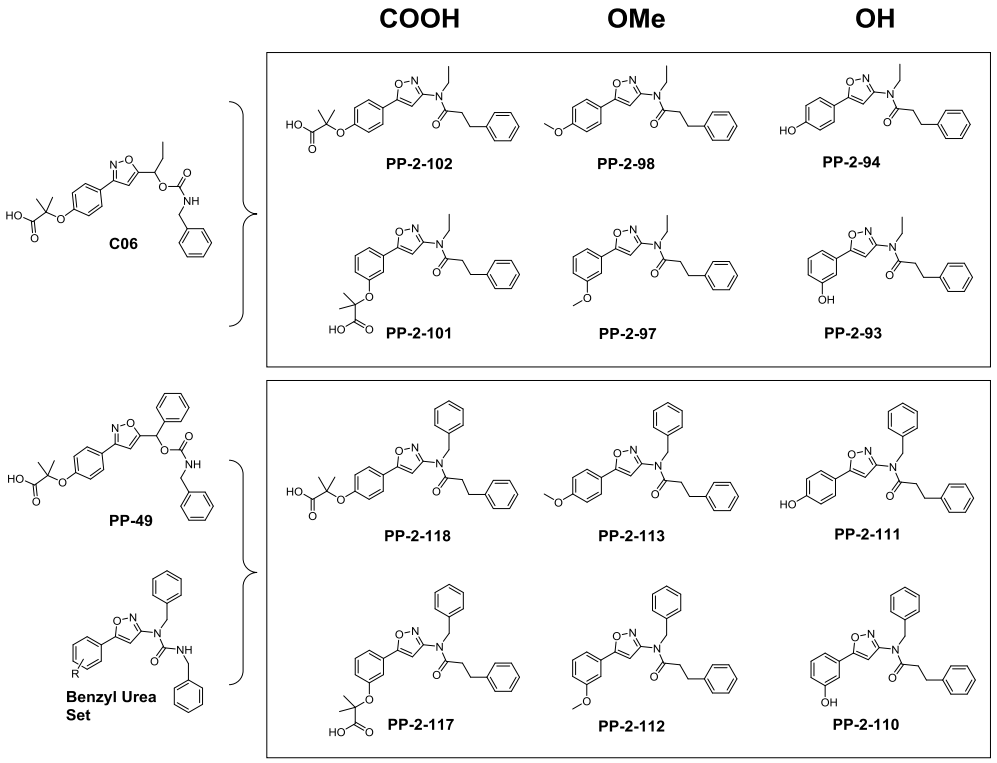

Figure 23. Amide-centered PPARγ ligand set. Derived from the carbamate set ligands C06 and PP-49 as well as the urea BP set. Compounds further split into carboxylic acid, methoxy and hydroxyl functionalized groups as well as into their respective para and meta isomers.

While the possibility of discovering a preferred orientation for the hydrocinnamoyl arm was quite enticing, a major concern for this modification was whether or not the added flexibility would disrupt the rest of the ligand from successfully docking with the LBD. Docking analysis data on the amide ligands did score lower than the urea and carbamate set compounds, but not low enough to write them off completely. First tested for their phosphorylation inhibition activity were the ethyl version ligands (Figure 24A). The collective lack of phosphorylation inhibition activity of the tested compounds, taken together with their relatively low docking scores, gives rise to the possibility that the ligands were unsuccessful in

binding with PPARγ. Similarly to the ethyl ligands, the benzyl ligands were not that much better, except for carboxylic acids PP-2-117 and PP-2-118 (Figure 24B).

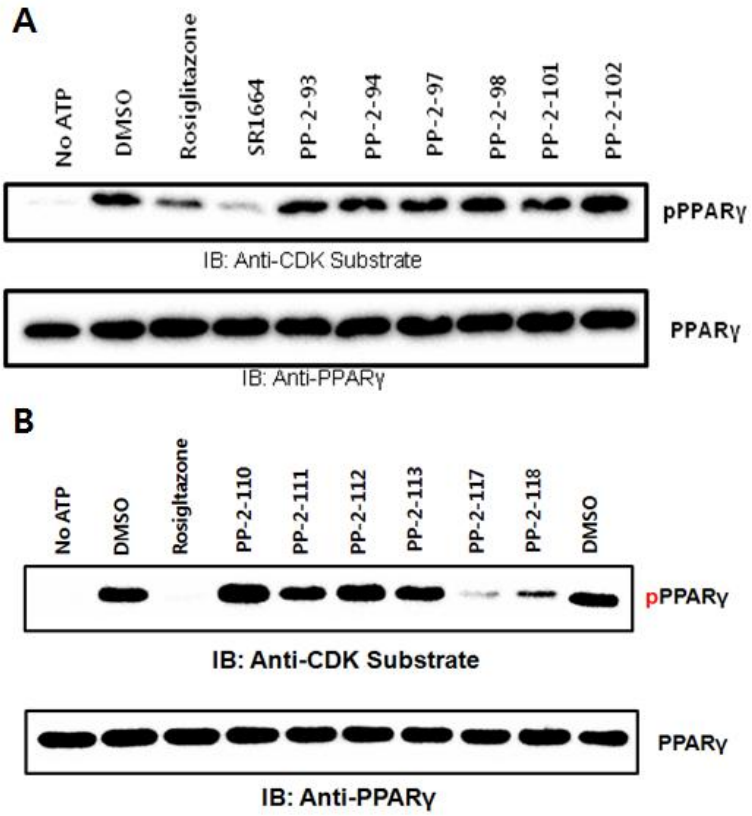

Figure 24. In vitro Cdk5 assay with a) (Ethyl ligands) Rosiglitazone, SR1664, PP-2-93, PP-2-94, PP-2-97, PP-2-98, PP-2-101 and PP-2-102 with PPARγ substrates. b) (Benzyl ligands) Rosiglitazone, PP-2-110, PP-2-111, PP-2-112, PP-2-113, PP-2-117 and PP-2-118 with PPARγ substrates

PP-2-117 showed almost full phosphorylation inhibition activity rivaling Rosiglitazone, and its para counterpart PP-2-118, while slightly less active was still able to induce partial inhibition. Transactivation assays of those compounds reveal both PP-2-117 and PP-2-118 behave as partial agonists relative to Rosiglitazone with EC50 values of 5.3μM and 1.5μM respectively (Figure 25). Nevertheless,

taking into account the entire amide set as a whole, using this amide scaffold for developing PPARγ ligands does not provide as large a window for modification possibilities as do the carbamate and urea sets.

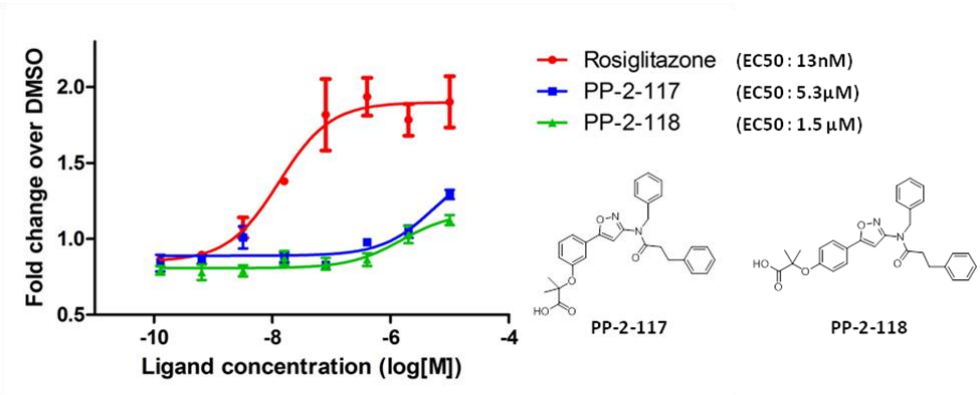

Figure 25. Transcriptional activity profile of a PPARγ-derived reporter gene in 293T cells after treatment with Rosiglitazone, PP-2-117 and PP-2-118.

1.6.1. Conclusion

A total of 3 libraries targeting PPARγ with the purpose of inhibiting its phosphorylation by Cdk-5 while inducing minimal to no activation of the host have been designed, synthesized and tested. Ligand design began from setting the partial agonist C06 as a template for subsequent modifications. While maintaining C06's low activation towards PPARγ, or even lowering it further, the goal was to functionalize it such that the new ligands also inhibit Cdk5-mediated phosphorylation.

The first series of modifications in the carbamate library provided a lot of useful information regarding the size and electronic environment threshold of newly attached substituents. PPARγ's large binding domain was found to have no problem accommodating ligands as large as PP-47 without its bulky 3-trifluoromethyl diphenylether group disrupting the isoxazole's H-bonding interaction with H3. This finding reveals that C06 can support relatively large modifications without it having

a detrimental effect on its binding within PPARγ's LBD. Furthermore, various modifications with C06's and BP's carboxylic acid groups confirmed the large role that the carboxylic acids have with both transcriptional activation and phosphorylation inhibition, however, their racemic nature complicated the elucidation of the SAR pertaining to their bio-activity. As a result, the next series of modifications have had all their chirality centers removed in order to eliminate this problem.

Of the three series, the urea series had the greatest amount of compounds that showed phosphorylation inhibition, encompassing all of the benzyl ligands as well as all of the carboxylic acid compounds. In addition, the benzyl substituted hydroxyl and methoxy ligands exhibited close to no agonism relative to Rosiglitazone.

The last amide series, based on consistent inability to inhibit phosphorylation, except for the benzyl substituted carboxylic acids PP-2-117 and PP-2-118, likely indicated failure to bind with PPARγ's LBD. While not overly exciting from an activity point of view, this observation does provide crucial information regarding the extent of how labile the arms of the PPAR ligand can be before it begins to affect its binding capacity. This information will most definitely be taken into consideration when designing future PPARγ ligands.

1.7.1. Experimental Section

1.7.1.1. General Information

All reactions were performed using oven-dried glassware that was kept in a dry argon environment. Solvents and other reagents were purchased from commercial venders and were used without further purification unless otherwise mentioned. 4-hydroxybenzaldehyde, t-butyl-α-bromo-isobutyrate, hydroxyamine hydrochloride, isocyanates, benzaldehydes, $CuBr_2$, CuCl, N-chlorosuccinimide, t-butyldimethylsilyl chloride (TBDMS-Cl), imidazole, 1-ethyl-3-(3-dimethylaminopropyl)carbodiimide (EDC) hydrochloride, 1-hydroxybenzotriazole (HOBt), triethylamine (TEA), $SnCl_4$, $LiAlH_4$ and trimethylsilyl chloride (TMS-Cl) were purchased from Sigma-Aldrich, USA. Trifluoroacetic acid, tetra-n-butylammonium fluoride (TBAF) and hydrocinnamoyl chloride were purchased from TCI [Tokyo Chemical Industry Co., Ltd., Japan]. The products were purified by flash column chromatography on silica gel (230 – 400 mesh) or preparative thin-layer chromatography (prep TLC) on pre-coated glass-backed plates (silica gel 60 F_{254}m 1.0 mm). Thin-layer chromatography was performed on pre-coated glass-backed plates (silica gel 60 F_{254}, 0.5 mm), and components were visualized by observation under UV light (254 and 365 nm) or by treating the plates with anisaldehyde, $KMnO_4$, and or phosphomolybdic acid followed by heating. Distilled water (DW) was polished by ion exchange and filtration. ^{1}H NMR and ^{13}C NMR spectra were recorded on a Bruker DRX-300 [Bruker Biospin, Germany] and Varian Inova-500 [Varian Assoc., USA] machines. Chemical shifts were measured in ppm, downfield from tetramethylsilane (TMS) as the internal standard. Multiplicites were indicated as follows: s (singlet), d (doublet), t (triplet), q (quartet), m (multiplet), dd (doublet of doublet), td (triplet of doublet), etc. Coupling constants were reported in Hz. Low resolution mass spectrometry (LRMS) analyses were performed with a Finnigan MSQ Plus Serveyer HPLC/MS system [Thermo Electron Corp., USA] using electron spray ionization (ESI).

1.7.1.2. Synthetic Procedures and Characterization

(1), *tert-butyl 2-(4-formylphenoxy)-2-methylpropanoate*

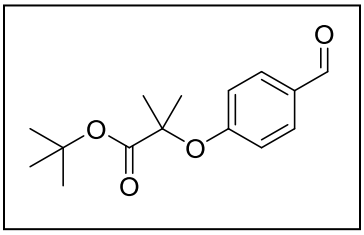

To a solution of 4-hydroxybenzaldehyde (5 g, 41.1 mmol) dissolved in dry DMF (100 mL) was added K_2CO_3 (22.6 g, 163.8 mmol), $MgSO_4$ (5.42 g, 45.0 mmol) and t-butyl-α-bromo-isobutyrate (23.7 mL, 122.8 mmol). The reaction mixture was stirred at 100°C for 28 h and then allowed to cool to room temperature. The crude mixture was diluted with distilled ice-water (100 mL) and extracted 3 times with EtOAc (100 mL). Afterwards, the combined organic layer was dried over anhydrous Na_2SO_4(s) and filtered through a celite-packed glass filter. The filtrate was concentrated *in vacuo* and purified with silica gel flash column chromatography (1:10 ~ 1:5 = EtOAC:n-hexanes, v/v) to provide 1 (10.1 g 93%). R_f = 0.92 (1:1 = EtOAc:Hex, v/v); ^{1}H NMR (400 MHz, $CDCl_3$-*d*) δ 9.78 (s, 1H), 7.68 (d, *J* = 8.9 Hz, 2H), 6.81 (d, *J* = 8.5 Hz, 1H), 1.54 (s, 6H), 1.31 (s, 9H). LRMS(ESI$^+$) m/z calcd for $C_{15}H_{20}O_4$ $[M+H]^+$ 265.14 Found; 264.94.

(2), *tert-butyl 2-(4-((hydroxyimino)methyl)phenoxy)-2-methylpropanoate*

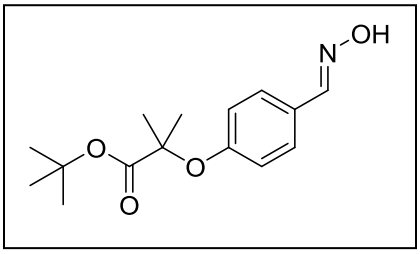

A solution of compound 1 (3.58 g, 13.54 mmol) and hydroxylamine hydrochloride (1.0 g, 14.9 mmol) dissolved in EtOH (75 mL) and DW (75 mL) was cooled to 0°C via an ice bath to which Na_2CO_3 (1.58 g, 14.9 mmol) was added. The reaction mixture was then heated to 65°C and was left stirring for 12 h. The solvents were evaporated *in vacuo*, and the remaining solid was dissolved with DW and chloroform. The organic layer was separated and the aqueous layer was further extracted two more times with chloroform. The separated and combined organic layers were dried over anhydrous Na_2SO_4(s) and filtered through a celite-

packed glass filter. The filtrate was concentrated under reduced pressure and purified with silica gel flash column chromatography (1:5 = EtOAc:*n*-hexanes, v/v) to provide 2 (2.7 g, 72%). R_f = 0.21 (1:5 = EtAOc:Hex, v/v); ^{1}H NMR (400 MHz, $CDCl_3$-*d*) δ 8.07 (s, 1H), 7.45 (d, *J* = 8.3 Hz, 2H), 7.28 (s, 1H), 6.84 (d, *J* = 8.7 Hz, 2H), 1.59 (s, 6H), 1.43 (s, 9H). LRMS(ESI$^+$) m/z calcd for $C_{15}H_{21}NO_4$ $[M+H]^+$ 280.15 Found 279.88.

(Alk-P), *1-phenylprop-2-yn-1-ol*

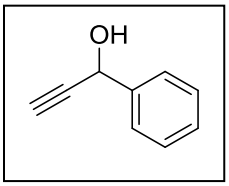

To a solution of dry THF (10 mL) cooled to -78^{o}C, was first added benzaldehyde (1 mL, 9.4 mmol) and then ethynyl magnesium bromide 0.5M in THF (22.6 mL, 11.3 mmol) dropwise over a 2 minute period. The mixture was left to stir for another 2.5 h, afterwards it was warmed to room temperature and then quenched with saturated NH_4Cl (25 mL). The crude product was extracted with DCM (50 mL) two times. The combined organic layers were dried over anhydrous $MgSO_4$ and filtered through a celite-packed glass filter. The filtrate was concentrated *in vacuo* and purified with silica gel flash column chromatography (1:5 = EtOAC:n-hexanes, v/v) to provide 1 (1.01 g 80%). R_f = 0.43 (1:5 = EtOAc:Hex, v/v); ^{1}H NMR (500 MHz, $CDCl_3$-*d*) δ 7.58 – 7.54 (m, 2H), 7.43 – 7.33 (m, 3H), 5.46 (d, *J* = 2.2 Hz, 1H), 2.67 (d, *J* = 2.3 Hz, 1H), 2.45 (s, 1H). ^{13}C NMR (125 MHz, $CDCl_3$-*d*) δ 140.1, 128.8, 128.7, 126.7, 83.6, 75.0, 64.5.

(Alk-CN), *4-(1-hydroxyprop-2-yn-1-yl)benzonitrile*

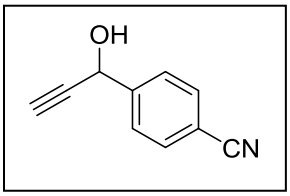

Synthesized according to the synthetic procedure of Alk-P, with p-cyanobenzaldehyde as the starting reagent. Yield 98%, R_f = 0.35 (1:2 = EtOAc:Hex, v/v); ^{1}H NMR (400 MHz, $CDCl_3$-*d*) δ 7.65 (s, 4H), 5.50 (dd, *J* = 5.8, 2.3 Hz, 1H), 3.17 (d, *J* = 5.7 Hz, 1H), 2.69 (d, *J* = 2.3 Hz, 1H). ^{13}C NMR (75 MHz, $CDCl_3$-*d*) δ 145.2, 132.5, 127.3, 118.7, 112.0, 82.6, 75.7, 63.4.

(Alk-CF3), *1-(3-(3-(trifluoromethyl)phenoxy)phenyl)prop-2-yn-1-ol*

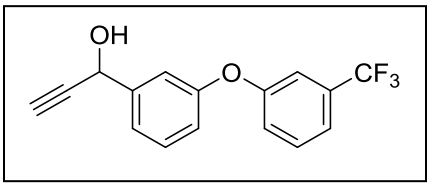

Synthesized according to the synthetic procedure of Alk-P, with 3-(3-(trifluoromethyl)phenoxy)benzaldehyde as the starting reagent. Yield 49%, R_f = 0.66 (1:2 = EtOAc:Hex, v/v); ^{1}H NMR (500 MHz, $CDCl_3$-*d*) δ 7.42 (t, *J* = 8.0 Hz, 1H), 7.39 – 7.32 (m, 3H), 7.26 (s, 2H), 7.15 (dd, *J* = 8.1, 2.3 Hz, 1H), 6.98 (d, *J* = 7.7 Hz, 1H), 5.44 (s, 1H), 2.65 (dd, *J* = 2.3, 0.7 Hz, 1H). ^{13}C NMR (125 MHz, $CDCl_3$-*d*) δ 157.6, 156.6, 142.5, 130.5, 130.4, 122.4, 121.9, 121.8, 120.1, 119.99, 119.96, 119.3, 117.7, 115.67, 115.64, 115.61, 115.58, 83.2, 75.3, 64.0.

(3 {P}), *tert-butyl*
2-(4-(5-(hydroxy(phenyl)methyl)isoxazol-3-yl)phenoxy)-2-methylpropanoate

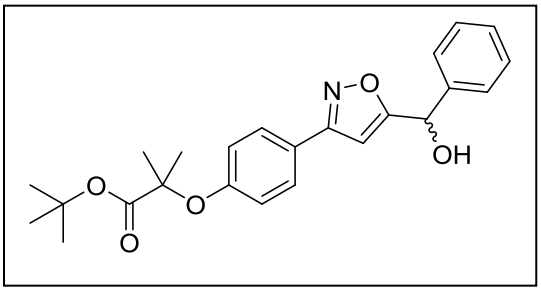

To a dry THF solution (10 mL) containing compound 2 (300 mg, 1.06 mmol) and N-chlorosuccinimide (158 mg, 0.11 mmol) was added pyridine (12 µL, 0.11 mmol). The mixture was stirred at 60^{o}C for 2h. To the stirring mixture was added Alk-P (144 µL, 1.1 mmol) pre-mixed with TEA (180 µL, 1.3 mmol). The solution was left stirring for 1 h and then quenched with brine (5 mL). The organic layer was separated and the aqueous layer was further extracted two more times with DCM. The separated and combined organic layers were dried over anhydrous $MgSO_4$(s) and filtered through a celite-packed glass filter. The filtrate was concentrated under reduced pressure and purified with silica gel flash column chromatography (1:10 ~ 1:5 = EtOAC:n-hexanes, v/v) to provide 3 {P}, (390 mg 99%). R_f = 0.52 (1:2 = EtOAc:Hex, v/v); ^{1}H NMR (400 MHz, $CDCl_3$-*d*) δ 7.64 (d, *J* = 8.8 Hz, 2H), 7.46 (d, *J* = 7.8 Hz, 2H), 7.43 – 7.33 (m, 2H), 6.87 (d, *J* = 8.8 Hz, 2H), 6.37 (s, 1H), 5.94 (s, 1H), 2.95 (s, 1H),

1.59 (s, 6H), 1.42 (s, 9H). ^{13}C NMR (75 MHz, $CDCl_3$-*d*) δ 173.9, 173.2, 162.0, 157.5, 139.7, 129.0, 128.9, 127.9, 126.8, 118.6, 99.8, 82.2, 79.7, 69.6, 27.9, 25.5 LRMS(ESI$^+$) m/z calcd for $C_{24}H_{27}NO_5$ $[M+H]^+$ 410.19 Found; 409.90.

(3 {CN}), *tert-butyl 2-(4-(5-((4-cyanophenyl)(hydroxy)methyl)isoxazol-3-yl)phenoxy)-2-methylpropanoate*

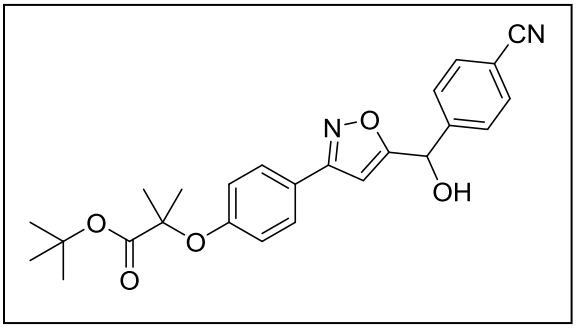

Synthesized according to the synthetic procedure of 3 {P}. Yield 58%, R_f = 0.33 (1:2 = EtOAc:Hex, v/v); ^{1}H NMR (500 MHz, $CDCl_3$-*d*) δ 7.69 (d, *J* = 8.4 Hz, 2H), 7.64 – 7.59 (m, 4H), 6.87 (d, *J* = 8.8 Hz, 2H), 6.37 (s, 1H), 6.02 (d, *J* = 3.9 Hz, 1H), 3.12 (d, *J* = 4.3 Hz, 1H), 1.59 (s, 6H), 1.42 (s, 9H). ^{13}C NMR (125 MHz, $CDCl_3$-*d*) δ 161.9, 157.4, 144.9, 132.4, 127.8, 127.2, 118.6, 99.8, 82.2, 79.7, 68.3, 27.7, 25.3

(3 {CF3}), *tert-butyl 2-(4-(5-(hydroxy(3-(3-(trifluoromethyl)phenoxy)phenyl)methyl)isoxazol-3-yl)phenoxy)-2-methylpropanoate*

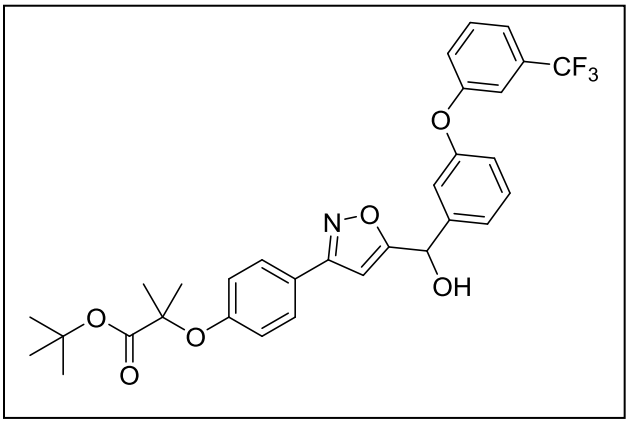

Synthesized according to the synthetic procedure of 3 {P}. Yield 26%, R_f = 0.53 (1:2 = EtOAc:Hex, v/v); ^{1}H NMR (500 MHz, $CDCl_3$-*d*) δ 7.63 (d, *J* = 8.8 Hz, 2H), 7.43 (t, *J* = 8.1 Hz, 1H), 7.40 – 7.33 (m, 2H), 7.25 (s, 1H), 7.19 (t,

J = 2.1 Hz, 1H), 7.15 (dd, *J* = 8.2, 2.2 Hz, 1H), 6.99 (ddd, *J* = 8.2, 2.5, 1.0 Hz, 1H), 6.88 (d, *J* = 8.9 Hz, 2H), 6.38 (d, *J* = 0.8 Hz, 1H), 5.94 (s, 1H), 1.60 (s, 6H), 1.42 (s, 9H). ^{13}C NMR (125 MHz, $CDCl_3$-*d*) δ 173.5, 173.2, 162..0, 157.5, 156.8, 142.1, 130.5, 127.9, 122.3, 122.0, 121.9, 120.1, 120.0, 119.4, 118.6, 117.6, 115.7, 115.6, 99.8, 82.2, 79.7, 69.0, 27.9, 25.5.

(4 {P}), *tert-butyl 2-(4-(5-(((benzylcarbamoyl)oxy)(phenyl)methyl)isoxazol-3-yl)phenoxy)-2-methylpropanoate*

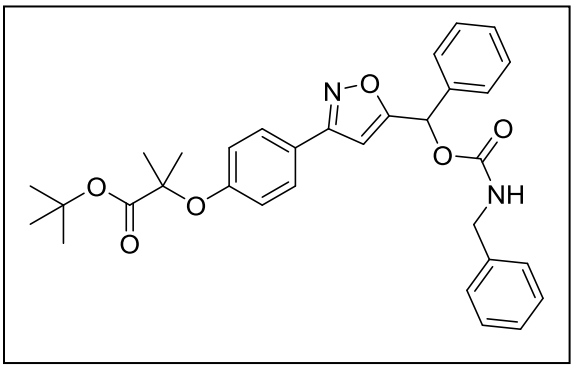

Compound 3 {P} (195 mg, 0.48 mmol) and copper (I) chloride (4.7 mg, 0.05 mmol) were dissolved in DCM (10 mL). To this mixture, pyridine (116 µL, 1.44 mmol) and benzyl isocyanate (71.0 µL, 0.58 mmol) were added and the reaction was left to stir at room temperature for 2 h. The reaction was quenched with saturated NH_4Cl (10 mL), then the organic layer was separated and the aqueous layer was extracted two times with DCM. The separated and combined organic layers were dried over anhydrous $MgSO_4$(s) and filtered through a celite-packed glass filter. The filtrate was concentrated under reduced pressure and purified with silica gel flash column chromatography (1:10 = Methanol:DCM, v/v) to provide 4 {P}, (210 mg 81%). R_f = 0.52 (1:2 = EtOAc:Hex, v/v); ^{1}H NMR (500 MHz, $CDCl_3$-*d*) δ 7.66 (d, *J* = 8.6 Hz, 2H), 7.47 (d, *J* = 3.8 Hz, 1H), 7.43 – 7.26 (m, 9H), 6.95 (s, 1H), 6.91 – 6.87 (m, 2H), 6.40 (s, 1H), 5.33 (t, *J* = 5.7 Hz, 1H), 4.40 (dd, *J* = 6.0, 3.7 Hz, 2H), 1.61 (s, 6H), 1.44 (s, 9H). ^{13}C NMR (125 MHz, $CDCl_3$-*d*) δ 173.1, 170.1, 161.2, 157.5, 155.1, 136.6, 129.1, 128.9, 128.8, 127.91, 127.88, 127.75, 127.69, 127.4, 122.0, 188.5, 101.1, 101.0, 82.1, 79.7, 70.4, 45.4, 27.9, 25.5 LRMS(ESI$^+$) m/z calcd for $C_{32}H_{34}N_2O_6$ $[M+H]^+$ 543.24 Found; 443.03.

(4 {CN}), *tert-butyl 2-(4-(5-(((benzylcarbamoyl)oxy)(4-cyanophenyl)methyl)isoxazol-3-yl)phenoxy)-2-methylpropanoate*

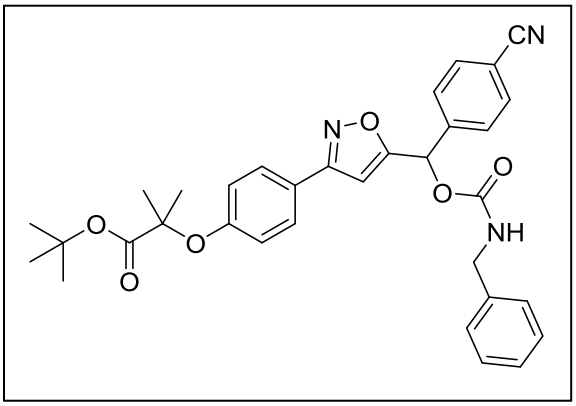

Synthesized according to the synthetic procedure of 4 {P}. Yield 68%, R_f = 0.48 (1:2 = EtOAc:Hex, v/v); ^{1}H NMR (500 MHz, $CDCl_3$-*d*) δ 7.67 (d, *J* = 8.3 Hz, 2H), 7.63 (d, *J* = 8.7 Hz, 2H), 7.56 (d, *J* = 8.9 Hz, 2H), 7.34 – 7.24 (m, 5H), 6.95 (s, 1H), 6.88 (d, *J* = 7.8 Hz, 2H), 6.44 (s, 1H), 5.50 (t, *J* = 6.1 Hz, 1H), 4.37 (d, *J* = 6.0 Hz, 2H), 1.60 (s, 6H), 1.42 (s, 9H). ^{13}C NMR (125 MHz, $CDCl_3$-*d*) δ 173.0, 169.0, 162.0, 157.6, 154.6, 141.6, 137.8, 132.6, 128.8, 127.83, 127.78, 127.6, 121.5, 118.5, 118.3, 112.9, 101.4, 82.1, 79.7, 69.3, 45.4, 27.8, 25.4.

(4 {CF3}), *tert-butyl 2-(4-(5-(((benzylcarbamoyl)oxy)(3-(3-(trifluoromethyl)phenoxy)phenyl)methyl) isoxazol-3-yl)phenoxy)-2-methylpropanoate*

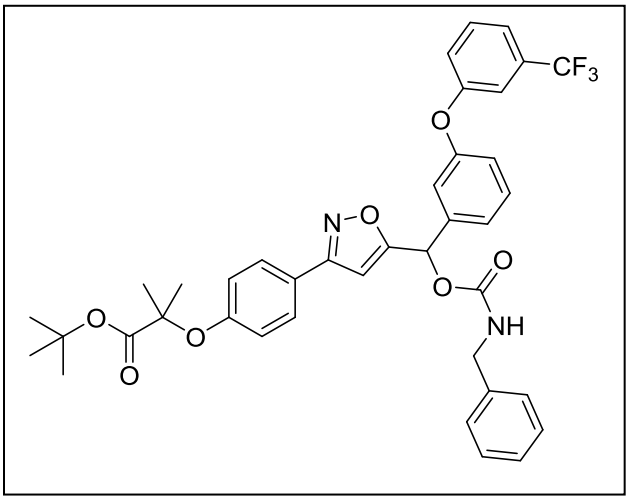

Synthesized according to the synthetic procedure of 4 {P}. Yield 85%, R_f = 0.51 (1:2 = EtOAc:Hex, v/v); ^{1}H NMR (400 MHz, $CDCl_3$-*d*) δ 7.64 (d, *J* = 8.4 Hz, 2H), 7.46 – 7.23 (m, 10H), 7.20 – 7.12 (m, 2H), 7.00 (dd, *J* = 8.1, 2.4 Hz, 1H), 6.92 (s, 1H), 6.88 (d, *J* = 8.7 Hz, 2H), 6.41 (s, 1H), 5.27 (s, 1H), 4.39 (dd, *J* = 6.0, 2.9 Hz, 2H), 1.60 (s, 6H), 1.42 (s, 9H).

^{13}C NMR (75 MHz, $CDCl_3$-*d*) δ 173.1, 170.0, 162.0, 157.6, 157.4, 156.7, 154.9, 138.9, 137.9, 130.6, 128.9, 127.9, 127.8, 127.7, 122.9, 121.93, 121.87, 120.2, 120.1, 119.6, 118.5, 118.1, 115.74, 155.70, 101.1, 82.1, 79.7, 69.8, 45.5, 27.9, 25.5 LRMS(ESI$^+$) m/z calcd for $C_{39}H_{37}F_3N_2O_7$ $[M+H]^+$ 703.26 Found; 703.13.

(5 {P}), *2-(4-(5-(((benzylcarbamoyl)oxy)(phenyl)methyl)isoxazol-3-yl)phenoxy)-2-methylpropanoic acid*

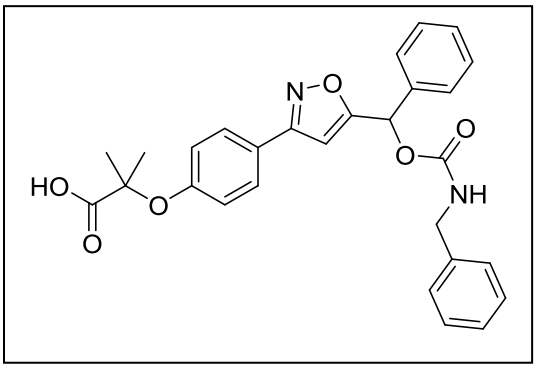

Compound 4 {P} (50 mg, 0.09 mmol) was dissolved in 10% (v/v) trifluoroacetic acid in DCM (1 mL). The mixture was stirred at room temperature for 10h and then quenched with aqueous Na_2CO_3. The organic layer was separated and the aqueous layer was further extracted two more times with DCM. The separated and combined organic layers were dried over anhydrous $MgSO_4$(s) and filtered through a celite-packed glass filter. The filtrate was concentrated under reduced pressure and purified with silica gel flash column chromatography (1:15 = Methanol:DCM + 1% acetic acid, v/v/v) to provide 5 {P}, (24.1 mg, 54%). R_f = 0.61 (1:10 = Methanol:DCM + 1% acetic acid, v/v/v); ^{1}H NMR (500 MHz, DMSO-d_6) δ 8.21 (t, *J* = 6.1 Hz, 1H), 7.62 (d, *J* = 8.3 Hz, 2H), 7.53 – 7.20 (m, 10H), 6.88 (s, 2H), 6.85 (s, 1H), 4.21 (d, *J* = 6.1 Hz, 2H), 1.42 (s, 6H). ^{13}C NMR (125 MHz, DMSO-d_6) δ 161.6, 158.5, 155.1, 139.3, 137.0, 128.7, 238.3, 127.4, 127.0, 126.93, 126.89, 119.5, 117.8, 100.9, 69.1, 44.0, 25.9. LRMS(ESI$^+$) m/z calcd for $C_{28}H_{26}N_2O_6$ $[M+H]^+$ 487.18 Found; 487.05

(5 {CN}), *2-(4-(5-(((benzylcarbamoyl)oxy)(4-cyanophenyl)methyl)isoxazol-3-yl)phenoxy)-2-methylpropanoic acid*

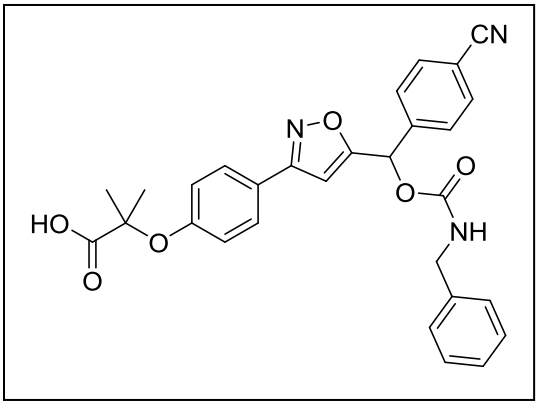

Synthesized according to the synthetic procedure of 5 {P}. Yield 75%, R_f = 0.64 (1:10 = Methanol:DCM + 1% acetic acid, v/v/v); ^{1}H NMR (400 MHz, DMSO-d_6) δ 8.32 (t, *J* = 6.1 Hz, 1H), 7.93 (d, *J* = 8.1 Hz, 2H), 7.76 – 7.70 (m, 3H), 7.37 – 7.19 (m, 6H), 7.19 – 7.10 (m, 1H), 7.06 (s, 1H), 6.96 – 6.89 (m, 3H), 4.24 (d, *J* = 6.1 Hz, 2H), 1.54 (s, 6H). ^{13}C NMR (75 MHz, DMSO-d_6) δ 169.6, 161.6, 157.5, 154.8, 142.3, 139.2, 137.4, 132.8, 128.9, 128.3, 127.8, 127.7, 127.1, 127.0, 125.3, 120.7, 118.5, 118.3, 111.6, 101.7, 68.2, 44.1, 25.3. LRMS(ESI$^+$) m/z calcd for $C_{29}H_{25}N_3O_6$ $[M+H]^+$ 512.17; Found 512.07

(5 {CF3}), *2-(4-(5-(((benzylcarbamoyl)oxy)(3-(3-(trifluoromethyl)phenoxy)phenyl)methyl)isoxazol-3-yl)phenoxy)-2-methylpropanoic acid*

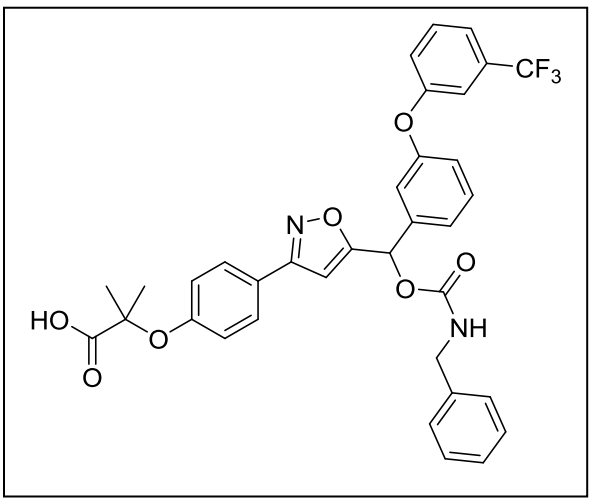

Synthesized according to the synthetic procedure of 5 {P}. Yield 75%, R_f = 0.64 (1:10 = Methanol:DCM + 1% acetic acid, v/v/v); ^{1}H NMR (400 MHz, DMSO-d_6) δ 8.21 (t, *J* = 6.2 Hz, 1H), 7.70 (d, *J* = 8.7 Hz, 2H), 7.62 (t, *J* = 8.0 Hz, 1H), 7.52 – 7.48 (m, 2H), 7.39 – 7.18 (m, 10H), 7.11 – 7.08 (m, 1H), 6.93 (s, 1H), 6.92 – 6.85 (m, 3H), 4.21 (d, *J* = 6.1 Hz, 2H), 1.50 (s, 6H). ^{13}C NMR (75

MHz, DMSO-d_6) δ 174.8, 170.3, 161.5, 157.8, 157.0, 156.0, 154.9, 139.5, 139.3, 131.5, 131.0, 130.8, 128.3, 127.7, 127.0, 126.9, 125.0, 122.6, 122.4, 120.3, 119.1, 118.1, 117.4, 101.3, 79.4, 68.3, 40.2, 25.5. LRMS(ESI^+) m/z calcd for $C_{35}H_{29}F_3N_2O_7$ $[M+H]^+$ 647.19 Found; 647.20

(6), *4-((tert-butyldimethylsilyl)oxy)benzaldehyde*

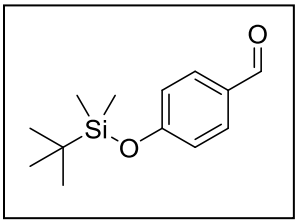

To a solution of 4-hydroxybenzaldehyde (10 g, 81.9 mmol) and imidazole (16.9 g, 245.6 mmol) in dry DMF (50 mL) cooled in an ice-water bath (0^{o}C) was added a solution of t-butyldimethylsilyl chloride (18.5 g, 123 mmol) in dry DMF (30 mL) followed by stirring at room temperature for 1 hour. The reaction mixture was then quenched with brine (60 mL) and extracted with EtOAc (80 mL) three times. The combined organic layer was dried over anhydrous $MgSO_4$, filtered, and concentrated under reduced pressure. The residue was purified by flash column chromatography (1:20 = EtOAC:n-hexanes, v/v) to provide 6, (17.22 g, 89%). R_f = 0.90 (1:10 = Methanol:DCM, v/v); ^{1}H NMR (400 MHz, $CDCl_3$-*d*) δ 9.88 (s, 1H), 7.78 (d, *J* = 8.3 Hz, 2H), 6.94 (d, *J* = 8.3 Hz, 2H), 0.99 (s, 9H), 0.25 (s, 6H).

(7), *(E)-4-((tert-butyldimethylsilyl)oxy)benzaldehyde oxime*

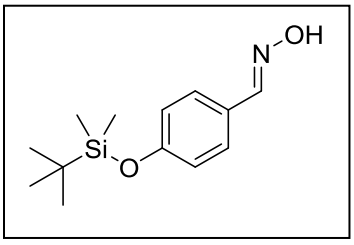

Synthesized according to the synthetic procedure of 2. Yield 65%, R_f = 0.38 (1:5 = EtOAc:Hex, v/v); ^{1}H NMR (400 MHz, $CDCl_3$-*d*) δ 8.08 (s, 1H), 7.50 – 7.42 (m, 3H), 6.85 (d, *J* = 8.1 Hz, 2H), 0.98 (s, 9H), 0.21 (s, 6H).

(8), *1-(3-(4-((tert-butyldimethylsilyl)oxy)phenyl)isoxazol-5-yl)propan-1-ol*

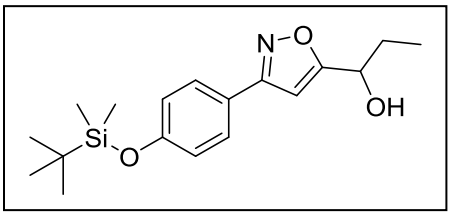

Synthesized according to the synthetic procedure of 3. Yield 63%, R_f = 0.18 (1:5 = EtOAc:Hex, v/v); ^{1}H NMR (400 MHz, $CDCl_3$-*d*) δ 7.68 (d, *J* = 8.8 Hz, 2H), 6.90 (d, *J* = 8.9 Hz, 2H), 6.45 (s, 1H), 4.86 – 4.79 (m, 1H), 2.14 (d, *J* = 5.5 Hz, 1H), 2.05 – 1.85 (m, 2H), 1.03 (t, *J* = 7.4 Hz, 3H), 0.99 (s, 9H), 0.22 (s, 6H). ^{13}C NMR (75 MHz, $CDCl_3$-*d*) δ 174.7, 162.1, 157.6, 128.3, 122.3, 120.7, 98.8, 68.7, 29.2, 25.8, 18.4, 9.5, -4.2. LRMS(ESI$^+$) m/z calcd for $C_{18}H_{27}NO_3Si$ $[M+H]^+$ 334.18 Found; 334.04

(PP-1-43), *1-(3-(4-((tert-butyldimethylsilyl)oxy)phenyl)isoxazol-5-yl)propyl benzylcarbamate*

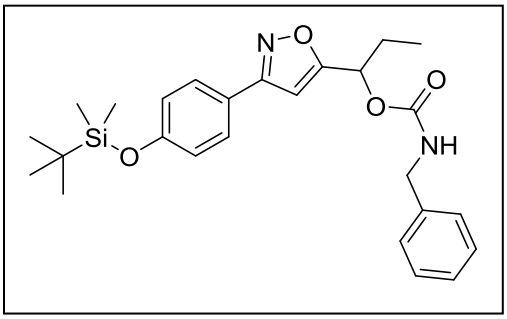

Synthesized according to the synthetic procedure of 4 {P}. Yield 92%, R_f = 0.70 (1:2 = EtOAc:Hex, v/v); ^{1}H NMR (400 MHz, $CDCl_3$-*d*) δ 7.67 (d, *J* = 8.5 Hz, 2H), 7.37 – 7.27 (m, 5H), 6.90 (d, *J* = 8.9 Hz, 2H), 6.46 (s, 1H), 5.85 (t, *J* = 6.8 Hz, 1H), 5.14 (t, *J* = 6.1 Hz, 1H), 4.40 – 4.37 (m, 2H), 2.08 – 1.97 (m, 2H), 0.99 (s, 9H), 0.99 – 0.94 (m, 3H), 0.22 (s, 6H). ^{13}C NMR (75 MHz, $CDCl_3$-*d*) δ 170.9, 162.1, 157.6, 155.7, 138.3, 129.0, 128.4, 127.8, 127.7, 122.2, 120.7, 100.5, 69.9, 45.4, 31.2, 26.6, 25.9, 18.5, 9.6, -4.2. LRMS(ESI$^+$) m/z calcd for $C_{26}H_{34}N_2O_4Si$ $[M+H]^+$ 467.23 Found; 466.88

(PP-1-44), *1-(3-(4-hydroxyphenyl)isoxazol-5-yl)propyl benzylcarbamate*

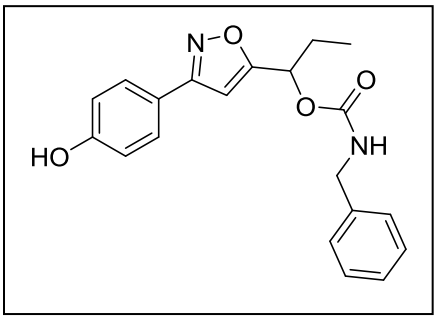

PP-1-43 (50 mg, 0.12 mmol) was dissolved in THF (1 mL) to which TBAF (1M in THF) (0.13 mL, 0.13 mmol) was added. The mixture was stirred at room temperature for 1 hour and then quenched with brine. The organic layer was separated and the aqueous layer was further extracted two more times with DCM. The separated and combined organic layers were dried over anhydrous $MgSO_4$(s) and filtered through a celite-packed glass filter. The filtrate was concentrated under reduced pressure and purified with silica gel flash column chromatography (1:2 = EtOAC:n-hexanes, v/v) to provide PP-1-44, (36 mg, 98%). R_f = 0.29 (1:2 = EtOAc:Hex, v/v); ^{1}H NMR (500 MHz, $CDCl_3$-*d*) δ 7.52 (d, *J* = 8.7 Hz, 2H), 7.34 – 7.19 (m, 5H), 6.82 (d, *J* = 8.6 Hz, 2H), 6.37 (s, 1H), 5.79 (t, *J* = 6.8 Hz, 1H), 5.57 – 5.50 (m, 1H), 4.41 – 4.31 (m, 3H), 2.03 – 1.97 (m, 2H), 0.96 (t, *J* = 7.4 Hz, 3H). ^{13}C NMR (75 MHz, $CDCl_3$-*d*) δ 170.5, 162.1, 158.4, 156.1, 137.9, 128.8, 128.5, 127.7, 127.6, 120.4, 116.1, 100.6, 70.1, 45.3, 26.4, 9.5. LRMS(ESI$^+$) m/z calcd for $C_{20}H_{20}N_2O_4$ $[M+H]^+$ 353.14 Found; 352.91

(PP-1-45), *1-(3-(4-((tert-butyldimethylsilyl)oxy)phenyl)isoxazol-5-yl)propyl benzyl(phenylcarbamoyl)carbamate*

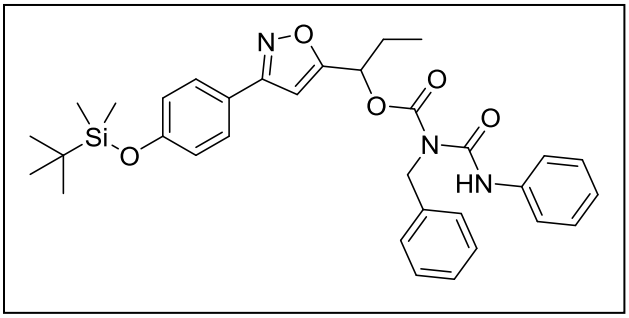

PP-1-43 (300 mg, 0.64 mmol) and copper (I) chloride (64 mg, 0.64 mmol) were dissolved in DCM (6.4 mL). To this mixture, TEA (272 µL, 1.93 mmol) and phenyl isocyanate (709.7 µL, 6.43 mmol) were added and the reaction was left to stir at room temperature for 24 hours. The reaction was quenched with brine (10 mL), then the organic layer was separated and the aqueous layer was extracted three times with DCM. The separated and combined organic layers were dried over anhydrous $MgSO_4$(s) and filtered through a celite-packed glass filter. The filtrate was concentrated under reduced pressure and purified with silica gel flash column chromatography (1:10 = EtOAC:n-hexanes, v/v) to provide PP-1-45, (334 mg, 89%). R_f = 0.89 (1:2 = EtOAc:Hex, v/v); ^{1}H NMR (500 MHz, $CDCl_3$-*d*) δ 10.78 (s, 1H), 7.60 (d, *J* = 8.7 Hz, 2H), 7.55 (d, *J* = 7.4 Hz, 2H), 7.39 – 7.31 (m, 6H), 7.31 – 7.25 (m, 1H), 7.14 – 7.10 (m, 1H), 6.91 (d, *J* = 8.6 Hz, 2H), 5.96 (s, 1H), 5.88 (t, *J* = 6.6 Hz, 1H), 5.13 (dd, *J* = 89.6, 15.3 Hz, 2H), 2.10 – 1.95 (m, 2H), 1.01 (s, 9H), 0.90 (t, *J* = 7.4 Hz, 3H), 0.24 (s, 6H). ^{13}C NMR (101 MHz, $CDCl_3$-*d*) δ 169.4, 162.1, 157.7, 155.6, 151.7, 138.1, 137.8, 129.1, 128.7, 128.4, 127.7, 127.6, 124.4, 121.8, 120.6, 120.5, 100.3, 72.3, 46.9, 26.5, 25.8, 18.4, 9.3, -4.3. LRMS(ESI$^+$) m/z calcd for $C_{33}H_{39}N_3O_5Si$ $[M+H]^+$ 586.27 Found; 586.01

(PP-1-46), *1-(3-(4-hydroxyphenyl)isoxazol-5-yl)propyl benzyl (phenylcarbamoyl)carbamate*

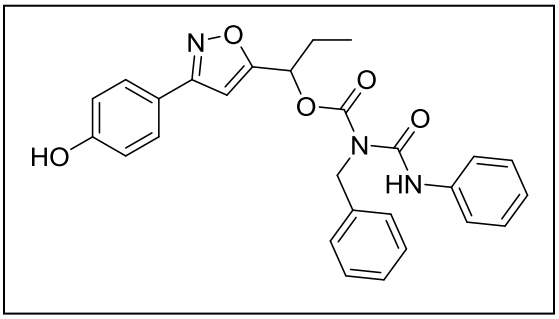

Synthesized according to the synthetic procedure of PP-1-44. Yield 91%, R_f = 0.44 (1:2 = EtOAc:Hex, v/v); ^{1}H NMR (400 MHz, $CDCl_3$-*d*) δ 10.77 (s, 1H), 7.57 (d, *J* = 8.8 Hz, 2H), 7.53 (dd, *J* = 8.7, 1.1 Hz, 2H), 7.37 – 7.30 (m, 6H), 7.29 – 7.23 (m, 1H), 7.15 – 7.08 (m, 1H), 6.89 (d, *J* = 8.8 Hz, 2H), 6.01 (s, 1H), 5.93 (s, 1H), 5.88 (t, *J* = 6.6 Hz, 1H), 5.12 (dd, *J* = 89.6, 15.3 Hz, 2H), 2.05 – 1.96 (m, 2H), 1.72 (s, 1H), 0.90 (t, *J* = 7.4 Hz, 3H). ^{13}C NMR (101 MHz, $CDCl_3$-*d*) δ 169.5, 162.1, 157.8, 155.6, 151.9, 138.0, 137.6, 129.2, 128.7, 128.6, 127.7, 127.6, 124.5, 120.9, 120.6, 116.0, 100.3, 72.3, 46.9, 26.5, 9.4. LRMS(ESI$^+$) m/z calcd for $C_{27}H_{25}N_3O_5$ $[M+H]^+$ 472.18 Found; 472.15

(PP-1-62), *1-(3-(4-((2-methyl-1-(methylamino)-1-oxopropan-2-yl)oxy)phenyl) isoxazol-5-yl)propyl benzyl((3,5 dimethoxyphenyl)carbamoyl)carbamate*

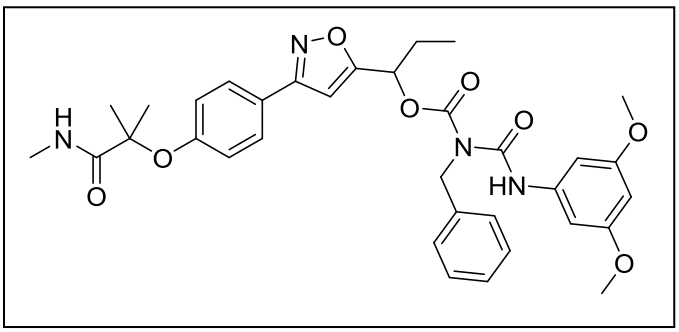

To a stirring solution of PP-1-61 (37 mg, 0.057 mmol) dissolved in 1,4-dioxane (1 mL) was added EDC-HCl (16.4 mg, 0.085 mmol) and HOBt (11.5 mg, 0.085 mmol). Afterwards, TEA (100 µL) was added and the reaction was left stirring for 22 hours. The reaction was then quenched with brine (1 mL), then the organic layer was separated and the aqueous layer was extracted three times with ethyl acetate.

The separated and combined organic layers were dried over anhydrous $MgSO_4$(s) and filtered through a celite-packed glass filter. The filtrate was concentrated under reduced pressure and purified with silica gel flash column chromatography (1:2 = EtOAC:n-hexanes + 1% acetic acid, v/v/v) to provide PP-1-62, (26 mg, 70%). R_f = 0.55 (1:1 = EtOAc:Hex + 1% acetic acid, v/v/v); ^{1}H NMR (400 MHz, $CDCl_3$-*d*) δ 10.75 (s, 1H), 7.61 (d, *J* = 8.9 Hz, 2H), 7.32 (d, *J* = 4.6 Hz, 4H), 7.31 – 7.23 (m, 1H), 6.95 (d, *J* = 8.8 Hz, 2H), 6.76 (d, *J* = 2.3 Hz, 3H), 6.23 (t, *J* = 2.3 Hz, 1H), 5.93 (s, 1H), 5.86 (t, *J* = 6.6 Hz, 1H), 5.10 (dd, *J* = 89.6, 15.3 Hz, 2H), 3.77 (s, 6H), 2.87 (d, *J* = 4.9 Hz, 3H), 2.04 – 1.95 (m, 2H), 1.54 (s, 6H), 0.88 (t, *J* = 7.4 Hz, 3H). ^{13}C NMR (75 MHz, $CDCl_3$-*d*) δ 175.4, 169.7, 161.7, 161.3, 156.1, 155.5, 151.5, 139.4, 138.0, 128.7, 128.1, 127.6, 123.5, 121.3, 100.3, 98.6, 97.0, 82.0, 72.8, 72.3, 55.5, 46.8, 26.5, 26.4, 25.21, 25.20, 9.3. LRMS(ESI$^+$) m/z calcd for $C_{34}H_{38}N_4O_8$ $[M+H]^+$ 631.27 Found; 631.22

(PP-1-69),*1-(3-(4-((2-methyl-1-(methylamino)-1-oxopropan-2-yl)oxy)phenyl) isoxazol-5-yl)propyl (benzo[d][1,3]dioxol-5-ylcarbamoyl)(benzyl)carbamate*

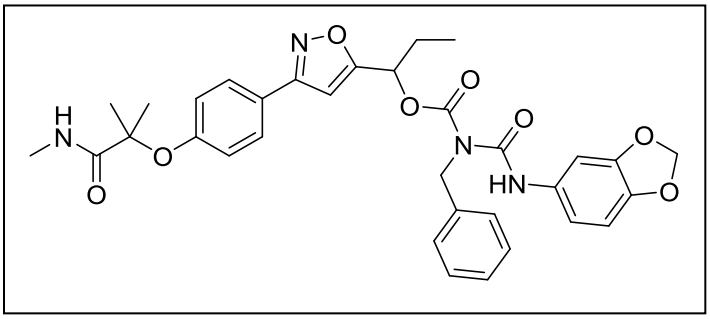

Synthesized according to the synthetic procedure of PP-1-62. Yield 54%, R_f = 0.48 (1:2 = EtOAc:Hex + 1% acetic acid, v/v/v); ^{1}H NMR (400 MHz, $CDCl_3$-*d*) δ 10.57 (s, 1H), 7.59 (d, *J* = 8.7 Hz, 2H), 7.33 – 7.23 (m, 5H), 7.17 (d, *J* = 2.1 Hz, 1H), 6.93 (d, *J* = 8.7 Hz, 2H), 6.81 – 6.68 (m, 4H), 5.93 – 5.88 (m, 2H), 5.83 (t, *J* = 6.6 Hz, 1H), 5.20 – 4.93 (m, 2H), 2.84 (d, *J* = 4.9 Hz, 3H), 2.00 – 1.94 (m, 2H), 1.51 (s, 6H), 0.88 – 0.81 (m, 3H). ^{13}C NMR (101 MHz, $CDCl_3$-*d*) δ 175.4, 169.8, 161.7, 156.1, 155.5, 151.9, 147.9, 144.4, 138.0, 131.8, 128.6, 128.1, 128.0, 127.6, 127.5, 123.5, 121.3, 119.5, 113.8, 108.1, 103.3, 101.3, 100.2, 82.0, 72.2, 46.9,

26.4, 26.4, 25.17, 20.9, 9.3. LRMS(ESI$^+$) m/z calcd for $C_{33}H_{34}N_4O_8$ $[M+H]^+$ 615.24 Found; 615.19

(9-p), *2-bromo-1-(4-hydroxyphenyl)ethan-1-one*

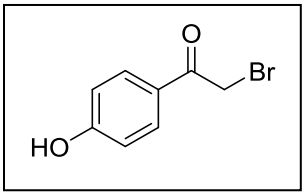

4-hydroxybenzophenone (1g, 7.27 mmol) was dissolved in EtOAc:DCM:MeOH (5:5:2, 100 mL) to which $CuBr_2$ (4.87 g, 21.81 mmol) was added. The reaction was left to stir at room temperature for 2 hours and was then quenched with water (40 mL). The organic layer was separated and the aqueous layer was extracted three times with DCM. The separated and combined organic layers were dried over anhydrous $MgSO_4$(s) and filtered through a celite-packed glass filter. The filtrate was concentrated under reduced pressure and purified with silica gel flash column chromatography (1:1 = EtOAC:n-hexanes, v/v) to provide 9-p, (1.54 g, 99%). R_f = 0.67 (1:1 = EtOAc:Hex, v/v); ^{1}H NMR (400 MHz, DMSO-d_6) δ 10.53 (s, 1H), 7.88 (d, *J* = 8.9 Hz, 2H), 6.87 (d, *J* = 8.9 Hz, 2H), 4.78 (s, 2H). ^{13}C NMR (101 MHz, DMSO-d_6) δ 189.87, 162.68, 131.47, 125.40, 115.43, 33.55. LRMS(ESI$^-$) m/z calcd for $C_8H_7BrO_2$ $[M+H]^-$ 212.96 Found; 212.83

(9-m), *2-bromo-1-(3-hydroxyphenyl)ethan-1-one*

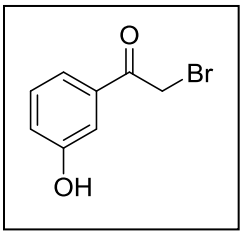

Synthesized according to the synthetic procedure of 9-p. Yield 91%, R_f = 0.80 (1:1 = EtOAc:Hex, v/v); ^{1}H NMR (500 MHz, DMSO-d_6) δ 9.89 (s, 1H), 7.48 – 7.42 (m, 1H), 7.38 – 7.30 (m, 2H), 7.08 – 7.05 (m, 1H), 4.88 (s, 2H). LRMS(ESI$^-$) m/z calcd for $C_8H_7BrO_2$ $[M+H]^-$ 212.96 Found; 212.84

(10-p), *3-(4-hydroxyphenyl)-3-oxopropanenitrile*

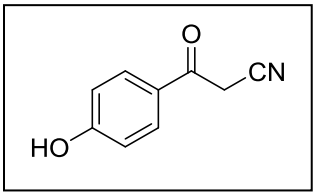

Compound 9 (1.4 g, 6.51 mmol) was dissolved in aqueous ethanol (EtOH:H_2O, 3:1, 100 mL). The solution was then cooled in an ice bath. To the stirring solution, NaCN (957.2 mg, 19.53 mmol) was carefully added in one portion. The solution was allowed to warm to room temperature and was then left stirring for 4 hours. The mixture was carefully acidified with 2M HCl (20 mL) and worked-up with DCM three times. The separated and combined organic layers were dried over anhydrous $MgSO_4$(s) and filtered through a celite-packed glass filter. The filtrate was concentrated under reduced pressure and purified with silica gel flash column chromatography (1:2 = EtOAC:n-hexanes, v/v) to provide 10-p, (0.84 g, 82%). R_f = 0.50 (1:1 = EtOAc:Hex, v/v); ^{1}H NMR (400 MHz, DMSO-d_6) δ 10.59 (s, 1H), 7.81 (d, *J* = 8.8 Hz, 2H), 6.88 (d, *J* = 8.8 Hz, 2H), 4.62 (s, 2H). LRMS(ESI$^-$) m/z calcd for $C_9H_7NO_2$ $[M+H]^-$ 160.05 Found; 159.96

(10-m), *3-(3-hydroxyphenyl)-3-oxopropanenitrile*

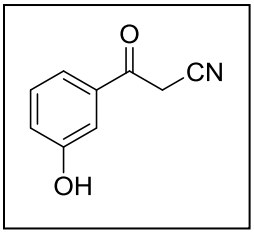

Synthesized according to the synthetic procedure of 10-p. Yield 88%, R_f = 0.50 (1:1 = EtOAc:Hex, v/v); ^{1}H NMR (400 MHz, DMSO-d_6) δ 9.93 (s, 1H), 7.39 – 7.36 (m, 2H), 7.29 – 7.28 (m, 1H), 7.10 – 7.07 (m, 1H), 4.70 (s, 2H). LRMS(ESI$^-$) m/z calcd for $C_9H_7NO_2$ $[M+H]^-$ 160.05 Found; 159.96

(11-p (3-amino)), *4-(3-aminoisoxazol-5-yl)phenol*

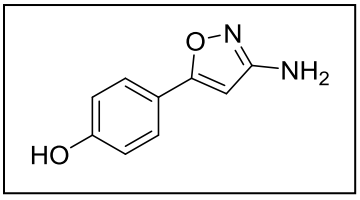

To a stirred solution of 10-p (500 mg, 3.103 mmol) dissolved in aqueous ethanol (EtOH:H_2O, 3:2, 30 mL) was added NaOH (until a pH of 8 was established, monitored by litmus paper). To this

mixture was then added NH_2OH-HCl (1.08 g, 15.5 mmol). The reaction was left to stir at room temperature for 24 hours and was then acidified with 2M HCl until a pH of 4 was established. The reaction was left to stir for 2 hours and was then quenched with brine (20 mL) and EA (50 mL). The organic layer was separated and the aqueous layer was extracted three times with EA. The separated and combined organic layers were dried over anhydrous $MgSO_4$(s) and filtered through a celite-packed glass filter. The filtrate was concentrated under reduced pressure and purified with silica gel flash column chromatography (1:1 = EtOAC:n-hexanes, v/v) to provide 11-p (3-amino), (508 mg, 93%). R_f = 0.46 (1:1 = EtOAc:Hex, v/v); ^{1}H NMR (400 MHz, DMSO-d_6) δ 9.71 (s, 1H), 7.49 (d, *J* = 8.6 Hz, 2H), 6.77 (d, *J* = 8.6 Hz, 2H), 6.61 (s, 2H), 5.23 (s, 1H). ^{13}C NMR (101 MHz, DMSO-d_6) δ 170.6, 162.3, 158.6, 127.7, 120.8, 115.5, 74.8. LRMS(ESI$^+$) m/z calcd for $C_9H_8N_2O_2$ $[M+H]^+$ 177.06 Found; 177.01

(11-p (5-amino)), *4-(5-aminoisoxazol-3-yl)phenol*

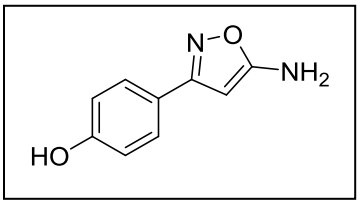

To a stirred solution of 10-p (500 mg, 3.103 mmol) dissolved in aqueous ethanol (EtOH:H_2O, 3:2, 30 mL) was added NaOH (until a pH of 12 was established, monitored by litmus paper). To this mixture was then added NH_2OH-HCl (1.08 g, 15.5 mmol). The reaction was left to stir at 85^{o}C for 24 hours and was then acidified with 2M HCl until a pH of 4 was established. The reaction was left to stir for 2 hours and was then quenched with brine (20 mL) and EA (50 mL). The organic layer was separated and the aqueous layer was extracted three times with EA. The separated and combined organic layers were dried over anhydrous $MgSO_4$(s) and filtered through a celite-packed glass filter. The filtrate was concentrated under reduced pressure and purified with silica gel flash column chromatography (1:1 = EtOAC:n-hexanes, v/v) to provide 11-p (5-amino), (208 mg, 38%). R_f = 0.36 (1:1 = EtOAc:Hex, v/v); ^{1}H NMR (400 MHz, DMSO-d_6) δ 9.95 (s, 1H), 7.56 (d, *J* = 8.8 Hz, 2H), 6.84 (d, *J* = 8.8 Hz, 2H),

6.08 (s, 1H), 5.56 (s, 2H). ^{13}C NMR (101 MHz, DMSO-d_6) δ 167.6, 164.5, 158.9, 127.0, 118.9, 115.7, 90.6. LRMS(ESI$^+$) m/z calcd for $C_9H_8N_2O_2$ $[M+H]^+$ 177.06 Found; 177.04

(11-m), *3-(3-aminoisoxazol-5-yl)phenol*

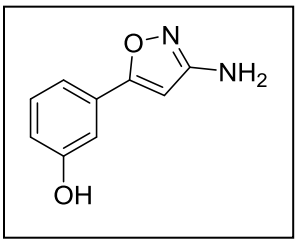

Synthesized according to the synthetic procedure of 11-p (3-amino). Yield 95%, R_f = 0.66 (2:1 = EtOAc:Hex, v/v); ^{1}H NMR (500 MHz, DMSO-d_6) δ 9.61 (s, 1H), 7.23 (t, J = 7.9 Hz, 1H), 7.14 (s, 2H), 6.83 (d, J = 9.3 Hz, 1H), 6.74 (s, 2H), 5.33 (s, 1H). ^{13}C NMR (101 MHz, DMSO-d_6) δ 171.0, 162.7, 157.6, 131.2, 130.0, 117.3, 116.7, 112.80, 75.3. LRMS(ESI$^+$) m/z calcd for $C_9H_8N_2O_2$ $[M+H]^+$ 177.06 Found; 177.04

(12-p), *5-(4-((tert-butyldimethylsilyl)oxy)phenyl)isoxazol-3-amine*

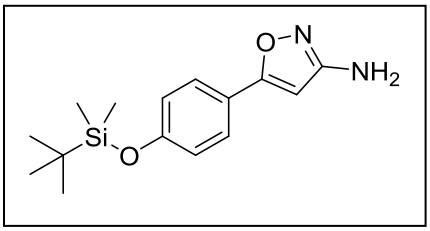

Synthesized according to the synthetic procedure of 6. Yield 78%, R_f = 0.74 (1:1 = EtOAc:Hex, v/v); ^{1}H NMR (500 MHz, $CDCl_3$-d) δ 7.59 (d, J = 8.6 Hz, 2H), 6.87 (d, J = 8.6 Hz, 2H), 5.35 (s, 1H), 4.66 (s, 2H), 0.98 (s, 9H), 0.21 (s, 6H).

(12-m), *-(3-((tert-butyldimethylsilyl)oxy)phenyl)isoxazol-3-amine*

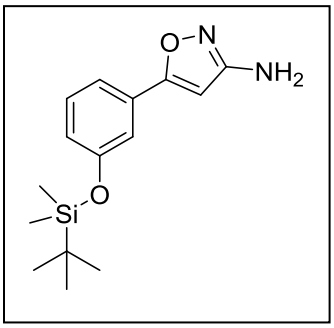

Synthesized according to the synthetic procedure of 6. Yield 87%, R_f = 0.80 (1:1 = EtOAc:Hex, v/v); ^{1}H NMR (500 MHz, $CDCl_3$-*d*) δ 7.27 (dd, *J* = 7.1, 2.2 Hz, 2H), 7.23 (t, *J* = 2.0 Hz, 1H), 6.92 – 6.85 (m, 1H), 5.38 (s, 1H), 4.70 (s, 2H), 0.99 (s, 9H), 0.21 (s, 6H).

(13-p {B}), *N-(5-(4-((tert-butyldimethylsilyl)oxy)phenyl)isoxazol-3-yl)benzamide*

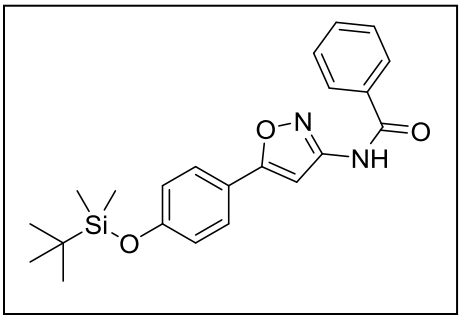

To an ice-bath cooled solution of 12-p (50 mg, 0.17 mmol) dissolved in DCM (2 mL) containing pyridine (24.6 µL, 0.30 mmol) was added benzoyl chloride (30.3 µL, 0.26 mmol). The reaction was stirred for 2 hours as the reaction vessel warmed to room temperature. The reaction was then diluted with DCM (10 mL) and quenched with aqueous $NaHCO_3$ (30 mL). The organic layer was separated and the aqueous layer was extracted three times with DCM. The separated and combined organic layers were dried over anhydrous $MgSO_4$(s) and filtered through a celite-packed glass filter. The filtrate was concentrated under reduced pressure and purified with silica gel flash column chromatography (2:5 = EtOAC:n-hexanes, v/v) to provide 13-p, (66 mg, 97%). R_f = 0.71 (1:2 = EtOAc:Hex, v/v); ^{1}H NMR (500 MHz, DMSO-d_6) δ 12.08 (s, 1H), 8.05 (d, *J* = 7.1 Hz, 2H), 7.79 (d, *J* = 8.6 Hz, 2H), 7.65 (t, *J* = 7.3 Hz, 1H), 7.56 (t, *J* = 7.7 Hz, 2H), 6.97 (d, *J* = 8.6 Hz, 2H), 6.88 (s, 1H), 0.96 (s, 9H), 0.22 (s, 6H).

(13-m {B}), *N-(5-(3-((tert-butyldimethylsilyl)oxy)phenyl)isoxazol-3-yl)benzamide*

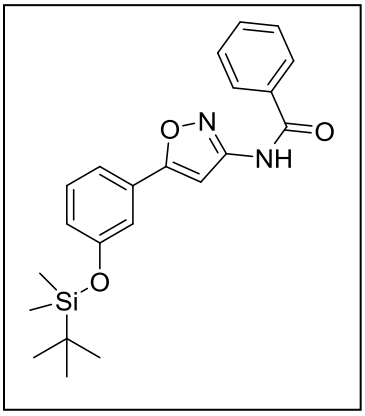

Synthesized according to the synthetic procedure of 13-p {B}. Yield 97%, R_f = 0.71 (1:1 = EtOAc:Hex, v/v); ^{1}H NMR (400 MHz, DMSO-d_6) δ 12.13 (s, 1H), 8.08 – 8.02 (m, 2H), 7.65 (ddt, *J* = 8.1, 6.7, 1.3 Hz, 1H), 7.56 (t, *J* = 7.4 Hz, 2H), 7.49 (ddd, *J* = 7.7, 1.6, 1.0 Hz, 1H), 7.40 (t, *J* = 7.8 Hz, 1H), 7.36 – 7.31 (m, 1H), 6.99 (ddd, *J* = 8.1, 2.5, 1.0 Hz, 1H), 6.93 (s, 1H), 0.97 (s, 9H), 0.22 (s, 6H).

(13-p {E}), *N-(5-(4-((tert-butyldimethylsilyl)oxy)phenyl)isoxazol-3-yl)acetamide*

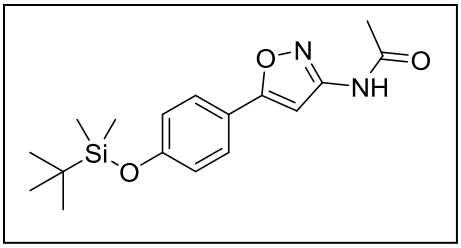

Synthesized according to the synthetic procedure of 13-p {B}. Yield 96%, R_f = 0.63 (1:1 = EtOAc:Hex, v/v); ^{1}H NMR (400 MHz, $CDCl_3$-*d*) δ 8.08 (s, 1H), 7.72 – 7.64 (m, 2H), 6.94 – 6.86 (m, 2H), 6.65 (s, 1H), 2.26 (s, 3H), 0.99 (s, 9H), 0.22 (s, 6H). LRMS(ESI$^+$) m/z calcd for $C_{17}H_{24}N_2O_3Si$ $[M+H]^+$ 333.16 Found; 333.03

(13-m {E}), *N-(5-(3-((tert-butyldimethylsilyl)oxy)phenyl)isoxazol-3-yl)acetamide*

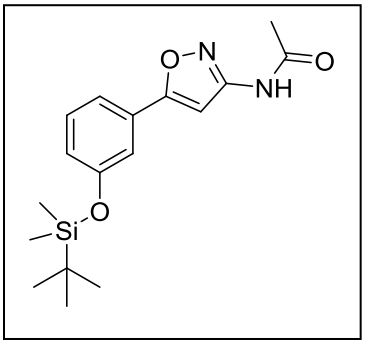

Synthesized according to the synthetic procedure of 13-p {B}. Yield 93%, R_f = 0.63 (1:1 = EtOAc:Hex, v/v); ^{1}H NMR (400 MHz, $CDCl_3$-*d*) δ 8.09 (s, 1H), 7.43 – 7.20 (m, 5H), 6.91 (d, *J* = 7.9 Hz, 1H), 6.66 (s, 1H), 2.26 (s, 3H), 0.99 (s, 9H), 0.21 (s, 6H). LRMS(ESI$^+$) m/z calcd for $C_{17}H_{24}N_2O_3Si$ $[M+H]^+$ 333.16 Found; 333.03

(14-p {B}), *N-benzyl-5-(4-((tert-butyldimethylsilyl)oxy)phenyl)isoxazol-3-amine*

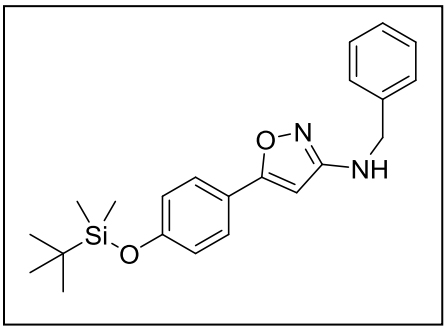

Under nitrogen atmosphere, compound 13-p {B} (1 g, 2.54 mmol) was dissolved in dry DCM (30 mL) and cooled in an ice bath. Trimethylsilyl chloride (394 µL, 3.04 mmol) was then added to the mixture, dropwise over a 10 minute period. After 1 hour, 1M $LiAlH_4$ in THF is then added dropwise over a 10 minute period to the cooled solution. After complete addition, the mixture is left to stir at 0^oC for 2 hours. After reaction completion (TLC), the reaction was quenched with slow dropwise addition of 2M NaOH (20 mL). The organic layer was then separated and the aqueous layer was extracted three times with DCM. The separated and combined organic layers were dried over anhydrous $MgSO_4$(s) and filtered through a celite-packed glass filter. The filtrate was concentrated under reduced pressure and purified with silica gel flash column chromatography (1:5 = EtOAC:n-hexanes, v/v) to provide 14-p {B}, (914 mg, 95%). R_f = 0.70 (1:2 = EtOAc:Hex, v/v); ^{1}H NMR (400 MHz, DMSO-d_6) δ 7.86 (t, *J* = 6.3 Hz, 1H), 7.61 (d, *J* = 8.8 Hz, 2H), 7.41 – 7.30 (m, 4H), 7.26 (d, *J* = 7.1 Hz, 1H), 6.90 (d, *J* = 8.7 Hz, 2H), 5.47 (s, 1H), 4.33 (d, *J* = 6.3 Hz, 2H), 0.94 (s, 9H), 0.19 (s, 6H). LRMS(ESI^+) m/z calcd for $C_{22}H_{28}N_2O_2Si$ $[M+H]^+$ 381.19 Found; 381.01

(14-m {B}), *N-benzyl-5-(3-((tert-butyldimethylsilyl)oxy)phenyl)isoxazol-3-amine*

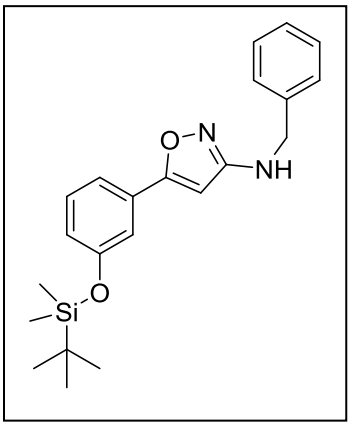

Synthesized according to the synthetic procedure of 14-p {B}. Yield 95%, R_f = 0.70 (1:2 = EtOAc:Hex, v/v); ^{1}H NMR (400 MHz, DMSO-d_6) δ 7.91 (t, *J* = 6.3 Hz, 1H), 7.42 – 7.22 (m, 7H), 7.18 – 7.16 (m, 1H), 6.91 (dt, *J* = 6.3, 2.6 Hz, 1H), 5.55 (s, 1H), 4.35 (d, *J* = 6.2 Hz, 2H), 0.95 (s, 9H), 0.19 (s, 6H). LRMS(ESI$^+$) m/z calcd for $C_{22}H_{28}N_2O_2Si$ $[M+H]^+$ 381.19 Found; 381.01

(14-p {E}), *5-(4-((tert-butyldimethylsilyl)oxy)phenyl)-N-ethylisoxazol-3-amine*

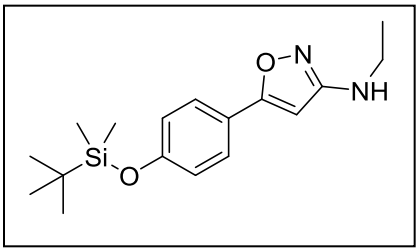

Synthesized according to the synthetic procedure of 14-p {B}. Yield 77%, R_f = 0.69 (1:2 = EtOAc:Hex, v/v); ^{1}H NMR (500 MHz, $CDCl_3$-*d*) δ 7.62 (d, *J* = 8.1 Hz, 2H), 6.87 (d, *J* = 8.8 Hz, 2H), 5.22 (s, 1H), 4.55 (s, 1H), 3.33 – 3.18 (m, 2H), 1.26 (t, *J* = 7.2 Hz, 3H), 0.99 (s, 9H), 0.21 (s, 6H). LRMS(ESI$^+$) m/z calcd for $C_{17}H_{26}N_2O_2Si$ $[M+H]^+$ 319.19 Found; 319.04

(14-m {E}), *5-(3-((tert-butyldimethylsilyl)oxy)phenyl)-N-ethylisoxazol-3-amine*

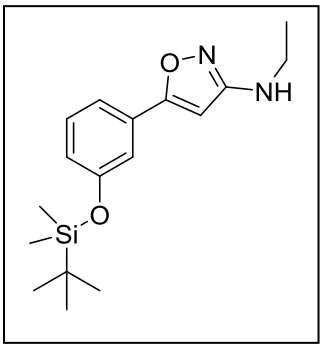

Synthesized according to the synthetic procedure of 14-p {B}. Yield 68%, R_f = 0.71 (1:2 = EtOAc:Hex, v/v); ^{1}H NMR (500 MHz, $CDCl_3$-*d*) δ 7.36 – 7.25 (m, 3H), 6.90 (ddd, *J* = 8.0, 2.5, 1.2 Hz, 1H), 5.26 (s, 1H), 4.59 (s, 1H), 3.28 (qd, *J* = 7.2, 5.8 Hz, 2H), 1.29 (t, *J* = 7.2 Hz, 3H), 1.01 (s, 9H), 0.23 (s, 6H). LRMS(ESI$^+$) m/z calcd for $C_{17}H_{26}N_2O_2Si$ $[M+H]^+$ 319.19 Found; 319.05

(15-p {B}), *1,3-dibenzyl-1-(5-(4-((tert-butyldimethylsilyl)oxy)phenyl)isoxazol-3-yl)urea*

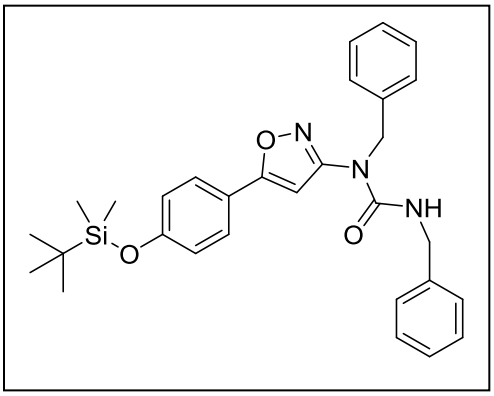

Synthesized according to the synthetic procedure of PP-1-45. Yield 52%, R_f = 0.65 (1:2 = EtOAc:Hex, v/v); ^{1}H NMR (400 MHz, DMSO-d_6) δ 7.92 (t, *J* = 5.8 Hz, 1H), 7.70 (d, *J* = 8.7 Hz, 2H), 7.38 – 7.18 (m, 10H), 6.95 (d, *J* = 8.6 Hz, 2H), 6.62 (s, 1H), 5.03 (s, 2H), 4.34 (d, *J* = 5.7 Hz, 2H), 0.95 (s, 9H), 0.21 (s, 6H). LRMS(ESI$^+$) m/z calcd for $C_{30}H_{35}N_3O_3Si$ $[M+H]^+$ 514.24 Found; 514.04

(15-m {B}), *1,3-dibenzyl-1-(5-(3-((tert-butyldimethylsilyl)oxy)phenyl)isoxazol-3-yl)urea*

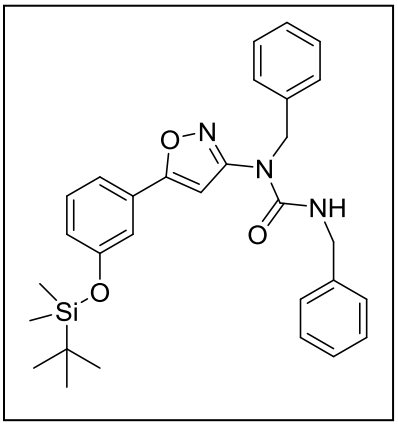

Synthesized according to the synthetic procedure of PP-1-45. Yield 58%, R_f = 0.68 (1:80 = Methanol:DCM, v/v); ^{1}H NMR (400 MHz, $CDCl_3$-*d*) δ 7.37 – 7.22 (m, 12H), 7.21 – 7.17 (m, 1H), 6.93 – 6.86 (m, 1H), 6.27 (t, *J* = 5.6 Hz, 1H), 5.96 (s, 1H), 5.06 (s, 2H), 4.52 (d, *J* = 5.6 Hz, 2H), 0.97 (s, 9H), 0.19 (s, 6H). LRMS(ESI$^+$) m/z calcd for $C_{30}H_{35}N_3O_3Si$ $[M+H]^+$ 514.24 Found; 514.02

(15-p {E}), *3-benzyl-1-(5-(4-((tert-butyldimethylsilyl)oxy)phenyl)isoxazol-3-yl)-1-ethylurea*

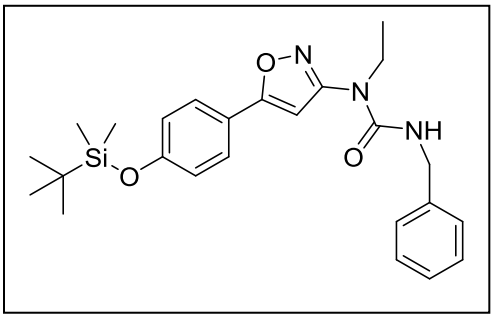

Synthesized according to the synthetic procedure of PP-1-45. Yield 68%, R_f = 0.60 (1:2 =EtOAc:Hex, v/v); ^{1}H NMR (500 MHz, $CDCl_3$-*d*) δ 7.65 (d, *J* = 8.6 Hz, 2H), 7.39 – 7.32 (m, 3H), 7.31 – 7.26 (m, 1H), 6.92 (d, *J* = 8.7 Hz, 2H), 6.35 (t, *J* = 5.6 Hz, 1H), 6.00 (s, 1H), 4.53 (d, *J* = 5.6 Hz, 2H), 3.90 (d, *J* = 7.1 Hz, 2H), 1.31 (t, *J* = 7.1 Hz, 3H), 1.01 (s, 9H), 0.24 (s, 6H). LRMS(ESI$^+$) m/z calcd for $C_{25}H_{33}N_3O_3Si$ $[M+H]^+$ 452.23 Found; 452.17

(15-m {E}), *3-benzyl-1-(5-(3-((tert-butyldimethylsilyl)oxy)phenyl)isoxazol-3-yl)-1-ethylurea*

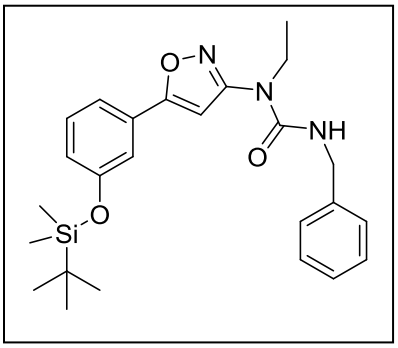

Synthesized according to the synthetic procedure of PP-1-45. Yield 56%, R_f = 0.60 (1:2 =EtOAc:Hex, v/v); ^{1}H NMR (500 MHz, $CDCl_3$-*d*) δ 7.41 – 7.24 (m, 7H), 6.95 (dt, *J* = 7.0, 2.2 Hz, 1H), 6.33 (t, *J* = 5.5 Hz, 1H), 6.04 (s, 1H), 4.54 (d, *J* = 5.5 Hz, 2H), 3.92 (q, *J* = 7.1 Hz, 2H), 1.33 (t, *J* = 7.1 Hz, 3H), 1.02 (s, 9H), 0.24 (s, 6H). LRMS(ESI$^+$) m/z calcd for $C_{25}H_{33}N_3O_3Si$ $[M+H]^+$ 452.23 Found; 452.17

(16-p {B}), *1,3-dibenzyl-1-(5-(4-hydroxyphenyl)isoxazol-3-yl)urea*

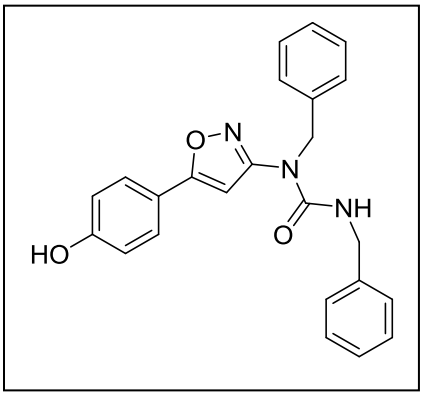

Synthesized according to the synthetic procedure of PP-1-44. Yield 90%, R_f = 0.21 (1:2 =EtOAc:Hex, v/v); ^{1}H NMR (400 MHz, DMSO-d_6) δ 9.91 (s, 1H), 7.90 (t, *J* = 5.8 Hz, 1H), 7.62 (d, *J* = 8.8 Hz, 2H), 7.42 – 7.11 (m, 10H), 6.85 (d, *J* = 8.8 Hz, 2H), 6.57 (s, 1H), 5.03 (s, 2H), 4.35 (d, *J* = 5.8 Hz, 2H). ^{13}C NMR (101 MHz, DMSO-d_6) δ 164.5, 162.6, 159.2, 153.8, 139.8, 137.5, 128.5, 128.2, 127.9, 127.2, 127.0, 126.8, 126.7, 119.6, 115.7, 88.9, 49.3, 43.9. LRMS(ESI$^+$) m/z calcd for $C_{24}H_{21}N_3O_3$ $[M+H]^+$ 400.16 Found; 400.05

(16-m {B}), *1,3-dibenzyl-1-(5-(3-hydroxyphenyl)isoxazol-3-yl)urea*

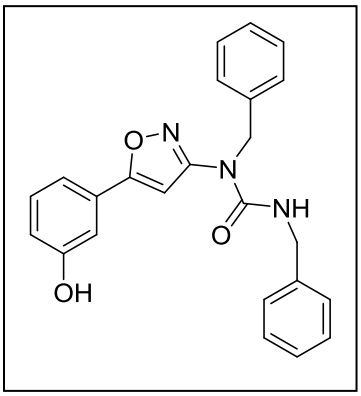

Synthesized according to the synthetic procedure of PP-1-44. Yield 81%, R_f = 0.21 (1:2 =EtOAc:Hex, v/v); ^{1}H NMR (400 MHz, DMSO-d_6) δ 9.71 (s, 1H), 7.94 (t, *J* = 5.8 Hz, 1H), 7.42 – 7.11 (m, 13H), 6.92 – 6.82 (m, 1H), 6.61 (s, 1H), 5.05 (s, 2H), 4.35 (d, *J* = 5.7 Hz, 2H). ^{13}C NMR (101 MHz, DMSO-d_6) δ 164.8, 162.8, 157.7, 153.7, 139.8, 137.4, 130.2, 130.0, 128.5, 128.2, 127.3, 127.0, 126.8, 126.7, 117.3, 117.3, 112.70, 89.2, 49.3, 43.9 LRMS(ESI$^+$) m/z calcd for $C_{24}H_{21}N_3O_3$ $[M+H]^+$ 400.16 Found; 400.05

(16-p {E}), *3-benzyl-1-ethyl-1-(5-(4-hydroxyphenyl)isoxazol-3-yl)urea*

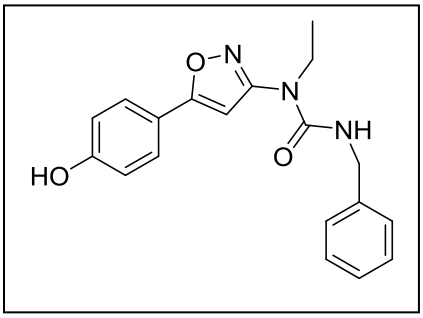

Synthesized according to the synthetic procedure of PP-1-44. Yield 71%, R_f = 0.25 (1:40 =Methanol:DCM, v/v); ^{1}H NMR (400 MHz, $CDCl_3$-*d*) δ 8.61 (s, 1H), 7.76 (t, *J* = 7.7 Hz, 1H), 7.58 (d, *J* = 8.6 Hz, 2H), 7.42 – 7.19 (m, 5H), 6.90 (d, *J* = 8.7 Hz, 2H), 6.34 – 6.30 (m, 1H), 5.98 (s, 1H), 4.50 (d, *J* = 5.5 Hz, 1H), 3.87 (q, *J* = 7.1 Hz, 2H), 1.28 (t, *J* = 7.1 Hz, 3H). ^{13}C NMR (101 MHz, $CDCl_3$-*d*) δ 164.8, 163.5, 158.8, 153.6, 148.9, 138.2, 137.2, 128.9, 128.4, 127.7, 116.2, 87.3, 45.2, 43.3, 13.6. LRMS(ESI$^+$) m/z calcd for $C_{19}H_{19}N_3O_3$ $[M+H]^+$ 338.14 Found; 338.02

(16-m {E}), *3-benzyl-1-ethyl-1-(5-(3-hydroxyphenyl)isoxazol-3-yl)urea*

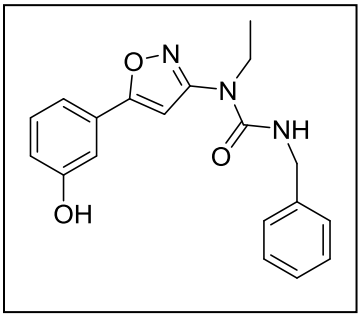

Synthesized according to the synthetic procedure of PP-1-44. Yield 74%, R_f = 0.25 (1:40 =Methanol:DCM, v/v); ^{1}H NMR (400 MHz, $CDCl_3$-*d*) δ 7.32 – 7.22 (m, 8H), 6.92 (d, *J* = 7.6 Hz, 1H), 6.27 (d, *J* = 5.0 Hz, 1H), 6.01 (d, *J* = 3.6 Hz, 1H), 4.50 (t, *J* = 4.5 Hz, 1H), 3.93 – 3.78 (m, 2H), 1.26 (t, *J* = 5.9 Hz, 3H). ^{13}C NMR (101 MHz, $CDCl_3$-*d*) δ 165.0, 163.7, 156.8, 153.5, 138.2, 130.4, 129.9, 128.9, 127.8, 127.7, 118.9, 117.8, 113.6, 87.7, 45.3, 43.3, 13.7. LRMS(ESI$^+$) m/z calcd for $C_{19}H_{19}N_3O_3$ $[M+H]^+$ 338.14 Found; 338.02

(17-p {B}), *1,3-dibenzyl-1-(5-(4-methoxyphenyl)isoxazol-3-yl)urea*

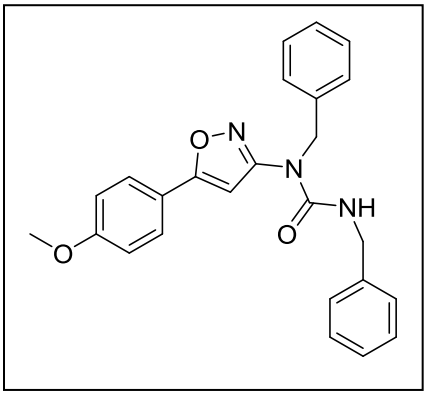

Compound 16-p {B} (25 mg, 0.06 mmol), methyl iodide (30.2 µL, 0.476 mmol), and potassium carbonate (41.5 mg, 0.3 mmol) were dissolved in acetone (3 mL) and refluxed overnight. The reaction mixture was filtered to remove the potassium salt, and the filtrate was evaporated under reduced pressure to dryness. The crude product was purified by prep TLC (1:3 = EtOAc:Hex, v/v); to provide 17-p {B}, (18.7 mg, 77%). R_f = 0.43 (1:2 = EtOAc:Hex, v/v); ^{1}H NMR (400 MHz, $CDCl_3$-*d*) δ 7.61 (d, *J* = 7.5 Hz, 2H), 7.43 – 7.20 (m, 10H), 6.91 (d, *J* = 7.5 Hz, 2H), 6.33 (t, *J* = 5.7 Hz, 1H), 5.92 (s, 1H), 5.04 (s, 2H), 4.52 (d, *J* = 5.5 Hz, 2H), 3.81 (s, 3H). ^{13}C NMR (101 MHz, $CDCl_3$-*d*) δ 164.9, 163.3, 161.3, 153.7, 138.3, 136.6, 129.0, 128.9, 128.8, 128.2, 127.9, 127.7, 127.2, 121.2, 114.4, 87.7, 55.5, 51.0, 45.3. LRMS(ESI$^+$) m/z calcd for $C_{25}H_{23}N_3O_3$ $[M+H]^+$ 414.17 Found; 414.15

(17-m {B}), *1,3-dibenzyl-1-(5-(3-methoxyphenyl)isoxazol-3-yl)urea*

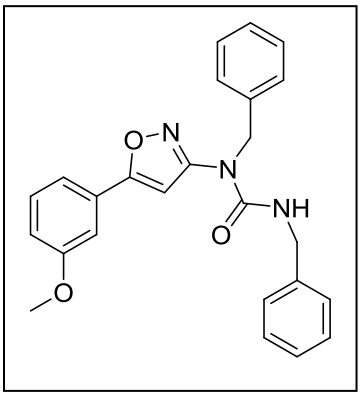

Synthesized according to the synthetic procedure of 17-p {B}. Yield 71%, R_f = 0.49 (1:2 =EtOAc:Hex, v/v); ^{1}H NMR (400 MHz, $CDCl_3$-*d*) δ 7.42 – 7.16 (m, 12H), 6.96 (ddd, *J* = 8.3, 2.6, 1.1 Hz, 1H), 6.28 (t, *J* = 5.5 Hz, 1H), 5.98 (s, 1H), 5.05 (s, 2H), 4.52 (d, *J* = 5.5 Hz, 2H), 3.81 (s, 3H). ^{13}C NMR (101 MHz, $CDCl_3$-*d*) δ 165.1, 163.7, 160.0, 153.7, 138.2, 136.5, 130.1, 130.0, 129.0, 128.9, 127.9, 127.7, 127.7, 127.2, 119.3, 116.5, 111.6, 88.0, 55.5, 51.0, 45.3. LRMS(ESI$^+$) m/z calcd for $C_{25}H_{23}N_3O_3$ $[M+H]^+$ 414.17 Found; 414.15

(17-p {E}), *3-benzyl-1-ethyl-1-(5-(4-methoxyphenyl)isoxazol-3-yl)urea*

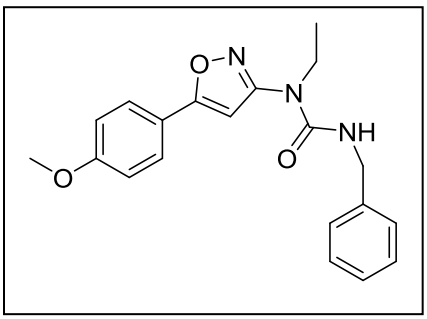

Synthesized according to the synthetic procedure of 17-p {B}. Yield 68%, R_f = 0.43 (1:2 =EtOAc:Hex, v/v); ^{1}H NMR (400 MHz, $CDCl_3$-*d*) δ 7.68 (d, *J* = 8.2 Hz, 2H), 7.41 – 7.17 (m, 5H), 6.95 (d, *J* = 8.1 Hz, 2H), 6.27 (t, *J* = 5.9 Hz, 1H), 5.96 (s, 1H), 4.50 (d, *J* = 5.5 Hz, 2H), 3.88 (q, *J* = 7.0 Hz, 2H), 3.84 (s, 3H), 1.29 (t, *J* = 7.1 Hz, 3H). ^{13}C NMR (101 MHz, $CDCl_3$-*d*) δ 165.1, 163.3, 161.4, 153.3, 138.5, 128.9, 128.2, 127.8, 127.7, 121.3, 114.5, 86.8, 55.5, 45.2, 43.2, 13.6. LRMS(ESI$^+$) m/z calcd for $C_{20}H_{21}N_3O_3$ $[M+H]^+$ 352.16 Found; 352.11

(17-m {E}), *3-benzyl-1-ethyl-1-(5-(3-methoxyphenyl)isoxazol-3-yl)urea*

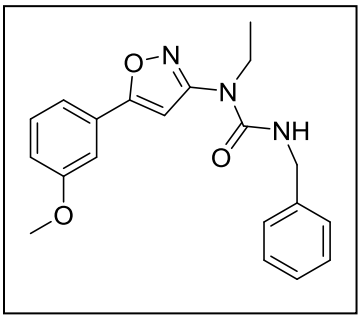

Synthesized according to the synthetic procedure of 17-p {B}. Yield 70%, R_f = 0.41 (1:2 =EtOAc:Hex, v/v); ^{1}H NMR (400 MHz, $CDCl_3$-*d*) δ 7.45 – 7.19 (m, 8H), 6.98 (dd, *J* = 8.8, 1.7 Hz, 1H), 6.25 (s, 1H), 6.02 (s, 1H), 4.51 (d, *J* = 5.6 Hz, 2H), 3.89 (q, *J* = 7.1 Hz, 2H), 3.84 (s, 3H), 1.29 (t, *J* = 7.1 Hz, 3H). ^{13}C NMR (101 MHz, $CDCl_3$-*d*) δ 165.3, 163.7, 160.1, 153.2, 138.4, 130.1, 128.9, 127.8, 127.7, 119.3, 116.6, 111.7, 87.1, 55.5, 45.2, 43.2, 13.7. LRMS(ESI$^+$) m/z calcd for $C_{20}H_{21}N_3O_3$ $[M+H]^+$ 352.16 Found; 352.11

(18-p {B}), *tert-butyl*
2-(4-(3-(1,3-dibenzylureido)isoxazol-5-yl)phenoxy)-2-methylpropanoate

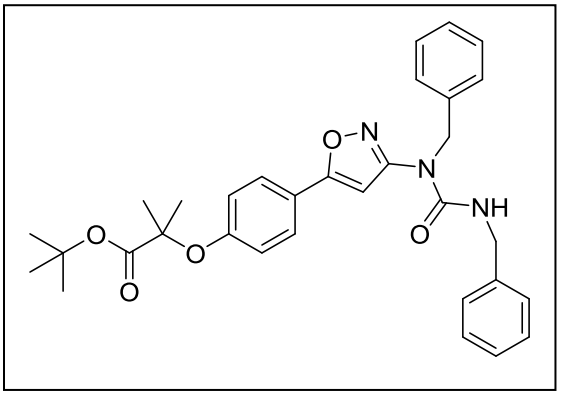

Synthesized according to the synthetic procedure of 1. Yield 19%, R_f = 0.53 (1:2 =EtOAc:Hex, v/v); ^{1}H NMR (400 MHz, $CDCl_3$-*d*) δ 7.56 (d, *J* = 7.3 Hz, 2H), 7.39 – 7.20 (m, 10H), 6.85 (d, *J* = 7.3 Hz, 2H), 6.30 (t, *J* = 5.8 Hz, 1H), 5.91 (d, *J* = 1.3 Hz, 1H), 5.04 (s, 2H), 4.52 (d, *J* = 5.5 Hz, 2H), 1.58 (s, 6H), 1.40 (s, 9H). ^{13}C NMR (101 MHz, $CDCl_3$-*d*) δ 173.1, 164.9, 163.3, 157.7, 153.7, 138.3, 136.6, 128.97, 128.95, 128.9, 127.9, 127.74, 127.68, 127.2, 121.8, 118.5, 87.7, 82.1, 79.7, 51.1, 45.3, 27.9, 25.5. LRMS(ESI$^+$) m/z calcd for $C_{32}H_{35}N_3O_5$ $[M+H]^+$ 542.26 Found; 542.33

(18-m {B}), *tert-butyl*

2-(3-(3-(1,3-dibenzylureido)isoxazol-5-yl)phenoxy)-2-methylpropanoate

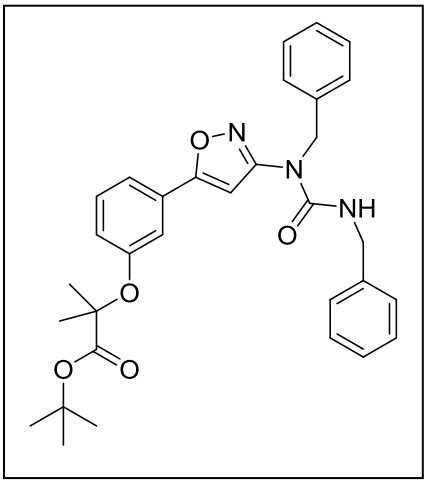

Synthesized according to the synthetic procedure of 1. Yield 19%, R_f = 0.53 (1:2 =EtOAc:Hex, v/v); ^{1}H NMR (400 MHz, $CDCl_3$-*d*) δ 7.37 – 7.22 (m, 12H), 7.18 (d, *J* = 1.5 Hz, 1H), 6.89 (ddd, *J* = 7.4, 1.7, 0.9 Hz, 1H), 6.31 (t, *J* = 5.7 Hz, 1H), 5.90 (d, *J* = 1.4 Hz, 1H), 5.04 (s, 2H), 4.53 (d, *J* = 5.0 Hz, 2H), 1.56 (s, 6H), 1.40 (s, 9H). ^{13}C NMR (101 MHz, $CDCl_3$-*d*) δ 173.1, 165.12, 163.5, 156.2, 153.7, 138.3, 136.6, 129.7, 129.7, 129.0, 128.9, 127.9, 127.7, 127.2, 120.4, 120.1, 117.2, 87.9,0 82.1, 79.8, 51.1, 45.3, 27.9, 25.5. LRMS(ESI$^+$) m/z calcd for $C_{32}H_{35}N_3O_5$ $[M+H]^+$ 542.26 Found; 542.33

(18-p {E}), *tert-butyl*

2-(4-(3-(3-benzyl-1-ethylureido)isoxazol-5-yl)phenoxy)-2-methylpropanoate

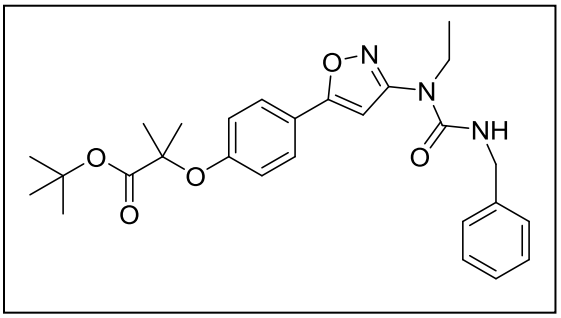

Synthesized according to the synthetic procedure of 1. Yield 33%, R_f = 0.50 (1:2 =EtOAc:Hex, v/v); ^{1}H NMR (400 MHz, $CDCl_3$-*d*) δ 7.61 (d, *J* = 8.8 Hz, 2H), 7.42 – 7.18 (m, 5H), 6.88 (d, *J* = 8.9 Hz, 2H), 6.29 (t, *J* = 5.5 Hz, 1H), 5.96 (s, 1H), 4.50 (d, *J* = 5.5 Hz, 2H), 3.87 (q, *J* = 7.1 Hz, 2H), 1.59 (s, 6H), 1.41 (s, 9H), 1.28 (t, *J* = 7.1 Hz, 3H). ^{13}C NMR (101 MHz, $CDCl_3$-*d*) δ 173.1, 165.1, 163.3, 157.7, 153.3, 138.5, 128.9, 127.8, 127.7, 127.7, 121.9, 118.5, 86.9, 82.1, 79.7, 45.2,

43.2, 27.9, 25.5, 13.6. LRMS(ESI$^+$) m/z calcd for $C_{27}H_{33}N_3O_5$ $[M+H]^+$ 480.24 Found; 480.14

(18-m {E}), *tert-butyl 2-(3-(3-(3-benzyl-1-ethylureido)isoxazol-5-yl)phenoxy)-2-methylpropanoate*

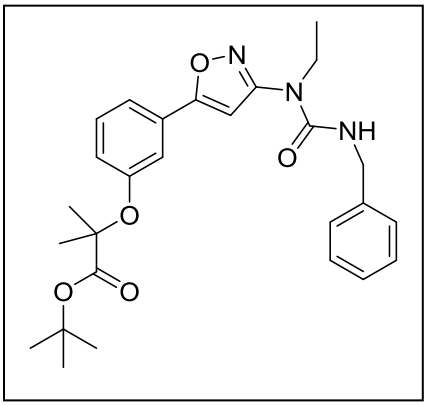

Synthesized according to the synthetic procedure of 1. Yield 29%, R_f = 0.44 (1:2 =EtOAc:Hex, v/v); ^{1}H NMR (400 MHz, $CDCl_3$-*d*) δ 7.41 – 7.18 (m, 8H), 6.96 – 6.87 (m, 1H), 6.28 (d, *J* = 6.0 Hz, 1H), 5.95 (s, 1H), 4.50 (d, *J* = 5.7 Hz, 2H), 3.87 (q, *J* = 7.2 Hz, 2H), 1.58 (s, 6H), 1.42 (s, 9H), 1.28 (t, *J* = 7.1 Hz, 3H). ^{13}C NMR (101 MHz, $CDCl_3$-*d*) δ 173.2, 165.2, 163.5, 156.3, 153.2, 138.4, 129.8, 129.7, 128.9, 127.8, 127.7, 120.5, 120.05, 117.2, 87.0, 82.1, 79.8, 45.2, 43.3, 27.9, 25.5, 13.6. LRMS(ESI$^+$) m/z calcd for $C_{27}H_{33}N_3O_5$ $[M+H]^+$ 480.24 Found; 480.14

(19-p {B}), *2-(4-(3-(1,3-dibenzylureido)isoxazol-5-yl)phenoxy)-2-methylpropanoic acid*

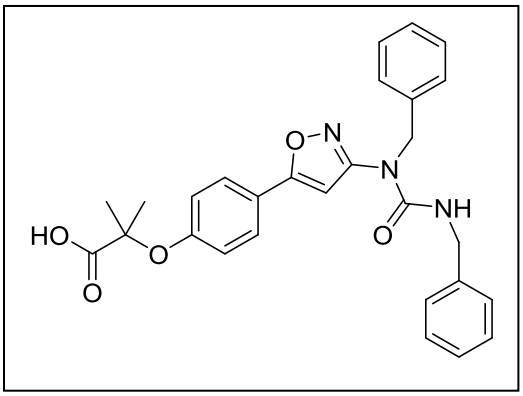

Synthesized according to the synthetic procedure of 5. Yield 89%, R_f = 0.32 (1:2 =EtOAc:Hex + 1% acetic acid, v/v/v); ^{1}H NMR (400 MHz, DMSO-d_6) δ 7.94 (t, *J* = 5.9 Hz, 1H), 7.67 (d, *J* = 8.1 Hz, 2H), 7.40 – 7.15 (m, 10H), 6.88 (d, *J* = 8.3 Hz, 2H), 6.60 (s, 1H), 5.03 (s, 2H), 4.34 (d, *J* = 5.9 Hz, 1H), 1.51 (s, 6H). ^{13}C NMR (101 MHz, DMSO-d_6) δ 168.2, 164.7, 162.4, 157.9, 157.3,

153.7, 139.8, 137.4, 128.5, 128.2, 127.5, 127.3, 127.0, 126.8, 126.7, 121.4, 118.2, 88.9, 49.3, 43.9, 25.3. LRMS(ESI$^+$) m/z calcd for $C_{27}H_{33}N_3O_5$ $[M+H]^+$ 486.20 Found; 486.08

(19-m {B}), *2-(3-(3-(1,3-dibenzylureido)isoxazol-5-yl)phenoxy)-2-methylpropanoic acid*

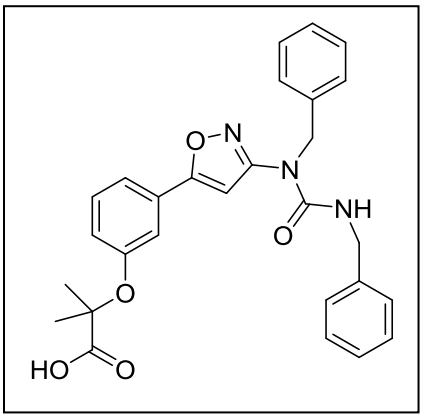

Synthesized according to the synthetic procedure of 5. Yield 82%, R_f = 0.32 (1:2 =EtOAc:Hex + 1% acetic acid, v/v/v); ^{1}H NMR (400 MHz, DMSO-d_6) δ 7.95 (t, *J* = 5.8 Hz, 1H), 7.39 – 7.18 (m, 13H), 6.96 – 6.91 (m, 1H), 6.63 (s, 1H), 5.04 (s, 2H), 4.34 (d, *J* = 5.7 Hz, 2H), 1.49 (s, 6H). ^{13}C NMR (101 MHz, DMSO-d_6) δ 164.91, 162.61, 153.68, 139.75, 137.38, 129.79, 128.49, 128.19, 127.25, 127.00, 126.78, 126.69, 89.14, 49.33, 43.85, 25.33. LRMS(ESI$^+$) m/z calcd for $C_{27}H_{33}N_3O_5$ $[M+H]^+$ 486.20 Found; 486.08

(19-p {E}), *2-(4-(3-(3-benzyl-1-ethylureido)isoxazol-5-yl)phenoxy)-2-methylpropanoic acid*

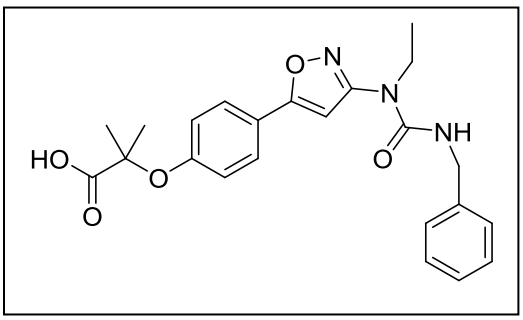

Synthesized according to the synthetic procedure of 5. Yield 77%, R_f = 0.33 (1:2 =EtOAc:Hex + 1% acetic acid, v/v/v); ^{1}H NMR (400 MHz, DMSO-d_6) δ 7.78 (t, *J* = 5.8 Hz, 1H), 7.66 (d, *J* = 7.1 Hz, 2H), 7.34 – 7.23 (m, 4H), 7.23 – 7.15 (m, 1H), 6.86 (s, 2H), 6.56 (s, 1H), 4.29 (d, *J* = 5.7 Hz, 2H), 3.78 (d, *J* = 7.0 Hz, 2H), 1.49 (s, 6H), 1.14 (t,

J = 7.7 Hz, 3H). ^{13}C NMR (101 MHz, DMSO-d_6) δ 164.6, 162.4, 153.3, 140.0, 128.2, 127.5, 127.1, 126.7, 121.7, 118.2, 109.6, 88.5, 43.7, 41.3, 40.4, 25.3, 14.1. LRMS(ESI$^+$) m/z calcd for $C_{23}H_{25}N_3O_5$ $[M+H]^+$ 424.18 Found; 424.19

(19-m {E}), *2-(3-(3-(3-benzyl-1-ethylureido)isoxazol-5-yl)phenoxy)-2-methylpropanoic acid*

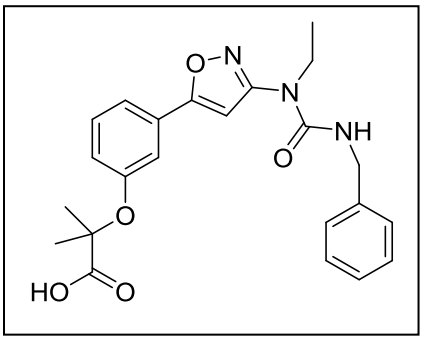

Synthesized according to the synthetic procedure of 5. Yield 97%, R_f = 0.45 (1:1 =EtOAc:Hex + 1% acetic acid, v/v/v); ^{1}H NMR (400 MHz, DMSO-d_6) δ 7.81 (t, *J* = 5.9 Hz, 1H), 7.43 – 7.13 (m, 8H), 6.90 (d, *J* = 7.6 Hz, 1H), 6.59 (s, 1H), 4.30 (d, *J* = 5.7 Hz, 2H), 3.79 (q, *J* = 7.0 Hz, 2H), 1.49 (s, 6H), 1.16 (t, *J* = 7.2 Hz, 3H). ^{13}C NMR (101 MHz, dmso) δ 165.0, 162.5, 155.8, 153.3, 140.0, 130.1, 130.0, 128.2, 127.1, 126.7, 120.1, 119.7, 115.9, 88.6, 43.7, 41.4, 40.4, 25.1, 14.1. LRMS(ESI$^+$) m/z calcd for $C_{23}H_{25}N_3O_5$ $[M+H]^+$ 424.18 Found; 424.19

(21-p), *1-benzyl-1-((3,5-dimethoxyphenyl)carbamoyl)-3-ethyl-3-(5-(4-hydroxyphenyl)isoxazol-3-yl)urea*

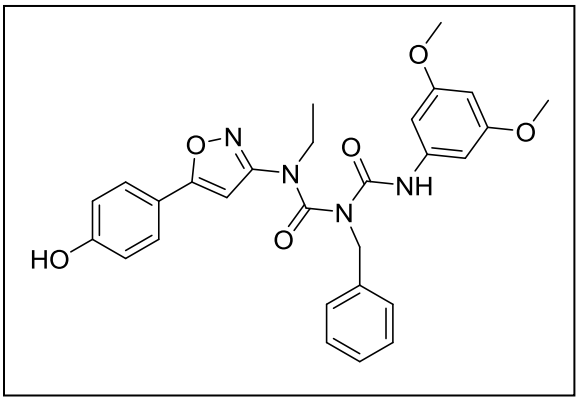

3,5-dimethoxyphenyl isocyanate (476.44 mg, 2.66 mmol) is dissolved in dry DCM (10 mL) to which $SnCl_4$ (157 µL, 1.33 mmol) is added dropwise over a 1 minute period. The reaction was left to stir for 30 minutes. Afterwards, compound 15-p {E} (120 mg, 0.266 mmol) pre-dissolved in dry DCM (1 mL) was added to the mixture

and was left to stir for 20 hours. After reaction completion (TLC), the reaction was quenched with brine (10 mL). The organic layer was separated and the aqueous layer was extracted three times with DCM. The separated and combined organic layers were dried over anhydrous $MgSO_4$(s) and filtered through a celite-packed glass filter. The filtrate was concentrated under reduced pressure to afford 98 mg of a crude mixture. The crude mixture was then dissolved in a 5% HF-Pyridine in THF solution (10 mL) and was left to stir for 2 hours. After reaction completion (TLC), the reaction was quenched with trimethylethoxy silane (5 mL) and crude product was evaporated under reduced pressure to dryness. The crude product was purified with preparatory think-layer chromatography (1:40 = Methanol:DCM, v/v); to provide 21-p {E}, (40.3 mg, 29%). R_f = 0.36 (1:1 = EtOAc:Hex, v/v); ^{1}H NMR (400 MHz, $CDCl_3$-*d*) δ 9.61 (s, 1H), 8.60 (d, *J* = 4.3 Hz, 1H), 7.59 (d, *J* = 8.6 Hz, 2H), 7.38 (dd, *J* = 7.7, 5.9 Hz, 1H), 7.33 – 7.18 (m, 5H), 6.88 (d, *J* = 8.6 Hz, 2H), 6.65 (d, *J* = 2.2 Hz, 2H), 6.21 (t, *J* = 2.2 Hz, 1H), 6.05 (s, 1H), 4.72 (s, 2H), 3.71 (s, 8H), 1.10 (t, *J* = 7.1 Hz, 3H). ^{13}C NMR (101 MHz, $CDCl_3$-*d*) δ 163.7, 163.6, 161.1, 159.1, 157.3, 152.4, 148.7, 139.2, 137.4, 136.9, 128.8, 128.4, 127.9, 127.4, 124.5, 120.0, 116.2, 98.7, 97.1, 91.2, 55.5, 49.3, 45.4, 13.3. LRMS(ESI^+) m/z calcd for $C_{28}H_{28}N_4O_6$ $[M+H]^+$ 517.20 Found; 517.19

(21-m), *1-benzyl-1-((3,5-dimethoxyphenyl)carbamoyl)-3-ethyl-3-(5-(3-hydroxyphenyl)isoxazol-3-yl)urea*

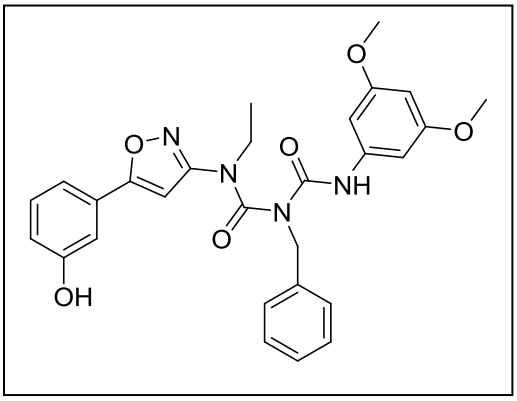

Synthesized according to the synthetic procedure of 21-p {E}. Yield 13%, R_f = 0.41 (1:2 =EtOAc:Hex, v/v); ^{1}H NMR (400 MHz, $CDCl_3$-*d*) δ 9.56 (s, 1H), 7.37 – 7.14 (m, 8H), 6.99 – 6.86 (m, 1H), 6.64 (d, *J* = 2.2 Hz, 2H), 6.20 (t, *J* = 2.2 Hz, 1H), 6.08 (s, 1H), 4.71 (s, 2H), 3.71 (s, 8H), 1.10 (t, *J* = 7.1

Hz, 3H). ^{13}C NMR (101 MHz, $CDCl_3$-*d*) δ 164.0, 163.8, 161.1, 157.3, 156.7, 152.4, 139.2, 136.9, 130.4, 129.6, 128.9, 128.0, 127.4, 119.0, 117.9, 113.7, 98.7, 97.2, 91.6, 55.5, 49.5, 45.4, 13.4. LRMS(ESI$^+$) m/z calcd for $C_{28}H_{28}N_4O_6$ $[M+H]^+$ 517.20 Found; 517.19

(PP-2-93), *N-ethyl-N-(5-(3-hydroxyphenyl)isoxazol-3-yl)-3-phenylpropanamide*

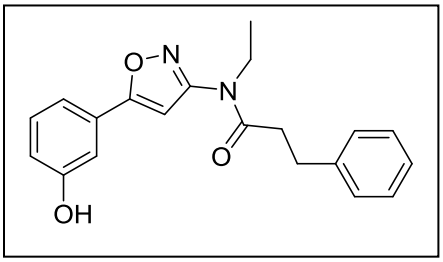

Compound 14-m {E} (250 mg, 0.785 mmol) and added to a solution containing hydrocinnamoyl chloride (357 µL, 2.36 mmol) and pyridine (127.73 µL, 1.57 mmol) dissolved in dry DCM (10 mL). The reaction was stirred at room temperature for 2 hours and the quenched with aqueous $NaHCO_3$. The organic layer was separated and the aqueous layer was extracted three times with DCM. The separated and combined organic layers were dried over anhydrous $MgSO_4$(s) and filtered through a celite-packed glass filter. The filtrate was concentrated under reduced pressure to afford 303 mg of a crude mixture. The crude mixture was then dissolved in a 5% HF-Pyridine in THF solution (15 mL) and was left to stir for 2 hours. After reaction completion (TLC), the reaction was quenched with trimethylethoxy silane (10 mL) and crude product was evaporated under reduced pressure to dryness. The crude product was purified with preparatory thin-layer chromatography (1:2 = EtOAC:n-hexanes, v/v) to provide PP-2-93, (168 mg, 81%). R_f = 0.38 (1:2 = EtOAc:Hex, v/v); ^{1}H NMR (400 MHz, $CDCl_3$-*d*) δ 7.53 (s, 1H), 7.39 – 7.09 (m, 8H), 7.03 – 6.93 (m, 1H), 6.06 (s, 1H), 3.81 (d, *J* = 7.3 Hz, 2H), 3.00 (t, *J* = 7.6 Hz, 2H), 2.68 (s, 2H), 1.21 (t, *J* = 7.1 Hz, 3H). ^{13}C NMR (101 MHz, $CDCl_3$-*d*) δ 172.1, 163.7, 157.0, 140.3, 130.32, 130.31, 129.7, 128.6, 128.5, 126.42, 126.40, 118.6, 117.9, 113.5, 43.3, 36.3, 31.3, 13.7.

(PP-2-94), *N-ethyl-N-(5-(4-hydroxyphenyl)isoxazol-3-yl)-3-phenylpropanamide*

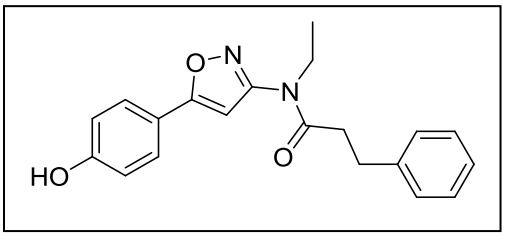

Synthesized according to the synthetic procedure of PP-2-93. Yield 81%, R_f = 0.33 (1:2 =EtOAc:Hex, v/v); ^{1}H NMR (400 MHz, $CDCl_3$-*d*) δ 8.25 (s, 1H), 7.69 – 7.60 (m, 2H), 7.34 – 7.10 (m, 5H), 7.00 (dd, *J* = 8.7, 2.1 Hz, 2H), 6.03 (s, 1H), 3.82 (d, *J* = 7.4 Hz, 2H), 3.02 (t, *J* = 7.7 Hz, 2H), 2.71 (s, 2H), 1.23 (t, *J* = 7.1 Hz, 3H). ^{13}C NMR (101 MHz, $CDCl_3$-*d*) δ 172.1, 163.6, 158.8, 140.3, 129.0, 128.6, 128.5, 128.3, 128.2, 126.4, 120.2, 116.1, 43.3, 36.3, 31.3, 13.6.

(PP-2-97), *N-ethyl-N-(5-(3-methoxyphenyl)isoxazol-3-yl)-3-phenylpropanamide*

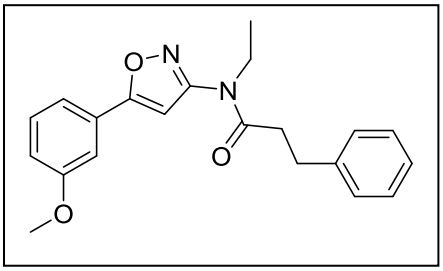

Synthesized according to the synthetic procedure of 17-p {B} with PP-2-93 as the starting material. Yield 83%, R_f = 0.33 (1:2 =EtOAc:Hex, v/v); ^{1}H NMR (400 MHz, $CDCl_3$-*d*) δ 7.41 – 7.12 (m, 8H), 6.99 (ddd, *J* = 8.1, 2.6, 1.2 Hz, 1H), 6.06 (s, 1H), 3.85 (s, 3H), 3.81 (d, *J* = 7.0 Hz, 2H), 3.00 (t, *J* = 7.6 Hz, 2H), 2.68 (s, 2H), 1.22 (t, *J* = 7.1 Hz, 3H). ^{13}C NMR (101 MHz, $CDCl_3$-*d*) δ 171.1, 163.7, 160.1, 140.7, 130.1, 128.6, 128.6, 126.4, 119.2, 116.6, 111.5, 55.5, 43.2, 36.4, 31.3, 13.8.

(PP-2-98), *N-ethyl-N-(5-(4-methoxyphenyl)isoxazol-3-yl)-3-phenylpropanamide*

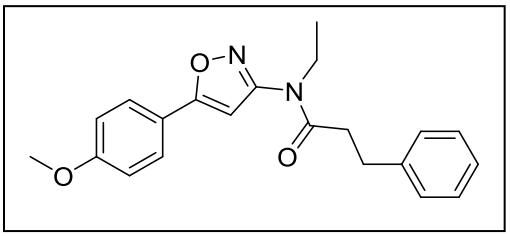

Synthesized according to the synthetic procedure of 17-p {B} with PP-2-94 as the starting material. Yield 78%, R_f = 0.50 (1:2 =EtOAc:Hex, v/v); ^{1}H NMR (400 MHz, $CDCl_3$-*d*) δ 7.69 (d, *J* = 8.8 Hz, 2H), 7.36 – 7.08 (m, 5H), 6.96 (d, *J* = 8.9 Hz, 2H), 6.01 (s, 1H), 3.84 (s, 3H), 3.80 (d, *J* = 7.5 Hz, 2H), 2.99 (t, *J* = 7.7 Hz, 2H), 2.67 (s, 2H), 1.21 (t, *J* = 7.2 Hz, 3H). ^{13}C NMR (101 MHz, $CDCl_3$-*d*) δ 163.4, 161.3, 157.8, 140.7, 128.6, 128.6, 128.1, 126.4, 121.4, 114.4, 55.5, 43.2, 36.3, 31.4, 13.8.

(PP-2-101), *2-(3-(3-(N-ethyl-3-phenylpropanamido)isoxazol-5-yl)phenoxy)-2-methylpropanoic acid*

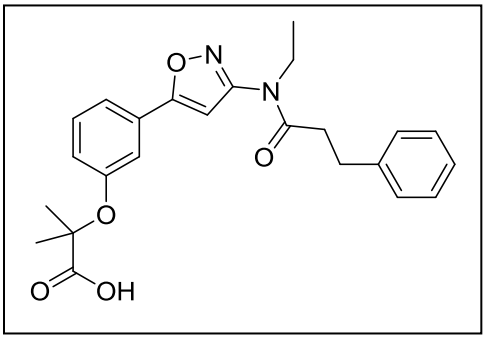

Compound PP-2-93 was reacted with t-butyl-alpha-isobutyrate as per the procedure outlined for 1. The crude mixture was then deprotected via HF-pyridine conditions under the same procedure as for 21-p to afford PP-2-101. Yield 54%, R_f = 0.48 (1:1 =EtOAc:Hex, v/v); ^{1}H NMR (400 MHz, DMSO-d_6) δ 7.56 – 7.07 (m, 9H), 6.95 (dd, *J* = 13.4, 5.2 Hz, 2H), 3.78 (s, 2H), 2.86 (t, *J* = 7.5 Hz, 2H), 2.75 (s, 2H), 1.54 (s, 6H), 1.15 (t, *J* = 7.4 Hz, 3H). ^{13}C NMR (101 MHz, DMSO-d_6) δ 170.5, 162.9, 156.0, 140.7, 137.4, 130.1, 129.6, 128.9, 128.4, 128.3, 128.2, 126.0, 125.3, 120.3, 119.7, 116.1, 78.9, 42.3, 35.4, 30.4, 25.2, 21.1, 13.6.

(PP-2-102), *2-(4-(3-(N-ethyl-3-phenylpropanamido)isoxazol-5-yl)phenoxy)-2-methylpropanoic acid*

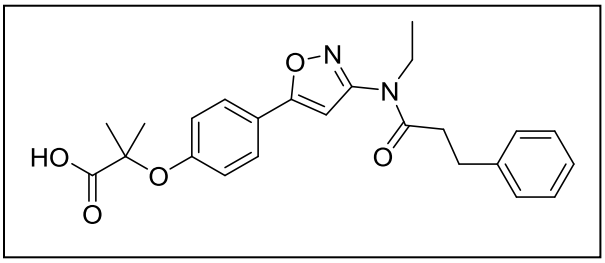

Compound PP-2-94 was reacted with t-butyl-alpha-isobutyrate as per the procedure outlined for 1. The crude mixture was then deprotected via HF-pyridine conditions under the same procedure as for 21-p to afford PP-2-102. Yield 90%, R_f = 0.48 (1:1 =EtOAc:Hex, v/v); ^{1}H NMR (400 MHz, DMSO-d_6) δ 7.76 (d, *J* = 7.9 Hz, 2H), 7.32 – 7.07 (m, 6H), 6.93 (d, *J* = 8.3 Hz, 2H), 6.87 (s, 1H), 3.76 (d, *J* = 7.3 Hz, 2H), 2.87 (t, *J* = 7.5 Hz, 2H), 2.71 (s, 2H), 1.56 (s, 6H), 1.13 (t, *J* = 7.1 Hz, 3H). ^{13}C NMR (101 MHz, DMSO-d_6) δ 170.50, 162.73, 157.28, 140.74, 137.36, 128.90, 128.35, 128.32, 128.20, 127.66, 126.03, 125.31, 121.48, 118.35, 78.83, 42.26, 35.44, 30.40, 25.17, 21.05, 13.55.

(PP-2-110), *N-benzyl-N-(5-(3-hydroxyphenyl)isoxazol-3-yl)-3-phenylpropanamide*

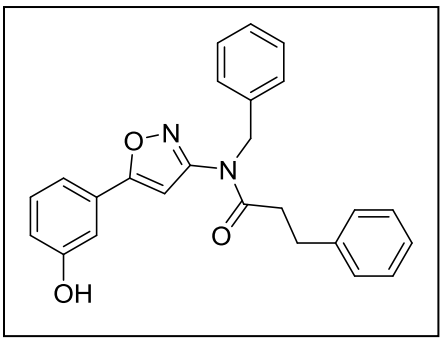

Synthesized according to the synthetic procedure of PP-2-93. Yield 79%, R_f = 0.39 (1:2 =EtOAc:Hex, v/v); ^{1}H NMR (400 MHz, $CDCl_3$-*d*) δ 7.32 – 7.13 (m, 11H), 7.15 – 7.08 (m, 2H), 6.92 (ddd, *J* = 8.1, 2.5, 1.1 Hz, 1H), 6.82 (s, 1H), 5.80 (s, 1H), 4.94 (s, 2H), 3.00 (t, *J* = 7.5 Hz, 2H), 2.71 (t, *J* = 7.5 Hz, 2H). ^{13}C NMR (101 MHz, $CDCl_3$-*d*) δ 172.0, 163.7, 156.7, 140.4, 136.0, 130.4, 129.8, 128.9, 128.7, 128.6, 128.0, 126.5, 118.9, 117.9, 113.4, 51.3, 36.4, 31.4. LRMS(ESI$^+$) m/z calcd for $C_{25}H_{22}N_2O_3$ $[M+H]^+$ 399.16 Found; 399.15

(PP-2-111), *N-benzyl-N-(5-(4-hydroxyphenyl)isoxazol-3-yl)-3-phenylpropanamide*

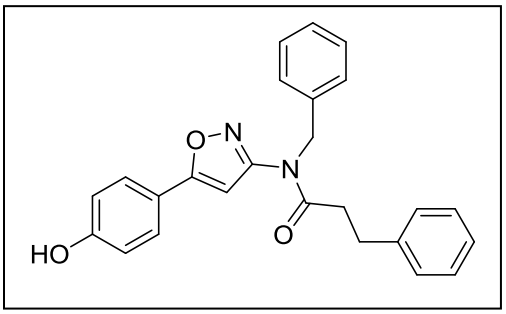

Synthesized according to the synthetic procedure of PP-2-93. Yield 59%, R_f = 0.31 (1:2 =EtOAc:Hex, v/v); ^{1}H NMR (400 MHz, DMSO-d_6) δ 9.99 (s, 1H), 7.62 (d, *J* = 8.7 Hz, 2H), 7.43 – 7.08 (m, 10H), 6.87 (d, *J* = 8.7 Hz, 2H), 6.76 (s, 1H), 4.97 (s, 2H), 2.89 (t, *J* = 7.2 Hz, 2H), 2.78 (t, *J* = 7.4 Hz, 2H). ^{13}C NMR (101 MHz, DMSO-d_6) δ 171.0, 162.9, 159.5, 140.6, 136.6, 128.5, 128.4, 128.3, 128.0, 127.4, 127.2, 126.1, 119.1, 115.8, 50.1, 48.6, 35.5, 30.4. LRMS(ESI$^+$) m/z calcd for $C_{25}H_{22}N_2O_3$ $[M+H]^+$ 399.16 Found; 399.15

(PP-2-112), *N-benzyl-N-(5-(3-methoxyphenyl)isoxazol-3-yl)-3-phenylpropanamide*

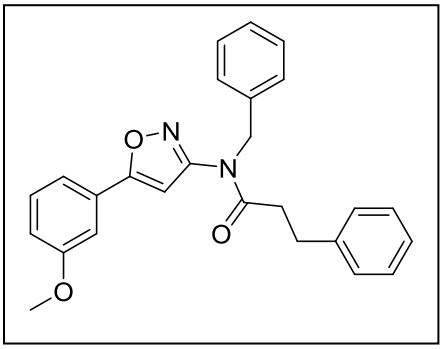

Synthesized according to the synthetic procedure of 17-p {B} with PP-2-110 as the starting material. Yield 98%, R_f = 0.63 (1:2 =EtOAc:Hex, v/v); ^{1}H NMR (400 MHz, $CDCl_3$-*d*) δ 7.42 – 7.06 (m, 11H), 6.97 (d, *J* = 8.4 Hz, 1H), 5.80 (s, 1H), 4.95 (s, 1H), 3.84 (s, 2H), 3.01 (td, *J* = 7.6, 2.9 Hz, 2H), 2.73 (t, *J* = 8.1 Hz, 2H). ^{13}C NMR (101 MHz, $CDCl_3$-*d*) δ 171.6, 163.6, 160.1, 140.5, 136.2, 130.1, 128.8, 128.7, 128.6, 128.0, 126.4, 119.2, 116.6, 111.5, 55.5, 36.3, 31.4, 29.8. LRMS(ESI$^+$) m/z calcd for $C_{26}H_{24}N_2O_3$ $[M+H]^+$ 413.18 Found; 413.13

(PP-2-113), *N-benzyl-N-(5-(4-methoxyphenyl)isoxazol-3-yl)-3-phenylpropanamide*

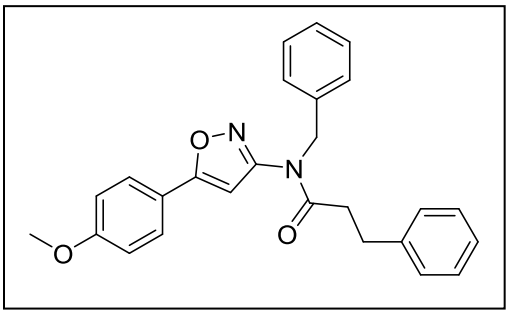

Synthesized according to the synthetic procedure of 17-p {B} with PP-2-111 as the starting material. Yield 99%, R_f = 0.62 (1:2 =EtOAc:Hex, v/v); ^{1}H NMR (400 MHz, $CDCl_3$-*d*) δ 7.62 (d, *J* = 8.2 Hz, 2H), 7.40 – 7.03 (m, 9H), 7.02 – 6.89 (m, 2H), 5.77 (s, 1H), 4.94 (s, 2H), 3.83 (s, 3H), 3.01 (td, *J* = 7.6, 2.8 Hz, 2H), 2.72 (t, *J* = 7.9 Hz, 2H). ^{13}C NMR (101 MHz, $CDCl_3$-*d*) δ 171.7, 163.3, 161.4, 140.6, 136.3, 128.8, 128.6, 128.1, 127.9, 126.4, 114.4, 55.5, 36.3, 31.4, 29.8. LRMS(ESI$^+$) m/z calcd for $C_{26}H_{24}N_2O_3$ $[M+H]^+$ 413.18 Found; 413.16

(PP-2-117), *2-(3-(3-(N-benzyl-3-phenylpropanamido)isoxazol-5-yl)phenoxy)-2-methylpropanoic acid*

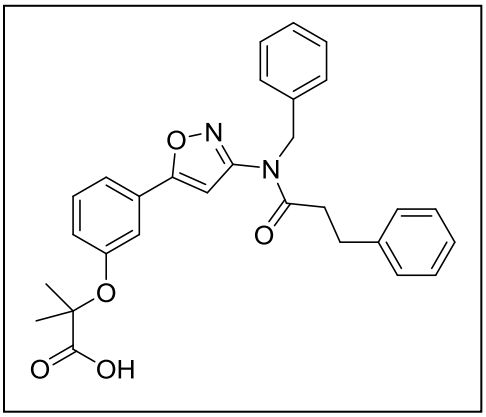

Compound PP-2-110 was reacted with t-butyl-alpha-isobutyrate as per the procedure outlined for 1. The crude mixture was then deprotected via HF-pyridine conditions under the same procedure as for 21-p to afford PP-2-117. Yield 54%, R_f = 0.48 (1:1 =EtOAc:Hex, v/v); ^{1}H NMR (400 MHz, DMSO-d_6) δ 7.45 – 7.12 (m, 13H), 6.99 – 6.92 (m, 1H), 6.90 (s, 1H), 5.00 (s, 2H), 2.90 (t, *J* = 6.8 Hz, 2H), 2.81 (t, *J* = 7.6 Hz, 2H), 1.53 (s, 6H). ^{13}C NMR (101 MHz, DMSO-d_6) δ 174.9, 171.0, 162.9, 156.0, 140.6, 136.6, 130.1, 129.4, 128.6, 128.4, 128.4, 127.5, 127.2, 126.1, 120.3, 119.7, 116.0, 78.9, 50.2, 40.4, 35.5, 30.4, 25.1, 21.2. LRMS(ESI$^+$) m/z calcd for $C_{29}H_{28}N_2O_5$ $[M+H]^+$ 485.20 Found; 485.19

(PP-2-118), *2-(4-(3-(N-benzyl-3-phenylpropanamido)isoxazol-5-yl)phenoxy)-2-methylpropanoic acid*

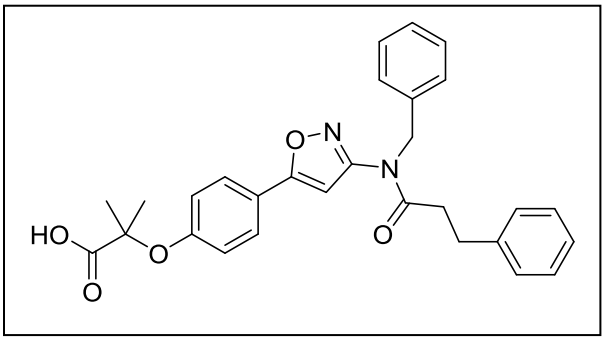

Compound PP-2-111 was reacted with t-butyl-alpha-isobutyrate as per the procedure outlined for 1. The crude mixture was then deprotected via HF-pyridine conditions under the same procedure as for 21-p to afford PP-2-118. Yield 98%, R_f = 0.25 (1:2 =EtOAc:Hex, v/v); ^{1}H NMR (400 MHz, DMSO-d_6) δ 7.70 (d, *J* = 8.4 Hz, 2H), 7.37 – 7.06 (m, 10H), 6.91 (d, *J* = 8.8 Hz, 2H), 6.81 (s, 1H), 4.98 (s, 2H), 2.89 (t, *J* = 7.4 Hz, 2H), 2.79 (t, *J* = 7.5 Hz, 2H), 1.54 (s, 6H). ^{13}C NMR (101 MHz, DMSO-d_6)) δ 174.9, 171.0, 162.7, 157.4, 140.6, 136.6, 128.6, 128.4, 128.3, 127.6, 127.5, 127.2, 126.1, 121.2, 118.3, 78.9, 50.1, 40.4, 35.5, 30.4, 25.2. LRMS(ESI$^+$) m/z calcd for $C_{29}H_{28}N_2O_5$ $[M+H]^+$ 485.20 Found; 485.19

1.8.1. References

1 Eric A. Finkelstein, Justin G. Trogdon, Joel W. Cohen, William Dietz, *Health Affairs*, 2009, 28, 5.

2 C. L. Ogden, M. D. *The Journal of the American Medical Association*, 2014, 311 (8), 806-814.

3 S. Low, M. C.-Y. *Annals of the Academy of Medicine Singapore,* 2009 38 (1), 57-59.

4 http://www.cdc.gov/chronicdisease/resources/publications/aag/ddt.htm

5 Ozcan U, *Science*, 2004, 306, no. 5695, 457-61

6 D. D. Sears, A. Hsiao, J. M. Ofrecio, J. Chapman, W. He, and J. M. Olefsky, *Biochemical and Biophysical Research Communications*, 2007, vol. 364, no. 3, 515–521

7 C. Yu, K. Markan, K. A. Temple, D. Deplewski, M. J. Brady, and R. N. Cohen, *Journal of Biological Chemistry*, 2005, vol. 280, no. 14, 13600–13605

8 J. N. Feige, L. Gelman, L. Michalik, B. Desvergne, and W. Wahli, *Progress in Lipid Research*, 2006, vol. 45, no. 2, 120–159

9 Scherer, P. E. *International Journal of Obesity*, 2005, S17-S23

10 G, P., *Nature,* 2005 473 (7059), 759-753.

11 Beekum, O. V., *Obesity,* 2009, 17, 213-219.

12 KA, B., *Biochim Biophys Acta*, 2007, 1771 (8), 952-960.

13 Choi JH., *Nature,* 2010, 466 (7305), 451-456.

14 Pershadsingh HA, Szollosi J, Benson S, Hyun WC, Feuerstein BG, Kurtz TW., *Hypertension*, 1993, 21 (6 Pt 2), 1020–3

15 L. Guo, L. Zhang, Y. Sun et al., *Molecular Diversity*, 2006, vol. 10, no. 3, pp. 349–360

16 Choi JH, Banks AS,. *Nature*. 2011, 477(7365), 477-81

17. Morikawa et al, *The EMBO Journal* (2010) 29, 3395-3407

18 S.B.Park et al, *Angew. Chem. Int. Ed.* 2014, 53, 5102

19 Takase, A.; Murabayashi, A.; Sumimoto, S., *Heterocycles* 1991,32, 1153.

20 L. Johnson, J. Powers, F. Ma, K. Jendza, B. Wang, E. Meredith, N. Mainolfi, *Synthesis*, 2013, *45*, 171-173.

Chapter 2

The Library Construction of Small Molecule Autophagy Modulators

2.1.1. Introduction

Alzheimer's disease is a progressive neurodegenerative disease that damages and eventually destroys brain cells, leading to irreversible memory loss and behavioral changes. The majority of those with the disease tend to be over 65, with a small percentage of patients found to contract the disease from as early 40, known as early-on-set Alzheimer's. As of 2015, there is believed to be an estimated 5.3 million people in the US living with Alzheimer's and that number is expected to almost triple to 13.8 million by 2050. Currently Alzheimer's is costing the US close to $226 billion annually and in the next 30 years the cost is projected to surpass $1 trillion[1]. With Alzheimer's being the only disease among the top 10 causes of death in the US that cannot be prevented, cured or even slowed, any developments in Alzheimer's research will have a profound effect for its sufferers, caregivers and humanity as a whole.

With the cause of Alzheimer's still remaining unknown, a considerable amount of research has been focused on developing various therapies that target different features of AD pathology in order to slow down the disease's progression. However, debate continues over which pathological features are central to its progression. A well accepted pathological biomarker for AD, is the formation of neuritic plaques composed of aggregated extracellular Amyloid Beta (AB) peptides. The formation of these plaques is believed to begin 10-20 years before the first clinical symptoms arise, with amyloid plaque formation beginning at the neocortex and gradually spreading throughout the rest of the brain[2]. Now before these plaques are able to form, first the individual monomer and oligomer constituents must be produced. These constituent parts to AB plaques, unsurprisingly, are called Amyloid Beta Oligomers and are produced from the cleavage of the conveniently named, Amyloid Precursor Protein (APP). APP can be cleaved resulting in two different outcomes; with or without the generation of Amyloid Beta, also referred to by their conveniently named pathways, Amyloidgenic Pathway and Non-Amyloidgenic Pathway, respectively. Which pathway is chosen depends on which enzyme is

cleaving APP. APP cleavage with Alpha-secratase will take the Non-Amyloidgenic pathway and cleavage with Beta and Γ-secratase follows the Amyloidgenic pathway[3]. However, for years researchers have been puzzled by the lack of correlation between the amount of neuritic plaque deposition and the degree of clinical dementia[3]. Gradually the notion that AB plaques were the cause of dementia symptoms began to fade, and rather, the quantity of soluble AB oligomers that are present in the brain became the primary indicator for predicting the extent of AD progression[4,5,6]. Increasing evidence has implicated these soluble AB oligomers to be the proximate effectors of synapse loss and neuronal injury and death through multiple channels[7-11]. An imbalance between the production and clearance of AB oligomers is the basis for AB plaque formation.

One such mechanism known to aid in AB clearance is autophagy. Autophagy is a lysosome-mediated, self-digesting degradation mechanism of long-lived, misfolded and aggregated proteins, as well as cytoplasmic organelles[12]. Impairment of this process is known to be a contributing factor to the progression of neurodegeneration and various neurodegenerative diseases including Parkinson's, Huntington's and Alzhiemer's[12,13]. As such, autophagy enhancement through the use of autophagy-inducing small molecules has become an attractive therapeutic strategy for combating neurodegenerative disorders.

Until recently an efficient method for the identification of small molecule autophagy modulators on a large scale has remained inaccessible. However, in 2013, our laboratory reported a novel high-content screening platform that monitors the degradation of lipid droplets (LD) via the autophagic process[14]. With the aim of using this technique, a small molecule library based off of an initial hit compound (P41-H06) that was discovered through the afore mentioned high-content screening method, has been constructed and tested for autophagy modulation. While various libraries based off of P41H06 are being synthesized in our laboratory, this thesis will focus on the synthesis of isoxazole-based derivatives of the P41-H06 hit compound.

2.1.2. Autophagy-Induced LD Degradation Sensing Overview

To connect the results obtained from this work it is important for the reader to have some familiarity with our laboratory's High Content Screening (HCS) method employed for the validation of the synthesized small molecule autophagy modulators presented in this chapter. This subsection 2.1.2, will serve as a brief overview of this HCS platform. For a detailed overview, please refer to reference 14.

Being able to visualize the progressive degradation of any of the constituents that autophagy consumes, could potentially serve as the basis for monitoring the progression of the autophagy process via a high content screening platform. By taking advantage of the unique fluorescent properties exhibited by our laboratory's compound SF44, image-based monitoring of the degradation of autophagy-consumed lipid droplets (LD) became possible. SF44's fluorescence is highly dependent on its environment; it is fluorescent in non-polar environments and dormant in polar environments (Figure 25b). Lipid droplets, being inherently hydrophobic, provide an ideal non-polar environment for situating SF44. Once the lipid droplet begins to be degraded by the autophagy process, the LD shell will be broken and SF44 will then enter the polar environment of the lysosome, immediately quenching its fluorescence and signaling the functioning of the autophagy process.

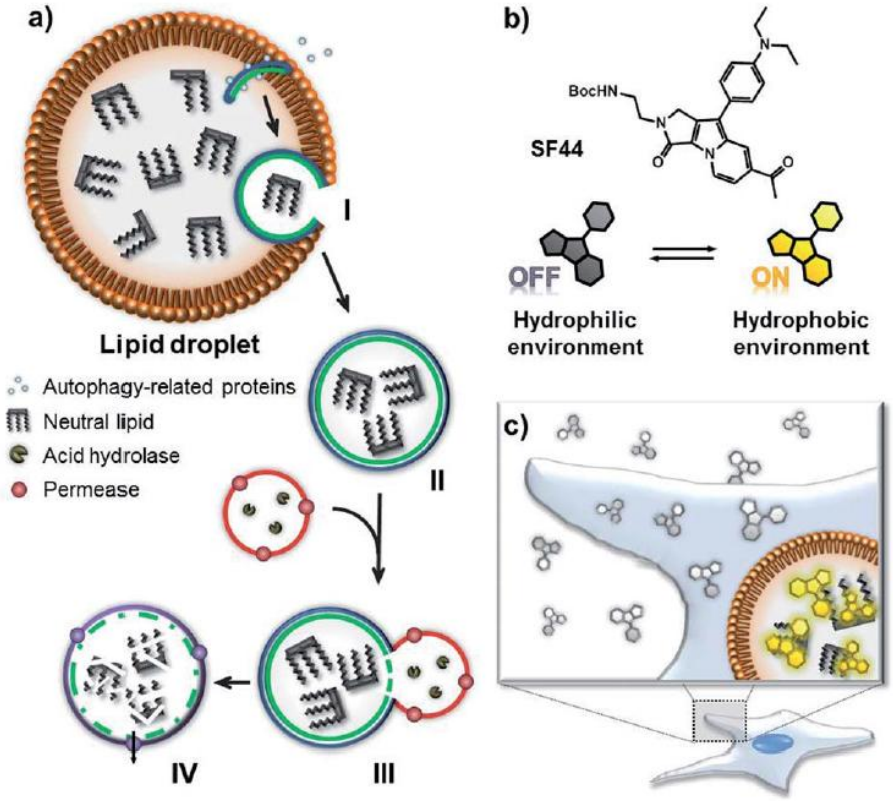

Figure 25. *(Chem. Sci., (2013), 4, 3282)* (a) Schematic illustration of lipid droplet (LD) degradation via the autophagic process. (b) Chemical structure of SF44 (Seoul-Fluor) and its fluorogenic features after exposure to a polar environment on the basis of positive solvatochromism. (c) Cellular visualization of LDs using SF44 without fixation and washing steps.

Currently the go-to method for monitoring the autophagy process involves the detection of two biomarker proteins: Light Chain 3 II (LC3 II) and P62. Increasing concentration of LC3 II is indicative of early-stage autophagy progression and the decrease in P62 (degraded in the autolysosome), signals late stage completion of the autophagy process (Figure 26). Western blot data confirming the appropriate concentration changes of these biomarkers enables the discrimination between compounds that are autophagy initiators and ones that are

late-stage inhibitors. Image-based high content screening of SF44-containing Lipid Droplet degradation, allows for the unambiguous identification of autophagy inducers on a large scale. After the identification of hit compounds that trigger LD degradation, organelle count and cell viability tests rule out potential cytotoxicity, and once ruled-out, dose-dependent analysis reveals the compound's potency.

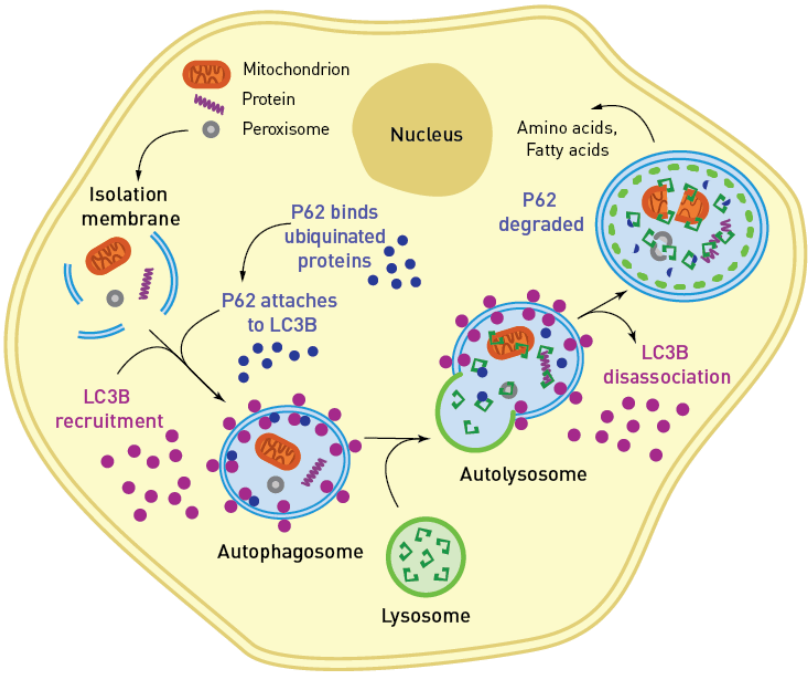

Figure 26. Schematic representation of the autophagy process[15].

2.2.1. Construction of an Isoxazole-based Small Molecule Autophagy Modulator Library

At the time of the start of this project, the target for which the synthesized isoxazole-based library was constructed for was unknown. As a result, a highly rationally designed approach, such as the one utilized in Chapter 1, was not implemented in this set. Instead, while the target identification component to this project was underway, a large library loosely based off of the hit compound P41H06

was developed. Once the target of P41H06 and any of its newly synthesized derivatives is discovered, the bio-activity data of P41H06 and its analogs will be instrumental to the progression of the activity modulation portion of the project.
Looking closely at the structure of P41H06 reveals three main areas for modification: the triazole ring, and the two regions neighboring it (Figure 27).

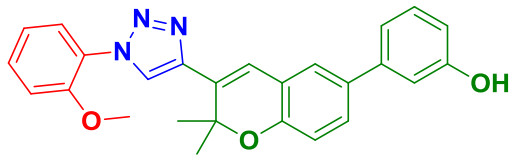

P41H06

Figure 27. Chemical structure of P41H06 with each modification area of interest highlighted in a different color.

Diversification of P41H06 first began by targeting its triazole core. Two identical libraries with only the triazole ring differing between them was first proposed (Figure 28). This thesis will focus on the synthesis of the isoxazole library.

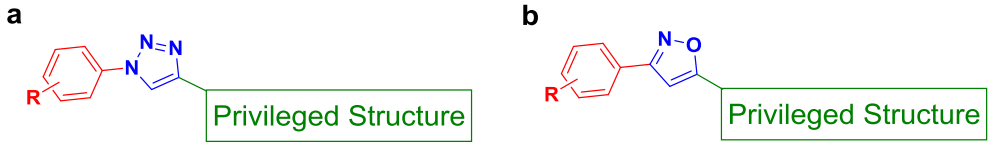

Figure 28. General representation of the initial two libraries constructed for the identification of small molecule autophagy modulators. a) triazole set and b) isoxazole set.

With the target for these compounds unknown, the starting point for P41H06 diversification was to place various well known bio-active privileged structures adjacent to the isoxazole ring (Figure 29a), as is the case with the 2-dimethylbenzopyran embedded moiety present in P41H06. Afterwards, the benzyl moiety, located opposite the privileged structure, adjacent to the isoxazole ring was

then functionalized. Common functional groups, possessing diverse electronic properties were included such as to explore their effects at all three ortho, meta and para positions (Figure 29b).

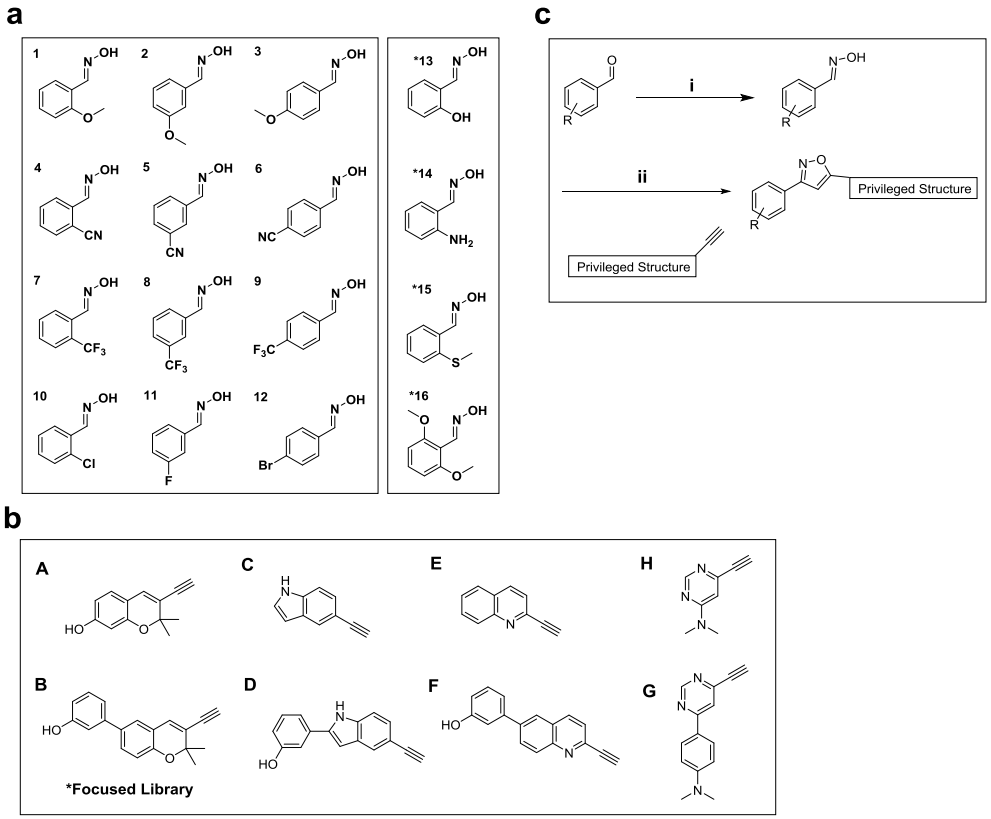

Figure 29. Overview of the building blocks and synthetic scheme used for the isoxazole library construction. a) Oxime components (*oximes 13-16 are for the focused library with privileged structure, alkyne B only) b) Alkynes containing the pre-selected privileged structures, and c) Synthetic scheme for generating the isoxazole from oxime (a) and alkyne (b) via a 2+3 cycloaddition reaction. [i) hydroxylamine, sodium acetate, MeOH, 65 ^{o}C, 20h, 40-97%, ii) oxime (a), NCS, pyridine, THF, 60 ^{o}C, 2h, then TEA, THF, 60 ^{o}C, 2h, 5-83%]

Construction of this library began with the synthesis of the oxime building blocks in Figure 29a, after which were each reacted in parallel with any given alkyne from Figure 29b via the procedure outlined in Figure 29c. While the isoxazole forming 2+3 cycloaddition reaction is quite standard, some large fluctuations in yields between various alkynes were observed. With the majority of the isoxazole forming reactions generating over 50% yields, the outliers were noted and their reaction condition optimizations were set to be carried out after the first run-through of all 2+3 cycloaddition reactions was completed. Improving the yields of the outliers after all the isoxazoles have been formed, was chosen as the best strategy because while the isoxazoles are being screened for their bioactivity there is then ample time to go back and optimize their conditions.

At the time of writing this thesis approximately one fourth of this library has been constructed. Isoxazoles originating from alkynes A, C and E have been either partially or fully synthesized as represented in Table 1.

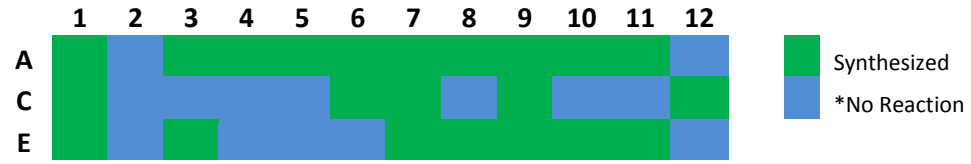

Table 1. Table illustrating the results of the first run-through of 2+3 cycloaddition reactions between oxime partners (1-12) and alkynes (A,C and E). **Cell blocks also include reactions that had yields under 10%.*

After synthesis of all oximes (Figure 29a), each were reacted with one alkyne (Figure 29b) at a time, making cross-comparisons between alkyne sets difficult. As such, in order to better elucidate the cause for what seems to be a random string of low yielding reactions, subsequent reactions will be performed with multiple alkynes reacting with one oxime at a time. That way whether the problem lies with the oxime or the alkyne, should be easier to resolve.

2.3.1 Conclusion

With the promise of being able to quickly and efficiently detect small molecule autophagy modulators through our laboratory's high throughput screening platform, construction of a library seeking to accomplish this task has begun. While still in its early stages, a starting point for the general design of the library has been developed and a simple 2 step synthetic pathway that generates the majority of the desired isoxazoles has been identified and utilized. Almost all of the 2+3 cycloaddition reactions produce enough product for submission for biotesting, however, some of the observed low yields leave room for improvement from the chemistry side of this project. Therefore, with the recent implementation of a slight alteration in the order in which the reactions are conducted, identification of the cause for some of the observed low yields is expected. Afterwards, reaction condition optimizations of isoxazoles with yields under 50% will be conducted.

2.4.1. Experimental Section

2.4.1.1. General Information

All reactions were performed using oven-dried glassware that was kept in a dry argon environment. Solvents and other reagents were purchased from commercial venders and were used without further purification unless otherwise mentioned. Hydroxyamine hydrochloride, N-chlorosuccinimide, triethylamine (TEA), and pyridine were purchased from Sigma-Aldrich, USA. All benzaldehyde reagents for the 1,3-dipolar cycloaddition reaction were purchased from TCI [Tokyo Chemical Industry Co., Ltd., Japan]. The alkyne partners A – F were synthesized by Minji Kim and alkynes H and G were synthesized by Heejun Kim. The products were purified by flash column chromatography on silica gel (230 – 400 mesh) or by preparative thin-layer chromatography (prep TLC) on pre-coated glass-backed plates (silica gel 60 F_{254}m 1.0 mm). Thin-layer chromatography was performed on

pre-coated glass-backed plates (silica gel 60 F_{254}, 0.5 mm), and components were visualized by observation under UV light (254 and 365 nm) or by treating the plates with anisaldehyde, $KMnO_4$, and or phosphomolybdic acid followed by heating. Distilled water (DW) was polished by ion exchange and filtration. ^{1}H NMR and ^{13}C NMR spectra were recorded on a Bruker DRX-300 [Bruker Biospin, Germany] and Varian Inova-500 [Varian Assoc., USA] machines. Chemical shifts were measured in ppm, downfield from tetramethylsilane (TMS) as the internal standard. Multiplicites were indicated as follows: s (singlet), d (doublet), t (triplet), q (quartet), m (multiplet), dd (doublet of doublet), td (triplet of doublet), etc. Coupling constants were reported in Hz. Low resolution mass spectrometry (LRMS) analyses were performed with a Finnigan MSQ Plus Serveyer HPLC/MS system [Thermo Electron Corp., USA] using electron spray ionization (ESI).

2.4.1.2. Synthetic Procedures and Characterization

Oximes (1-16)

To a heated (60^{o}C) solution of a respective benzaldehyde (1 eq) and hydroxylamine hydrochloride (1.2 eq) dissolved in MeOH was added sodium acetate (1.2 eq). The reaction was left to stir between 4-20 hours until the aldehyde was fully consumed (TLC). The reaction was then quenched with brine and the product was extracted with ethyl acetate 3 times. The separated and combined organic layers were dried over anhydrous Na_2SO_4(s) and filtered through a celite-packed glass filter. The filtrate was concentrated under reduced pressure and purified with silica gel flash column chromatography (Yields 28-97%).

(3), 4-methoxybenzaldehyde oxime

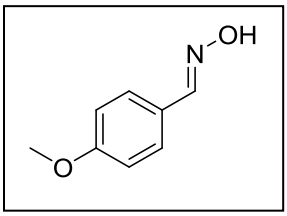

4-methoxybenzaldehyde (1.0 g, 7.35 mmol), reaction time: 12 hours, yield: 93%, R_f = 0.55 (1:2 = EtOAc:Hex, v/v); ^{1}H NMR (400 MHz, $CDCl_3$-*d*) δ 9.36 (s, 1H), 8.11 (s, 1H), 7.50 (d, *J* = 8.2 Hz, 2H), 6.89 (d, *J* = 7.9 Hz, 2H), 3.80 (s, 3H). ^{13}C NMR (101 MHz, $CDCl_3$-*d*) δ 160.2, 148.9, 132.2, 127.7, 123.5, 113.4, 76.5, 76.2, 75.8, 54.4. LRMS(ESI$^+$) m/z calcd for $C_8H_9NO_2$ $[M+H]^+$ 152.06 Found; 152.09

(5), 3-((hydroxyimino)methyl)benzonitrile

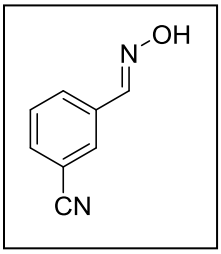

3-cyanobenzaldehyde (1.0 g, 7.63 mmol), reaction time: 12 hours, yield: 93%, R_f = 0.33 (1:2 = EtOAc:Hex, v/v); ^{1}H NMR (400 MHz, DMSO-d_6) δ 11.60 (s, 1H), 8.20 (s, 1H), 7.98 (s, 1H), 7.93 (d, *J* = 8.2 Hz, 1H), 7.83 (d, *J* = 8.2 Hz, 1H), 7.60 (t, *J* = 7.8 Hz, 1H). ^{13}C NMR (101 MHz, DMSO-d_6) δ 146.6, 134.4, 132.6, 130.5, 130.0, 118.5, 111.9, 101.5.

(7), 2-(trifluoromethyl)benzaldehyde oxime

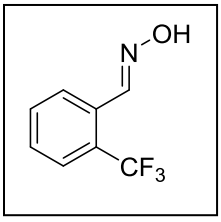

2-trifluoromethylbenzaldehyde (1.0 g, 7.63 mmol), reaction time: 12 hours, yield: 40%, R_f = 0.67 (1:2 = EtOAc:Hex, v/v); ^{1}H NMR (400 MHz, $CDCl_3$-*d*) δ 8.52 (s, 1H), 7.97 (d, *J* = 7.6 Hz, 1H), 7.68 (d, *J* = 7.6 Hz, 1H), 7.55 (t, *J* = 7.6 Hz, 1H), 7.48 (t, *J* = 7.5 Hz, 1H). ^{13}C NMR (101 MHz, $CDCl_3$-*d*) δ 147.38, 147.36, 132.20, 132.19, 132.2, 129.9, 127.4, 126.18, 126.12, 126.07, 126.01.

(12), 4-bromobenzaldehyde oxime

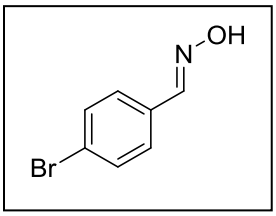

4-bromobenzaldehyde (1.0 g, 7.63 mmol), reaction time: 16 hours, yield: 28%, R_f = 0.73 (1:2 = EtOAc:Hex, v/v); ^{1}H NMR (400 MHz, $CDCl_3$-*d*) δ 8.39 (s, 1H), 8.10 (s, 1H), 7.61 – 7.35 (m, 4H). ^{13}C NMR (101 MHz, $CDCl_3$-*d*) δ 149.5, 132.2, 131.0, 128.6, 124.4

Isoxazoles (A1-E11)

To a dry THF solution containing the respective oxime (1-16) (1 eq) and N-chlorosuccinimide (1.1 eq) was added pyridine (0.1 eq). The mixture was stirred at 60^{o}C for 2h. To the stirring mixture was added the respective alkyne (A-H) (1 eq) pre-mixed with TEA (1.2 eq). [*For Alkyne A which has its hydroxyl group protected with TBDMS, 5% HF-Pyridine in THF solution was added to the mixture and left to stir for 2 hours. After reaction completion (TLC), the reaction was quenched with trimethylethoxy silane and the crude product was evaporated under reduced pressure to dryness. The crude product was purified with preparatory thin-layer chromatography (1:2 = EtOAC:n-hexanes, v/v) to provide isoxazoles A, yield: 20-65%*] The solution was left stirring for 1 h and then quenched with brine. The organic layer was separated and the aqueous layer was further extracted two more times with EA. The separated and combined organic layers were dried over anhydrous $MgSO_4$(s) and filtered through a celite-packed glass filter. The filtrate was concentrated under reduced pressure and purified with preparatory thin-layer chromatography (1:2 = EtOAC:n-hexanes, v/v) to provide isoxazoles C and E, yield: 20-65%]

(A1), *3-(3-(2-methoxyphenyl)isoxazol-5-yl)-2,2-dimethyl-2H-chromen-7-ol*

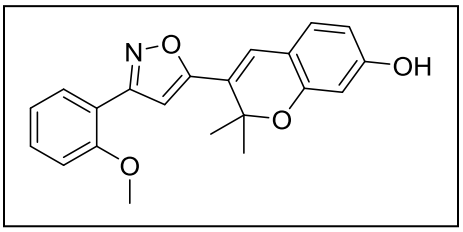

Oxime 1 (35 mg, 0.23 mmol), reaction time: 10 hours, yield: 46%, R_f = 0.40 (1:2 = EtOAc:Hex, v/v); ^{1}H NMR (400 MHz, $CDCl_3$-*d*) δ 8.63 (s, 1H), 7.88 (d, *J* = 7.6 Hz, 1H), 7.47 – 7.33 (m, 1H), 7.11 – 6.95 (m, 3H), 6.93 (s, 1H), 6.77 (d, *J* = 1.3 Hz, 1H), 6.48 – 6.36 (m, 2H), 3.92 (s, 3H), 1.69 (s, 6H).

(A3), *3-(3-(4-methoxyphenyl)isoxazol-5-yl)-2,2-dimethyl-2H-chromen-7-ol*

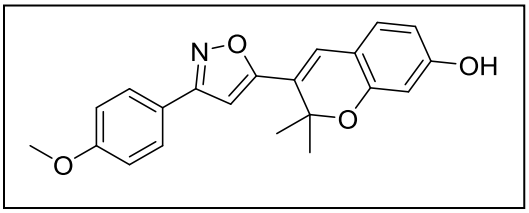

Oxime 3 (20 mg, 0.13 mmol), reaction time: 20 hours, yield: 28%, R_f = 0.38 (1:2 = EtOAc:Hex, v/v); ^{1}H NMR (400 MHz, Methanol-d_4) δ 7.78 (d, *J* = 8.3 Hz, 2H), 7.05 – 6.95 (m, 4H), 6.82 (s, 1H), 6.37 (dd, *J* = 8.2, 2.4 Hz, 1H), 6.27 (d, *J* = 3.1 Hz, 1H), 3.83 (s, 3H), 1.64 (s, 6H).

(A4), *2-(5-(7-hydroxy-2,2-dimethyl-2H-chromen-3-yl)isoxazol-3-yl)benzonitrile*

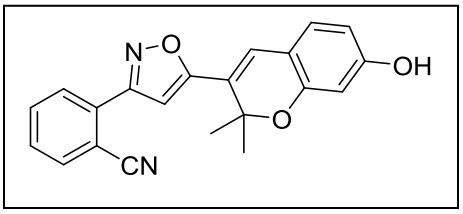

Oxime 4 (20 mg, 0.13 mmol), reaction time: 20 hours, yield: 28%, R_f = 0.34 (1:2 = EtOAc:Hex, v/v); ^{1}H NMR (400 MHz, Acetone-d_6) δ 8.84 (s, 1H), 7.99 (dddd, *J* = 11.9, 7.7, 1.5, 0.8 Hz, 2H), 7.87 (tdd, *J* = 7.9, 1.4, 0.8 Hz, 1H), 7.73 (tt, *J* = 7.7, 1.0 Hz, 1H), 7.20 – 7.05 (m, 3H), 6.47 (ddd, *J* = 8.2, 2.3, 0.8 Hz, 1H), 6.36 (d, *J* = 2.3 Hz, 1H), 1.68 (s, 6H).

(A5), *3-(5-(7-hydroxy-2,2-dimethyl-2H-chromen-3-yl)isoxazol-3-yl)benzonitrile*

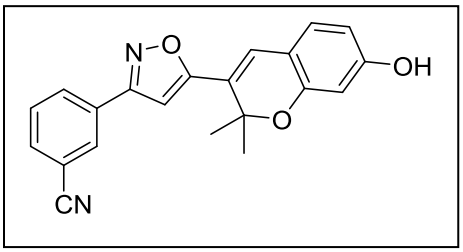

Oxime 5 (20 mg, 0.13 mmol), reaction time: 20 hours, yield: 29%, R_f = 0.36 (1:2 = EtOAc:Hex, v/v); ^{1}H NMR (400 MHz, $CDCl_3$-*d*) δ 8.09 (d, *J* = 8.8 Hz, 2H), 7.75 (d, *J* = 7.6 Hz, 1H), 7.59 (t, *J* = 6.4 Hz, 1H), 7.01 (d, *J* = 8.2 Hz, 1H), 6.97 (s, 1H), 6.57 (s, 1H), 6.43 (dd, *J* = 8.1, 2.4 Hz, 1H), 6.38 (s, 1H), 1.69 (s, 6H).

(A6), *4-(5-(7-hydroxy-2,2-dimethyl-2H-chromen-3-yl)isoxazol-3-yl)benzonitrile*

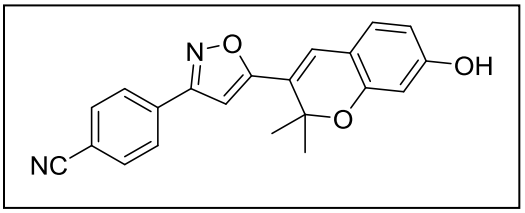

Oxime 6 (20 mg, 0.13 mmol), reaction time: 20 hours, yield: 30%, R_f = 0.37 (1:2 = EtOAc:Hex, v/v); ^{1}H NMR (400 MHz, Acetone-d_6) δ 8.86 (s, 1H), 8.15 (d, *J* = 8.4 Hz, 2H), 7.94 (d, *J* = 8.4 Hz, 2H), 7.16 (d, *J* = 23.9 Hz, 2H), 7.11 (d, *J* = 8.2 Hz, 1H), 6.47 (dd, *J* = 8.2, 2.3 Hz, 1H), 6.36 (d, *J* = 2.0 Hz, 1H), 1.68 (s, 6H).

(A7), *2,2-dimethyl-3-(3-(2-(trifluoromethyl)phenyl)isoxazol-5-yl)-2H-chromen-7-ol*

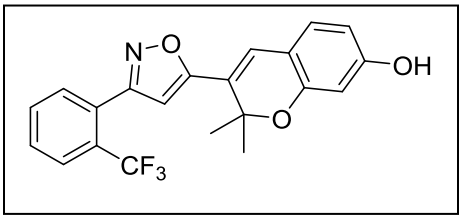

Oxime 7 (20 mg, 0.10 mmol), reaction time: 20 hours, yield: 25%, R_f = 0.25 (1:2 = EtOAc:Hex, v/v); ^{1}H NMR (400 MHz, $CDCl_3$-*d*) δ 7.82 (d, *J* = 7.2 Hz, 1H), 7.72 – 7.55 (m, 3H), 7.00 (d, *J* = 8.1 Hz, 1H), 6.96 (s, 1H), 6.45 (s, 1H), 6.40 (dd, *J* = 8.1, 2.4 Hz, 1H), 6.37 (d, *J* = 2.4 Hz, 1H), 1.68 (s, 6H).

(A8), *2,2-dimethyl-3-(3-(3-(trifluoromethyl)phenyl)isoxazol-5-yl)-2H-chromen-7-ol*

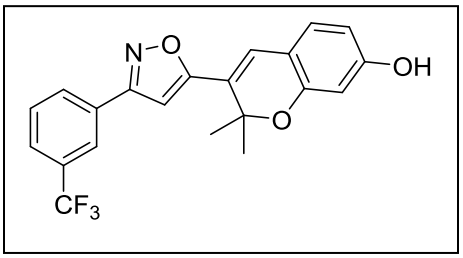

Oxime 8 (20 mg, 0.13 mmol), reaction time: 20 hours, yield: 31%, R_f = 0.22 (1:2 = EtOAc:Hex, v/v); ^{1}H NMR (400 MHz, $CDCl_3$-*d*) δ 8.06 (s, 1H), 8.03 (d, *J* = 8.0 Hz, 1H), 7.72 (d, *J* = 8.5 Hz, 1H), 7.61 (t, *J* = 7.8 Hz, 1H), 7.01 (d, *J* = 8.2 Hz, 1H), 6.97 (s, 1H), 6.60 (s, 1H), 6.42 (dd, *J* = 8.1, 2.4 Hz, 1H), 6.38 (d, *J* = 2.4 Hz, 1H), 1.70 (s, 6H).

(A9), *2,2-dimethyl-3-(3-(4-(trifluoromethyl)phenyl)isoxazol-5-yl)-2H-chromen-7-ol*

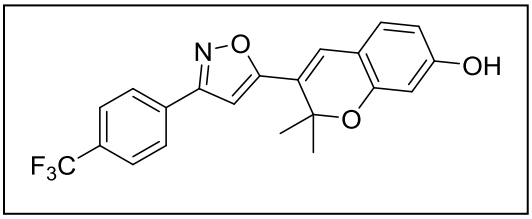

Oxime 9 (20 mg, 0.13 mmol), reaction time: 18 hours, yield: 32%, R_f = 0.20 (1:2 = EtOAc:Hex, v/v); ^{1}H NMR (400 MHz, $CDCl_3$-*d*) δ 7.95 (d, *J* = 8.1 Hz, 2H), 7.74 (d, *J* = 8.2 Hz, 2H), 7.01 (d, *J* = 8.2 Hz, 1H), 6.97 (s, 1H), 6.59 (s, 1H), 6.42 (d, *J* = 8.1 Hz, 1H), 6.39 (s, 1H), 1.70 (s, 6H).

(C1), *5-(1H-indol-6-yl)-3-(2-methoxyphenyl)isoxazole*

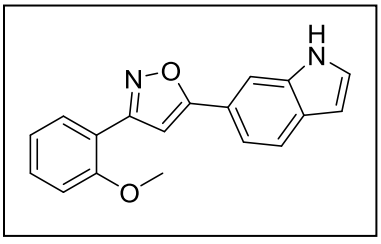

Oxime 1 (30 mg, 0.20 mmol), reaction time: 18 hours, yield: 62%, R_f = 0.33 (1:2 = EtOAc:Hex, v/v); ^{1}H NMR (500 MHz, $CDCl_3$-*d*) δ 8.73 (s, 1H), 8.20 (dt, *J* = 1.6, 0.7 Hz, 1H), 7.98 (dd, *J* = 7.6, 1.8 Hz, 1H), 7.70 (dd, *J* = 8.5, 1.7 Hz, 1H), 7.50 – 7.41 (m, 2H), 7.27 (dd, *J* = 3.3, 2.3 Hz, 1H), 7.09 (td, *J* = 7.5, 1.1 Hz, 1H), 7.05 (dd, *J* = 8.3, 1.0 Hz, 1H), 7.02 (s, 1H), 6.66 – 6.65 (m, 1H), 3.94 (s, 3H).

(C6), *4-(5-(1H-indol-6-yl)isoxazol-3-yl)benzonitrile*

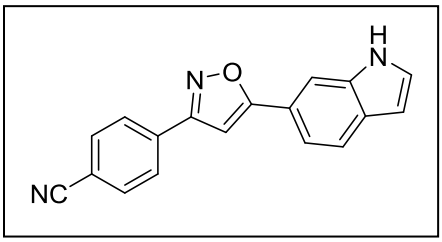

Oxime 6 (30 mg, 0.21 mmol), reaction time: 20 hours, yield: 10%, R_f = 0.31 (1:2 = EtOAc:Hex, v/v); ^{1}H NMR (500 MHz, DMSO-d_6) δ 11.46 (s, 1H), 8.17 – 8.09 (m, 3H), 8.04 (d, *J* = 8.0 Hz, 2H), 7.69 – 7.54 (m, 3H), 7.48 (t, *J* = 2.8 Hz, 1H), 6.59 (td, *J* = 2.1, 1.0 Hz, 1H).

(C7), *5-(1H-indol-6-yl)-3-(2-(trifluoromethyl)phenyl)isoxazole*

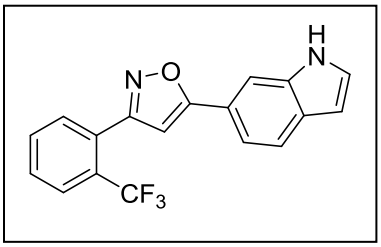

Oxime 7 (30 mg, 0.16 mmol), reaction time: 20 hours, yield: 77%, R_f = 0.43 (1:2 = EtOAc:Hex, v/v); ^{1}H NMR (500 MHz, $CDCl_3$-*d*) δ 8.64 (s, 1H), 8.22 – 8.16 (m, 1H), 7.84 (d, *J* = 7.1 Hz, 1H), 7.73 (d, *J* = 7.6 Hz, 1H), 7.70 – 7.63 (m, 2H), 7.63 – 7.58 (m, 1H), 7.47 (d, *J* = 8.5 Hz, 1H), 7.28 – 7.26 (m, 1H), 6.70 (d, *J* = 0.9 Hz, 1H), 6.66 (ddd, *J* = 3.1, 2.0, 0.9 Hz, 1H).

(C9), *5-(1H-indol-6-yl)-3-(4-(trifluoromethyl)phenyl)isoxazole*

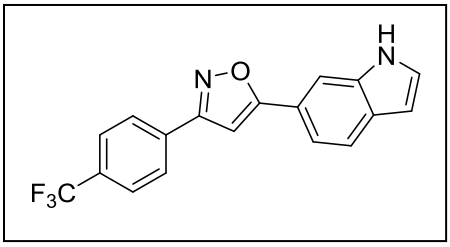

Oxime 9 (30 mg, 0.16 mmol), reaction time: 20 hours, yield: 41%, R_f = 0.45 (1:2 = EtOAc:Hex, v/v); ^{1}H NMR (500 MHz, DMSO-d_6) δ 11.47 (s, 1H), 8.20 – 8.10 (m, 3H), 7.91 (d, *J* = 8.1 Hz, 2H), 7.66 (dd, *J* = 8.5, 1.7 Hz, 1H), 7.57 (d, *J* = 12.4 Hz, 2H), 7.48 (t, *J* = 2.7 Hz, 1H), 6.59 (s, 1H).

(C12), *3-(4-bromophenyl)-5-(1H-indol-6-yl)isoxazole*

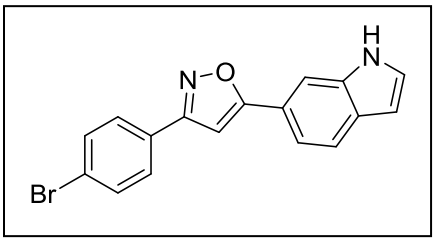

Oxime 12 (30 mg, 0.15 mmol), reaction time: 20 hours, yield: 22%, R_f = 0.46 (1:2 = EtOAc:Hex, v/v); ^{1}H NMR (500 MHz, DMSO-d_6) δ 11.44 (s, 1H), 8.14 (s, 1H), 7.88 (d, *J* = 8.5 Hz, 2H), 7.76 (d, *J* = 8.6 Hz, 2H), 7.60 (ddd, *J* = 38.4, 8.4, 1.2 Hz, 2H), 7.47 (s, 2H), 6.58 (td, *J* = 2.1, 1.0 Hz, 1H).

(E1), *3-(2-methoxyphenyl)-5-(quinolin-2-yl)isoxazole*

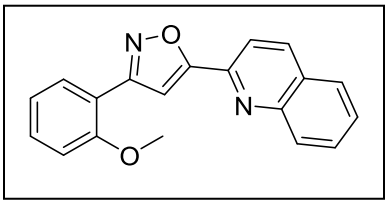

Oxime 1 (30 mg, 0.19 mmol), reaction time: 24 hours, yield: 70%, R_f = 0.67 (DCM); ^{1}H NMR (400 MHz, Acetone-d_6) δ 8.47 (d, *J* = 8.4 Hz, 1H), 8.18 – 8.05 (m, 2H), 8.03 – 7.93 (m, 2H), 7.82 (t, *J* = 8.4 Hz, 1H), 7.69 – 7.58 (m, 2H), 7.54 – 7.42 (m, 1H), 7.19 (td, *J* = 5.9, 5.5, 2.5 Hz, 1H), 7.09 (t, *J* = 7.5 Hz, 1H), 3.97 (s, 3H).

(E3), *3-(4-methoxyphenyl)-5-(quinolin-2-yl)isoxazole*

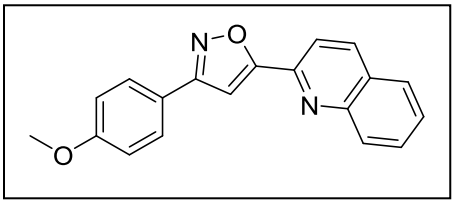

Oxime 3 (30 mg, 0.19 mmol), reaction time: 24 hours, yield: 25%, R_f = 0.53 (DCM); ^{1}H NMR (500 MHz, $CDCl_3$-*d*) δ 8.30 (d, *J* = 8.5 Hz, 1H), 8.16 (d, *J* = 8.5 Hz, 1H), 8.06 (d, *J* = 8.5 Hz, 1H), 7.91 – 7.83 (m, 3H), 7.80 – 7.74 (m, 1H), 7.63 – 7.57 (m, 1H), 7.38 (s, 1H), 7.01 (d, *J* = 8.5 Hz, 2H), 3.87 (s, 3H).

(E7), *5-(quinolin-2-yl)-3-(2-(trifluoromethyl)phenyl)isoxazole*

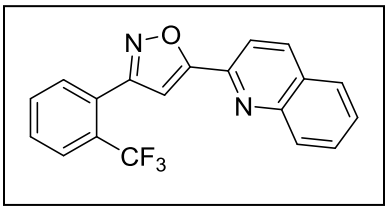

Oxime 7 (30 mg, 0.15 mmol), reaction time: 24 hours, yield: 76%, R_f = 0.70 (DCM); ^{1}H NMR (500 MHz, Acetone-d_6) δ 8.53 (d, *J* = 8.5 Hz, 1H), 8.13 (dd, *J* = 8.5, 3.4 Hz, 2H), 8.02 (d, *J* = 8.2 Hz, 1H), 7.96 (d, *J* = 7.8 Hz, 1H), 7.88 – 7.75 (m, 4H), 7.67 (ddd, *J* = 8.1, 6.5, 1.2 Hz, 1H), 7.39 (s, 1H).

(E8), *5-(quinolin-2-yl)-3-(3-(trifluoromethyl)phenyl)isoxazole*

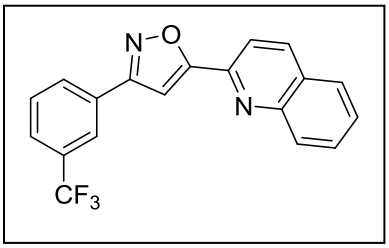

Oxime 8 (30 mg, 0.15 mmol), reaction time: 24 hours, yield: 49%, R_f = 0.75 (DCM); ^{1}H NMR (400 MHz, $CDCl_3$-*d*) δ 8.42 – 8.30 (m, 1H), 8.29 – 8.05 (m, 4H), 7.98 – 7.74 (m, 3H), 7.73 – 7.59 (m, 2H), 7.56 – 7.50 (m, 1H).

(E9), *5-(quinolin-2-yl)-3-(4-(trifluoromethyl)phenyl)isoxazole*

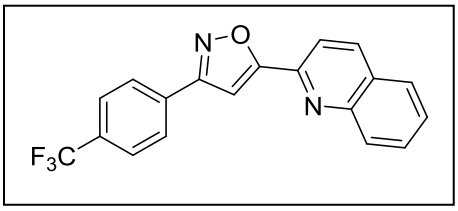

Oxime 9 (30 mg, 0.15 mmol), reaction time: 24 hours, yield: 55%, R_f = 0.75 (DCM); ^{1}H NMR (400 MHz, $CDCl_3$-*d*) δ 8.32 (dd, *J* = 8.7, 4.0 Hz, 1H), 8.17 (dd, *J* = 8.7, 3.8 Hz, 1H), 8.09 – 8.05 (m, 3H), 7.88 (dd, *J* = 8.2, 3.7 Hz, 1H), 7.82 – 7.76 (m, 3H), 7.66 – 7.56 (m, 1H), 7.47 (d, *J* = 5.5 Hz, 1H).

(E10), *3-(2-chlorophenyl)-5-(quinolin-2-yl)isoxazole*

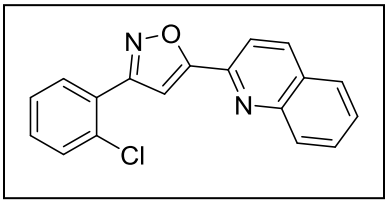

Oxime 10 (30 mg, 0.18 mmol), reaction time: 24 hours, yield: 4%, R_f = 0.56 (DCM); ^{1}H NMR (400 MHz, Acetone-d_6) δ 8.59 (d, *J* = 8.6 Hz, 1H), 8.21 – 8.12 (m, 2H), 8.07 (d, *J* = 7.8 Hz, 1H), 7.89 – 7.85 (m, 2H), 7.75 – 7.50 (m, 5H).

(E11), *3-(3-fluorophenyl)-5-(quinolin-2-yl)isoxazole*

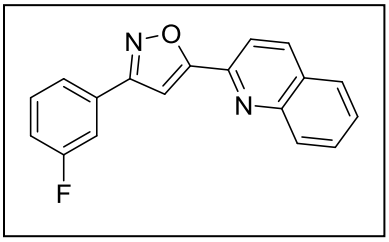

Oxime 11 (30 mg, 0.20 mmol), reaction time: 24 hours, yield: 5%, R_f = 0.55 (DCM); ^{1}H NMR (400 MHz, Acetone-d_6) δ 8.58 (d, *J* = 8.5 Hz, 1H), 8.15 (d, *J* = 8.6 Hz, 2H), 8.06 (d, *J* = 8.4 Hz, 1H), 7.96 – 7.79 (m, 3H), 7.77 – 7.58 (m, 3H), 7.39 – 7.28 (m, 1H).

2.5.1 References

1 https://www.alz.org/facts/overview.asp

2 Braak H, Braak E., *Acta Neuropathol*, 1991, 82, 239–259

3 Ganesh M Shankar, *Molecular Neurodegeneration* 2009, **4**, 48

4 K. Broerson., *Alzheimers Res. Ther.*, 2010, 2[4]

5 Rosenblum, William I. *Neurobiology of Aging*, 2013, 35(5), 969-974

6 Walsh DM., *J Neurochem*. 2007 Jun, 101(5), 1172-84

7 Bruce T. Lamb., *The Journal of Neuroscience*, 2008, 28(43): 10786-10793

8 William L. Klein., *The Journal of Biological Chemistry*, 2007, 282, 11590-11601

9 William L. Klein., *FASEB J*, 2008, 22:246-260

10 U. Ebert., C. Bruehl., *The Journal of Neuroscience*, 2008, 28(4): 788-797

11 Klionsky D. J., Emr S. D., *Science*, 2000, 290, 1717–1721

12 Komatsu M., *Nature*, 2006, *441, 880–884*

13 Mizushima N., Levine B., Cuervo A. M., Klionsky D. J., *Nature*, 2008, *451, 1069–1075*

14 S.B. Park, *Chem. Sci*., 2013, 4, 3282

15 http://www.lifetechnologies.com/content/dam/LifeTech/migration/images/cell-analysis/data.par.89173.image.-1.-1.1.gif

국문초록

Pavel Printsev (현수)
서울대학교 자연과학대학원 화학부

1장: 핵 호르몬 수용체인 퍼옥시좀 증식자 활성화 수용체 (peroxisome proliferator-activated receptors, PPAR) 는 포도당 및 지방 대사에서 중요한 역할을 담당하는 전사 인자이다. 많은 연구자들은 PPAR 단백질들과 상호작용 할 수 있는 저분자 물질을 발굴하고 이를 통해 유전자 발현을 조절하여 원하는 생물학적 변화를 유도하는데 관심을 기울이고 있다. 하지만 PPARγ 의 과도한 활성은 일련의 심각한 부작용들과 연관이 있으며, 최근의 연구들을 통해 사이클린의존성 인산화효소 5 (CDK5) 매개 PPARγ 인산화 저해는 인슐린 민감 유전자들을 상향 조절한다는 결과들이 발표되고 있다. 이러한 연구 결과들을 고려하여, 본 학위 논문에서는 PPARγ에 아고니즘 효과가 없으면서 동시에 PPARγ 의 Ser273 자리에 인산화를 저해하기 위한 아이소옥사졸 기반 저분자 물질의 합리적 디자인과 이들의 생물학적 결과에 대한 연구 성과를 기술하고 있다.
본 논문에서의 분자들은 크게 세 가지 종류 (카바메이트, 유레아, 아마이드)로 나뉘는데 각각의 분자군들은 분자 경직성과 곁가지의 전자적 환경에 차이를 두어 디자인되었다. 세 분자군의 합성과 생물학적 평가는 병렬적으로 진행되었으며, 각각 분자군들에서 도출된 생물학적 결과들은 타 분자군의 새로운 물질을 디자인할 때 상호적으로 영향을 주어, 궁극적으로 가장 우수한 효과를 지니는 분자의 도출로 수렴되고 있다. 합성된 모든 분자들은 웨스턴 블로팅을 통해 CDK5 매개 인산화에 대한 저해 효과를 관찰하였고, 이 중 선별된 분자들은 전사 활성 분석 시험을 통해 PPARγ 에 대한 아고니즘 효과를 관찰하였다. 그리고 도킹 시뮬레이션을 수행하여 합성된 리간드와 PPARγ 결합포켓와의 가능한 상호작용을 알아보고 이를 생물학적 결과와 비교해 보았으며, 이를 통해 새로운 분자

디자인을 위한 정보들을 도출하고자 하였다. 결과적으로 유레아 분자군이 전반적으로 PPARγ 에 낮은 아고니즘 효과와 우수한 인산화 저해 효과를 보이는 분자군임이 밝혀졌고, 카바메이트 그리고 아마이드 분자군이 그 뒤를 이었다.

2장 : 1장에서 연구한 아이소옥사졸 기반 리간드를 바탕으로 자가소화작용 조절을 위한 새로운 분자 라이브러리 합성을 진행하였다. 자가소화작용은 기능이 손상되었거나 불필요해진 세포질 물질들을 라이소솜으로 보내 분해하는 중요한 생체 내 분해 시스템이다. 뇌 세포의 안팎에서 발생하는 아밀로이드 베타 플라크들의 응집은 자가소화작용과 연관관계가 있음이 밝혀지고 있으며, 아밀로이드 베타 플라크들의 축적은 알츠하이머 질병을 일으키는 가장 중요한 원인이 된다. 기존에 표현형 기반 HTS을 통해 찾아낸 유효화합물(P41H06)에서부터 시작하여 우리는 자가소화작용을 조절할 수 있는 새로운 화합물들을 발견하고자 확장된 라이브러리를 디자인하였다. 자가소화작용의 과도한 증가로 발생할 수 있는 여러 부작용들로부터 벗어나기 위해, 새로 합성하는 라이브러리는 세포 독성이 없이 비침습적으로 자가소화작용을 조절할 수 있는 분자의 도출에 초점을 맞추고 있다.

주요어 : PPAR, 합리적 분자 디자인, 인산화 저해, Ser273, 파셜 아고니스트, 아밀로이드 베타, 자가소화작용 조절, 저분자 조절 물질, SF44

학번 : 2013-22445

Appendix

(NMR Spectra)

Chapter 1

The Rational Design and Synthesis of novel PPARγ Phosphorylation Inhibiting Agonism-Free Ligands

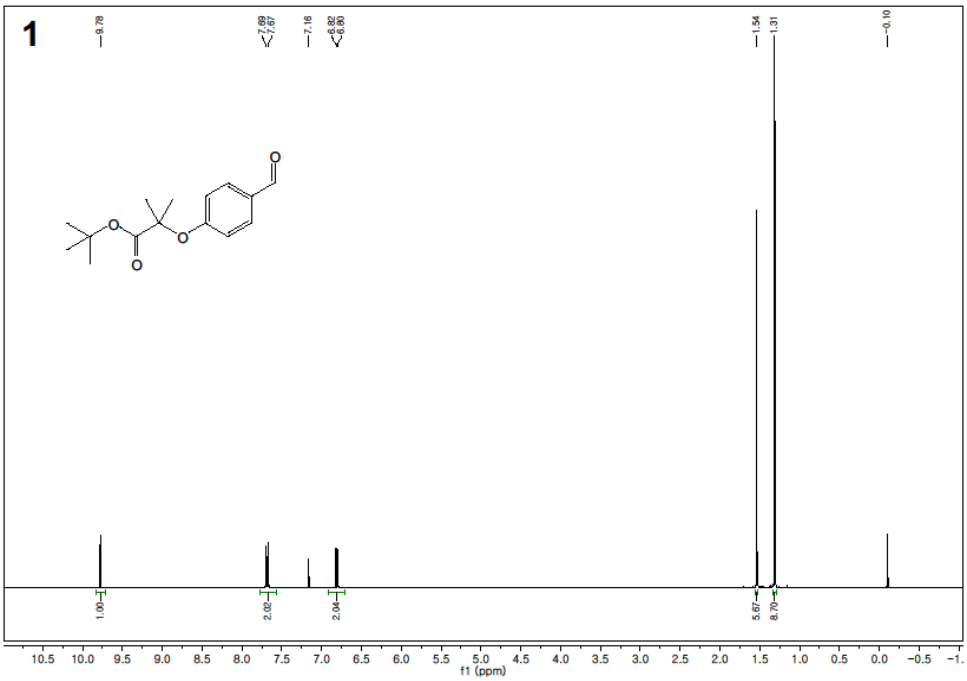
1
9.78
7.69
7.67
7.16
6.82
6.80
1.54
1.31
0.10
O
O
O
O
1.00
2.02
2.04
5.67
8.70
f1 (ppm)

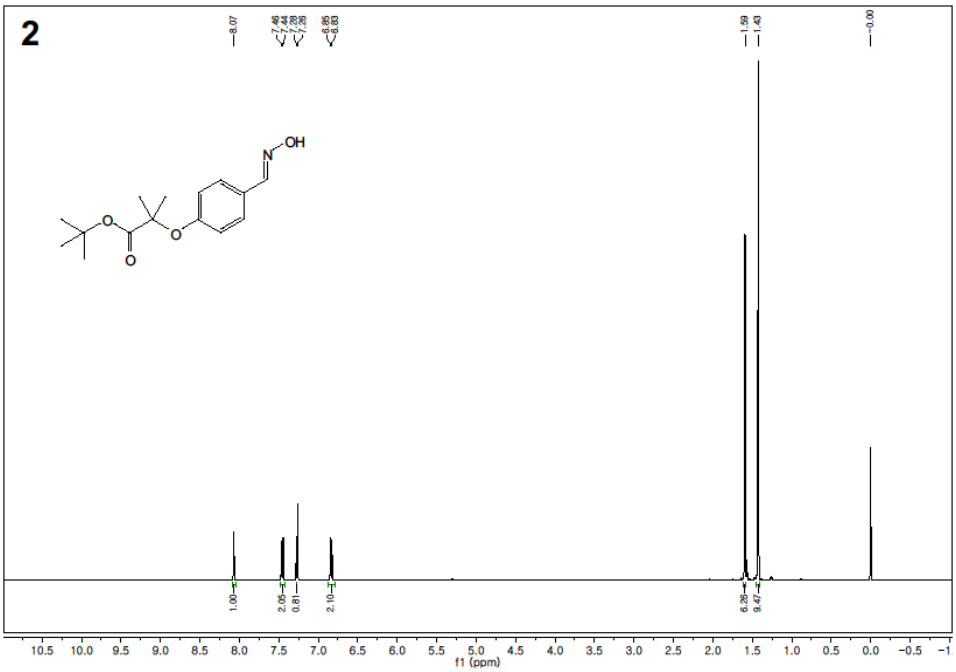
2
8.07
7.46
7.44
7.29
7.26
6.85
6.83
1.59
1.43
0.00
N
OH
O
O
O
1.00
2.05
0.81
2.10
6.26
9.47
f1 (ppm)

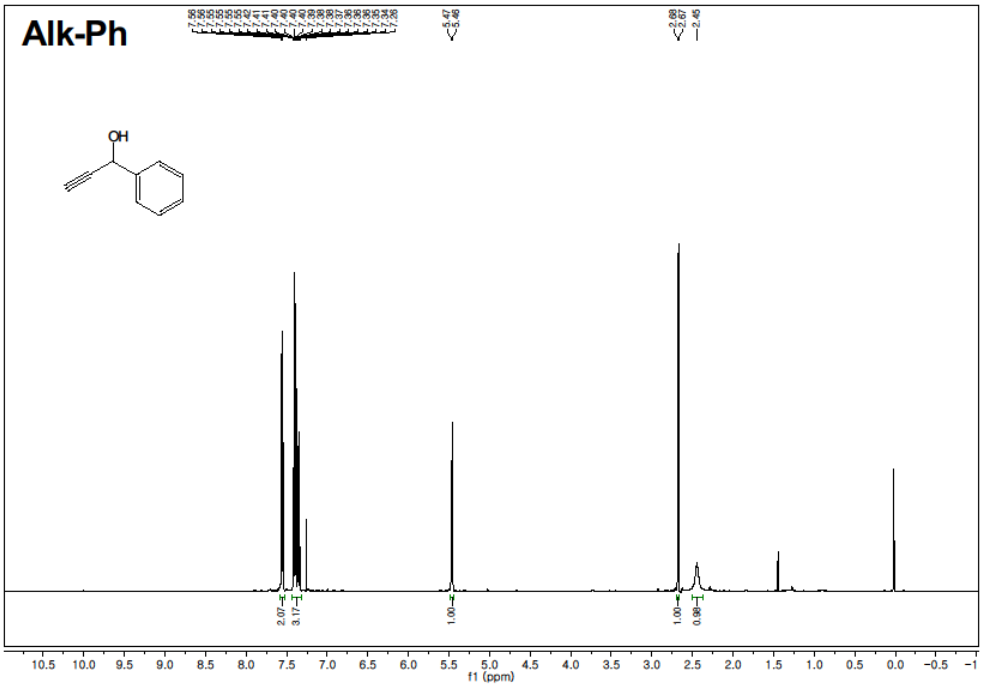
Alk-Ph
OH
7.56
7.55
7.55
7.55
7.55
7.55
7.55
7.52
7.42
7.41
7.40
7.40
7.40
7.40
7.39
7.39
7.39
7.37
7.36
7.36
7.35
7.35
7.34
7.26
5.47
5.46
2.68
2.67
2.45
2.07
3.17
1.00
1.00
0.88
10.5 10.0 9.5 9.0 8.5 8.0 7.5 7.0 6.5 6.0 5.5 5.0 4.5 4.0 3.5 3.0 2.5 2.0 1.5 1.0 0.5 0.0 −0.5 −1
f1 (ppm)

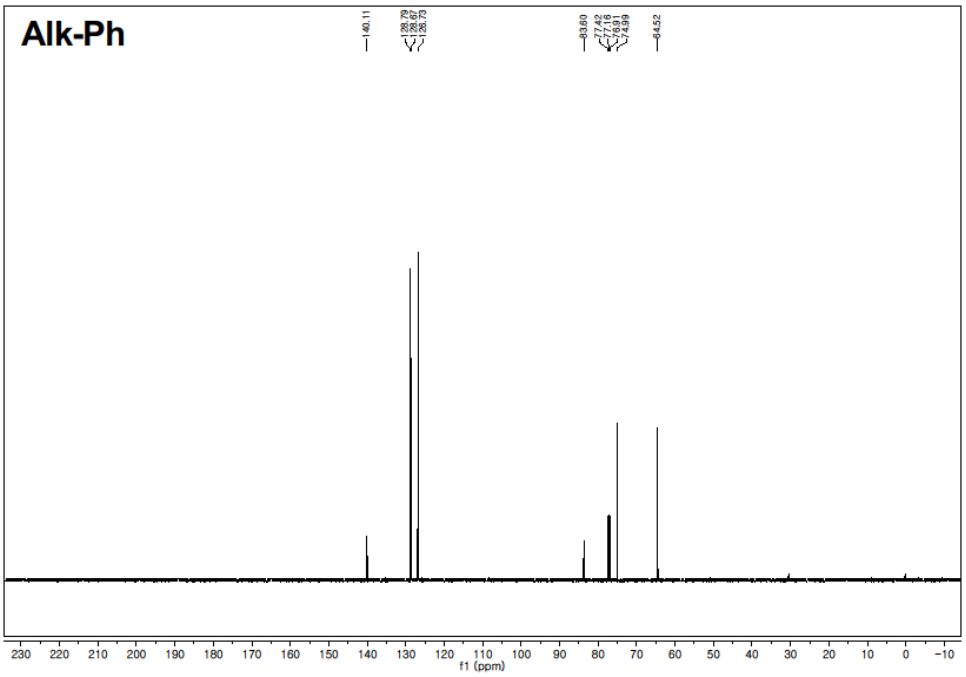
Alk-Ph
140.11
128.79
128.67
128.70
83.60
77.42
77.16
76.91
74.99
64.52
230 220 210 200 190 180 170 160 150 140 130 120 110 100 90 80 70 60 50 40 30 20 10 0 −10
f1 (ppm)

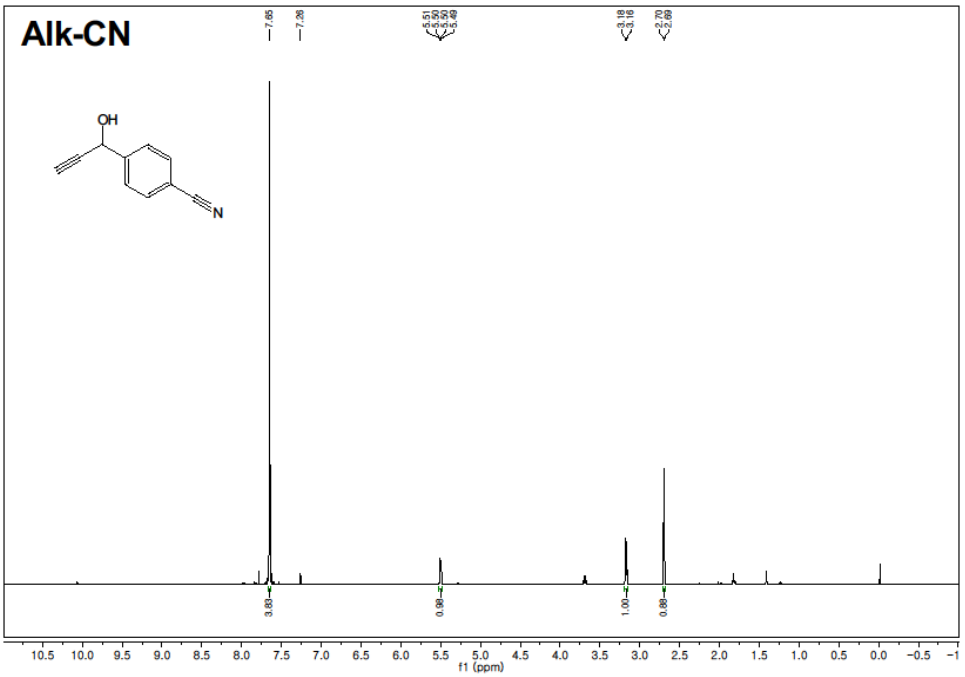
Alk-CN
OH
N
7.65
7.36
5.51
5.50
5.50
5.49
3.18
3.16
2.70
2.69
3.83
0.98
1.00
0.88
f1 (ppm)

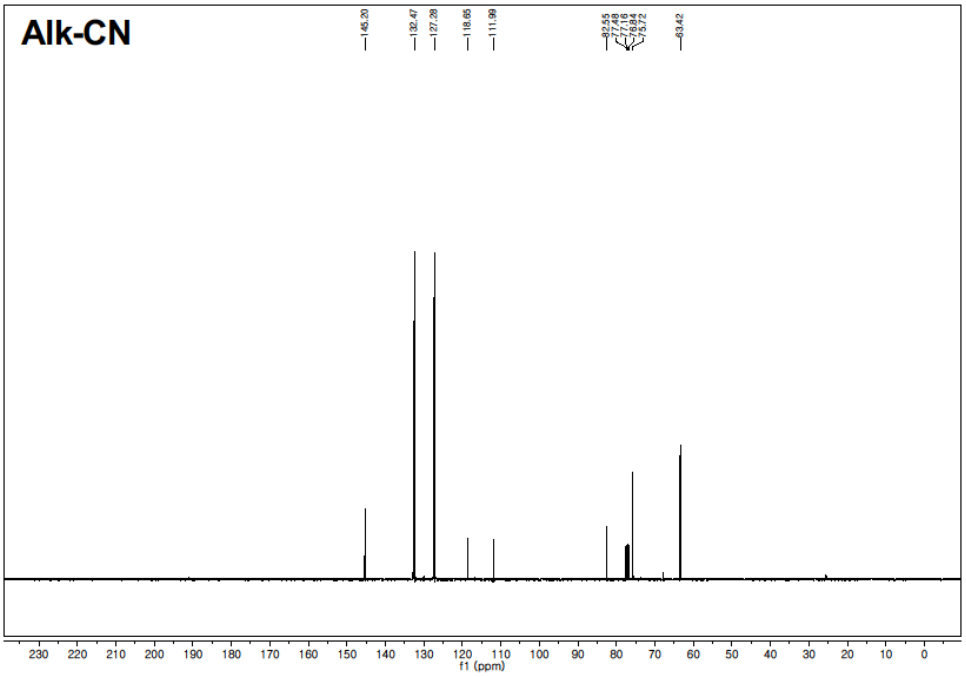
Alk-CN
145.20
132.47
127.28
118.65
111.99
82.55
77.48
77.16
76.84
75.72
63.42
f1 (ppm)

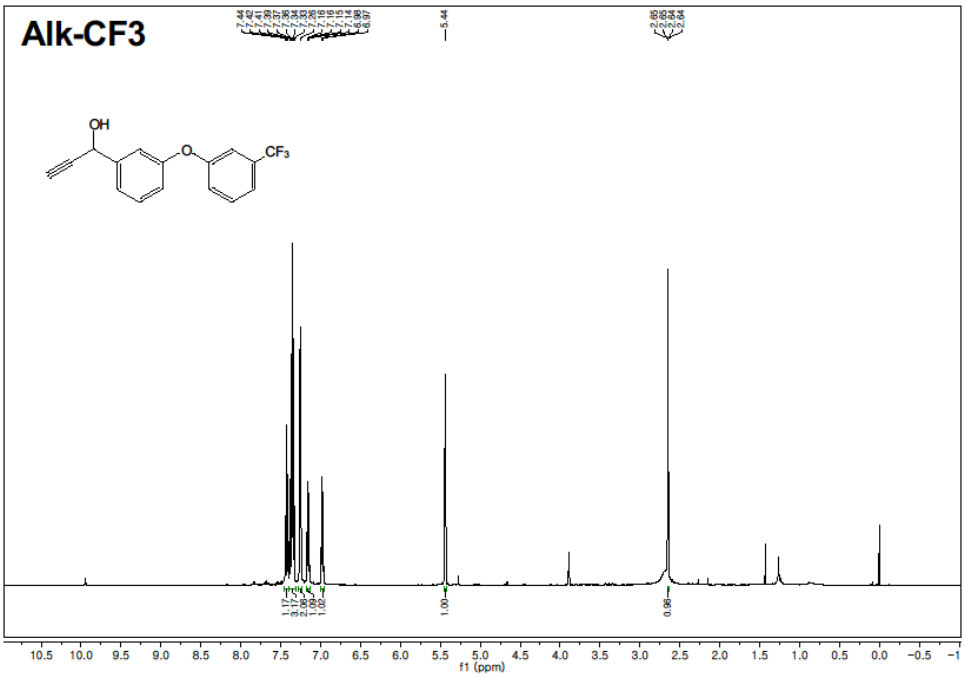
Alk-CF3
OH
O
CF3
f1 (ppm)

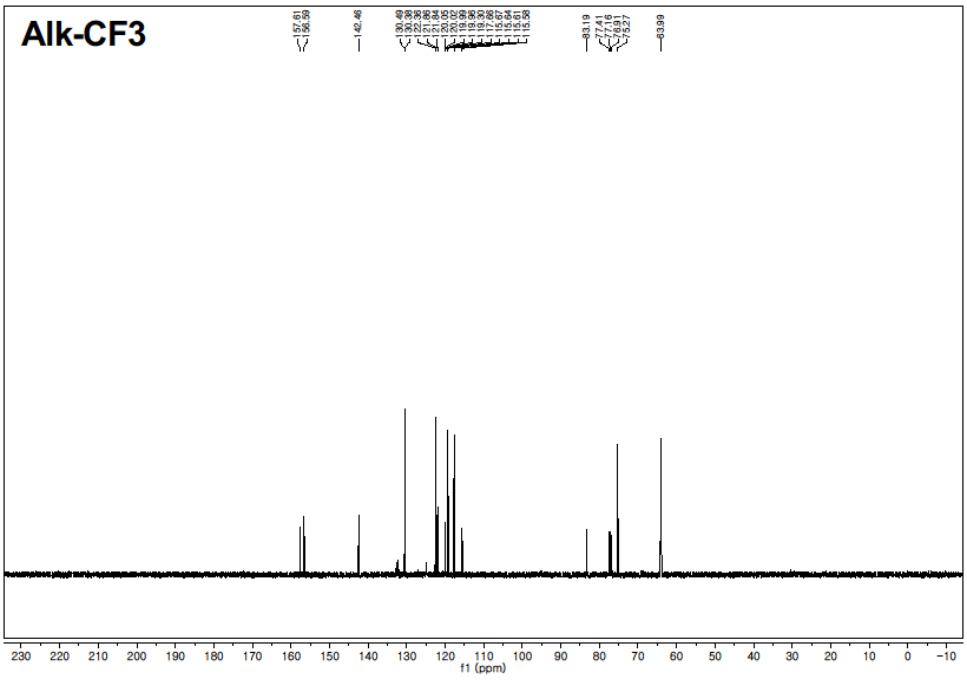
Alk-CF3
f1 (ppm)

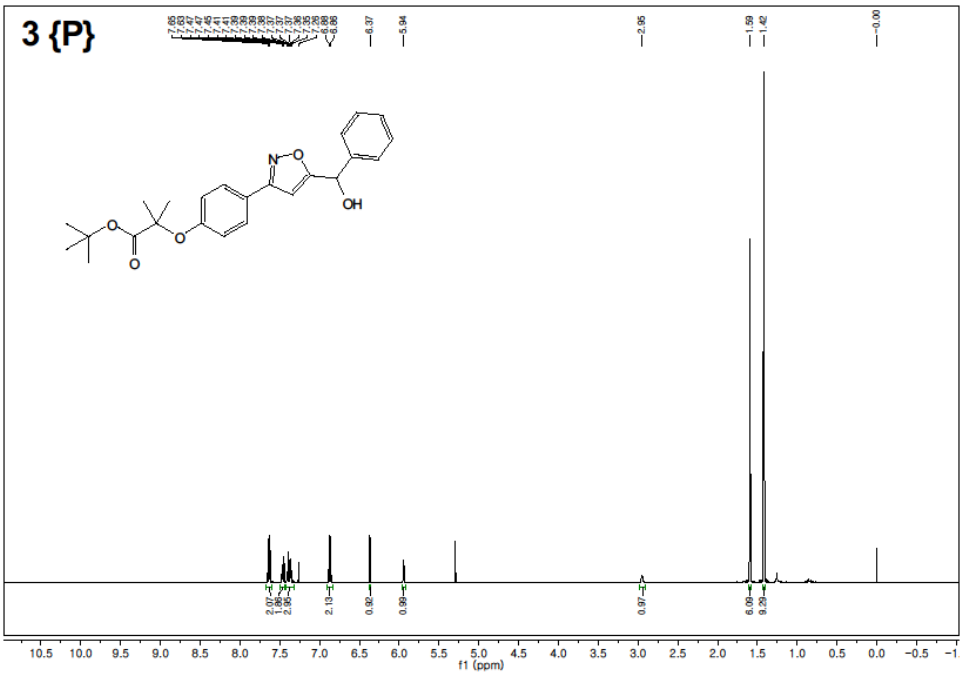
3 {P}
f1 (ppm)

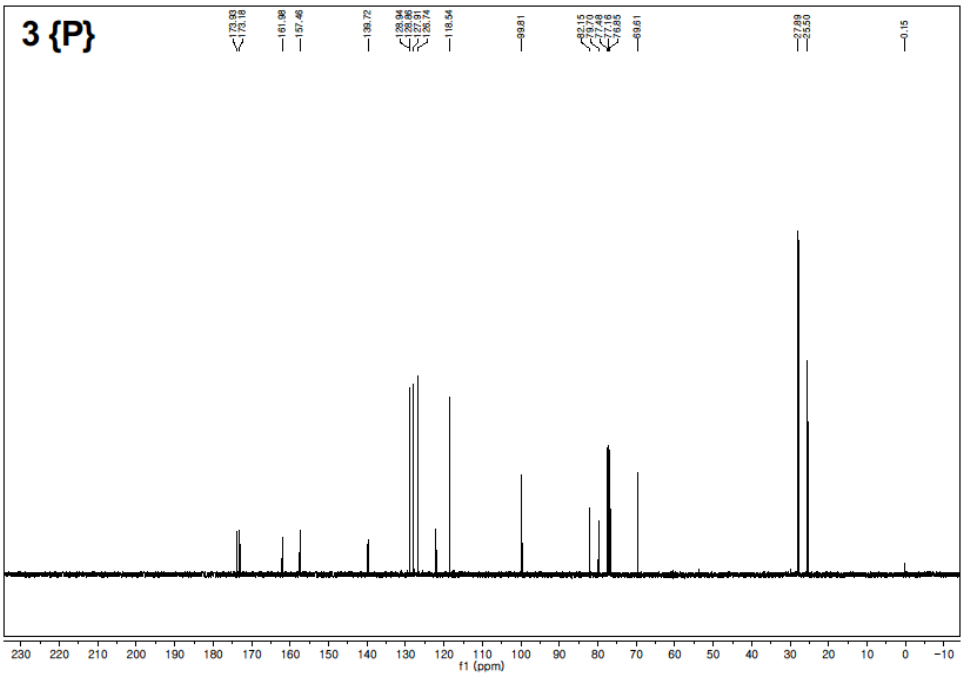
3 {P}
f1 (ppm)

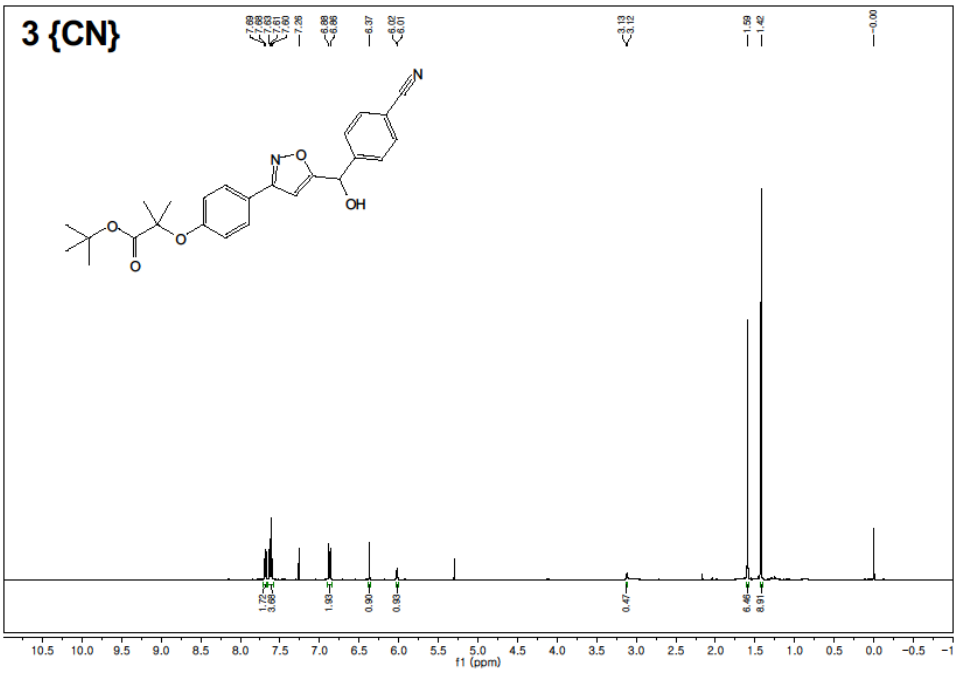
3 {CN}
7.69
7.68
7.61
7.60
7.60
7.26
6.88
6.86
8.37
6.02
6.01
3.13
3.12
1.59
1.42
0.00
N
O
OH
O
O
O
1.72
3.68
1.83
0.90
0.83
0.47
6.46
8.91
10.5 10.0 9.5 9.0 8.5 8.0 7.5 7.0 6.5 6.0 5.5 5.0 4.5 4.0 3.5 3.0 2.5 2.0 1.5 1.0 0.5 0.0 −0.5 −1
f1 (ppm)

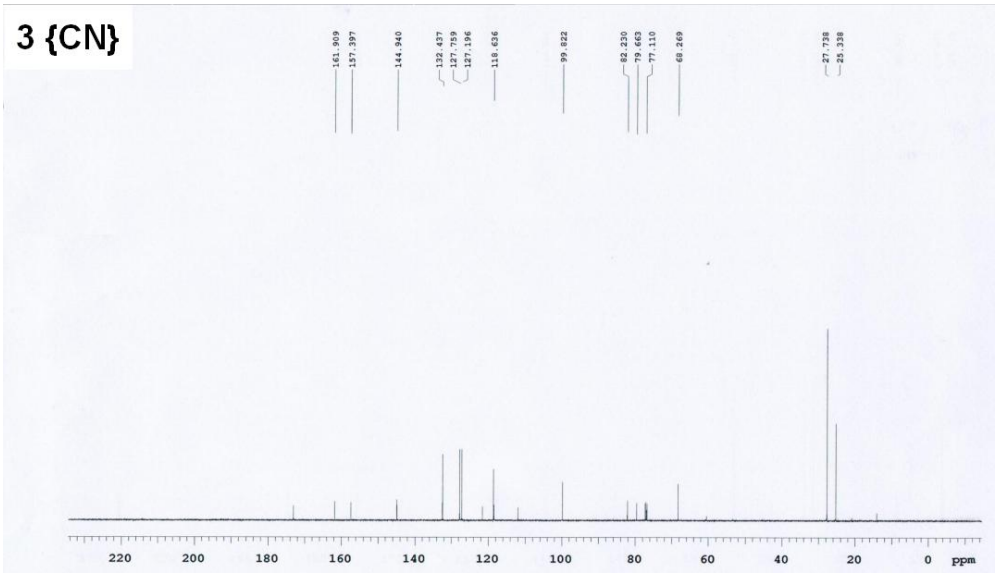
3 {CN}
161.909
157.397
144.940
132.437
127.759
127.196
118.636
99.822
82.230
79.663
77.110
69.269
27.738
25.338
220 200 180 160 140 120 100 80 60 40 20 0 ppm

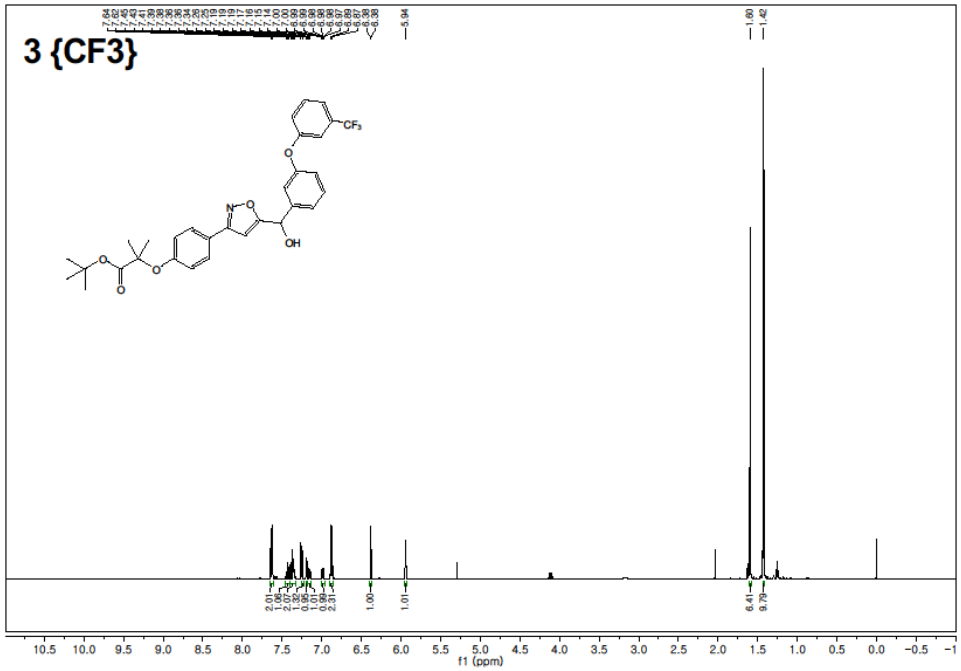
3 {CF3}
CF3
O
N
O
OH
O
O
O
f1 (ppm)

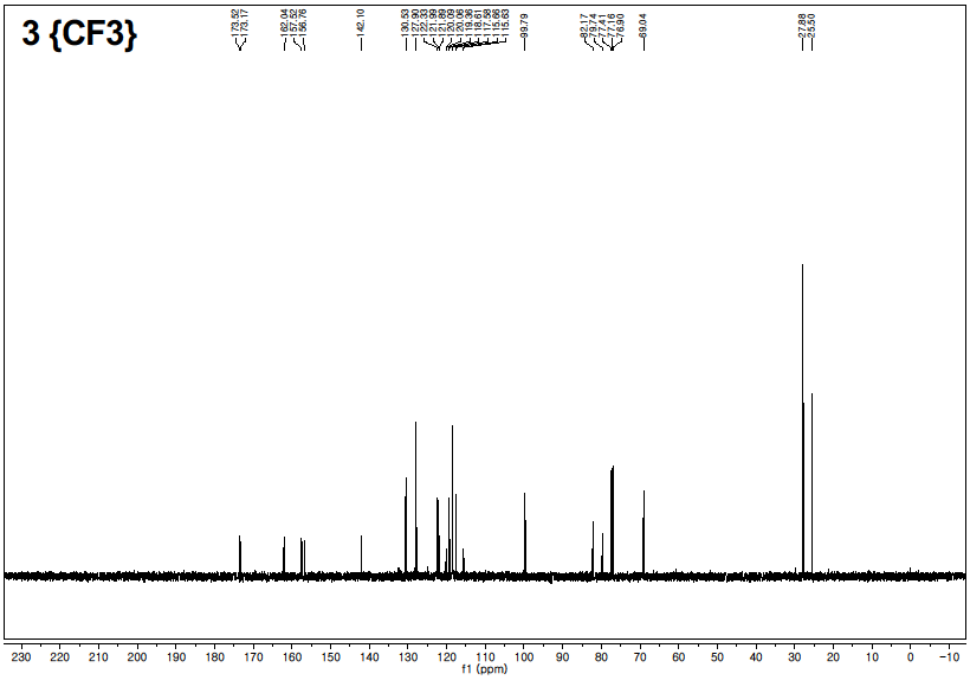
3 {CF3}
f1 (ppm)

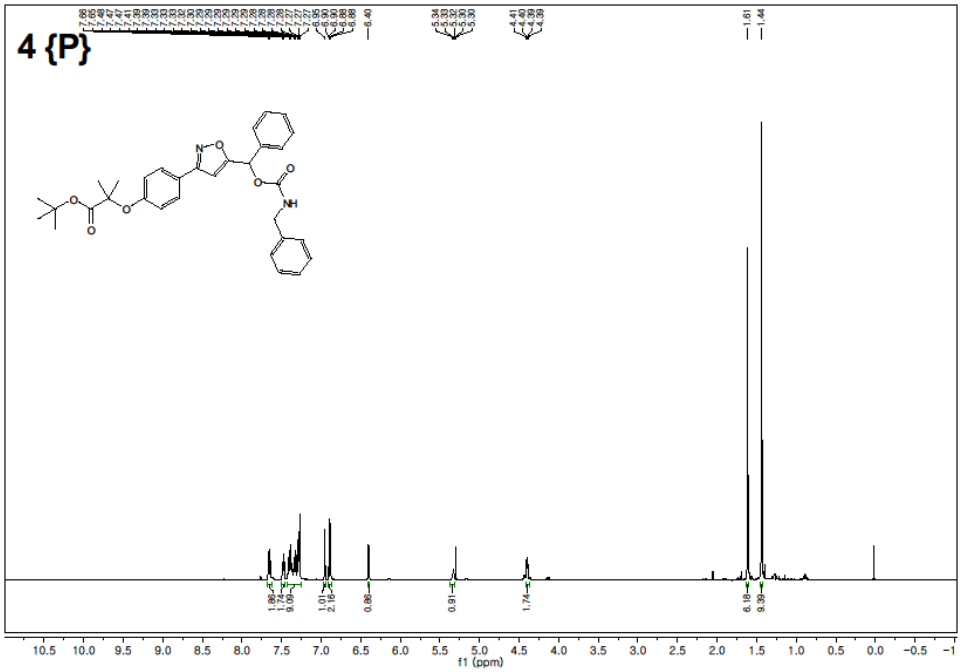
4 {P}
f1 (ppm)

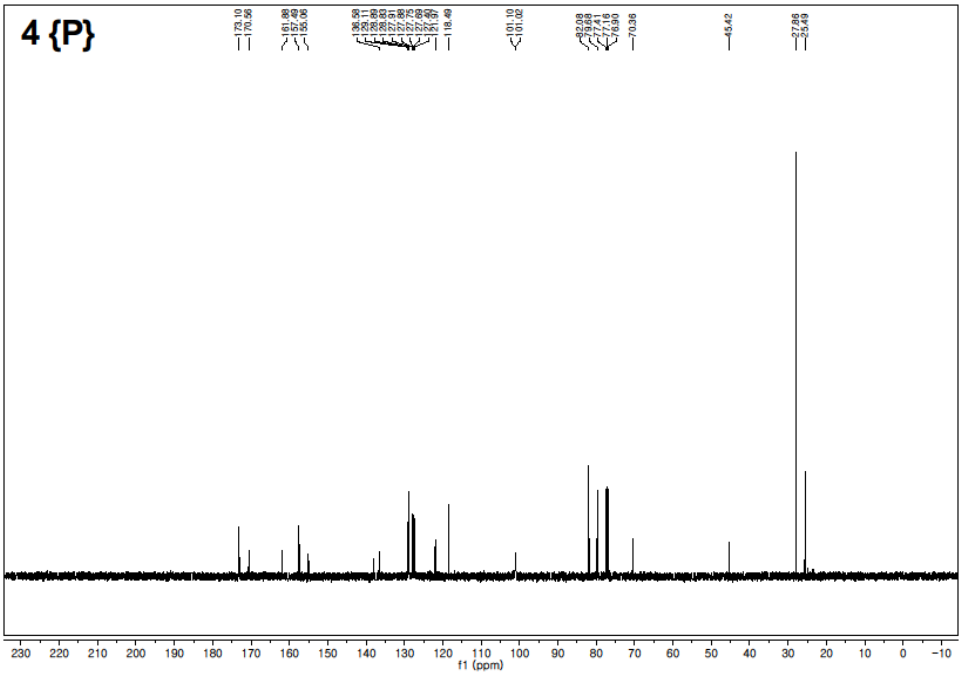
4 {P}
f1 (ppm)

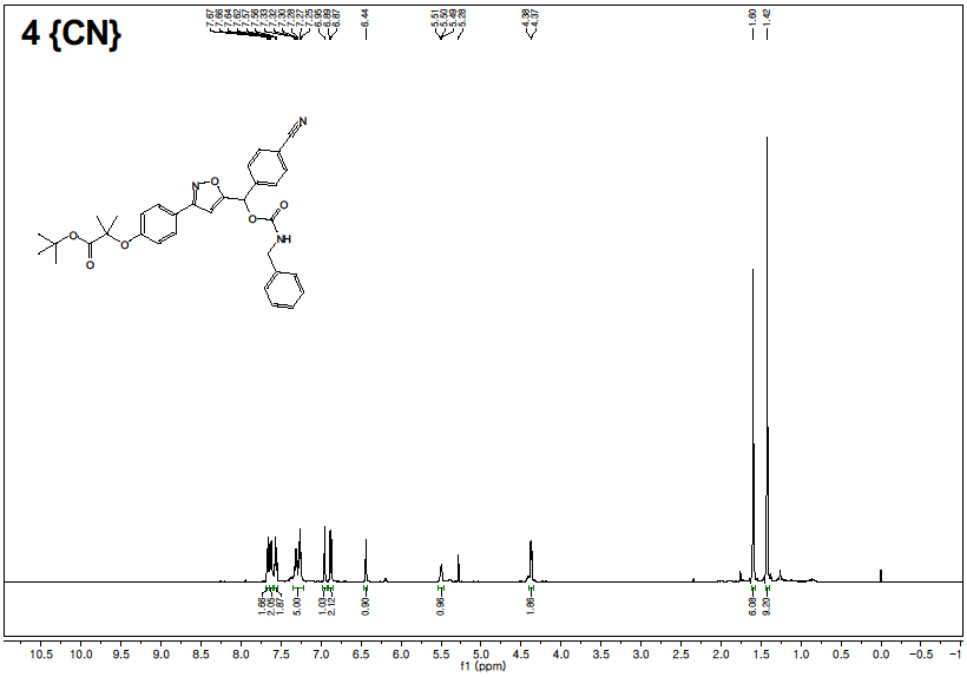
4 {CN}
f1 (ppm)

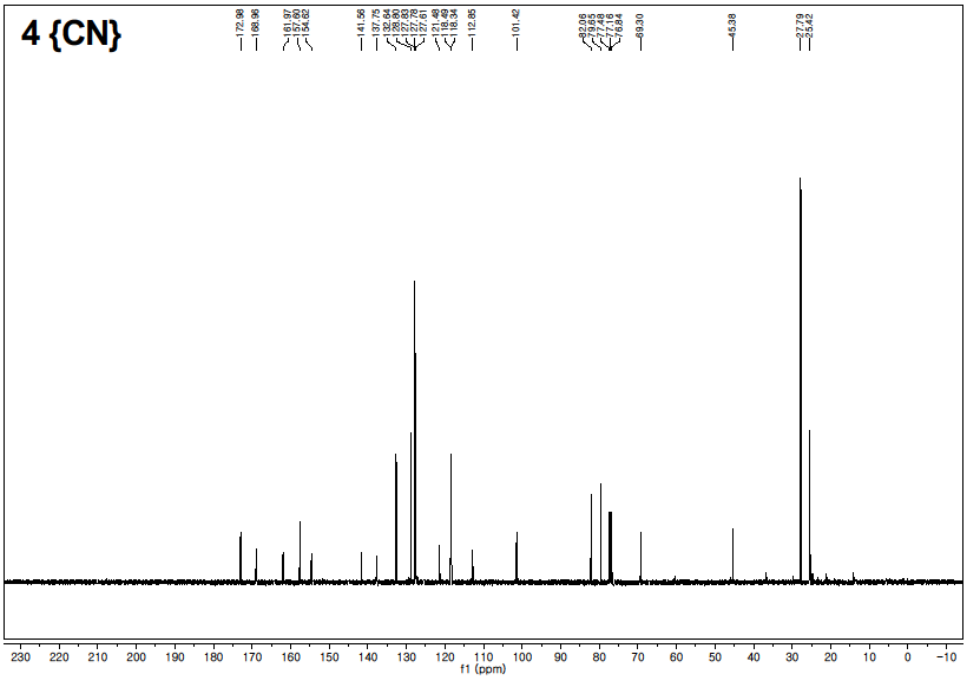
4 {CN}
f1 (ppm)

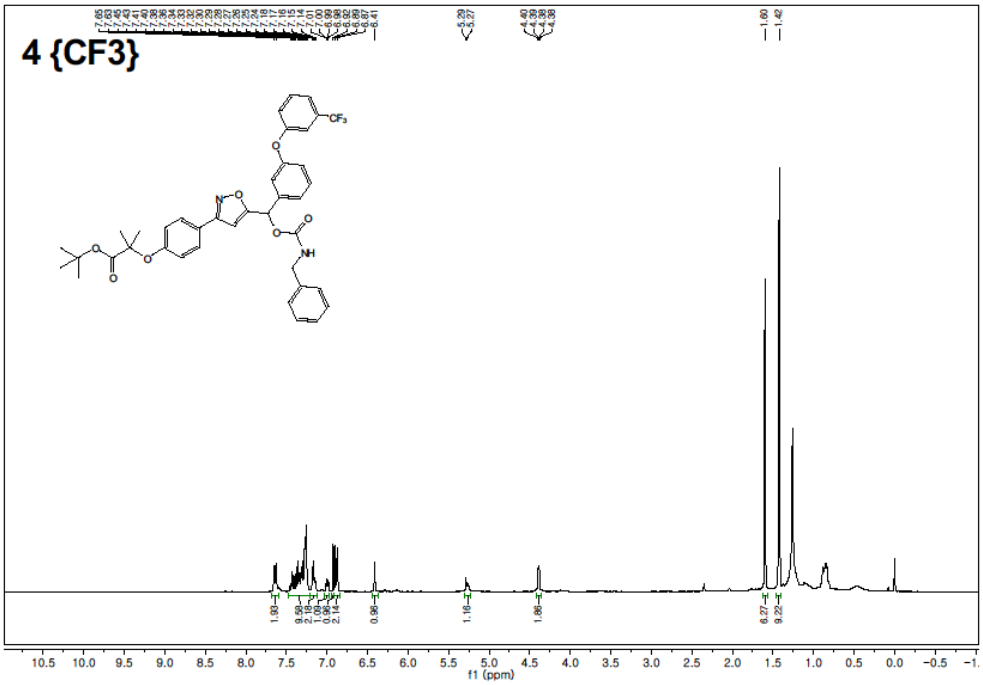
4 {CF3}
CF3
O
N
O
O
O
O
NH
f1 (ppm)

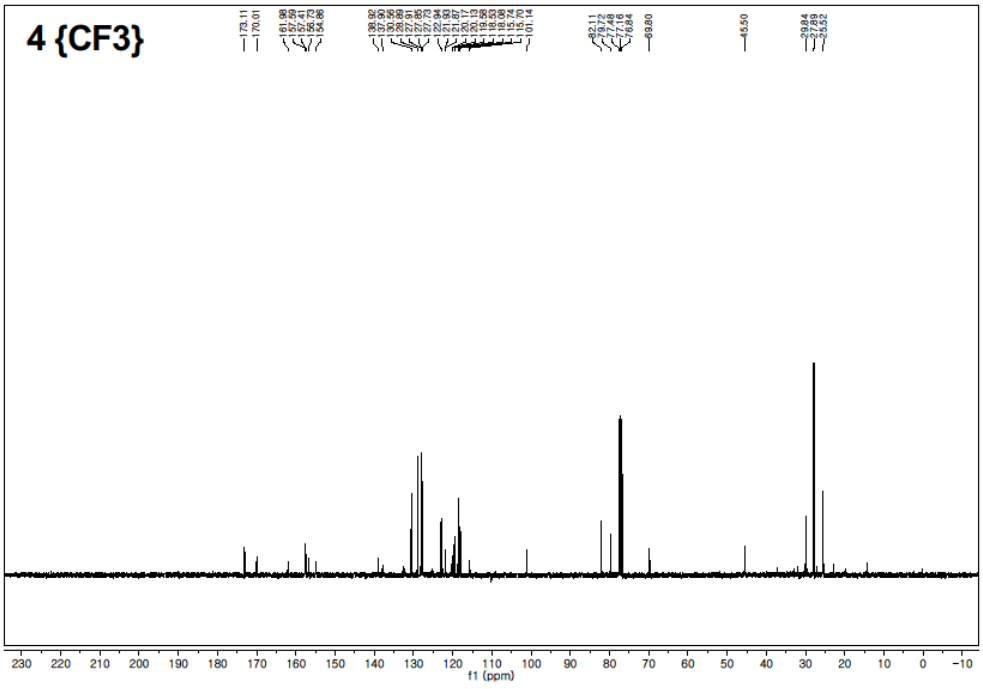
4 {CF3}
f1 (ppm)

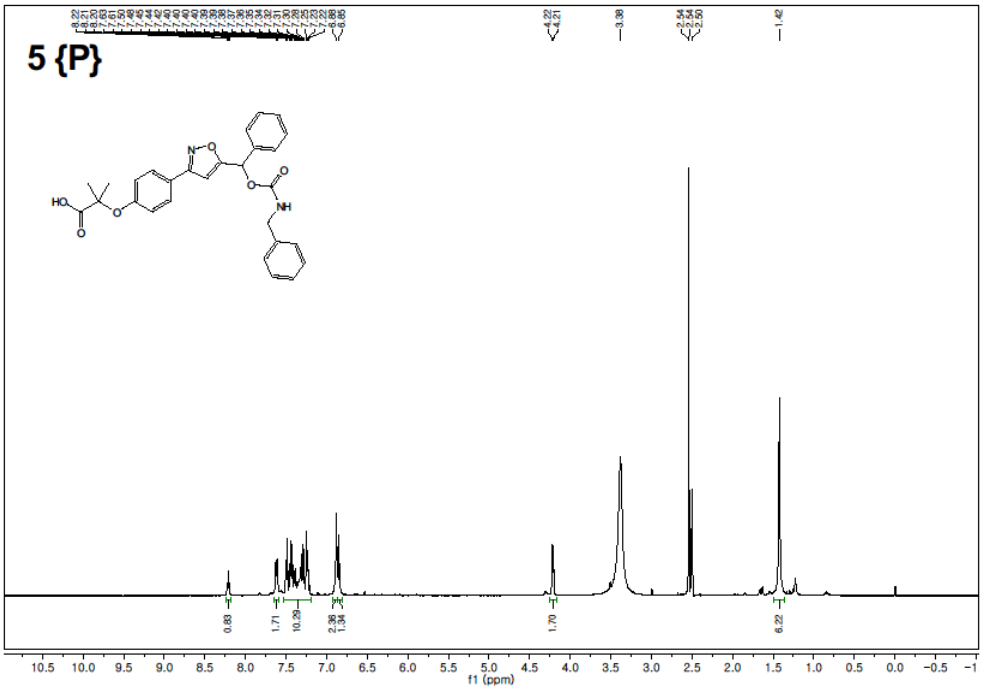
5 {P}
HO
O
O
N
O
O
NH
f1 (ppm)

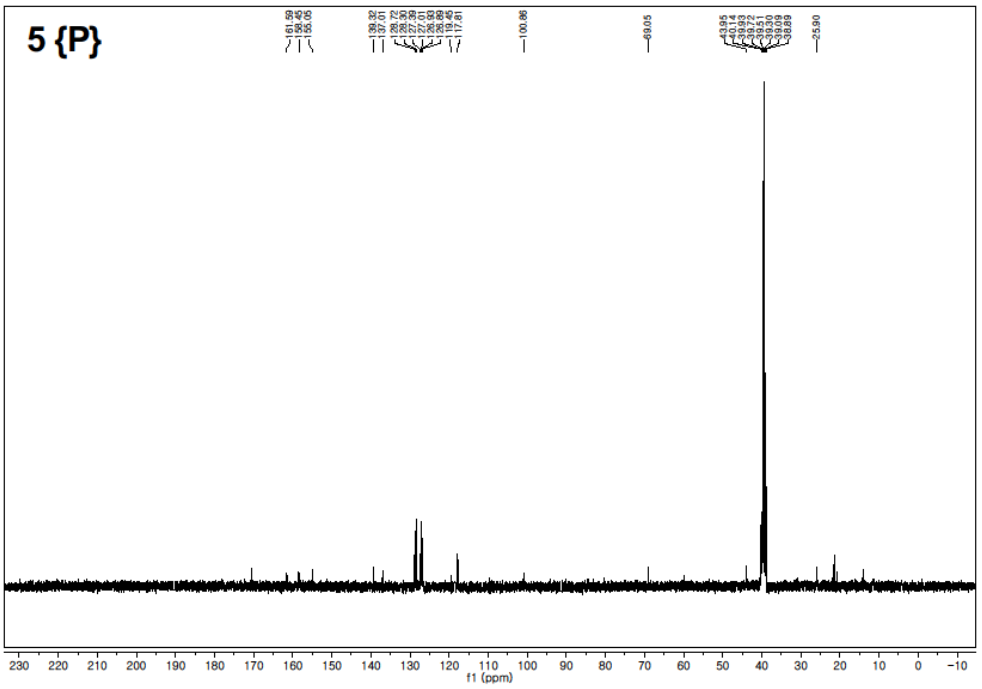
5 {P}
f1 (ppm)

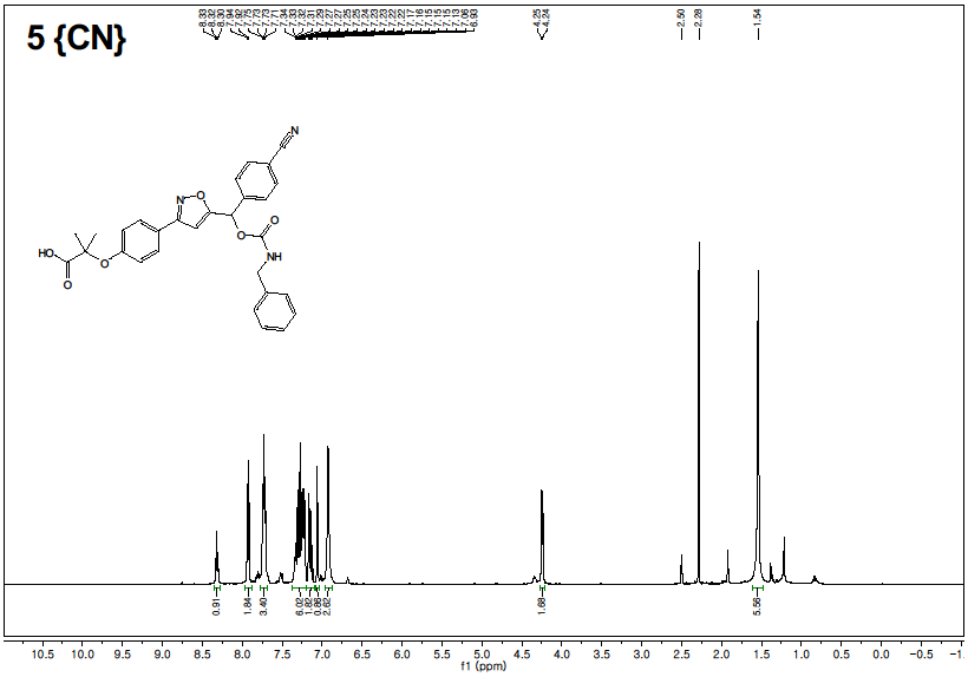
5 {CN}
f1 (ppm)

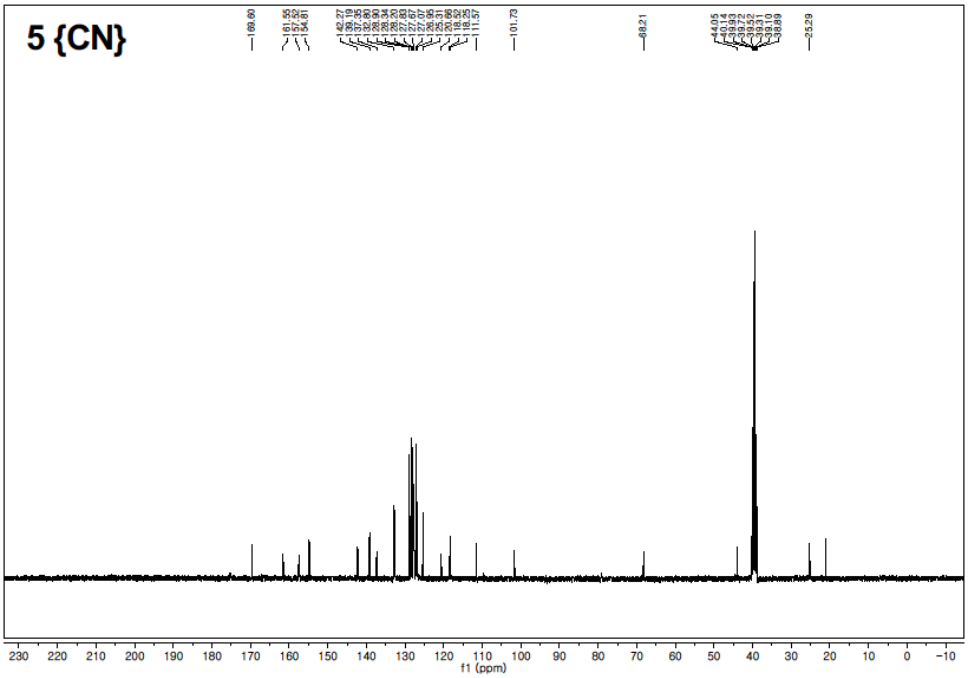
5 {CN}
f1 (ppm)

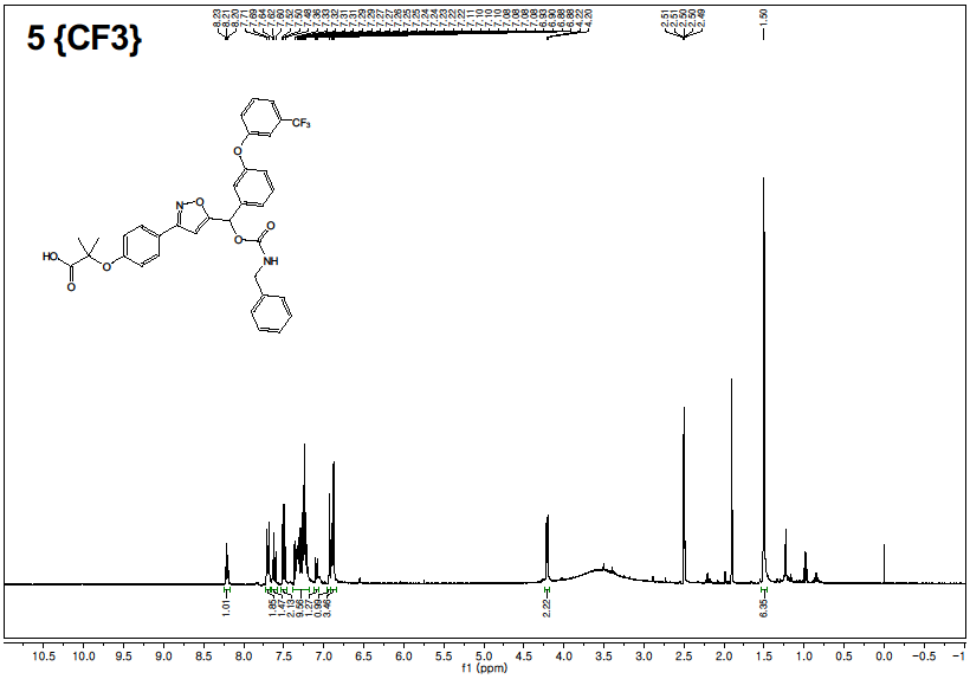
5 {CF3}
CF3
HO
O
N
NH
f1 (ppm)

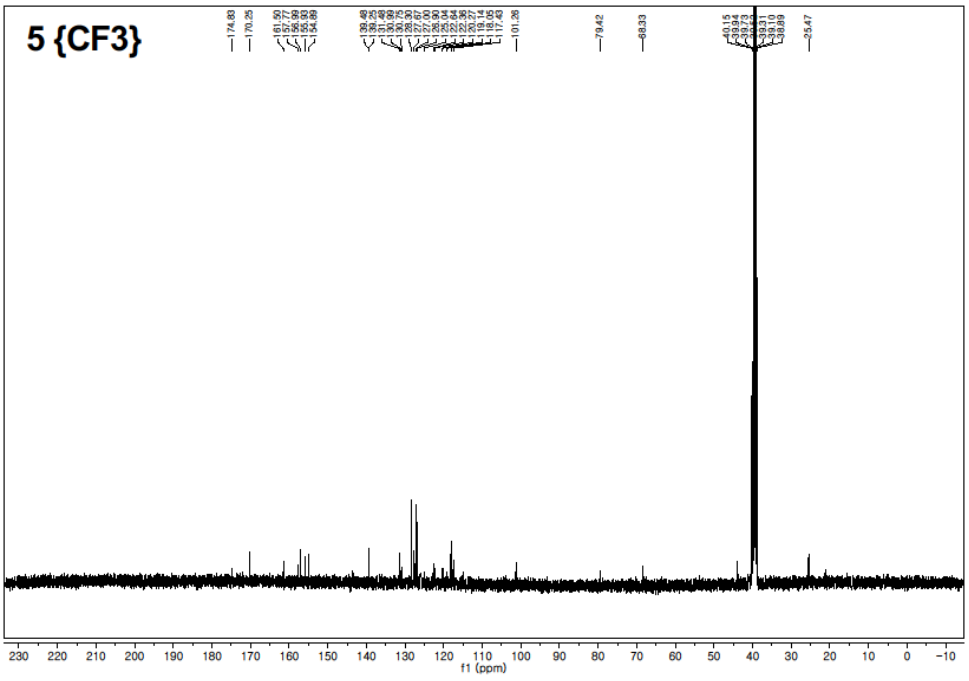
5 {CF3}
f1 (ppm)

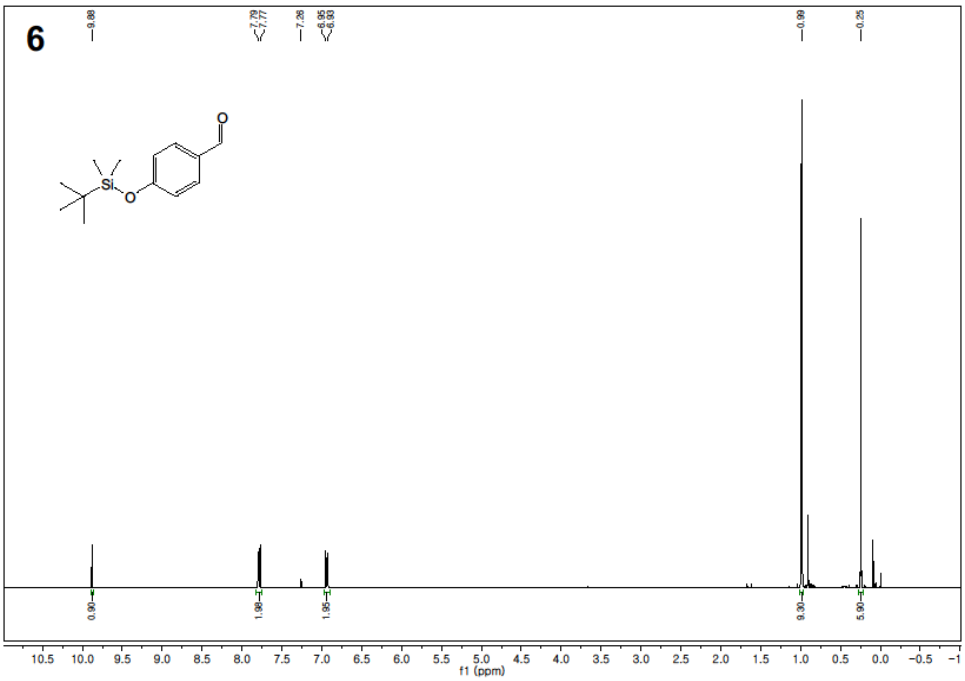
6
9.88
7.79
7.77
7.26
6.95
6.93
0.99
0.25
O
Si
O
0.90
1.98
1.95
9.30
5.90
10.5 10.0 9.5 9.0 8.5 8.0 7.5 7.0 6.5 6.0 5.5 5.0 4.5 4.0 3.5 3.0 2.5 2.0 1.5 1.0 0.5 0.0 −0.5 −1
f1 (ppm)

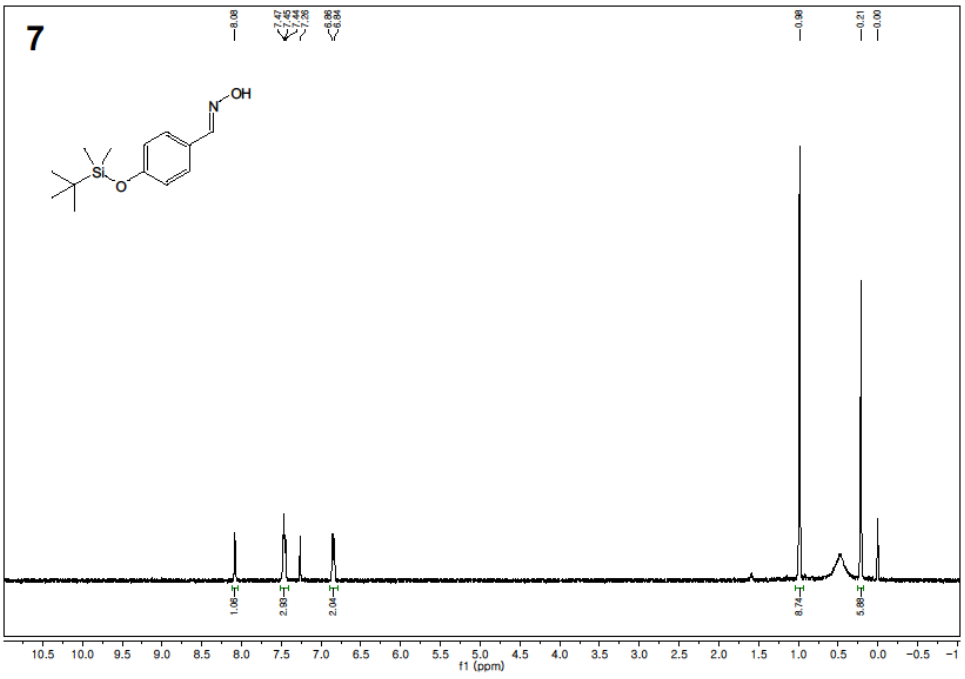
7
8.06
7.47
7.45
7.44
7.26
6.88
6.84
0.98
0.21
0.00
N
OH
Si
O
1.06
2.93
2.04
8.74
5.88
10.5 10.0 9.5 9.0 8.5 8.0 7.5 7.0 6.5 6.0 5.5 5.0 4.5 4.0 3.5 3.0 2.5 2.0 1.5 1.0 0.5 0.0 −0.5 −1
f1 (ppm)

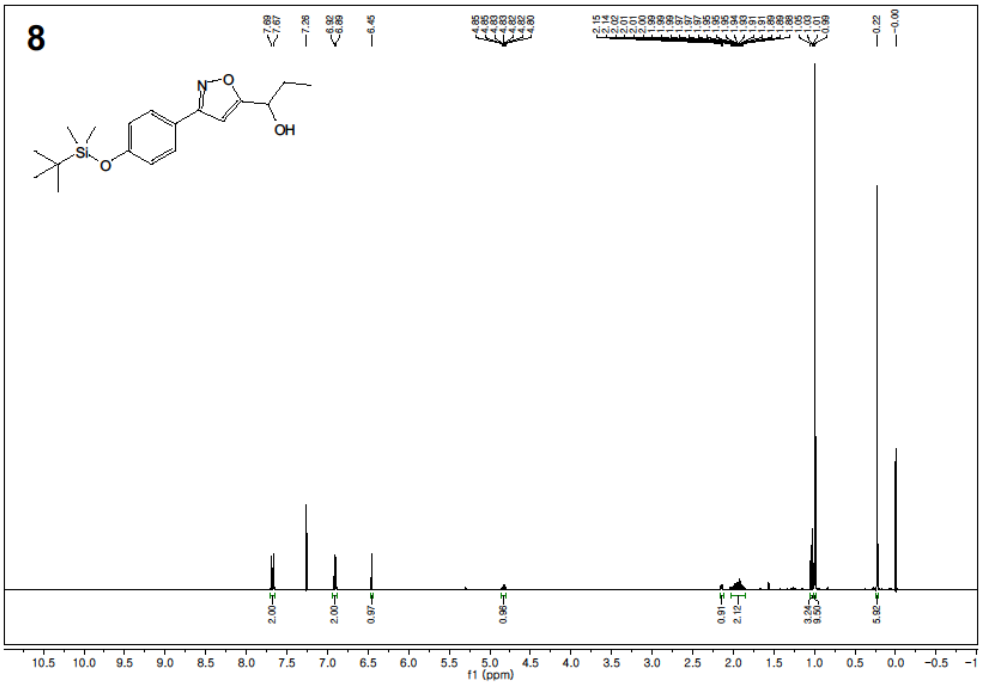
8
7.69
7.67
7.26
6.92
6.89
6.45
4.85
4.84
4.83
4.82
4.82
4.80
2.15
2.14
2.02
2.01
2.01
2.00
1.99
1.99
1.97
1.97
1.95
1.95
1.94
1.91
1.91
1.89
1.88
1.05
1.03
1.01
0.99
0.22
-0.00
N
O
OH
Si
O
2.00
2.00
0.97
0.98
0.91
2.12
3.24
9.50
5.92
10.5 10.0 9.5 9.0 8.5 8.0 7.5 7.0 6.5 6.0 5.5 5.0 4.5 4.0 3.5 3.0 2.5 2.0 1.5 1.0 0.5 0.0 -0.5 -1
f1 (ppm)

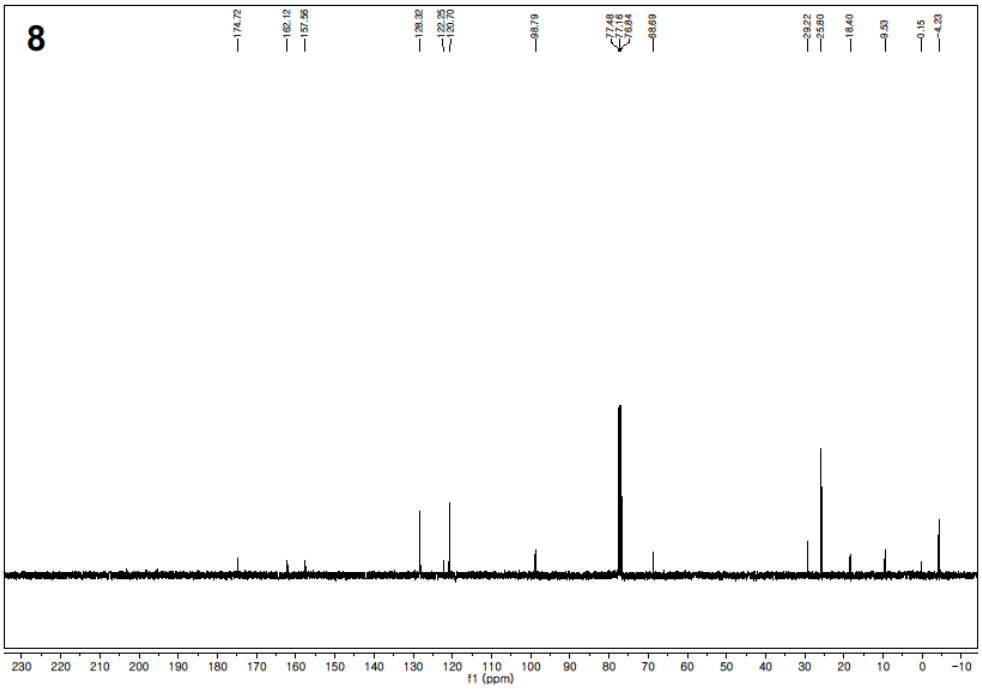
8
174.72
162.12
157.56
138.32
132.25
130.70
98.79
77.48
77.16
76.84
68.69
29.22
25.80
18.40
-9.53
-0.15
-4.23
230 220 210 200 190 180 170 160 150 140 130 120 110 100 90 80 70 60 50 40 30 20 10 0 -10
f1 (ppm)

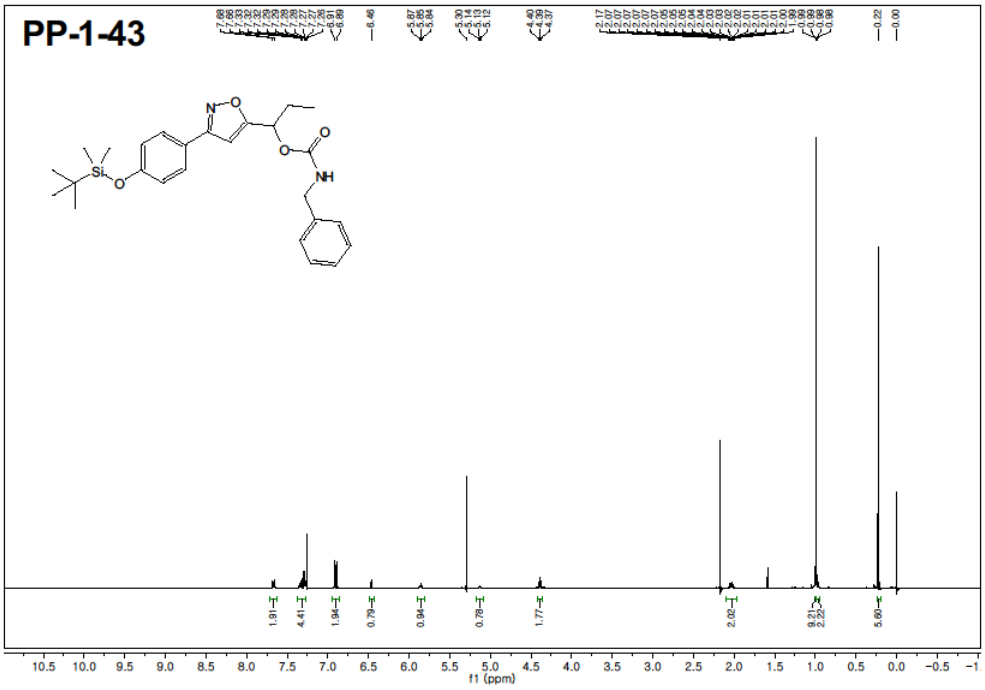
PP-1-43
f1 (ppm)

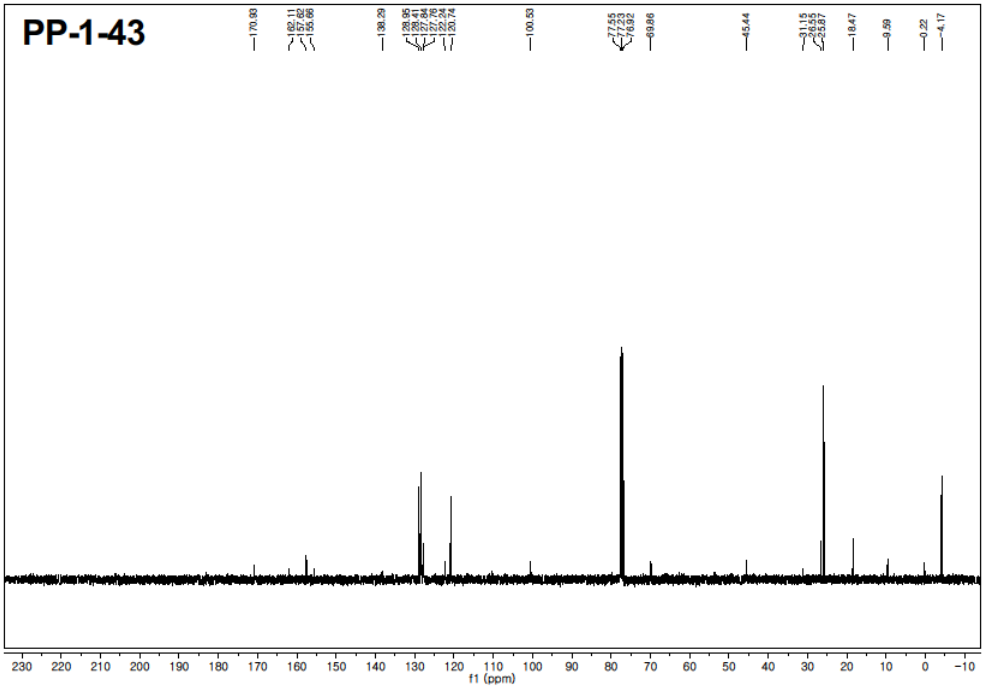
PP-1-43
f1 (ppm)

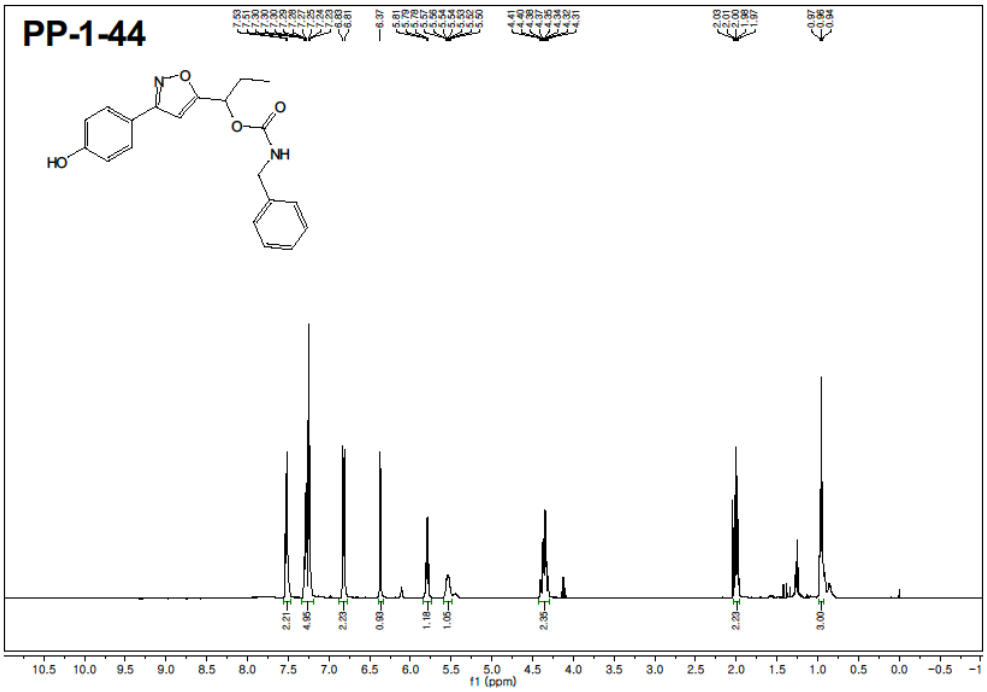
PP-1-44
HO
N
O
O
O
NH
f1 (ppm)

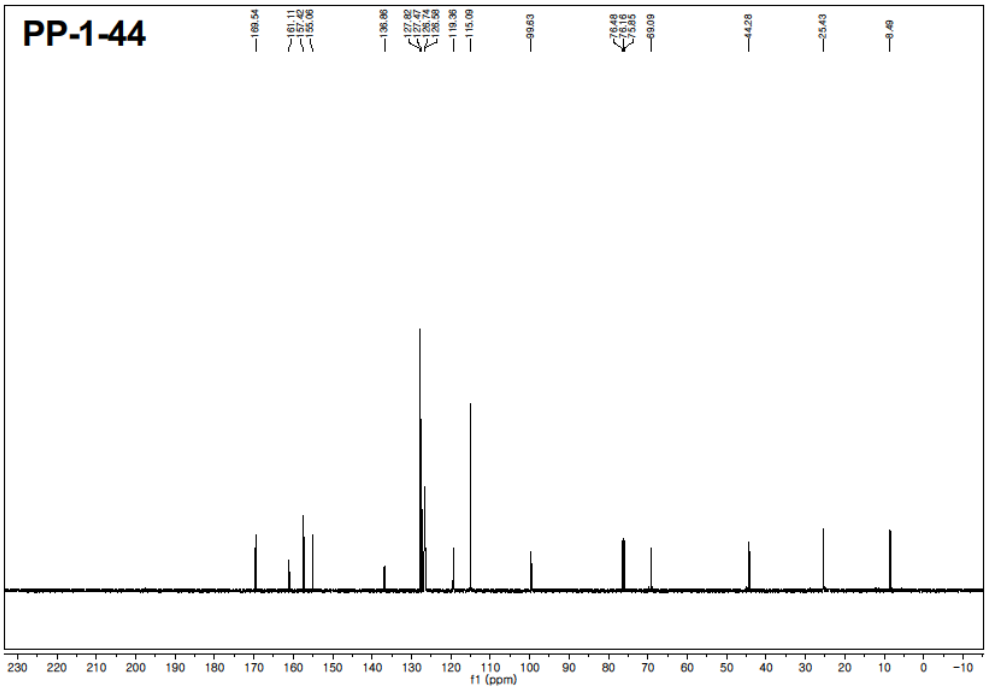
PP-1-44
f1 (ppm)

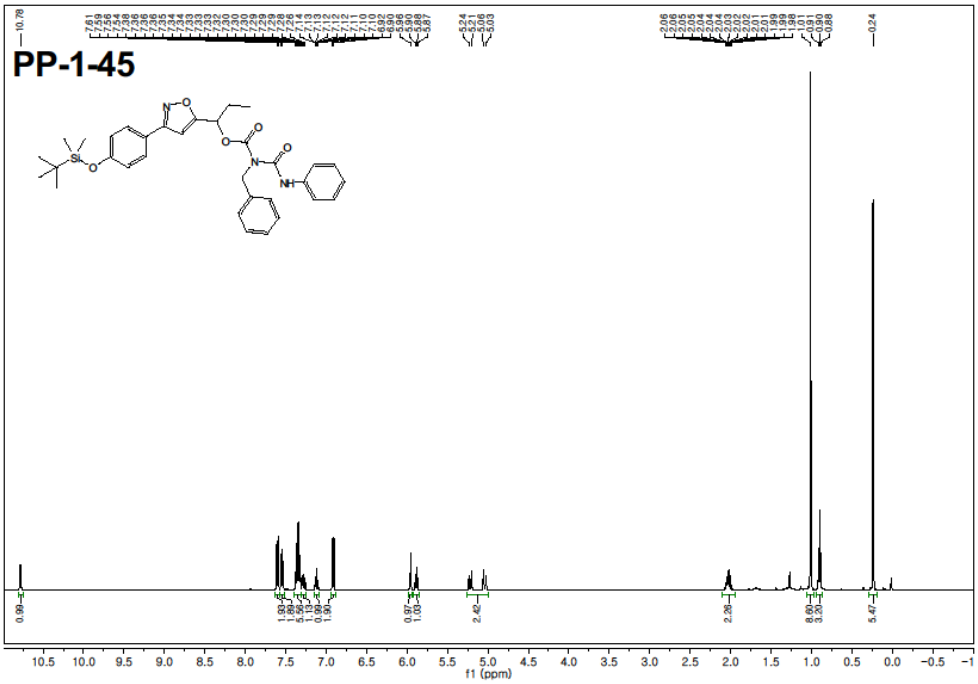
PP-1-45
f1 (ppm)

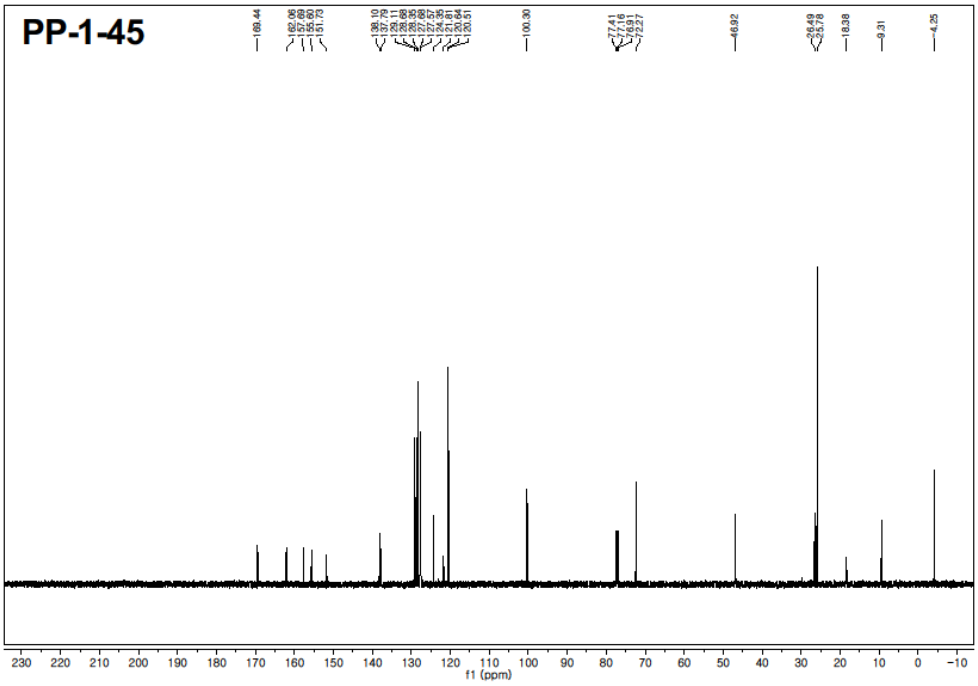
PP-1-45
f1 (ppm)

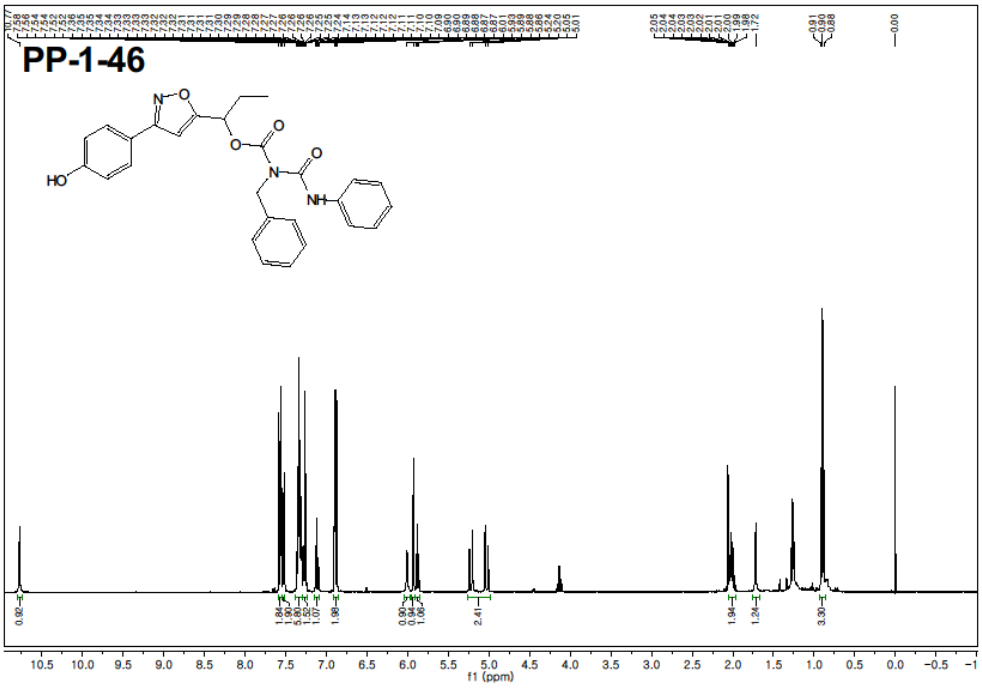
PP-1-46
HO
N
O
O
O
N
O
NH
f1 (ppm)

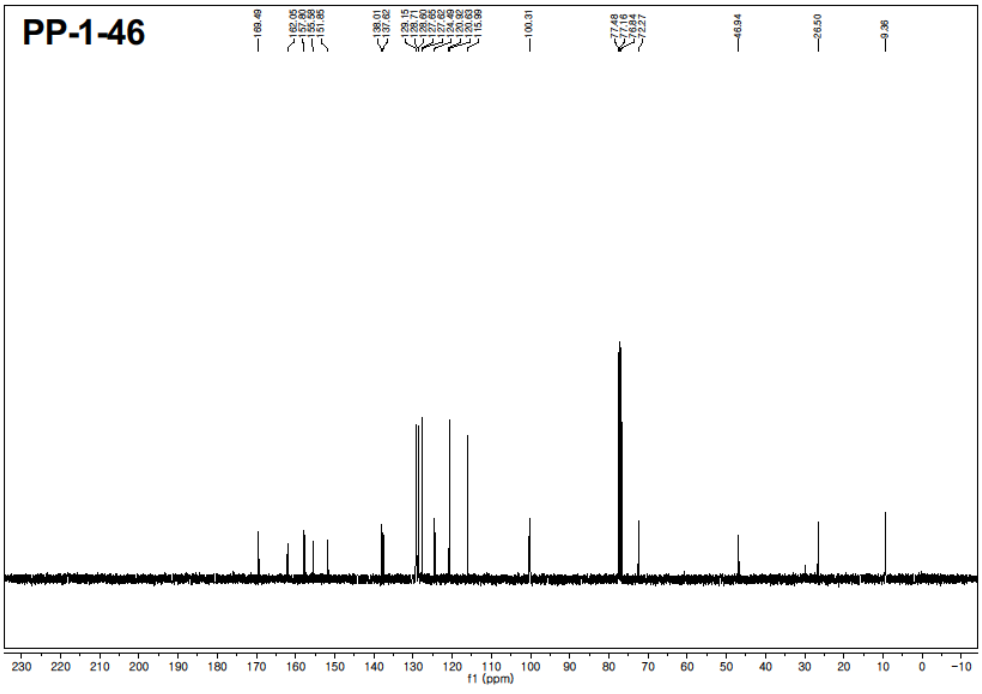
PP-1-46
f1 (ppm)

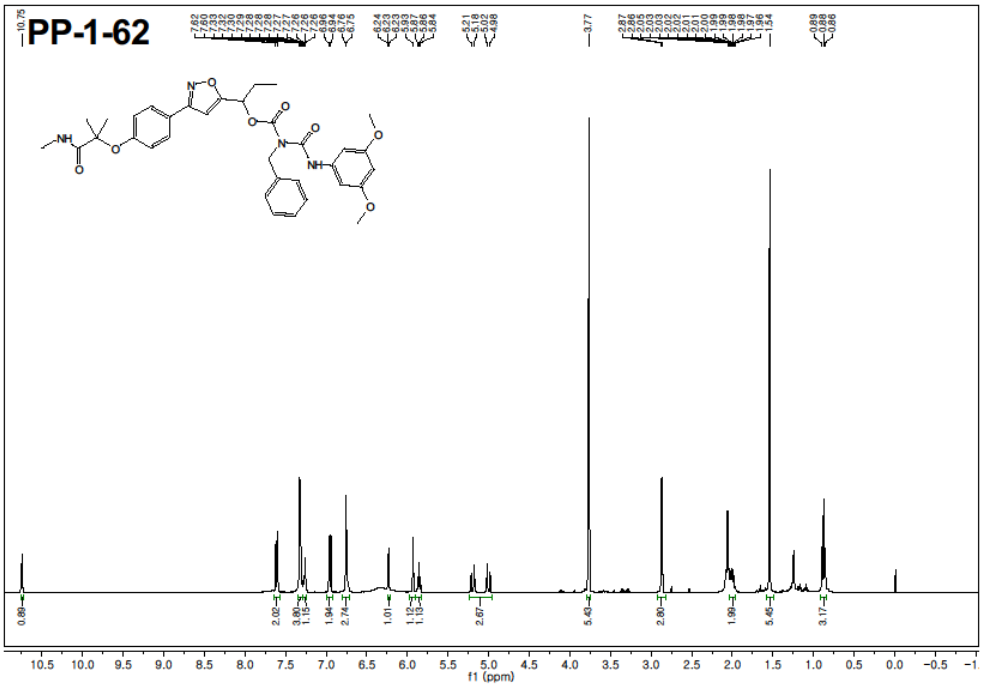
PP-1-62
f1 (ppm)

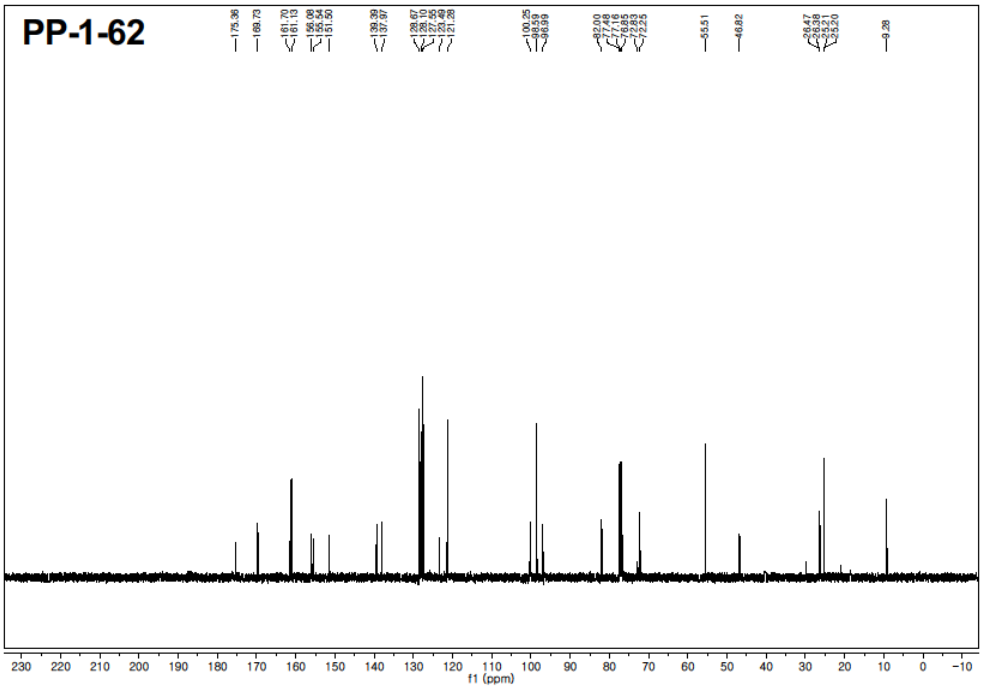
PP-1-62
f1 (ppm)

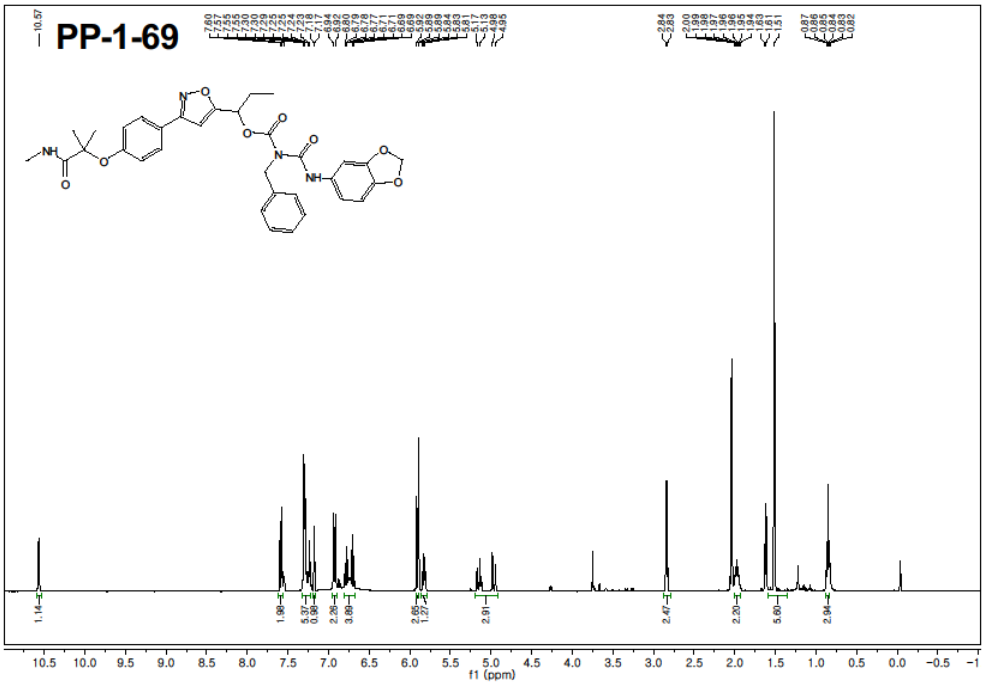
PP-1-69
f1 (ppm)

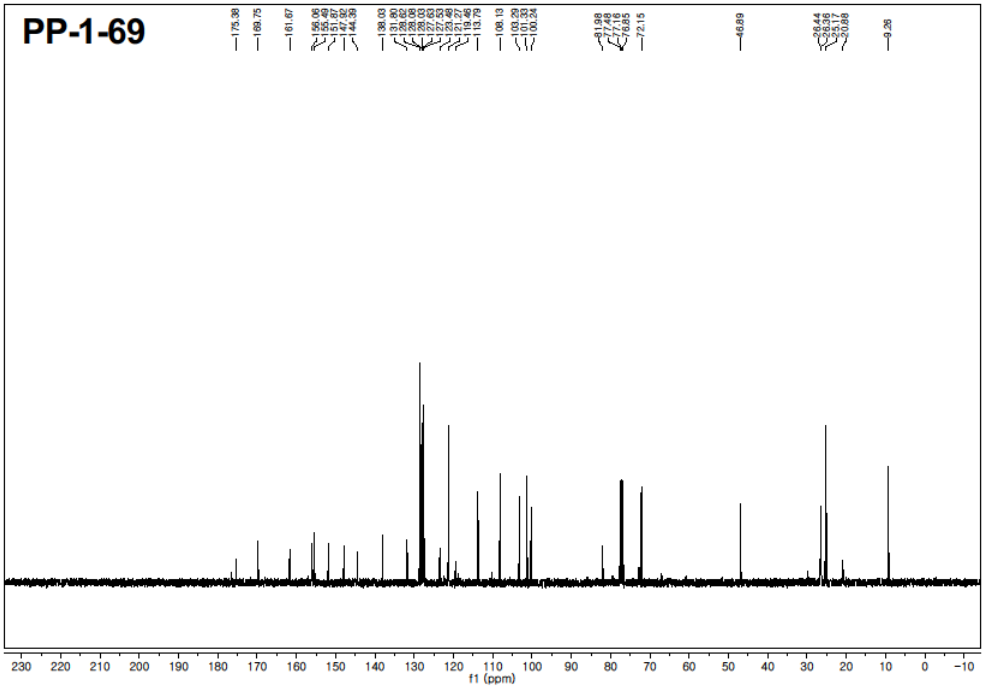
PP-1-69
f1 (ppm)

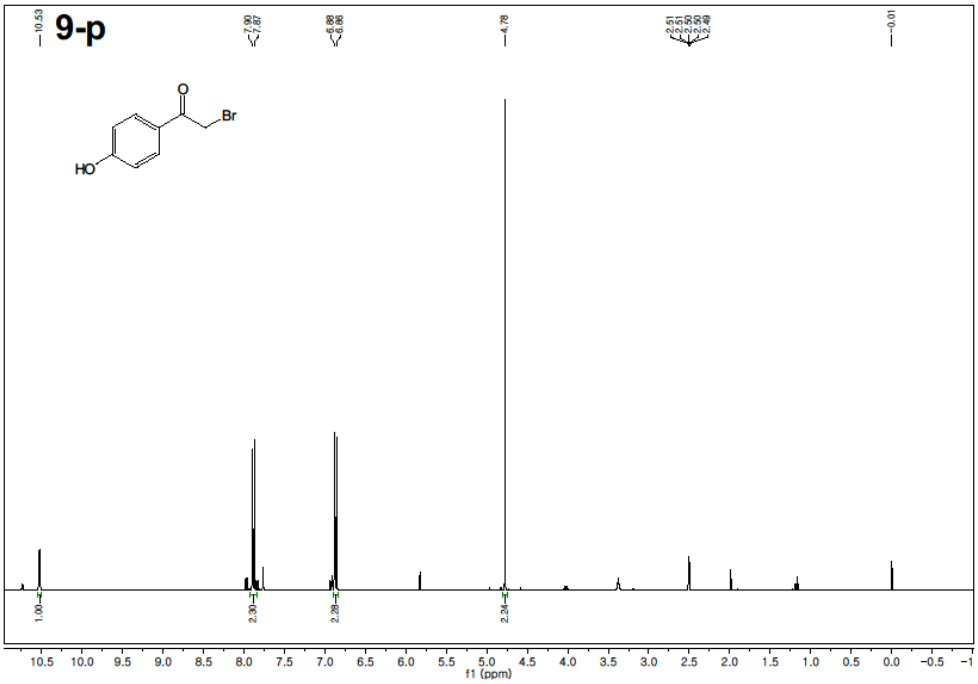
9-p
10.53
7.90
7.87
6.88
6.86
4.78
2.51
2.51
2.50
2.49
-0.01
O
Br
HO
1.00
2.30
2.28
2.24
f1 (ppm)

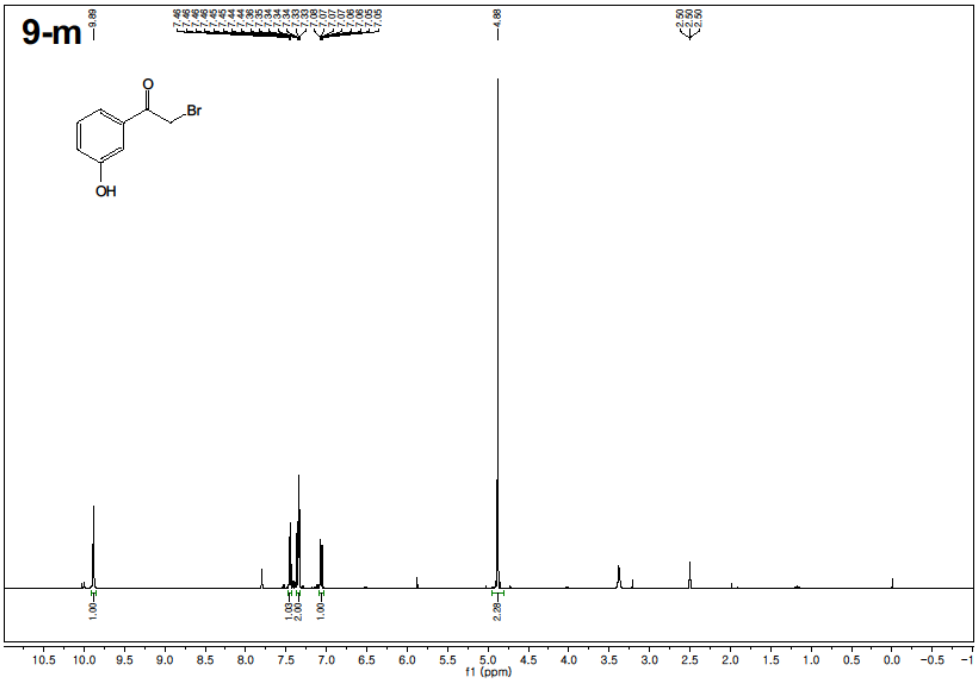
9-m
9.89
4.88
2.50
2.50
2.50
O
Br
OH
1.00
1.03
2.00
1.00
2.28
f1 (ppm)

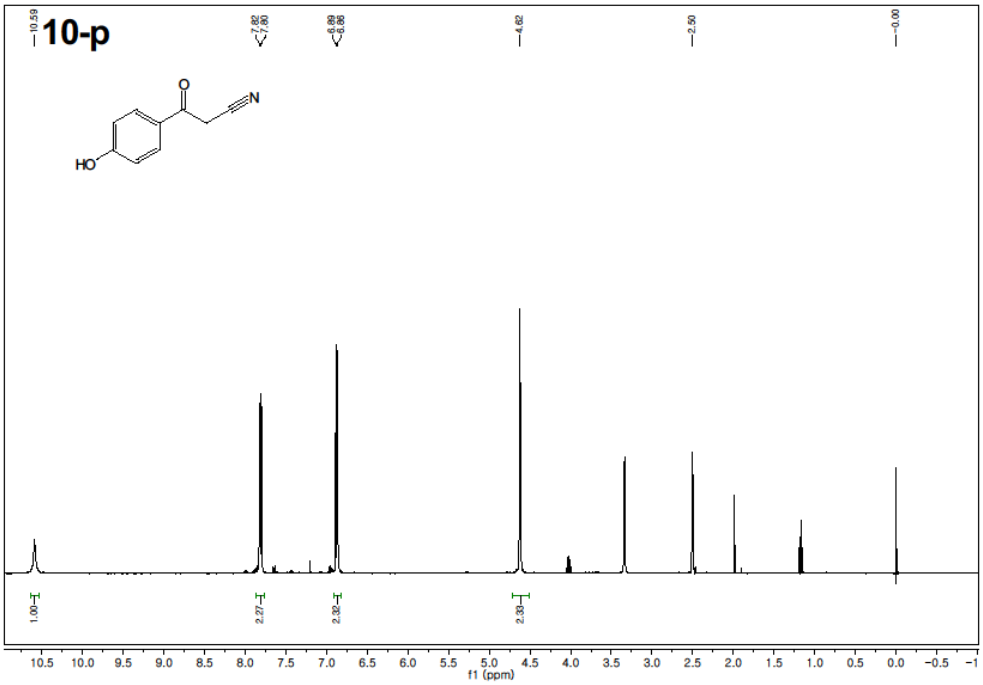
10-p
HO
O
N
10.59
7.82
7.80
6.89
6.88
4.62
2.50
0.00
1.00
2.27
2.32
2.33
f1 (ppm)

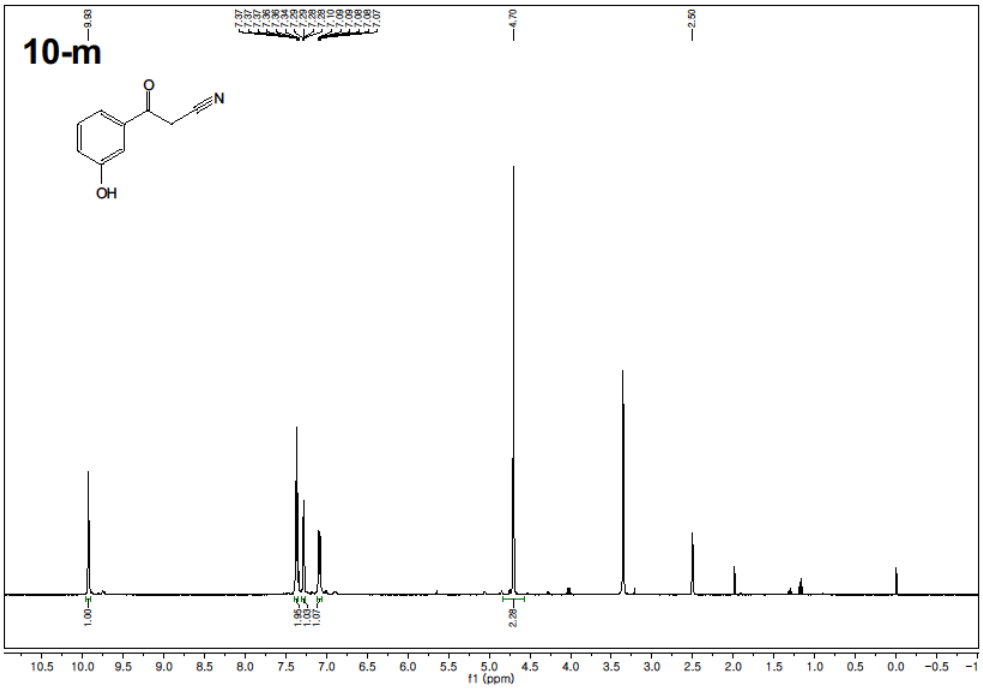
10-m
OH
O
N
9.93
7.37
7.36
7.35
7.34
7.33
7.32
7.31
7.30
7.29
7.28
7.27
7.26
7.25
7.24
7.23
7.22
7.21
7.20
7.19
7.18
7.17
7.16
7.15
7.14
7.13
7.12
7.11
7.10
7.09
7.08
7.07
4.70
2.50
1.00
1.95
1.00
1.07
2.28
f1 (ppm)

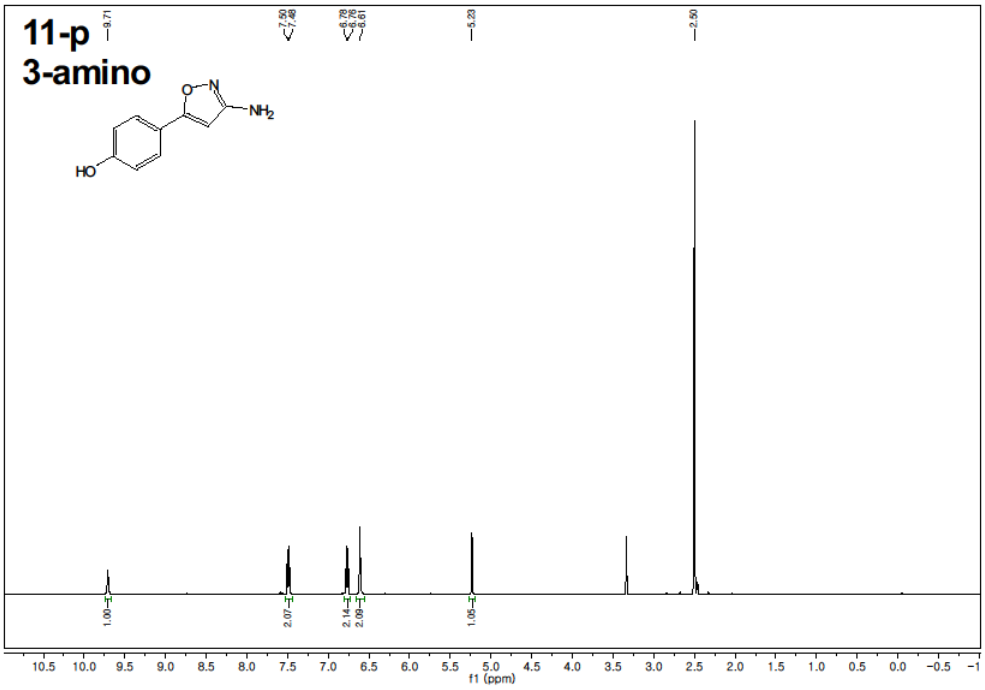
11-p
3-amino
NH2
HO
9.71
7.50
7.48
6.78
6.76
6.61
5.23
2.50
1.00
2.07
2.14
2.09
1.06
f1 (ppm)

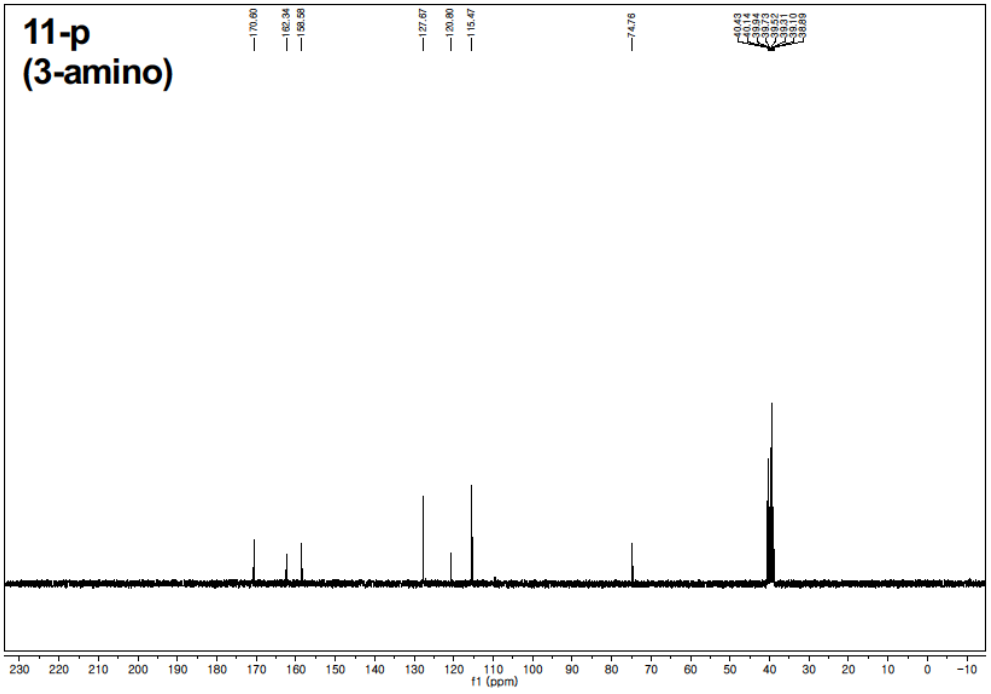
11-p
(3-amino)
170.60
162.34
158.58
127.67
120.80
115.47
74.76
40.43
40.14
39.94
39.73
39.52
39.31
39.10
38.89
f1 (ppm)

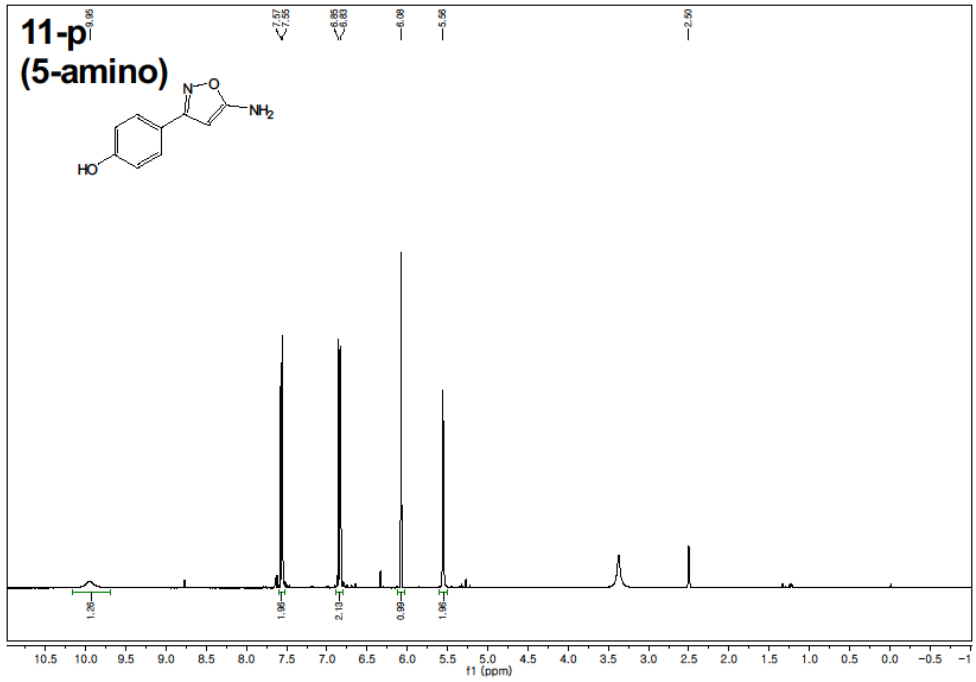
11-p
(5-amino)
9.95
7.57
7.55
6.85
6.83
6.08
5.56
2.50
1.26
1.96
2.13
0.99
1.96
f1 (ppm)

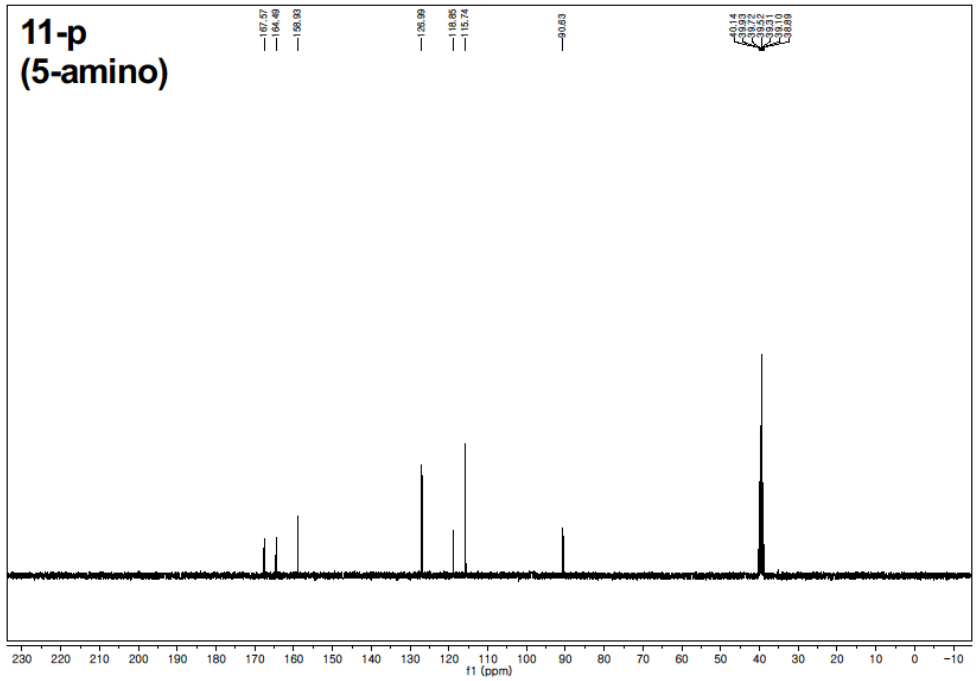
11-p
(5-amino)
167.57
164.49
158.93
126.99
118.85
115.74
90.63
40.14
39.93
39.72
39.51
39.31
39.10
38.89
f1 (ppm)

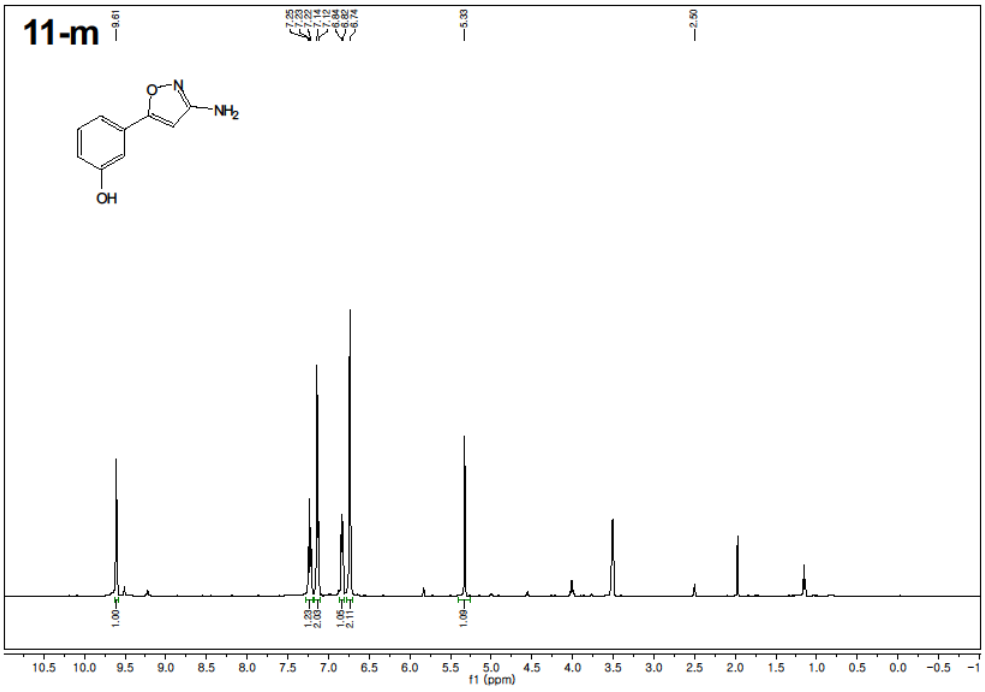
11-m
9.61
7.25
7.20
7.22
7.14
7.12
6.84
6.82
6.74
5.33
2.50
O
N
NH2
OH
1.00
1.23
2.08
1.06
2.11
1.00
10.5 10.0 9.5 9.0 8.5 8.0 7.5 7.0 6.5 6.0 5.5 5.0 4.5 4.0 3.5 3.0 2.5 2.0 1.5 1.0 0.5 0.0 −0.5 −1
f1 (ppm)

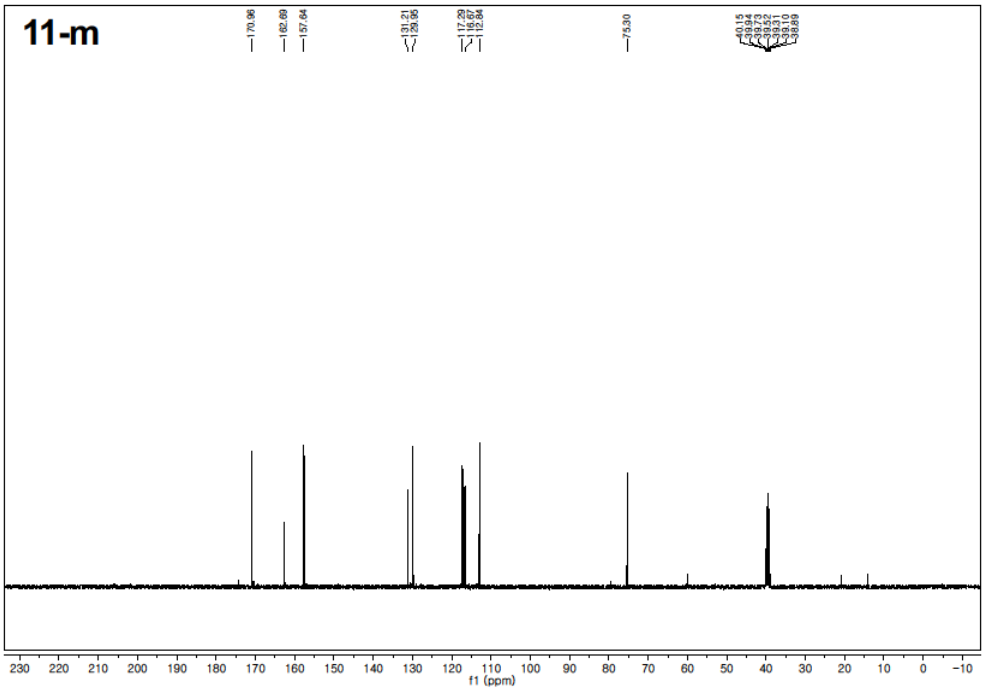
11-m
170.96
162.69
157.64
131.21
129.96
117.29
116.67
112.84
75.30
40.15
39.94
39.73
39.52
39.31
39.10
38.89
230 220 210 200 190 180 170 160 150 140 130 120 110 100 90 80 70 60 50 40 30 20 10 0 −10
f1 (ppm)

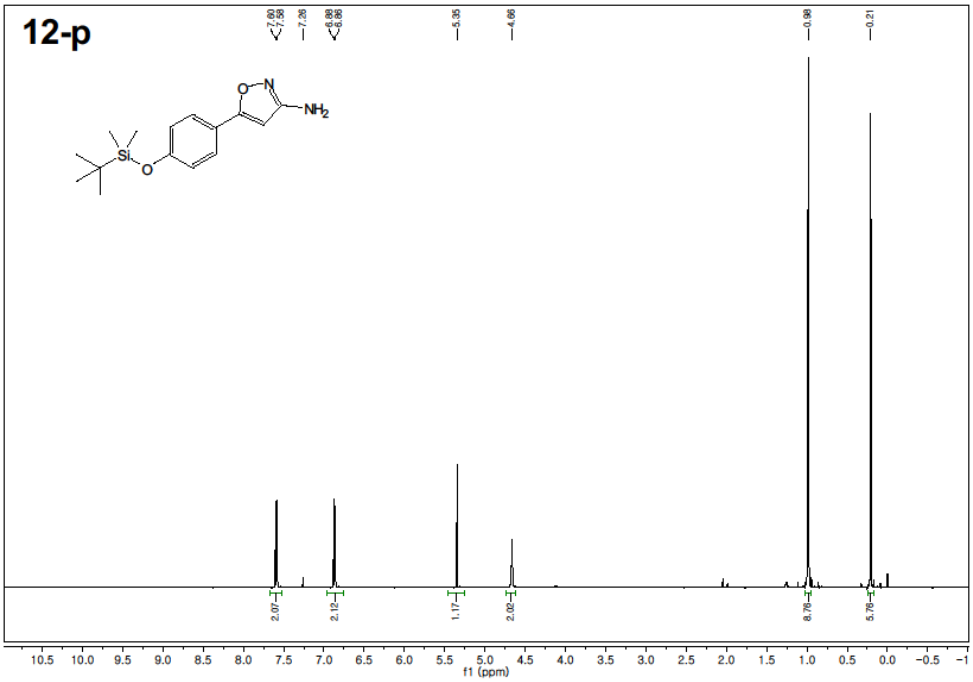
12-p
7.60
7.59
7.26
6.88
6.86
5.35
4.66
0.98
0.21
O
N
NH2
Si
O
2.07
2.12
1.17
2.02
8.76
5.78
10.5 10.0 9.5 9.0 8.5 8.0 7.5 7.0 6.5 6.0 5.5 5.0 4.5 4.0 3.5 3.0 2.5 2.0 1.5 1.0 0.5 0.0 −0.5 −1
f1 (ppm)

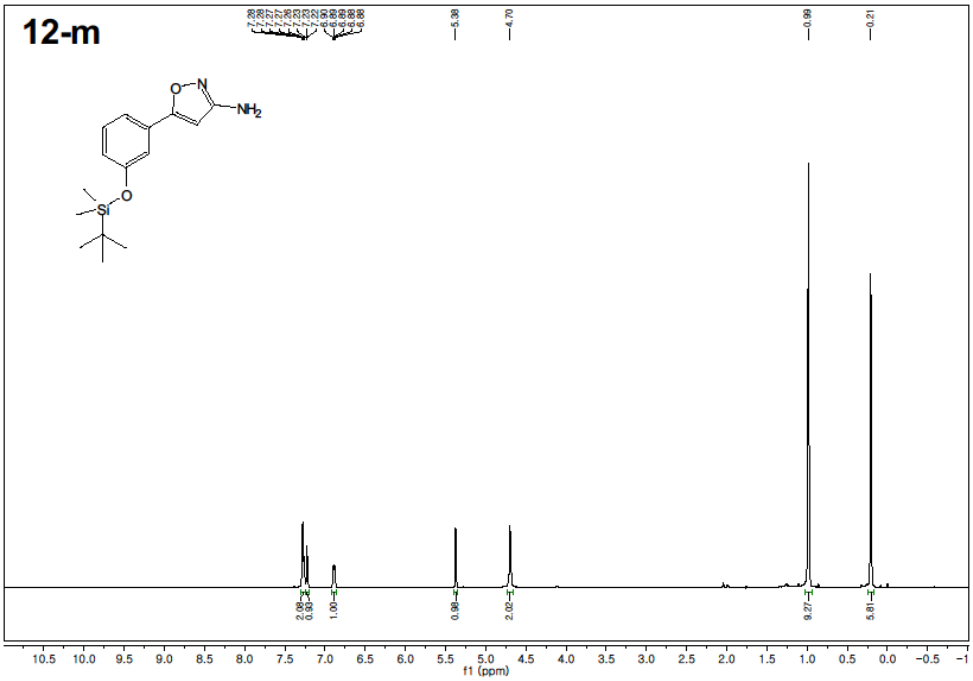
12-m
5.38
4.70
0.99
0.21
O
N
NH2
Si
O
2.08
0.98
1.00
0.98
2.02
9.27
5.81
10.5 10.0 9.5 9.0 8.5 8.0 7.5 7.0 6.5 6.0 5.5 5.0 4.5 4.0 3.5 3.0 2.5 2.0 1.5 1.0 0.5 0.0 −0.5 −1
f1 (ppm)

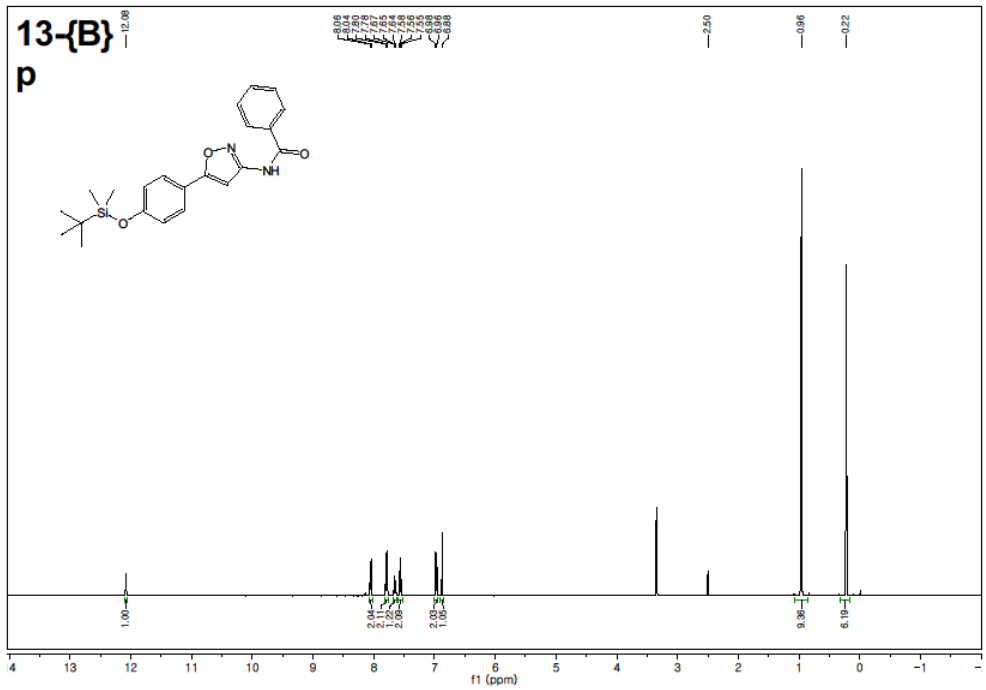
13-{B}
p
f1 (ppm)

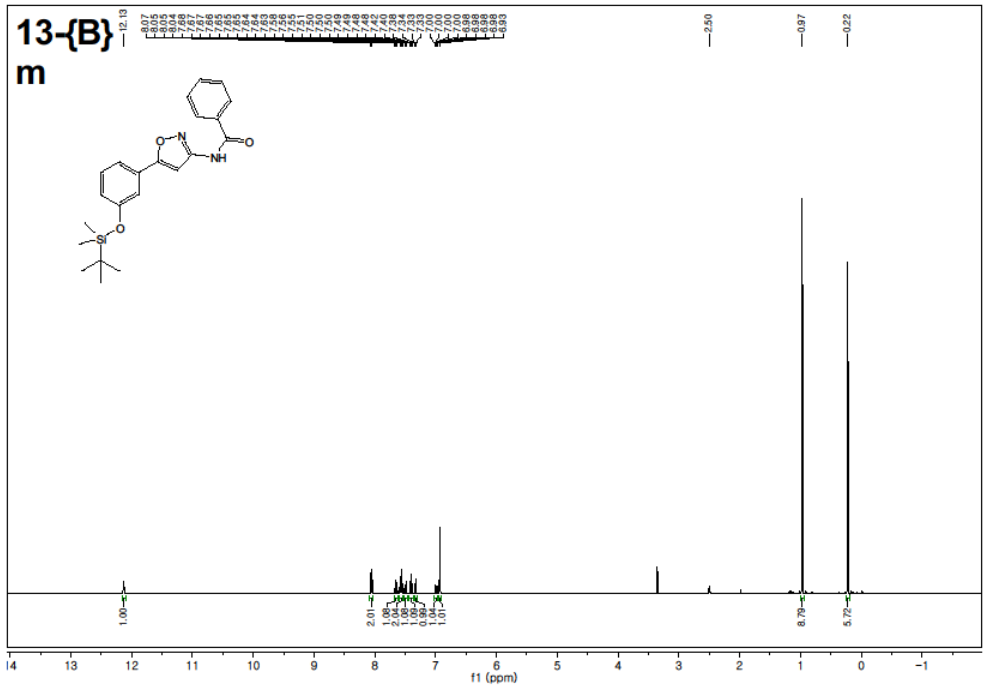
13-{B}
m
f1 (ppm)

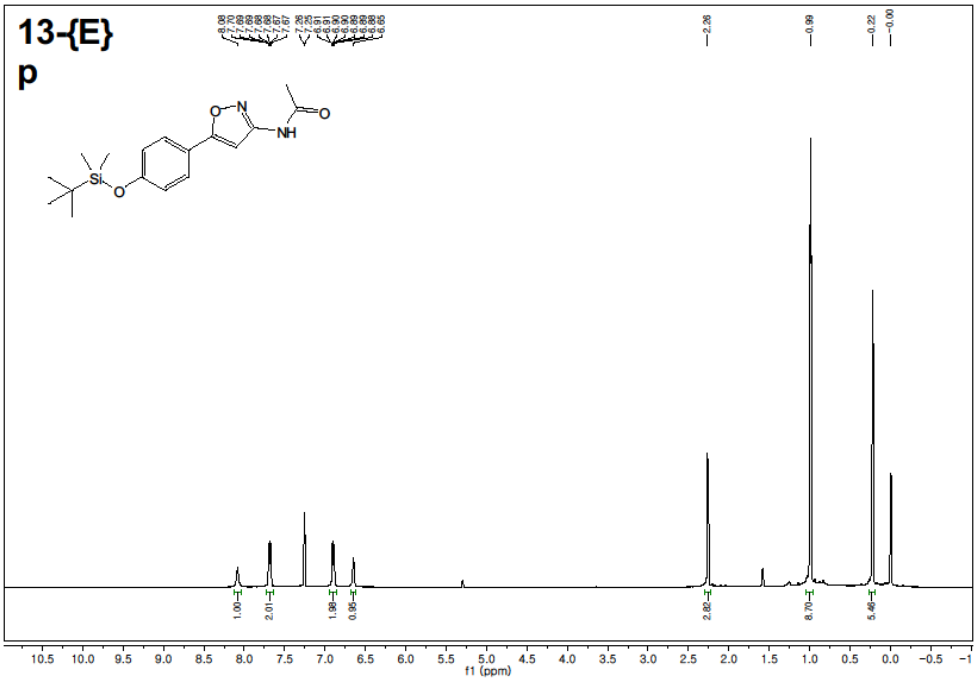
13-{E}
p
f1 (ppm)

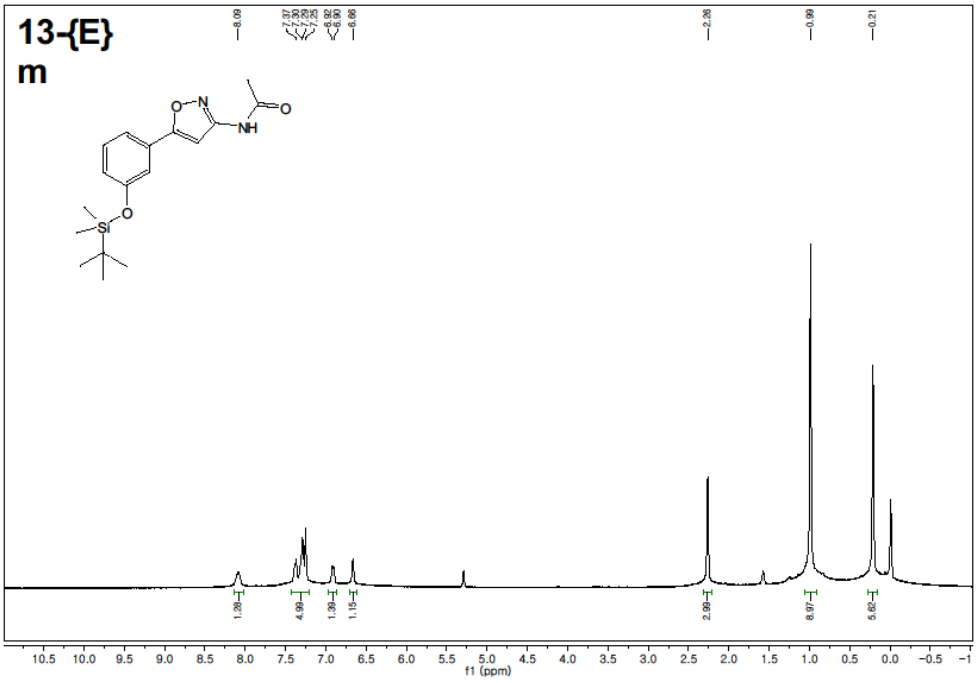
13-{E}
m
f1 (ppm)

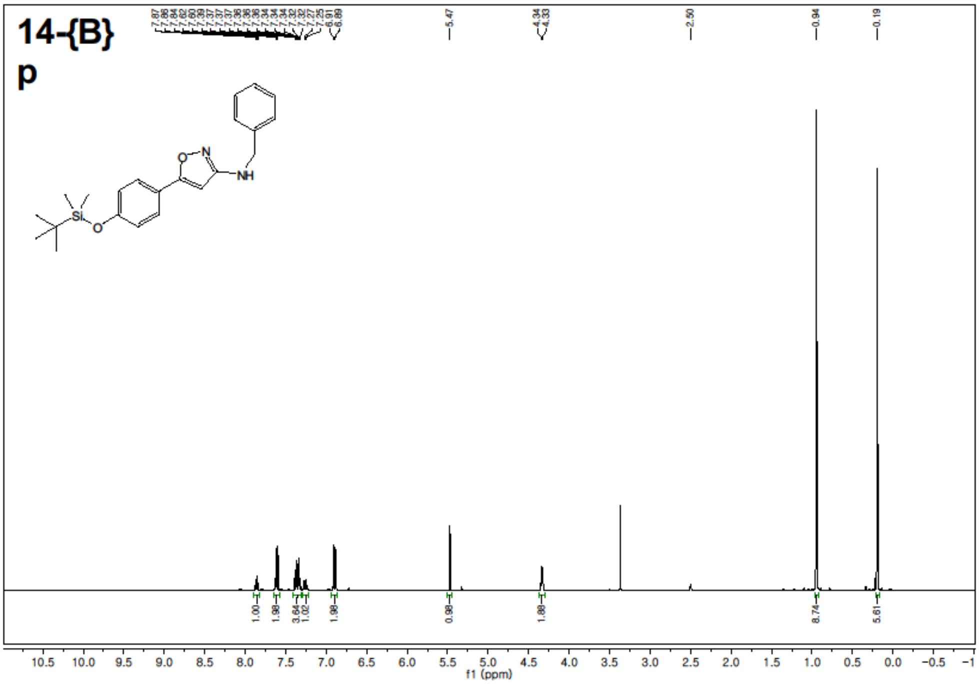
14-{B}
p
O
N
NH
Si
O
5.47
4.34
4.33
2.50
0.94
0.19
1.00
1.98
3.64
1.02
1.98
0.98
1.88
8.74
5.61
f1 (ppm)

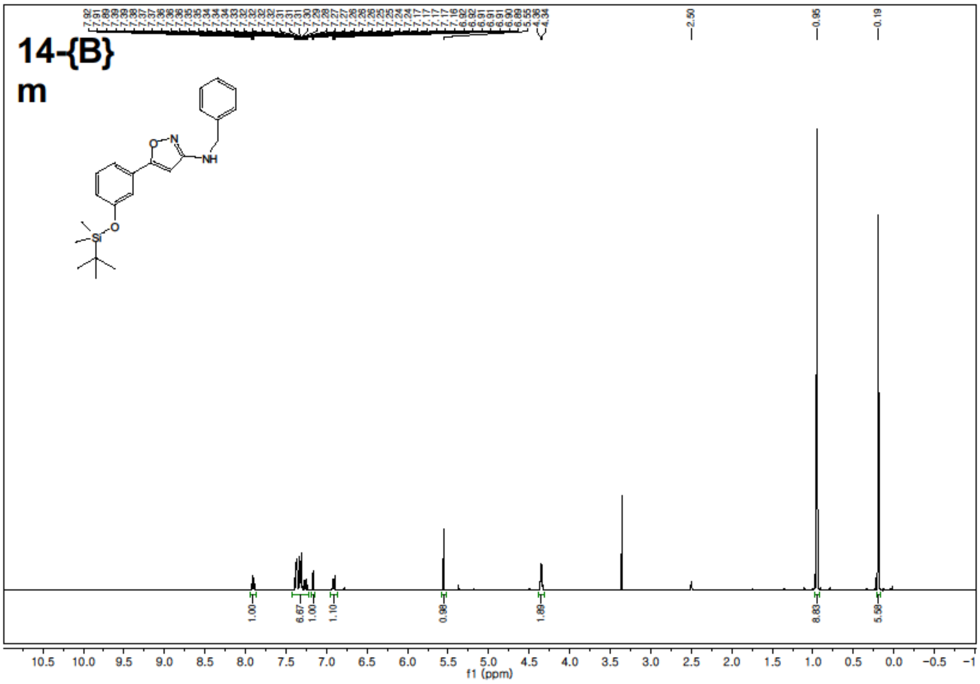
14-{B}
m
O
N
NH
Si
O
2.50
0.95
0.19
1.00
6.67
1.00
1.10
0.98
1.89
8.83
5.58
f1 (ppm)

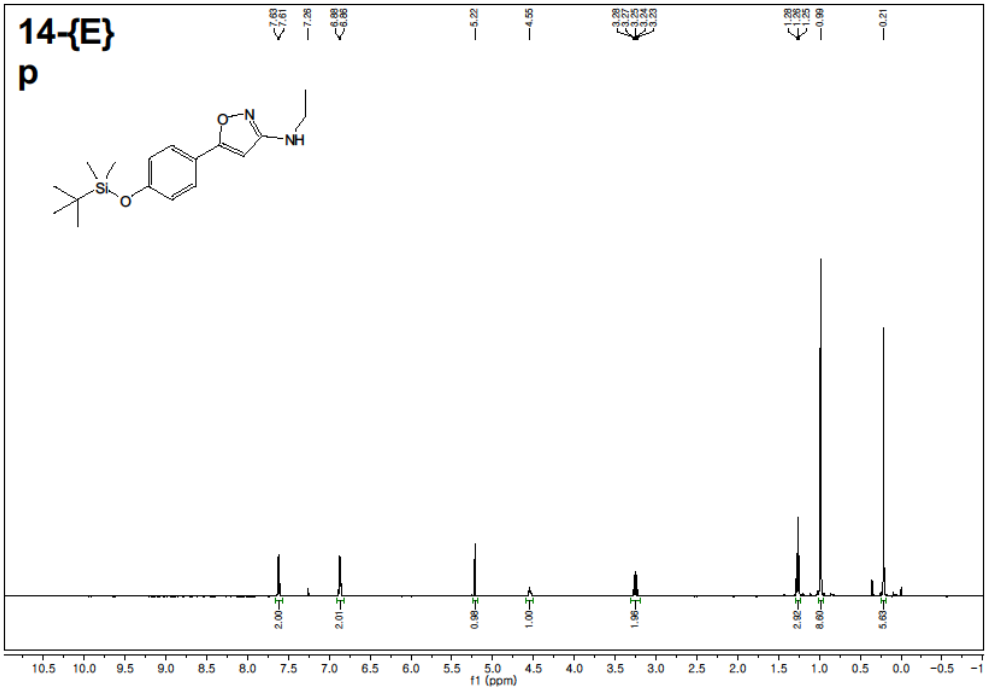
14-{E}
p
O
N
NH
Si
O
f1 (ppm)

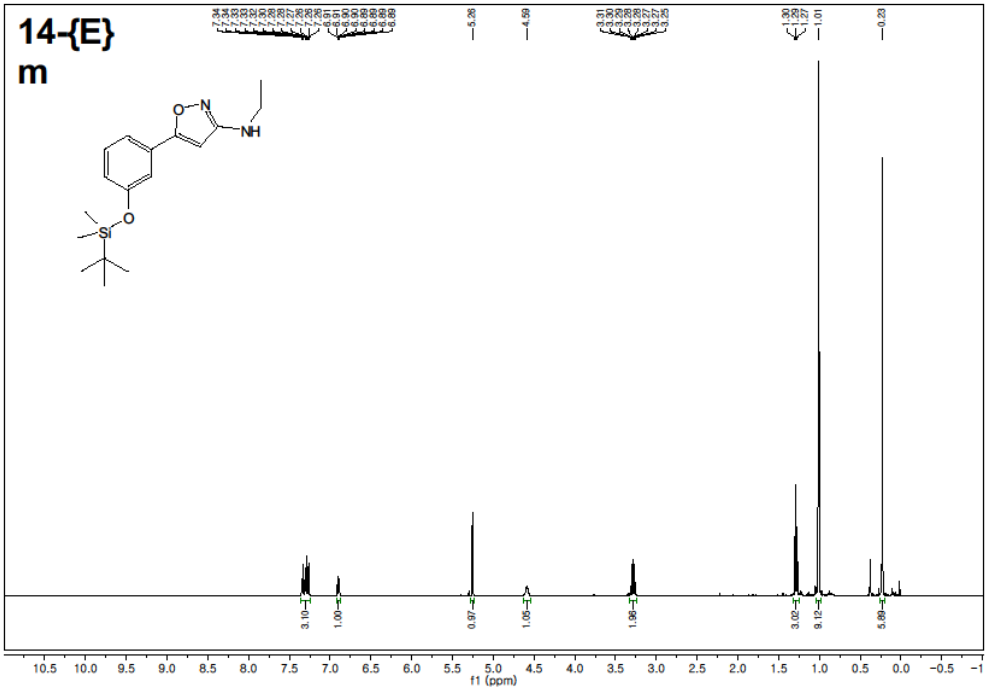
14-{E}
m
O
N
NH
Si
O
f1 (ppm)

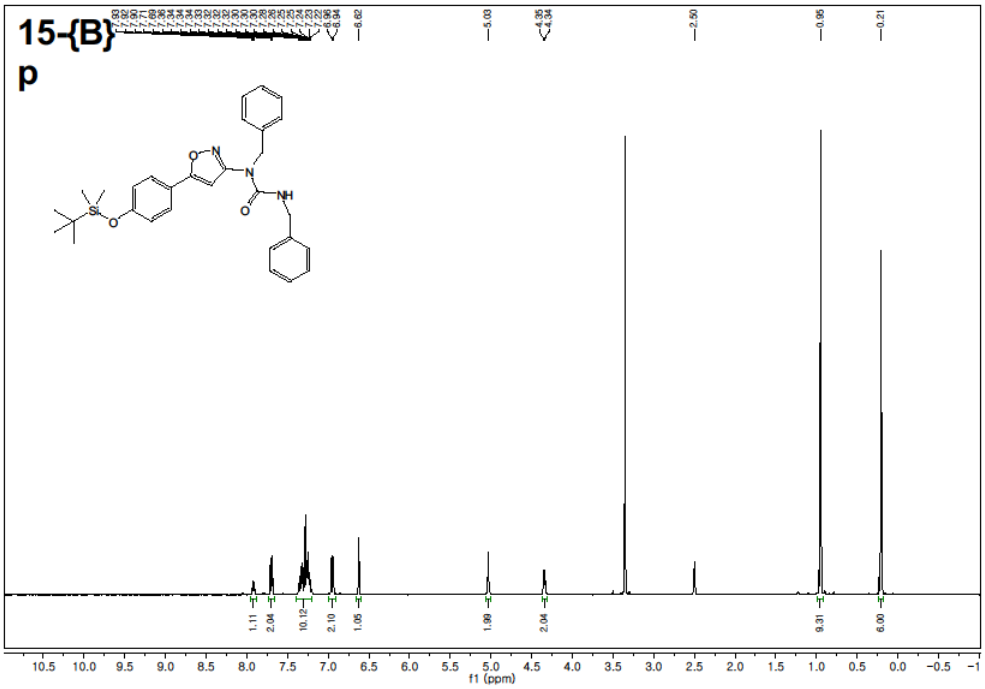
15-{B}
p
f1 (ppm)

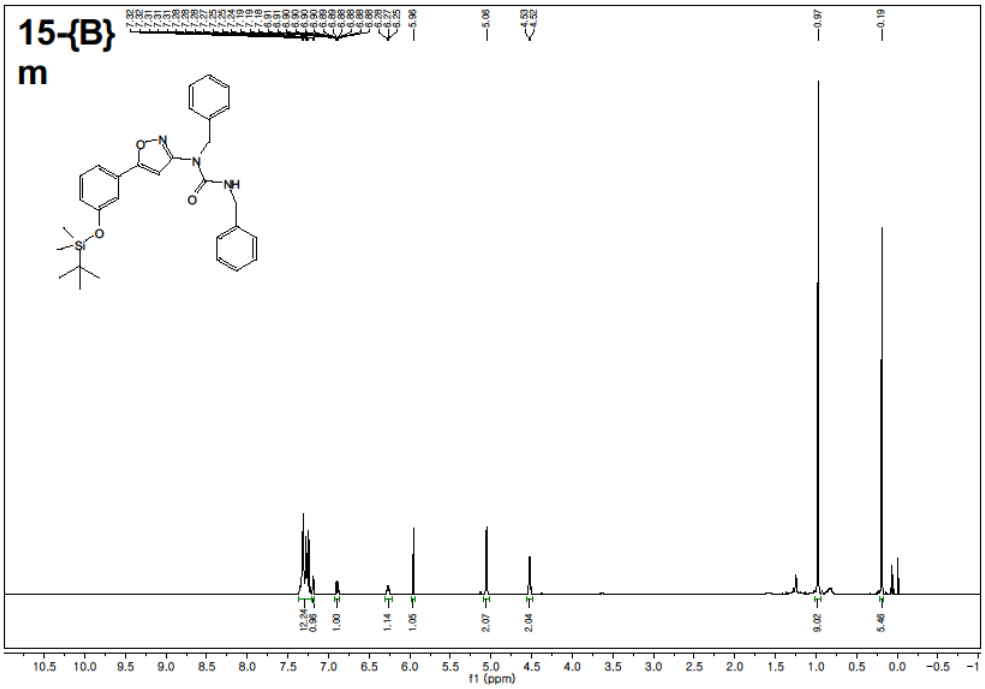
15-{B}
m
f1 (ppm)

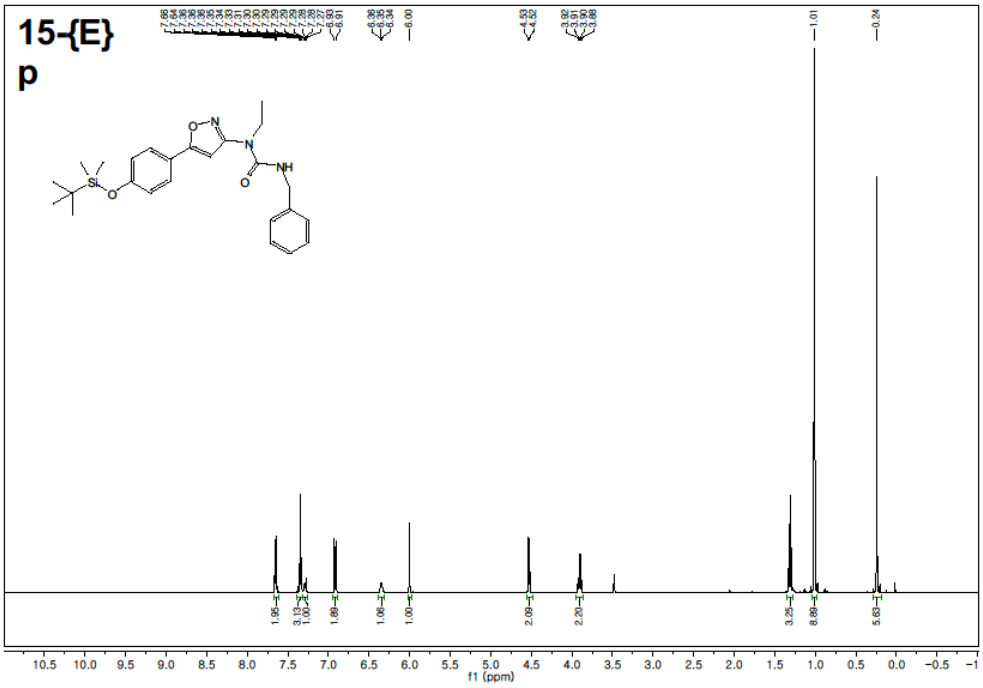
15-{E}
p
f1 (ppm)

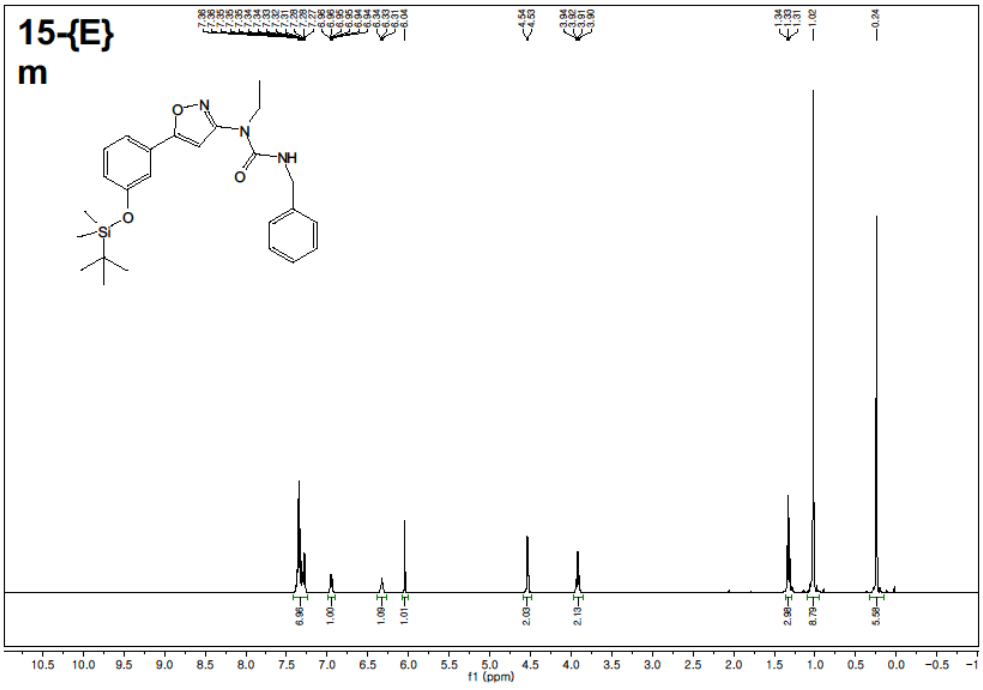
15-{E}
m
f1 (ppm)

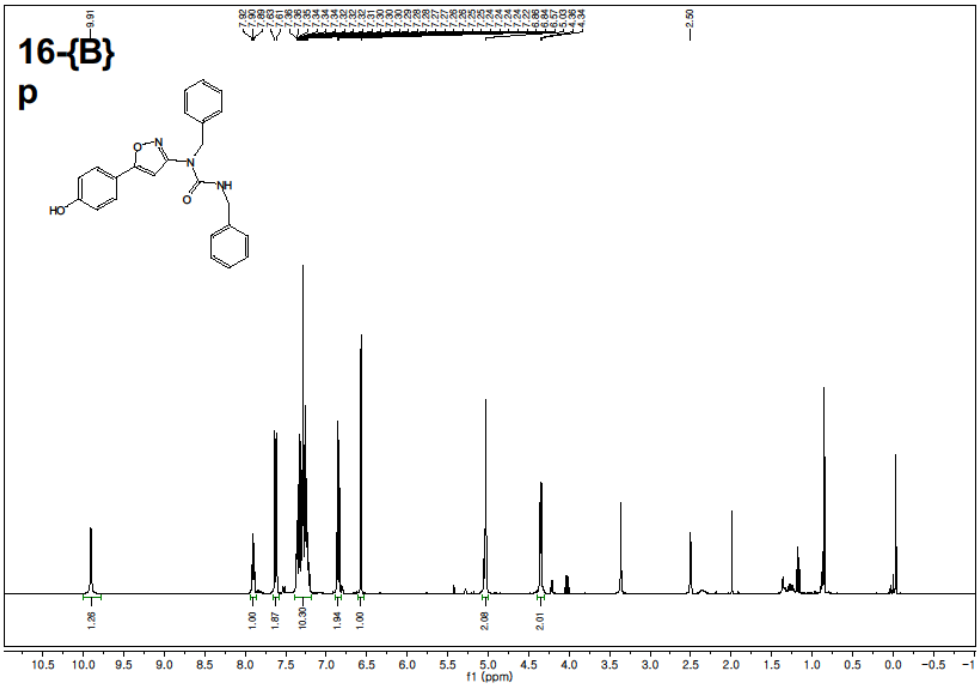
16-{B}
p
HO
O
N
NH
f1 (ppm)

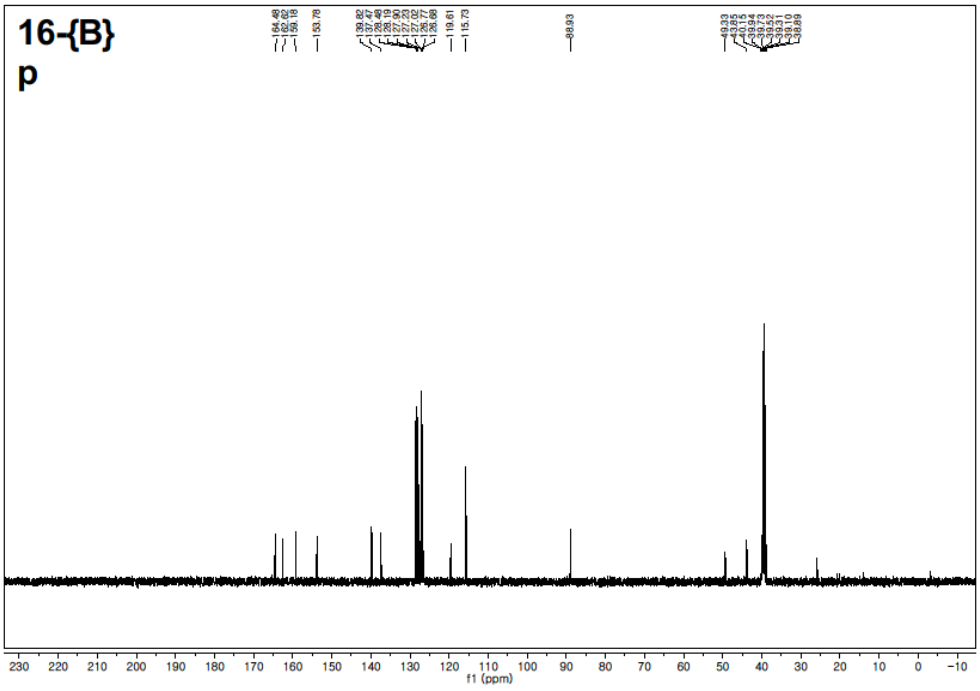
16-{B}
p
f1 (ppm)

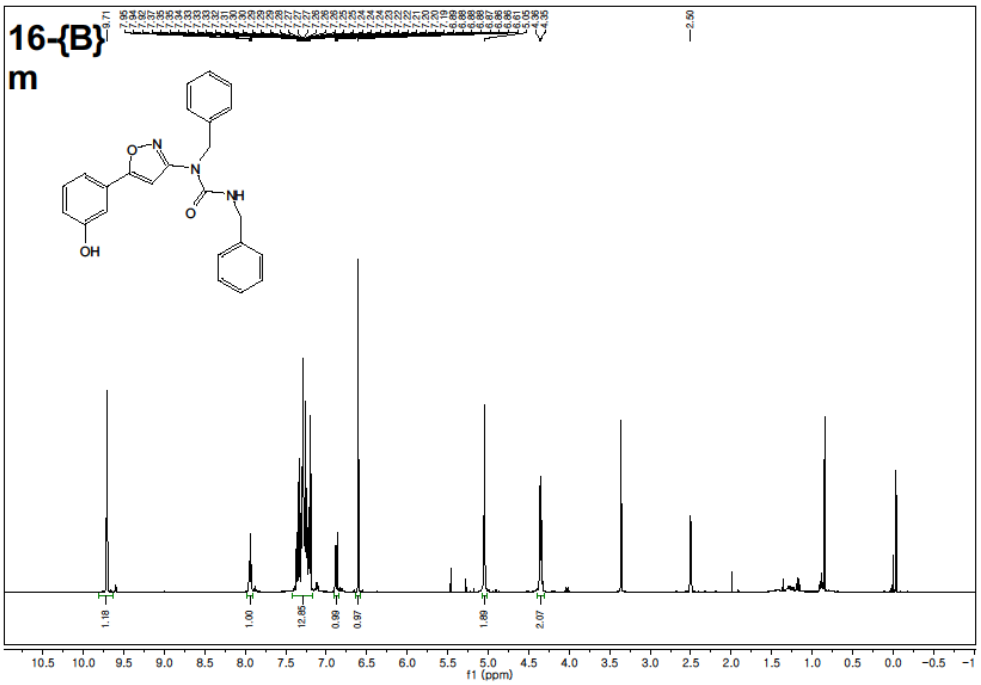
16-{B}
m
OH
NH
1.18
1.00
12.85
0.99
0.97
1.89
2.07
f1 (ppm)

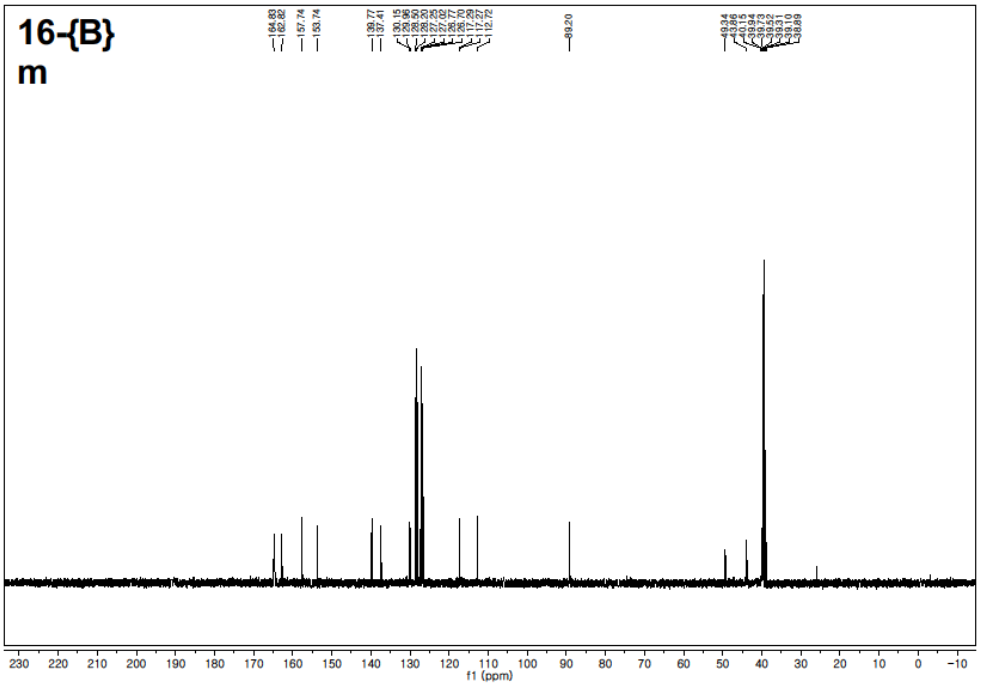
16-{B}
m
f1 (ppm)

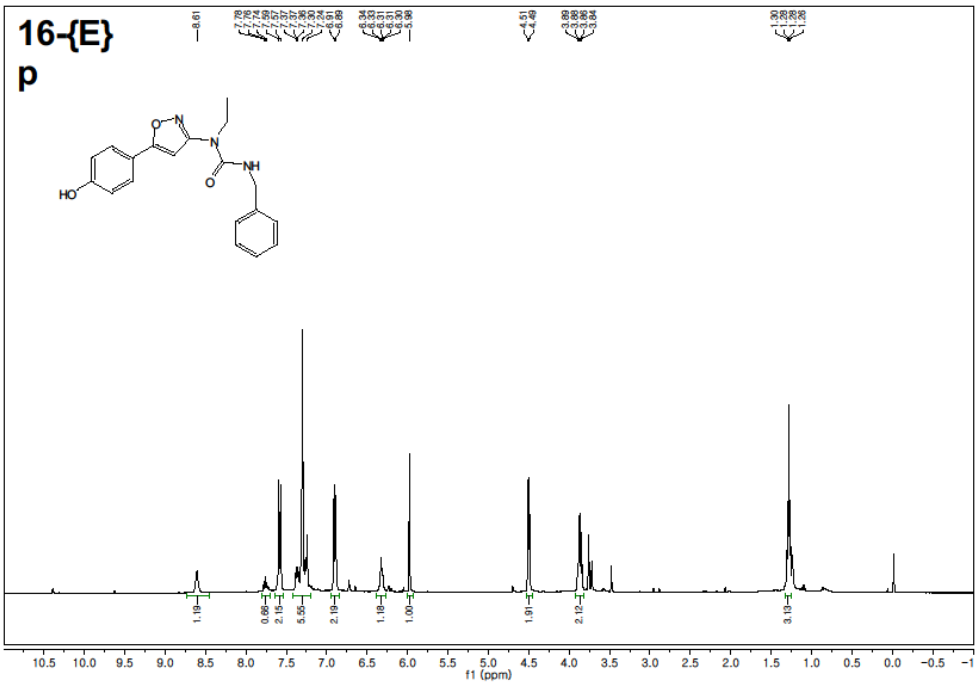
16-{E}
p
HO
O
N
NH
O
f1 (ppm)

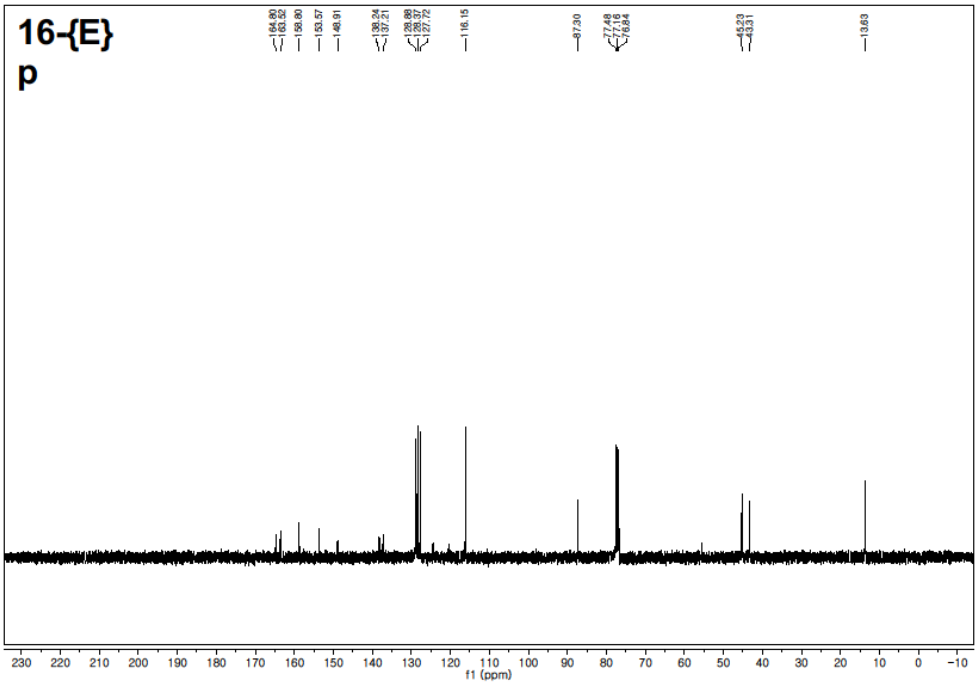
16-{E}
p
f1 (ppm)

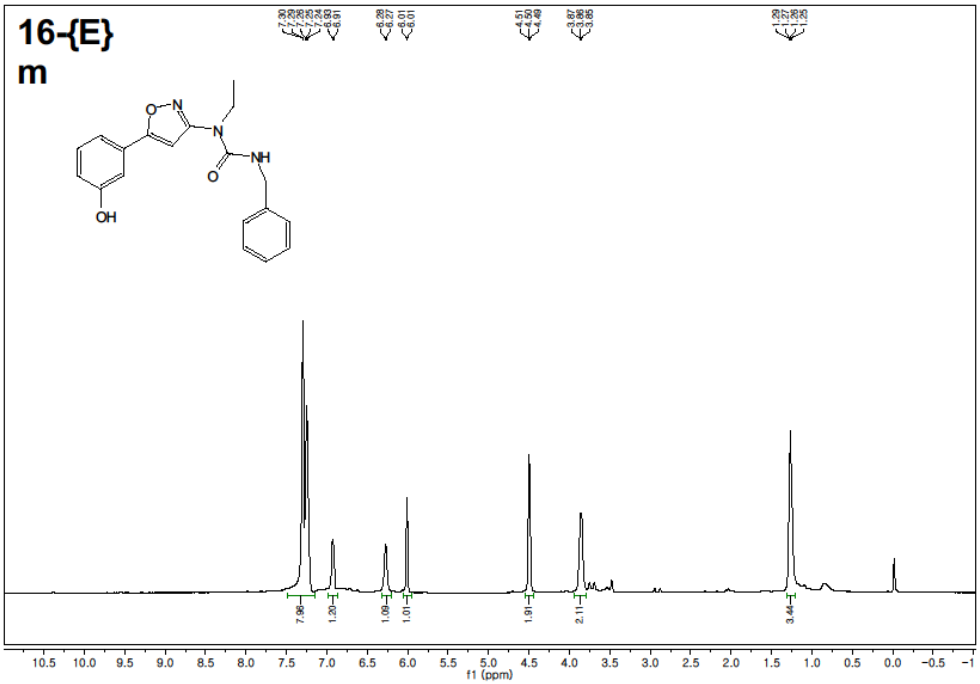
16-{E}
m
O
N
N
O
NH
OH
7.30
7.29
7.26
7.25
7.24
6.93
6.91
6.28
6.27
6.01
6.01
4.51
4.50
4.49
3.87
3.86
3.86
1.29
1.27
1.26
1.25
7.06
1.20
1.09
1.01
1.91
2.11
3.44
f1 (ppm)

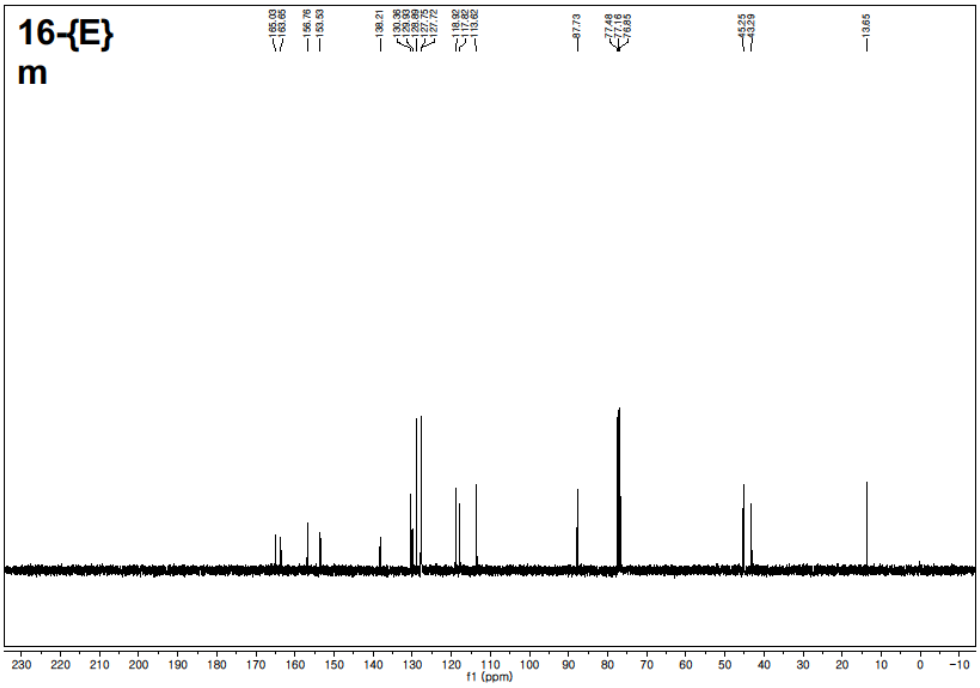
16-{E}
m
165.03
163.66
156.76
153.53
138.21
130.36
129.00
128.69
127.72
127.72
119.92
117.77
113.62
87.73
77.48
77.16
76.85
45.25
43.29
13.65
f1 (ppm)

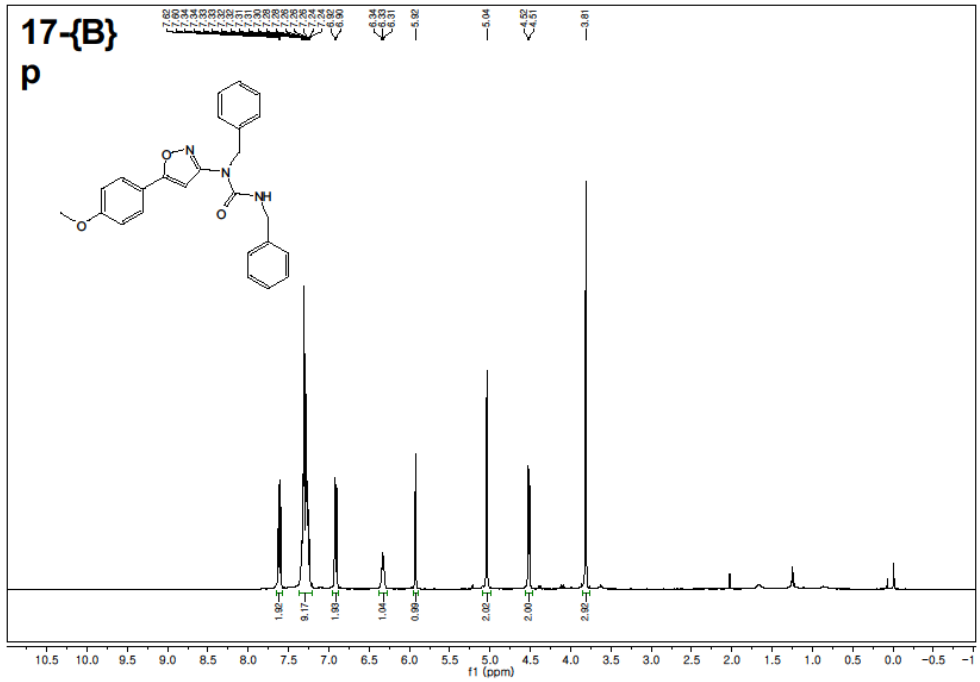
17-{B}
p
f1 (ppm)

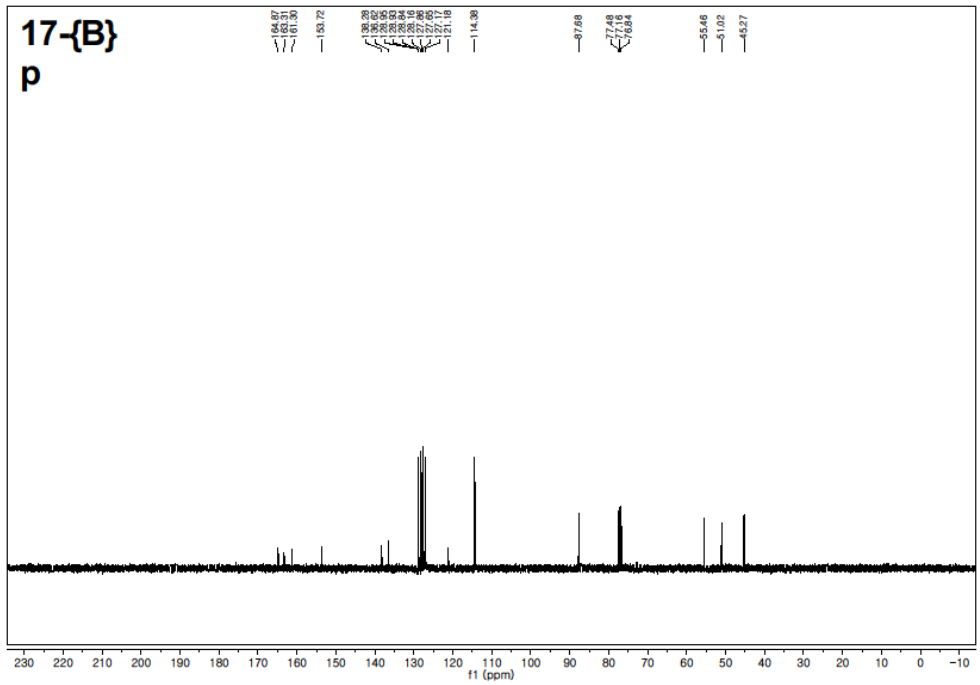
17-{B}
p
f1 (ppm)

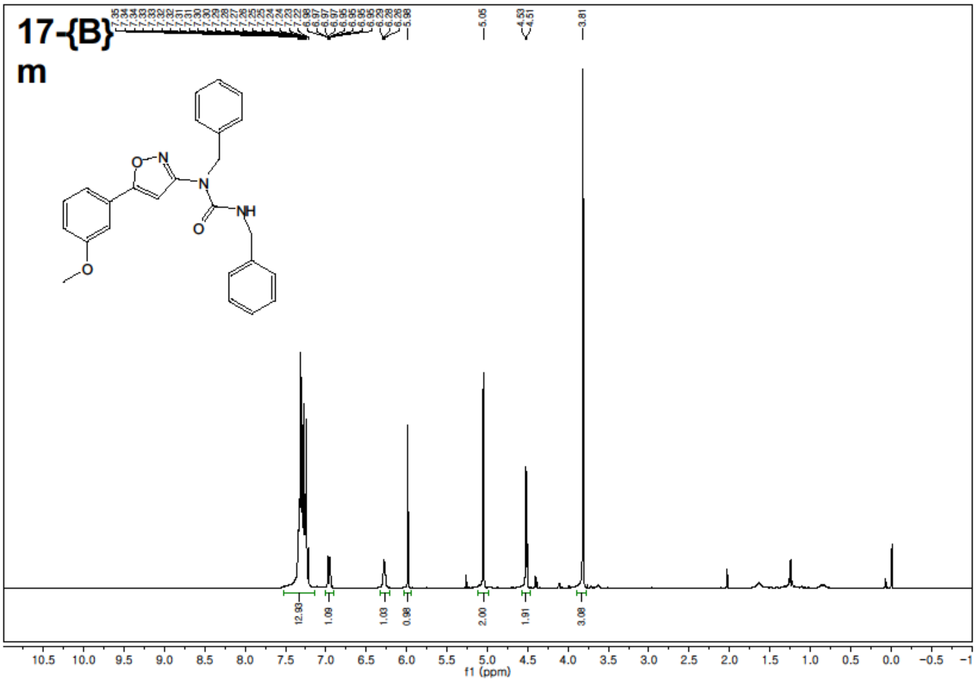

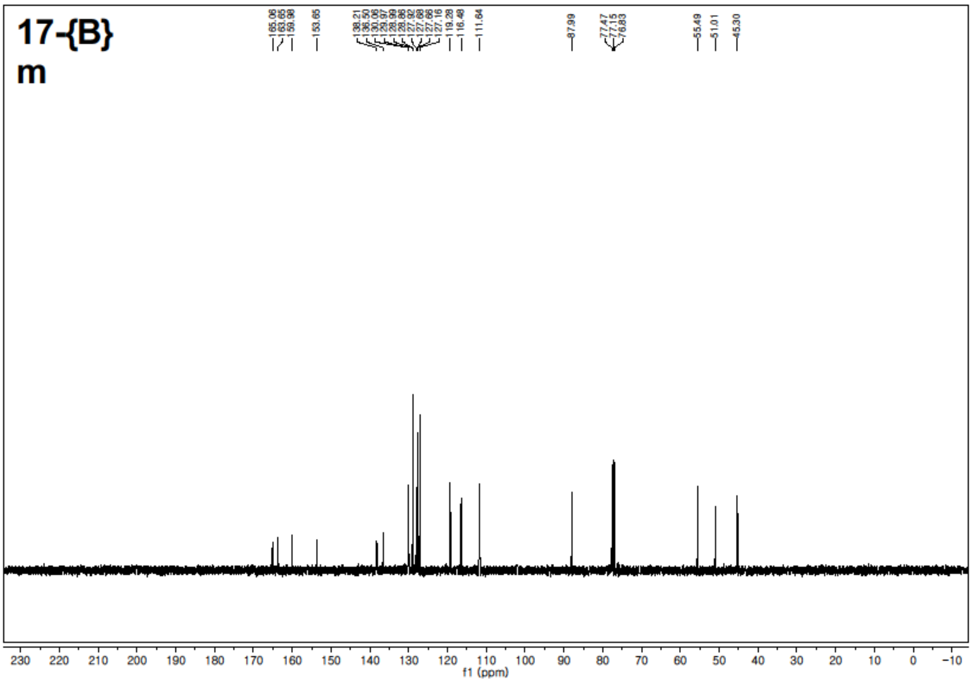

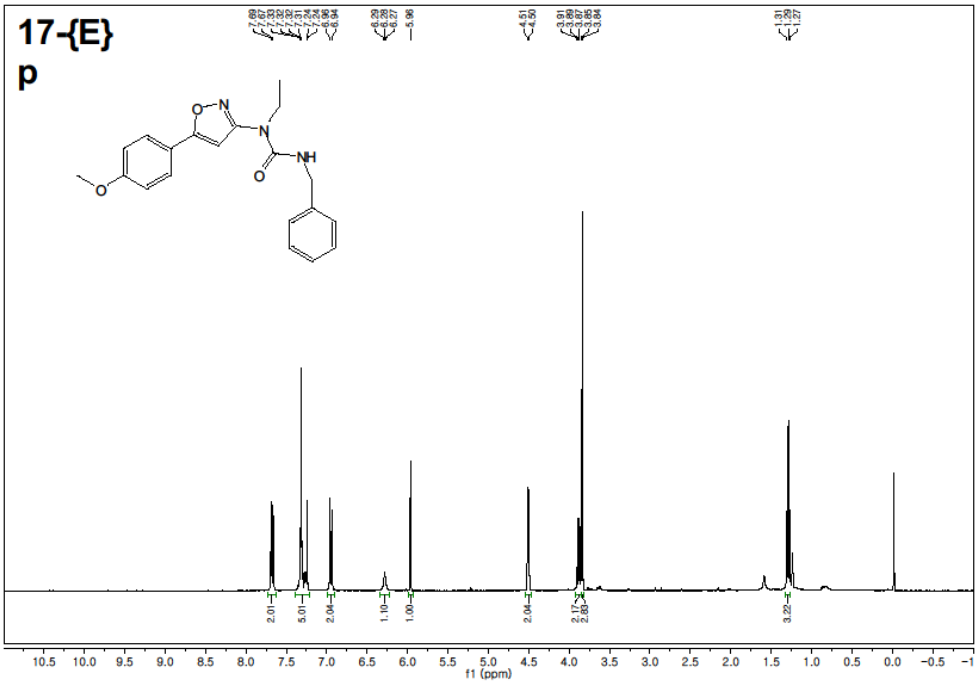
17-{E}
p
f1 (ppm)

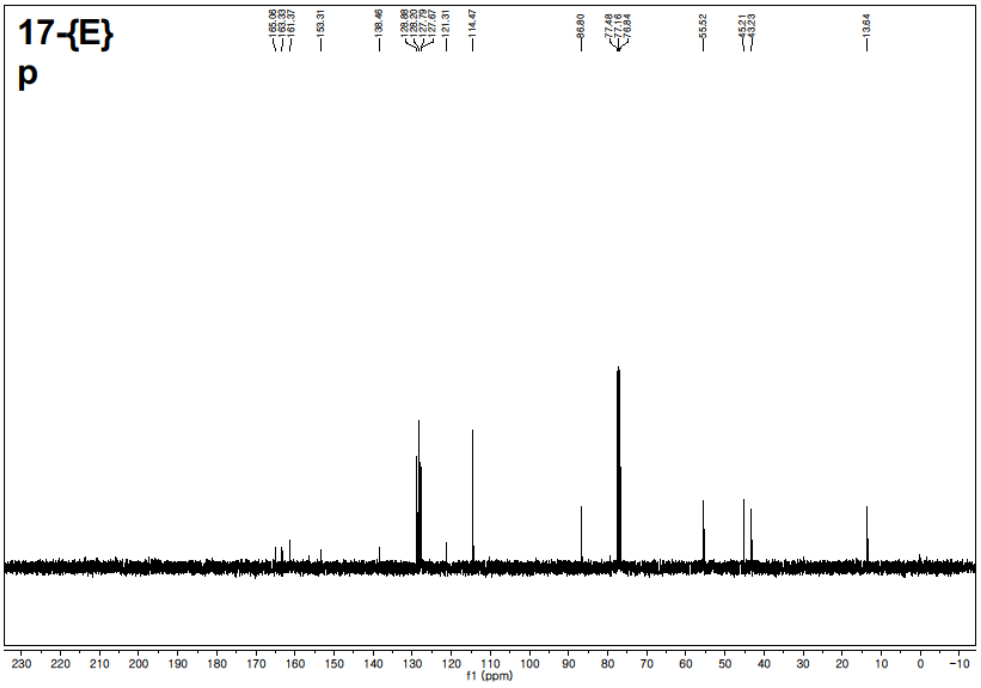
17-{E}
p
f1 (ppm)

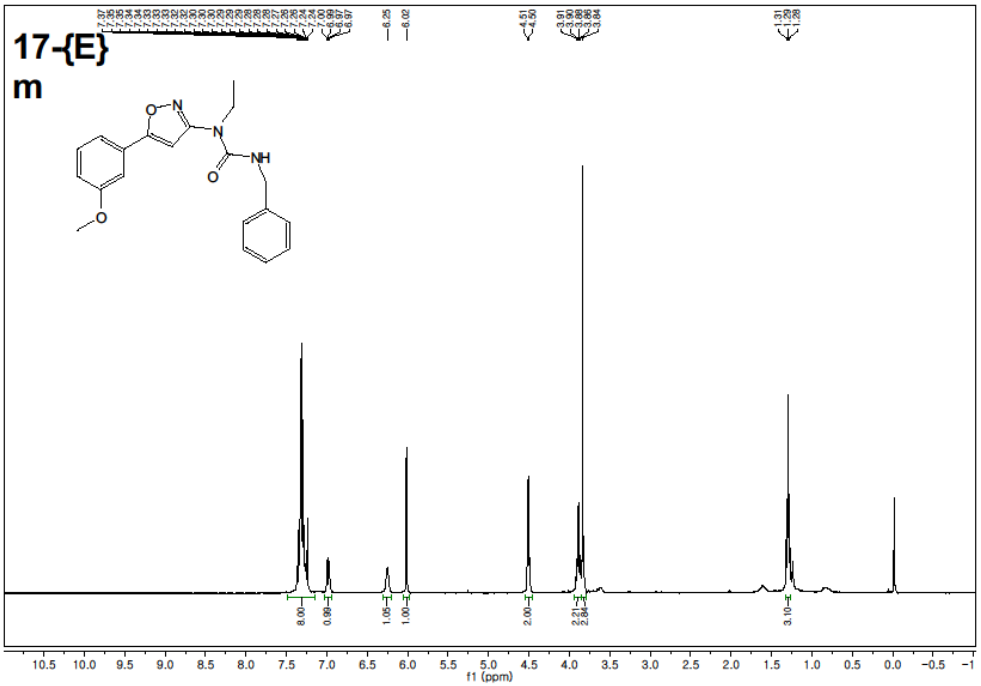
17-{E}
m
f1 (ppm)

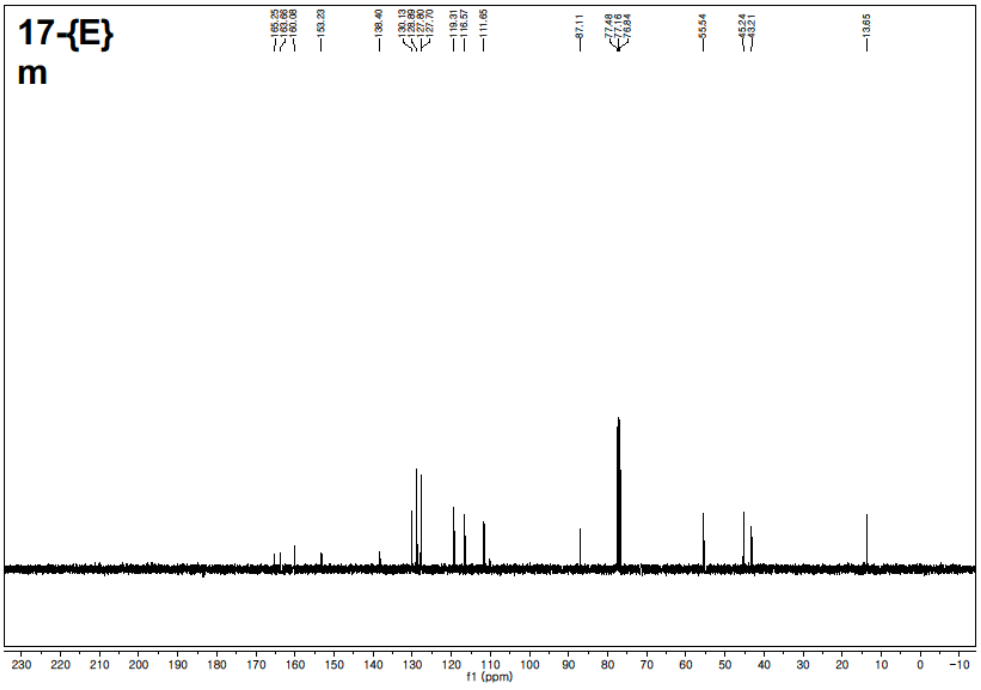
17-{E}
m
f1 (ppm)

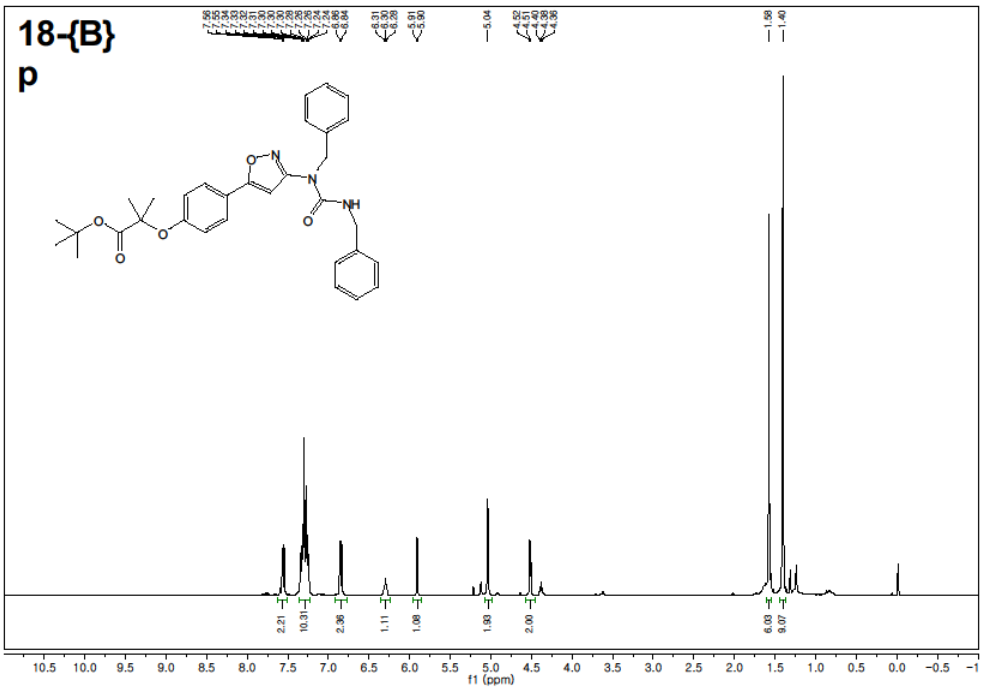
18-{B}
p
f1 (ppm)

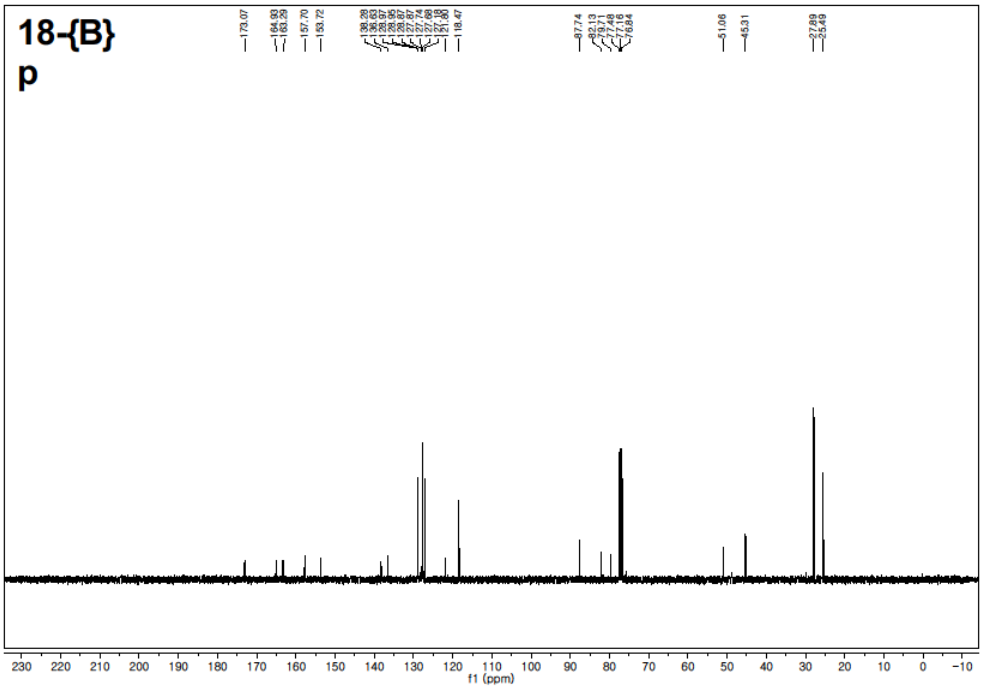
18-{B}
p
f1 (ppm)

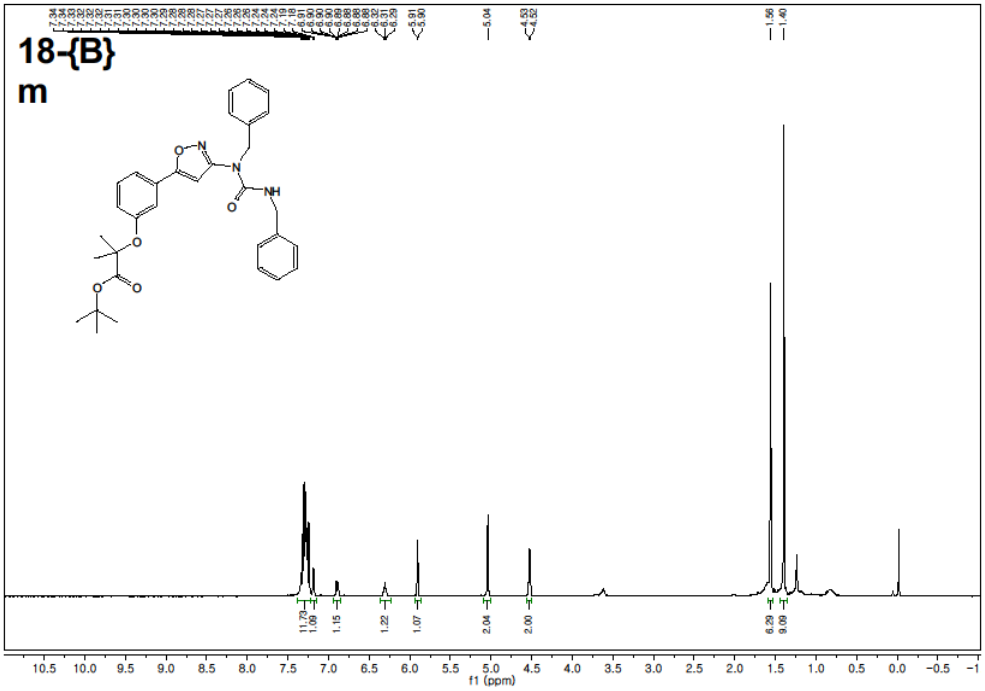
18-{B}
m
f1 (ppm)

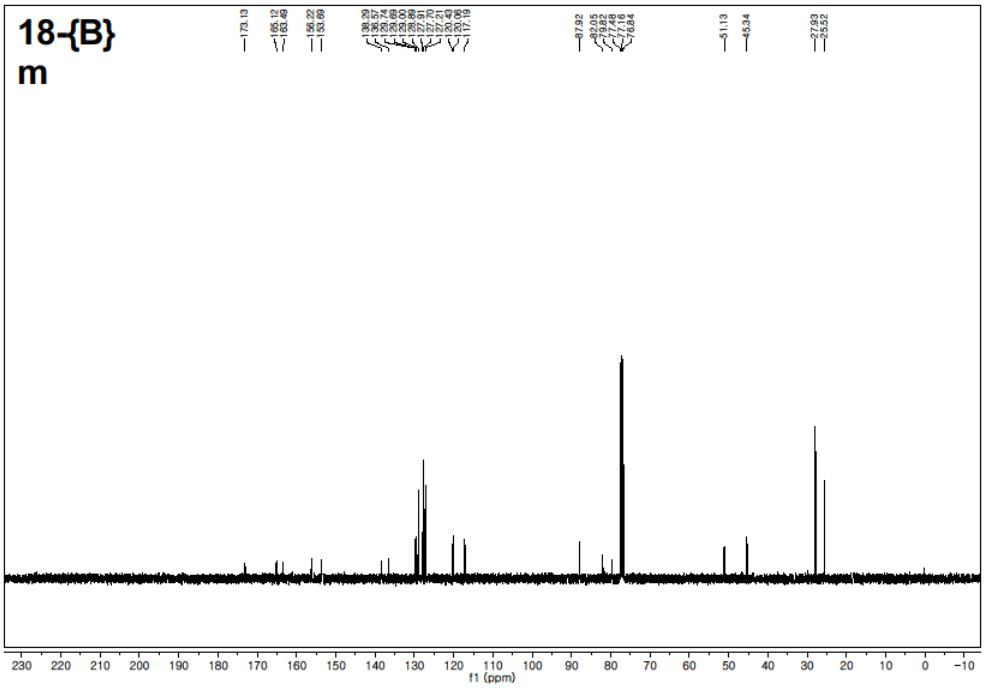
18-{B}
m
f1 (ppm)

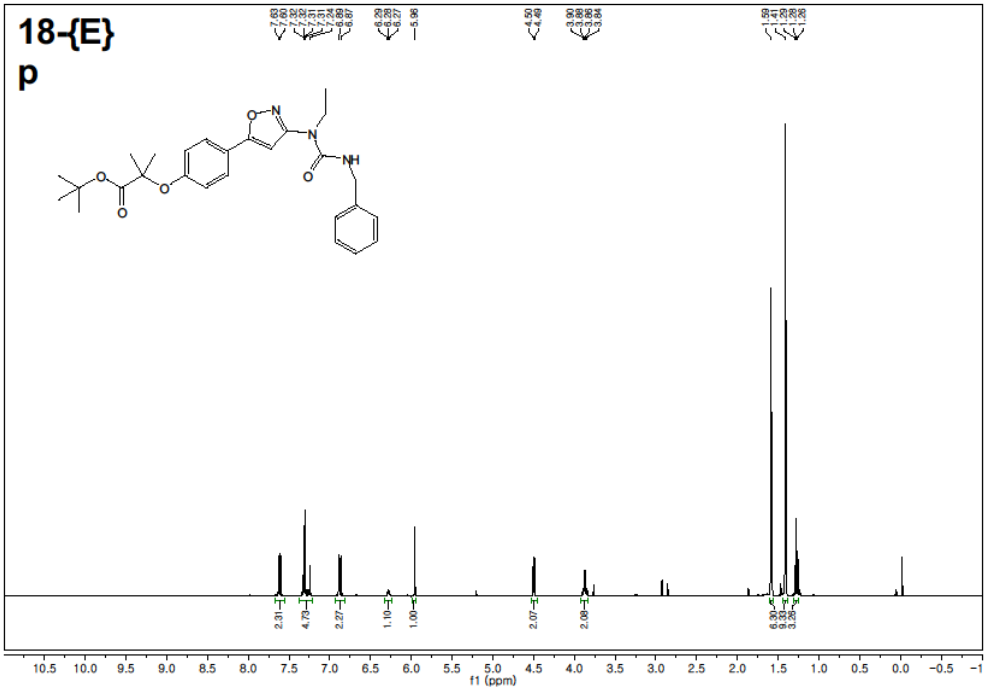
18-{E}
p
f1 (ppm)

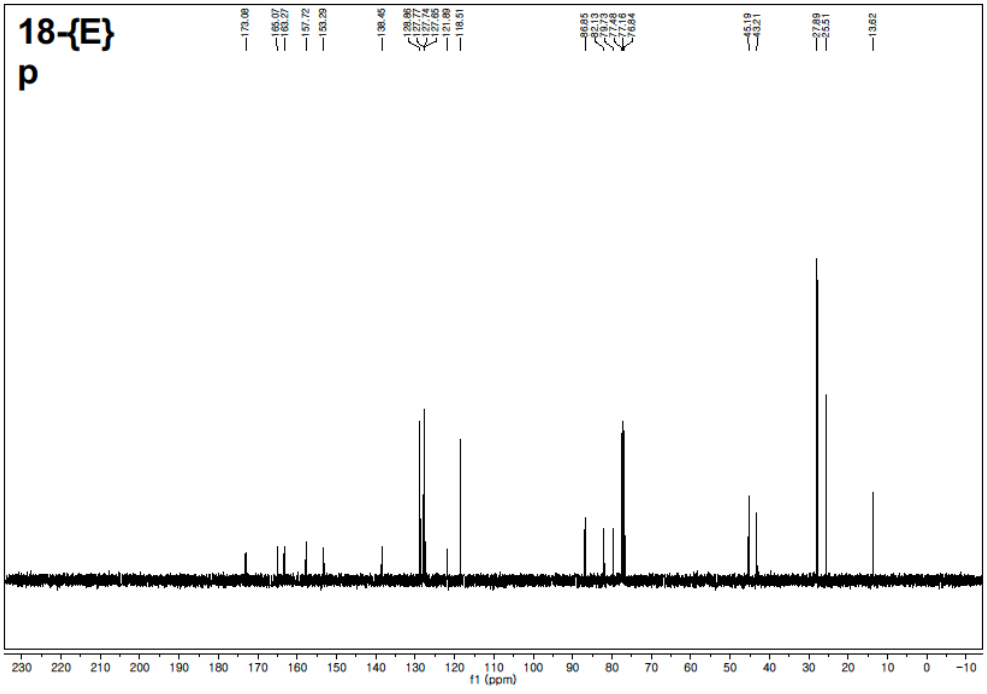
18-{E}
p
f1 (ppm)

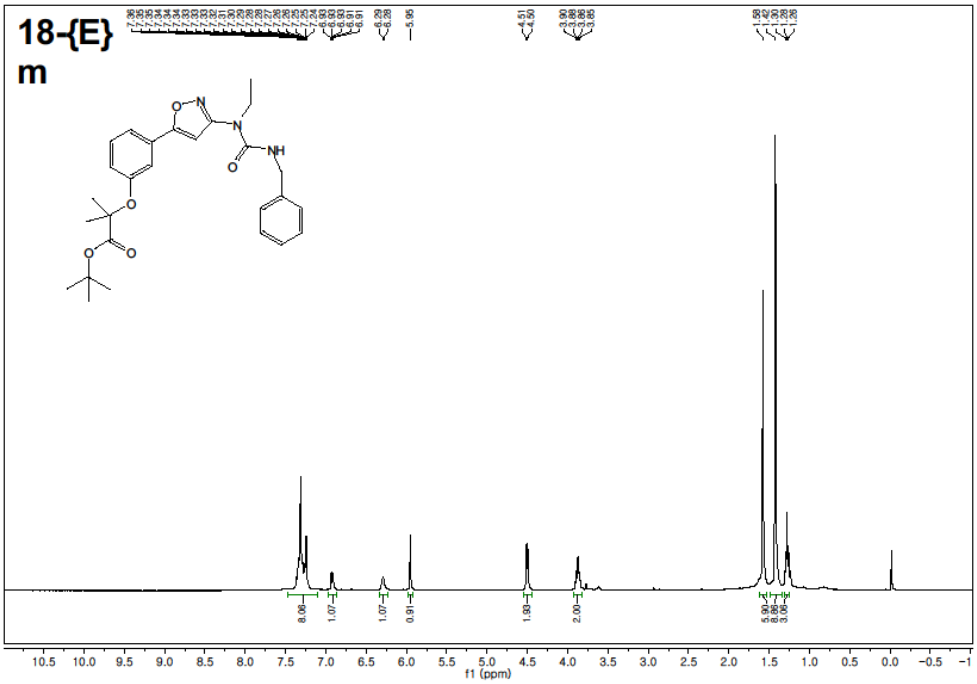
18-{E}
m
f1 (ppm)

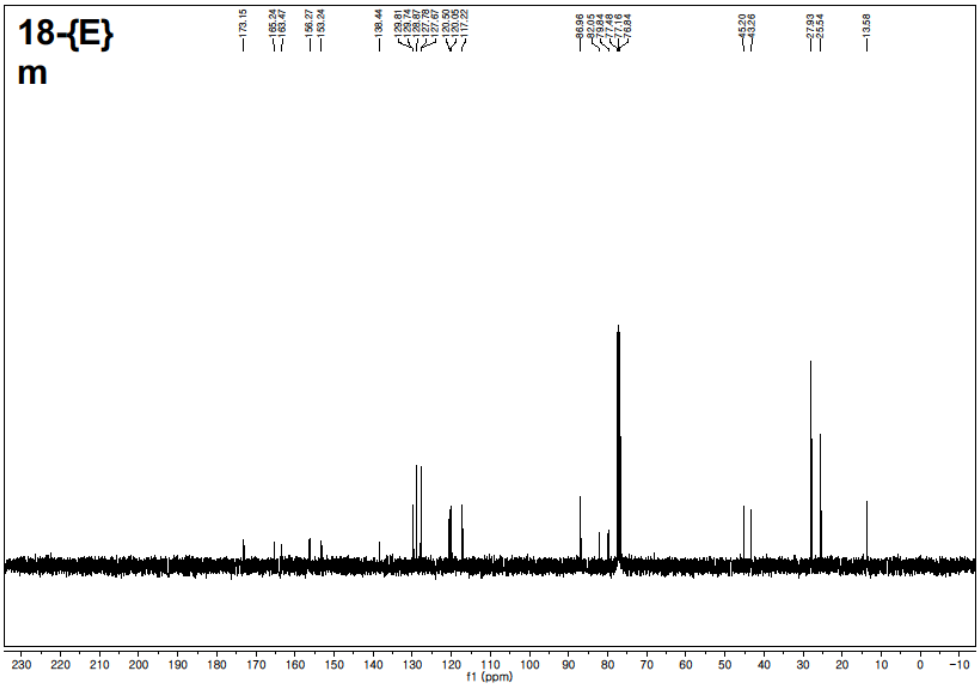
18-{E}
m
f1 (ppm)

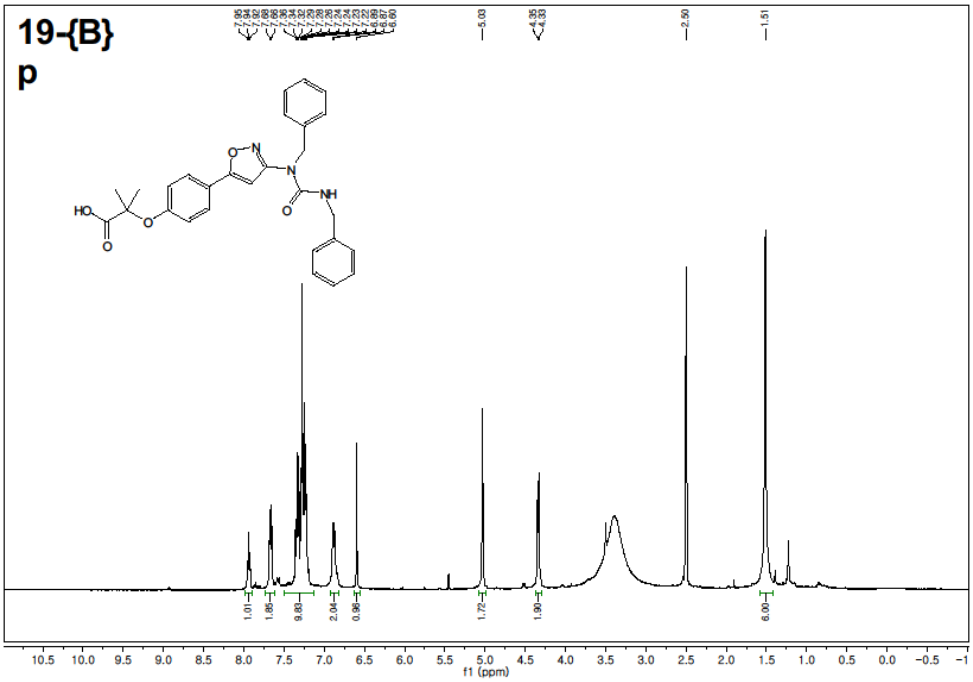
19-{B}
p
f1 (ppm)

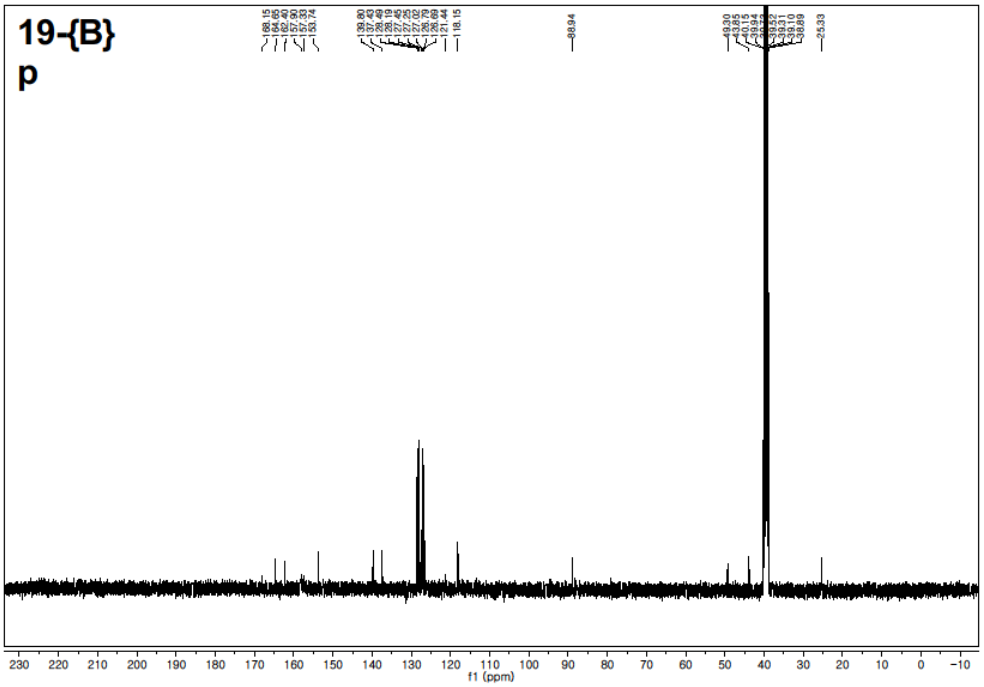
19-{B}
p
f1 (ppm)

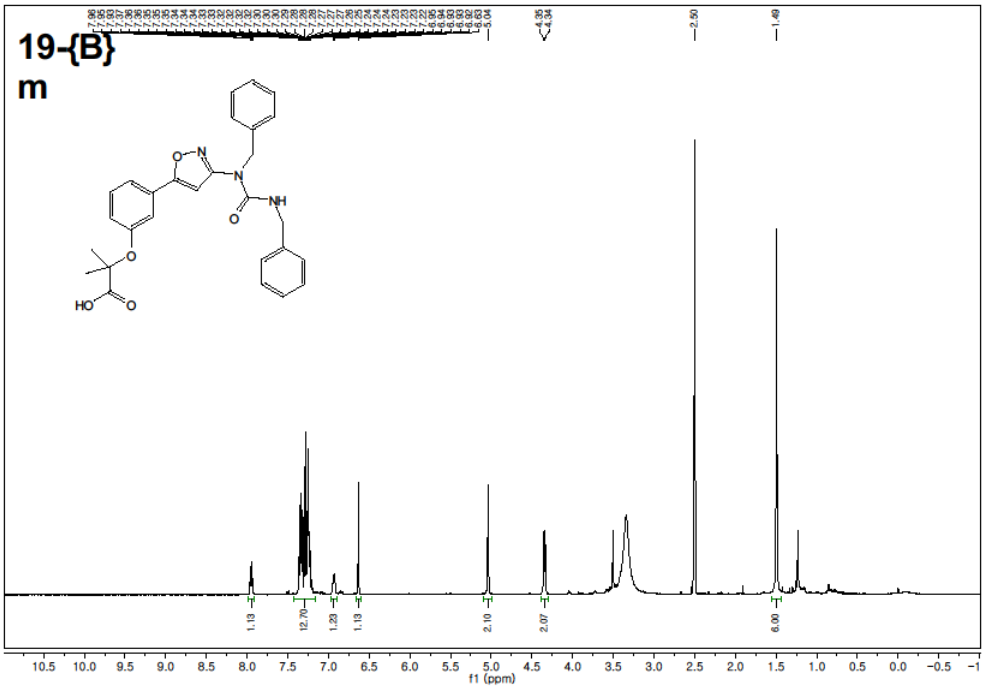
19-{B}
m
f1 (ppm)

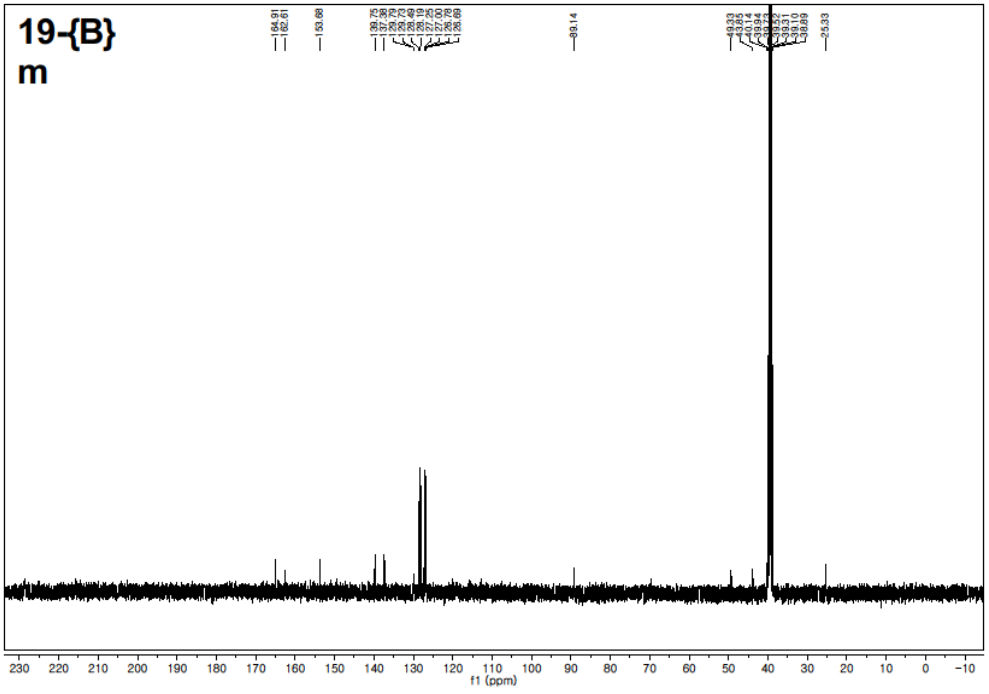
19-{B}
m
f1 (ppm)

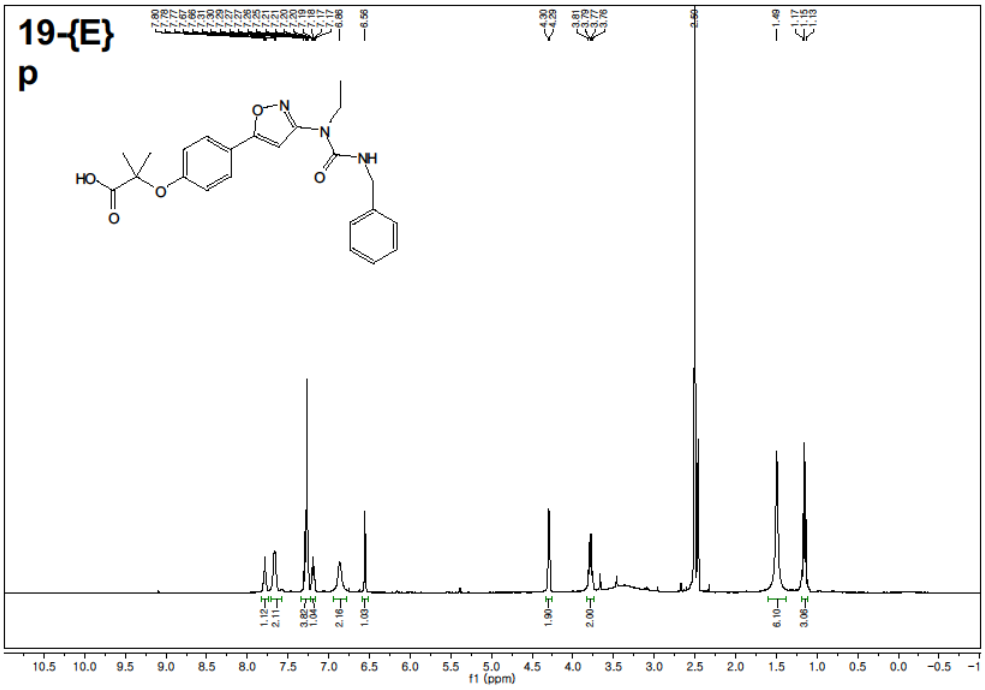
19-{E}
p
HO
O
O
N
N
NH
O
f1 (ppm)

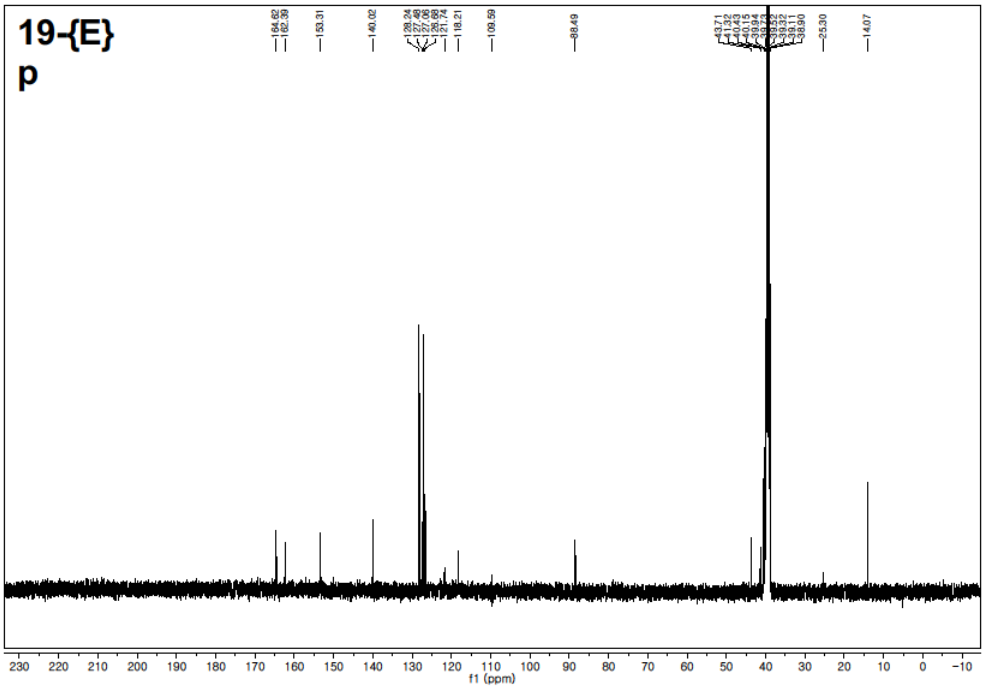
19-{E}
p
f1 (ppm)

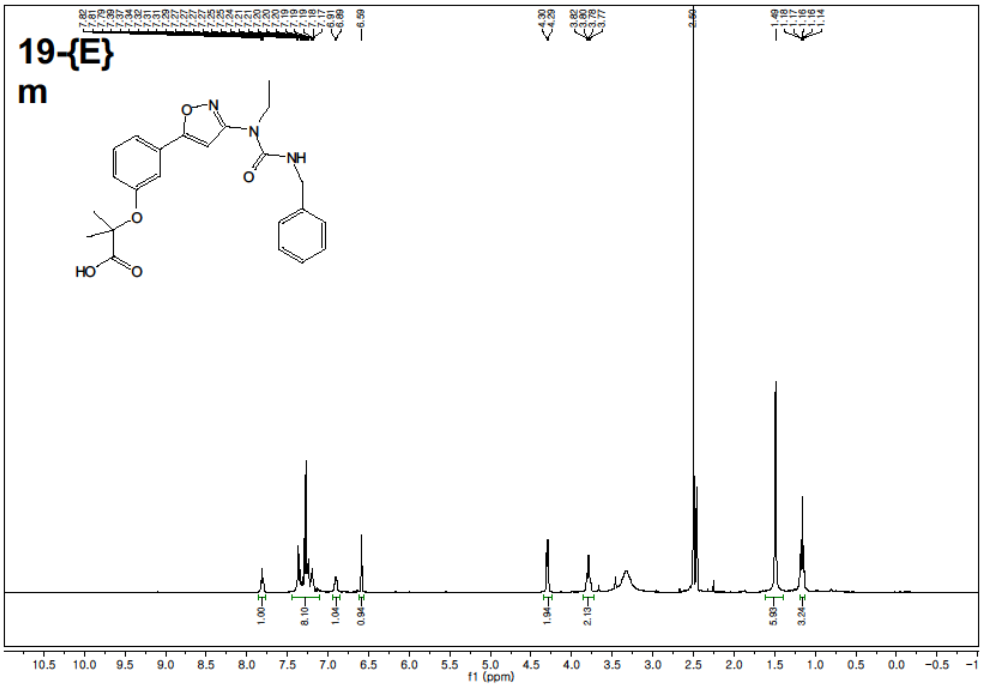
19-{E}
m
f1 (ppm)

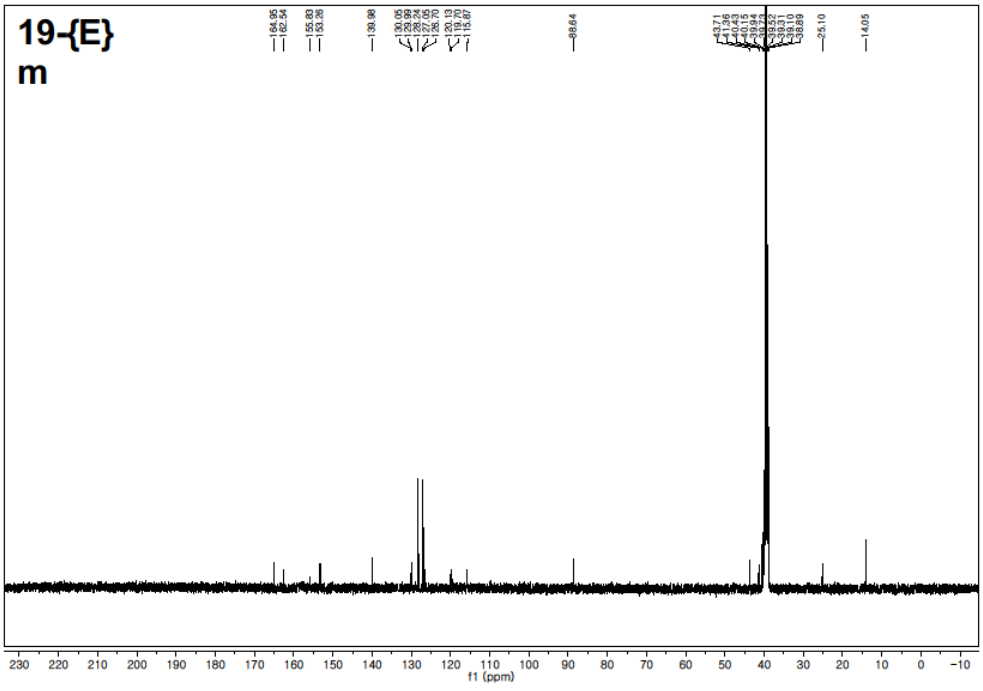
19-{E}
m
f1 (ppm)

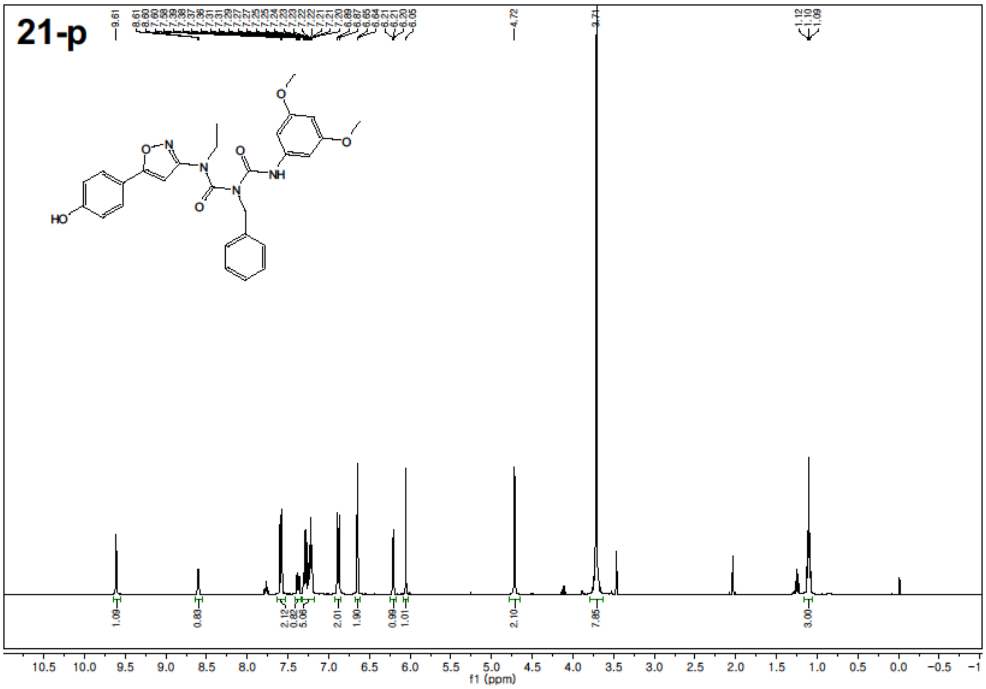
21-p
HO
O
N
NH
f1 (ppm)

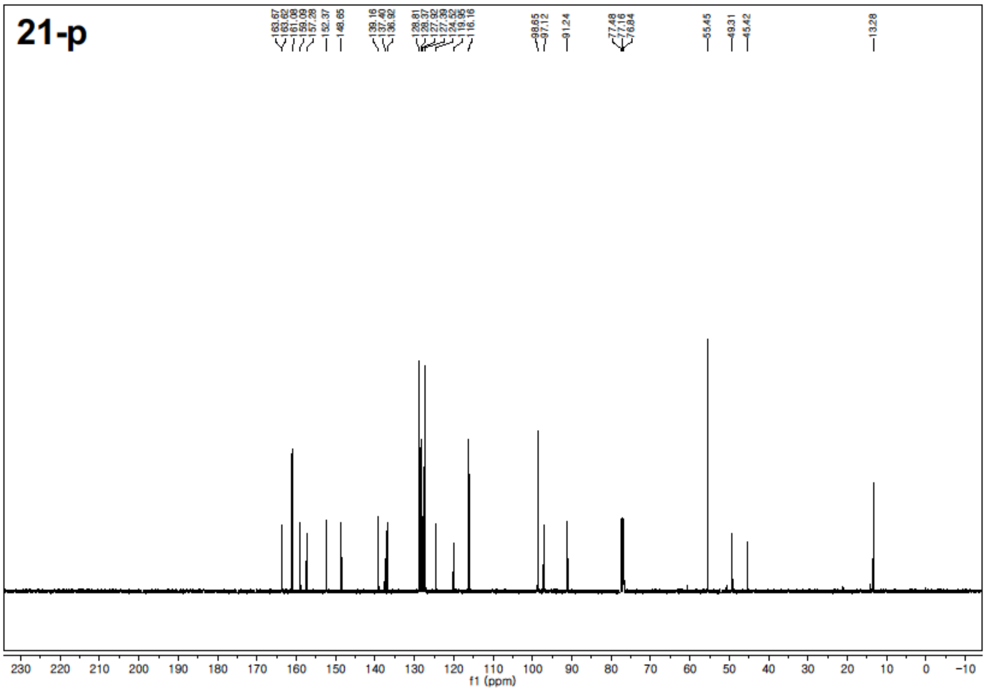
21-p
f1 (ppm)

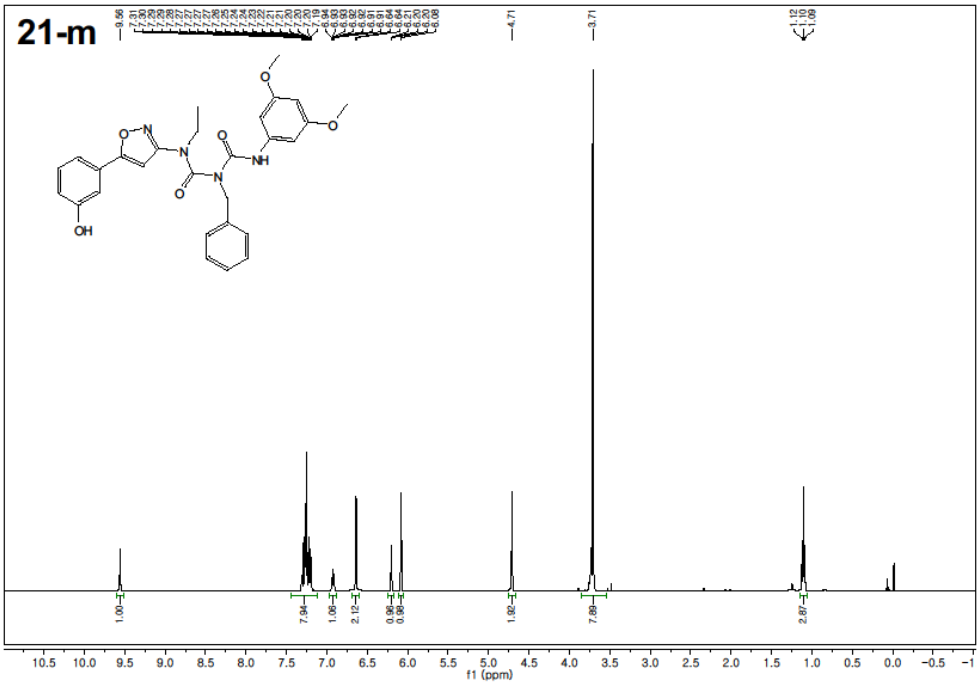
21-m
f1 (ppm)

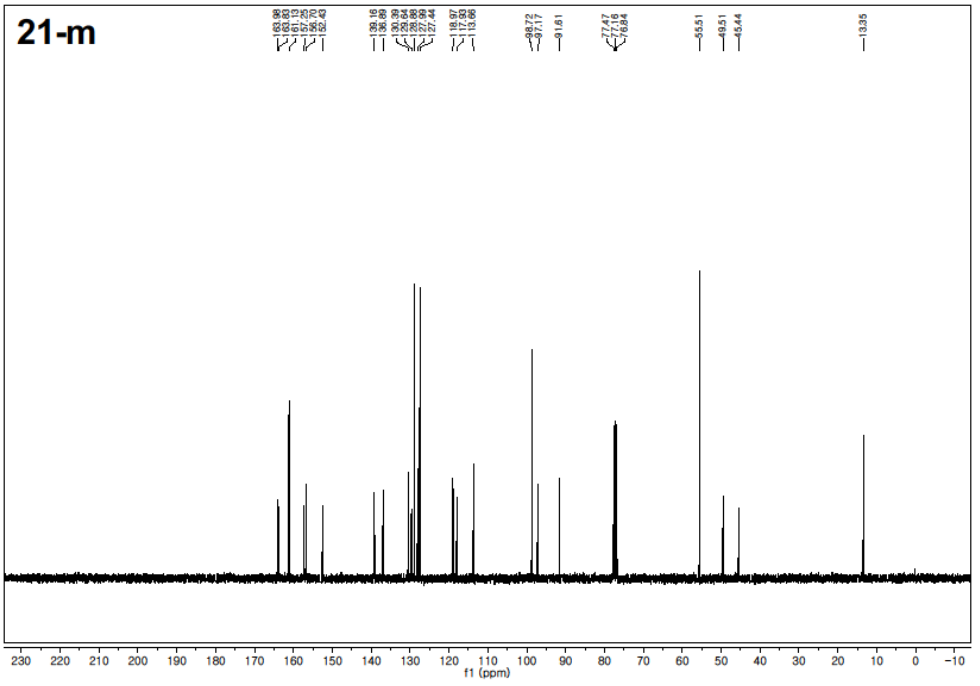
21-m
f1 (ppm)

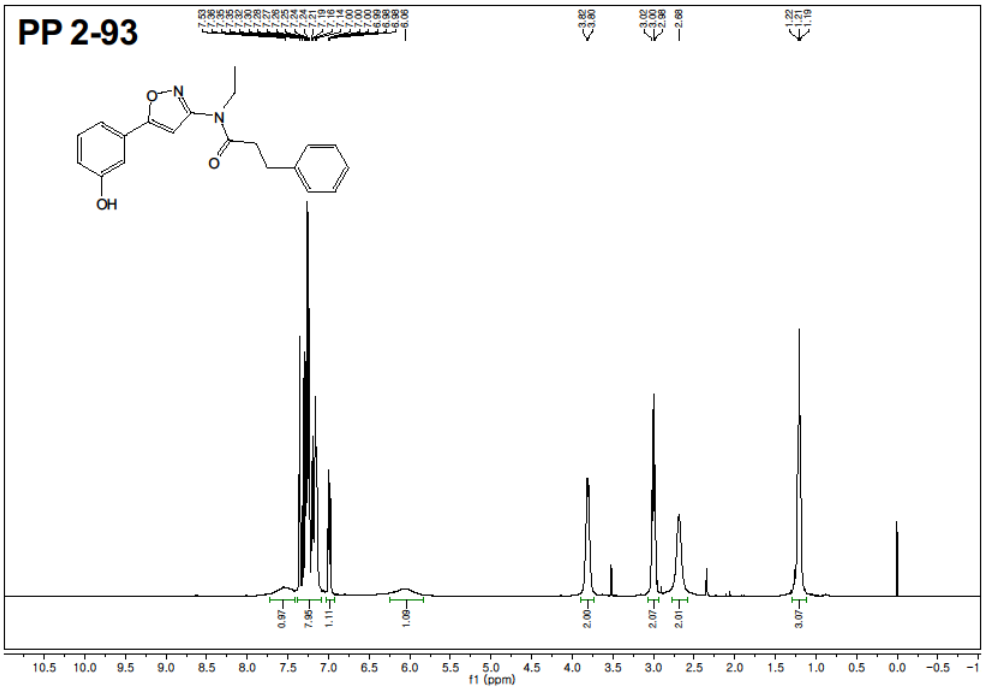
PP 2-93
O
N
N
O
OH
f1 (ppm)

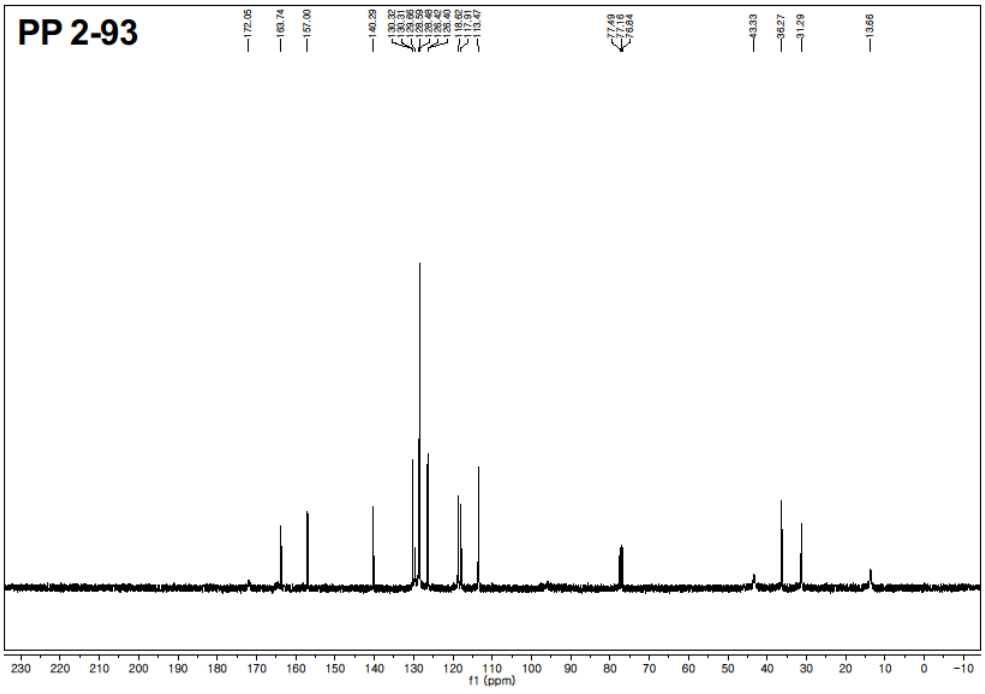
PP 2-93
f1 (ppm)

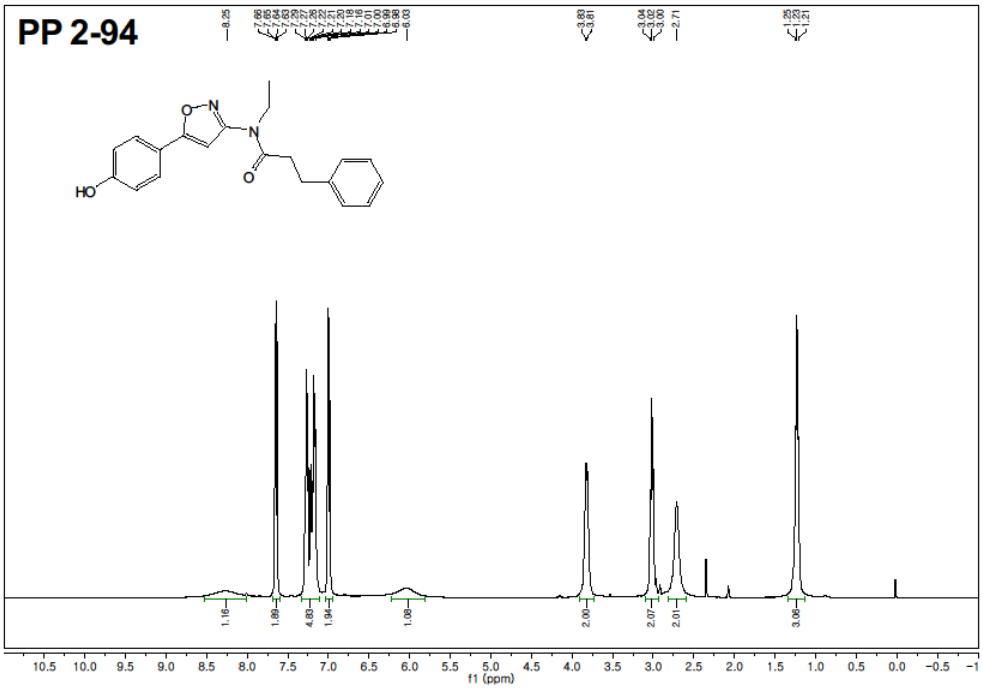
PP 2-94
HO
O
N
N
O
f1 (ppm)

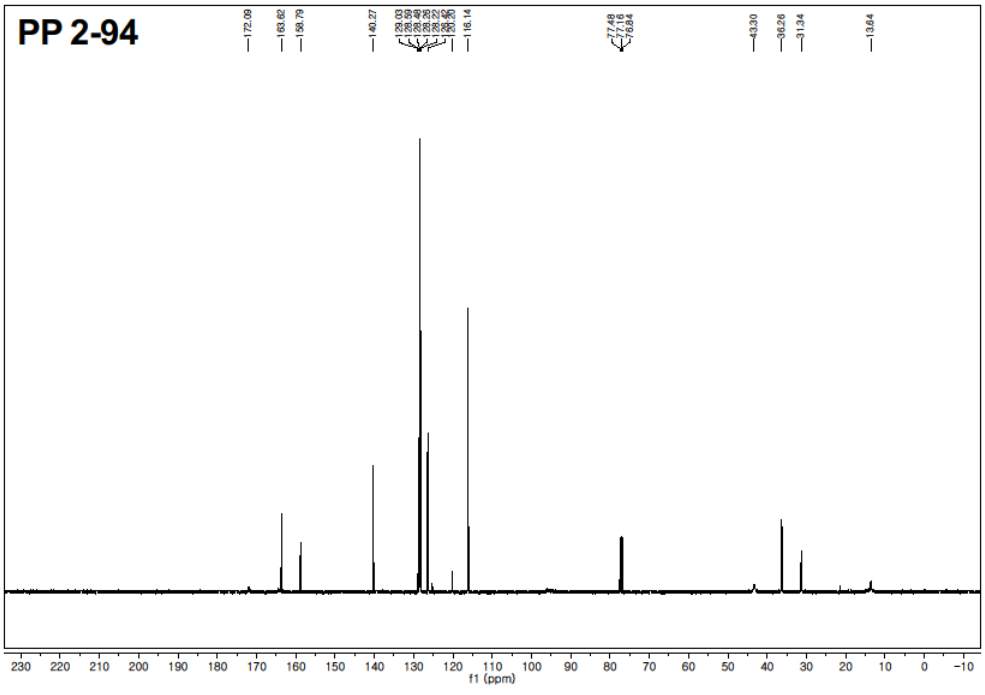
PP 2-94
f1 (ppm)

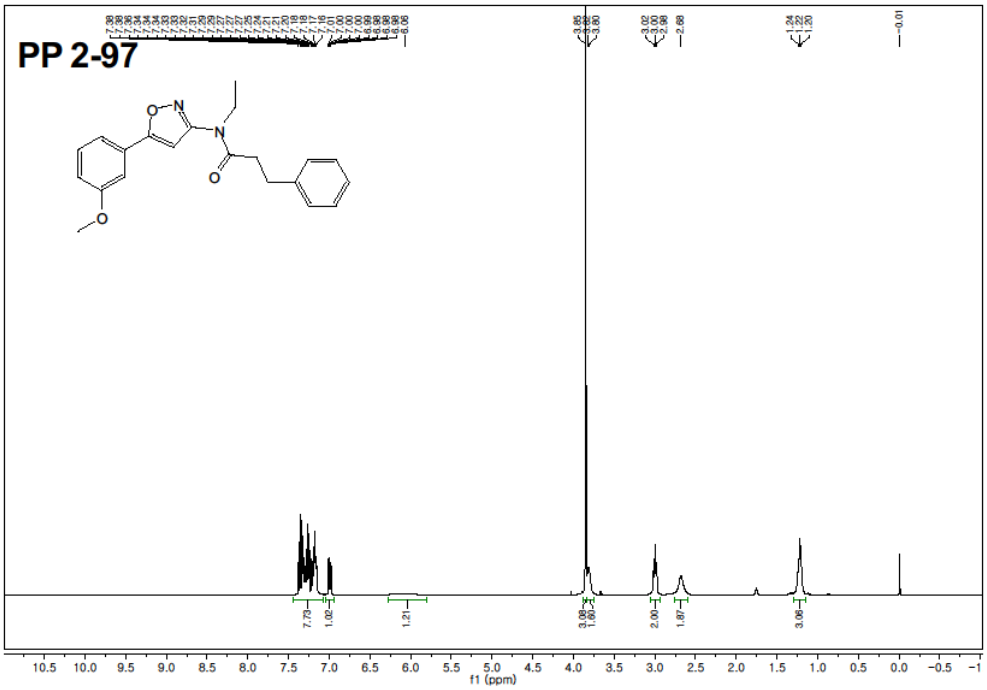
PP 2-97
f1 (ppm)

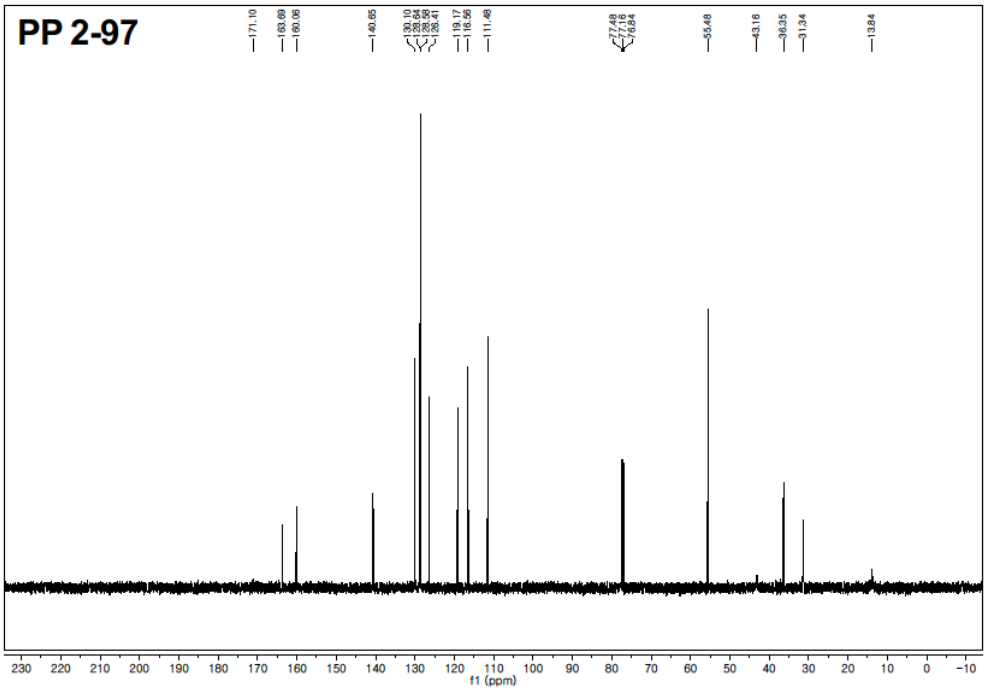
PP 2-97
f1 (ppm)

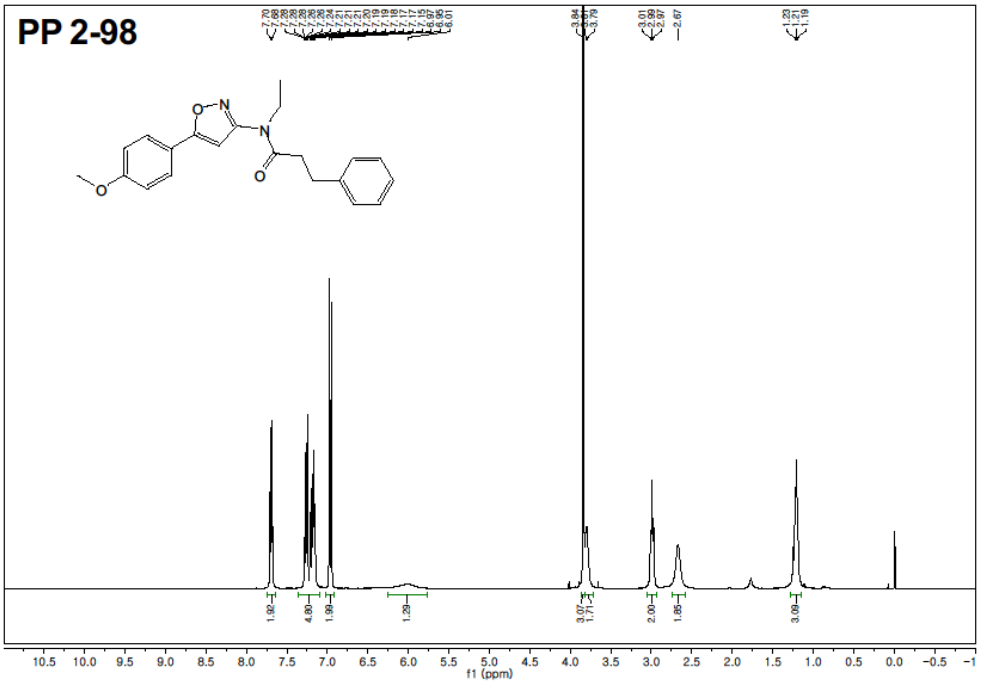
PP 2-98
f1 (ppm)

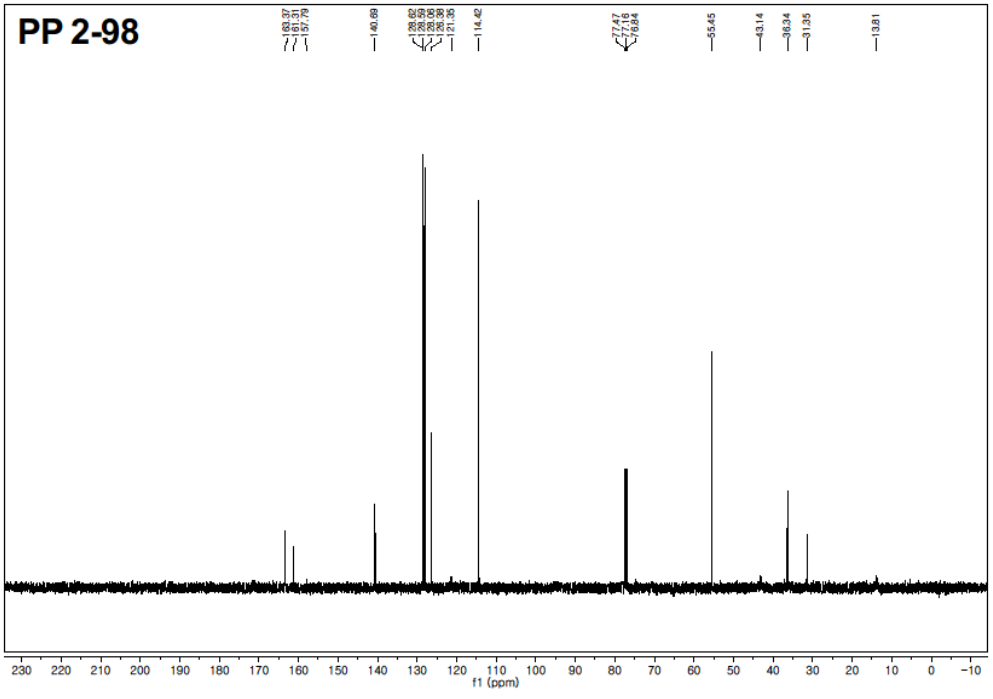
PP 2-98
f1 (ppm)

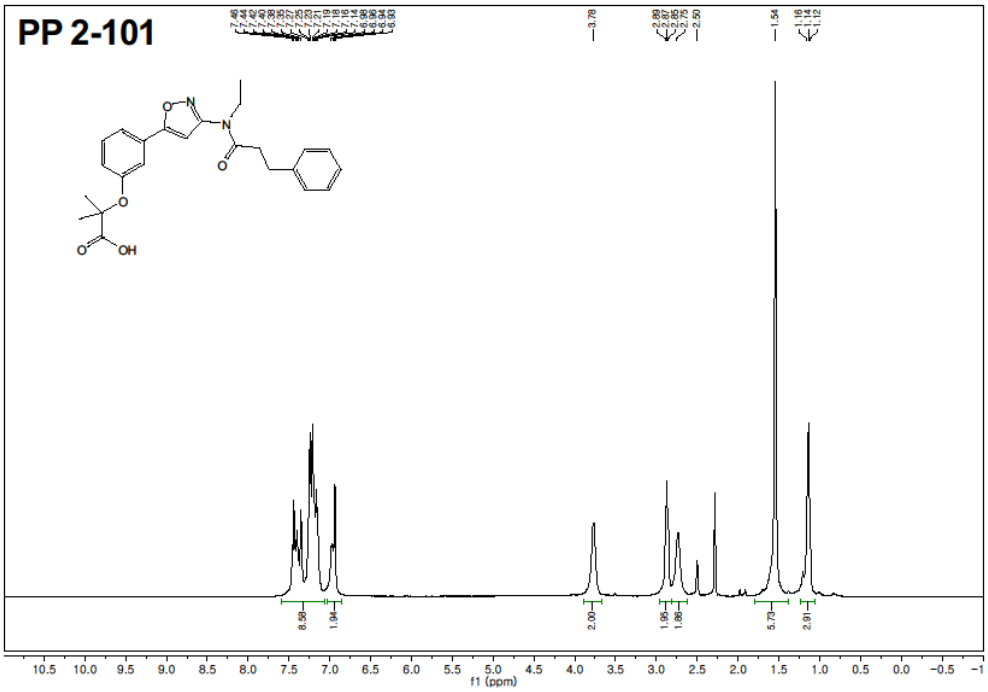
PP 2-101
3.78
2.89
2.87
2.85
2.75
2.50
1.54
1.16
1.14
1.12
O
N
O
N
O
O
O
OH
8.58
1.94
2.00
1.95
1.88
5.70
2.91
f1 (ppm)

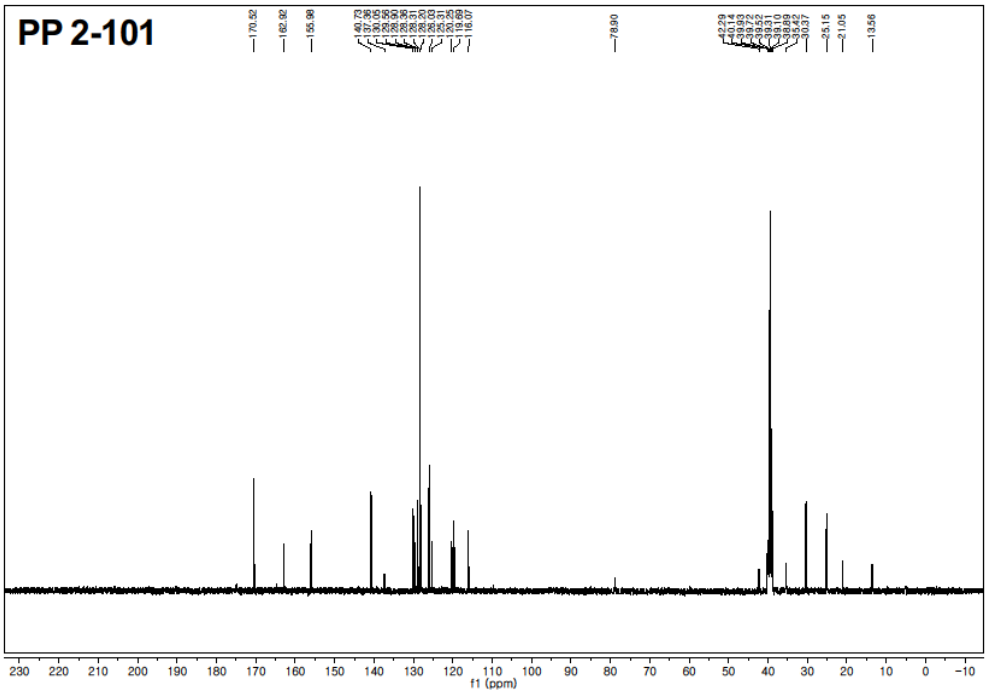
PP 2-101
170.52
162.92
155.98
78.90
25.15
21.05
13.56
f1 (ppm)

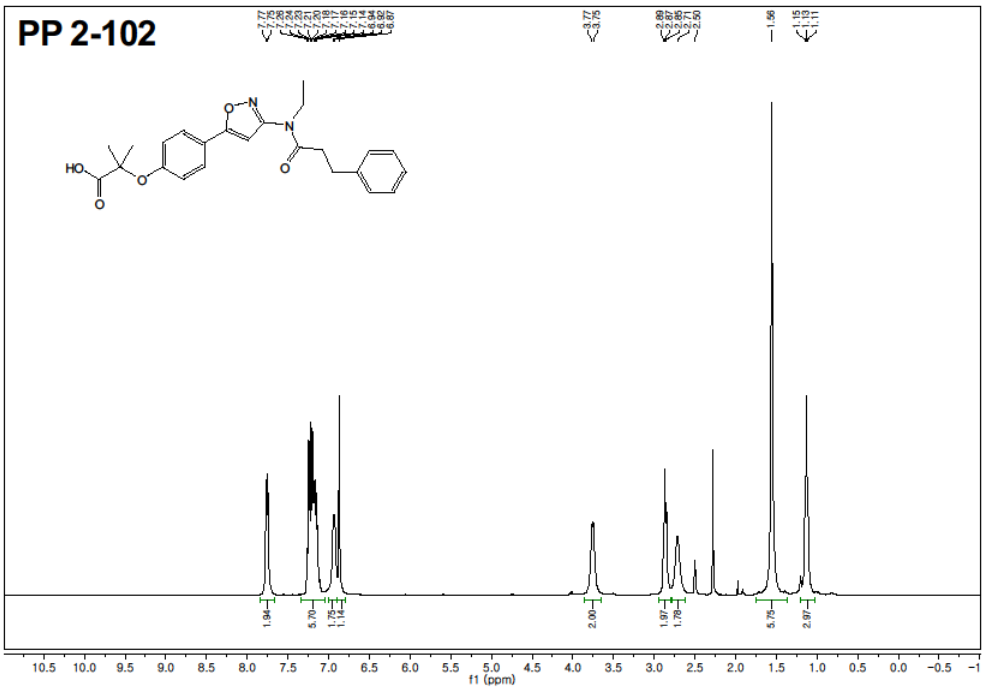
PP 2-102
HO
O
O
N
O
f1 (ppm)

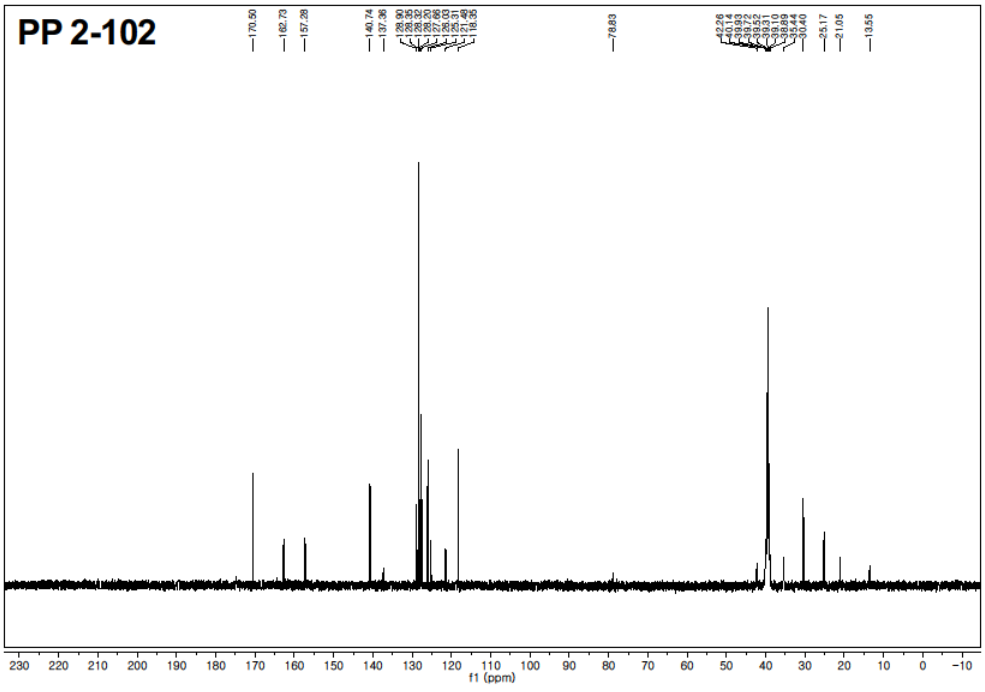
PP 2-102
f1 (ppm)

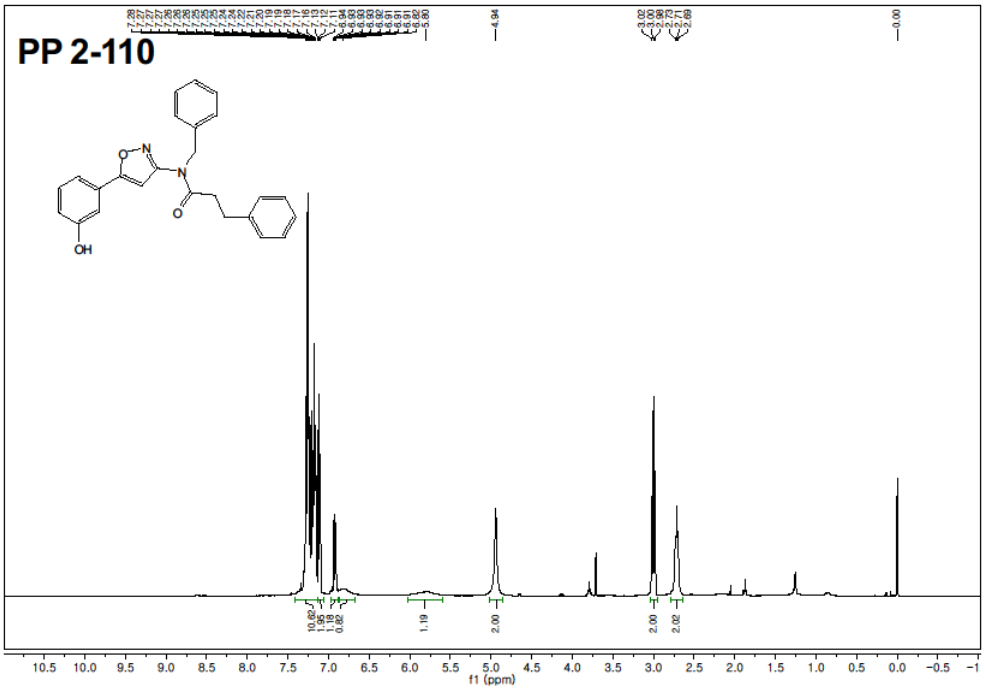
PP 2-110
O
N
O
N
OH
10.62
1.95
1.18
0.82
1.19
2.00
2.00
2.02
f1 (ppm)

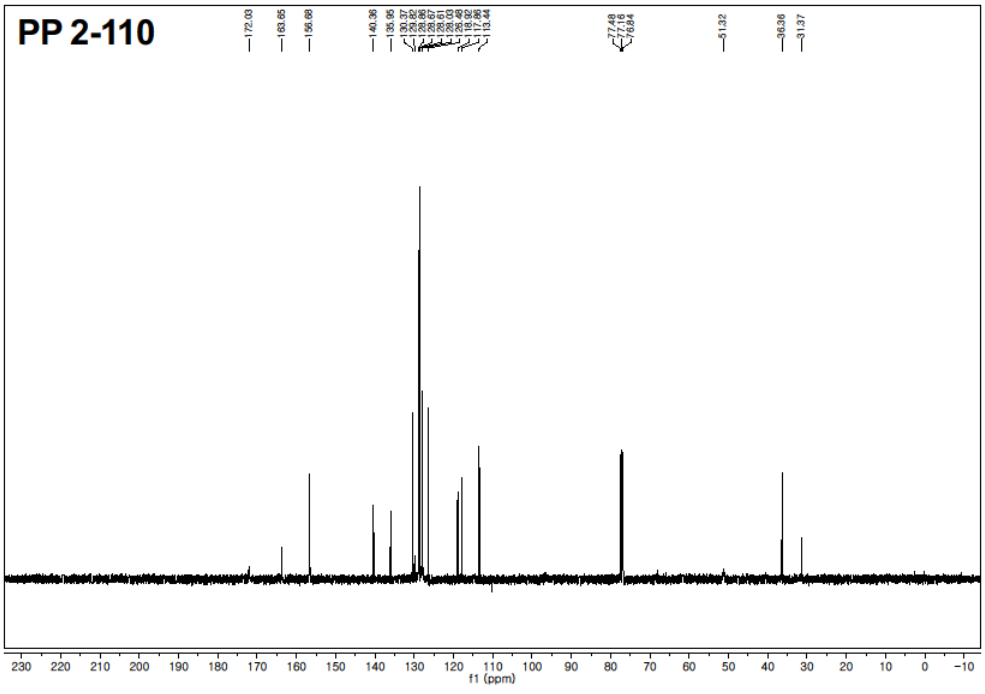
PP 2-110
172.03
163.65
156.68
140.36
135.95
130.37
129.82
128.67
128.61
126.53
126.49
117.02
113.44
77.48
77.16
76.84
51.32
36.36
31.37
f1 (ppm)

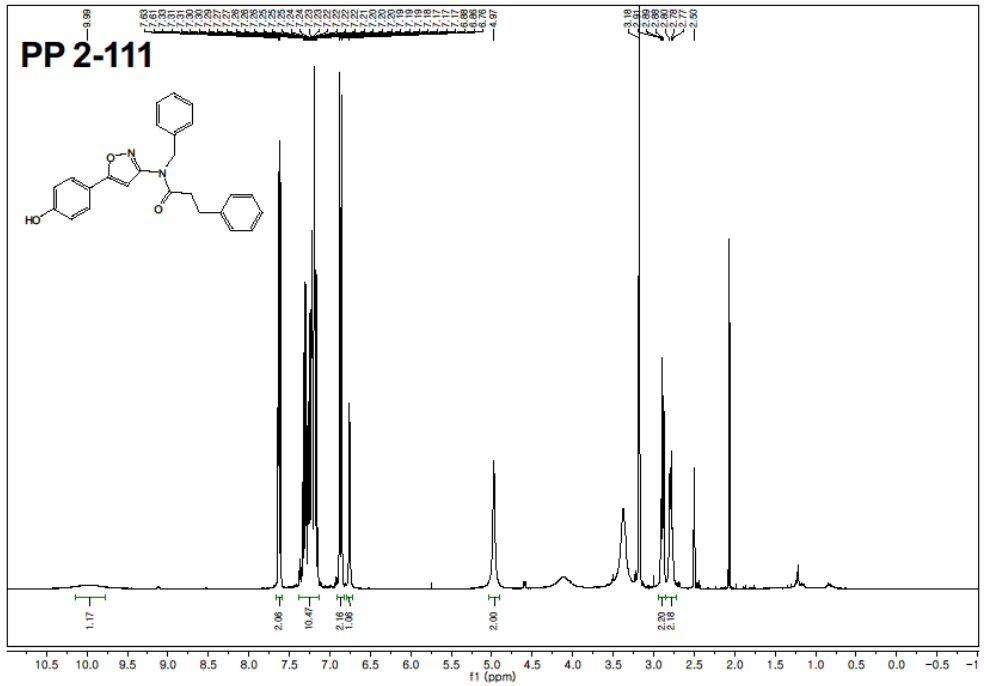
PP 2-111
HO
O
N
O
N
f1 (ppm)

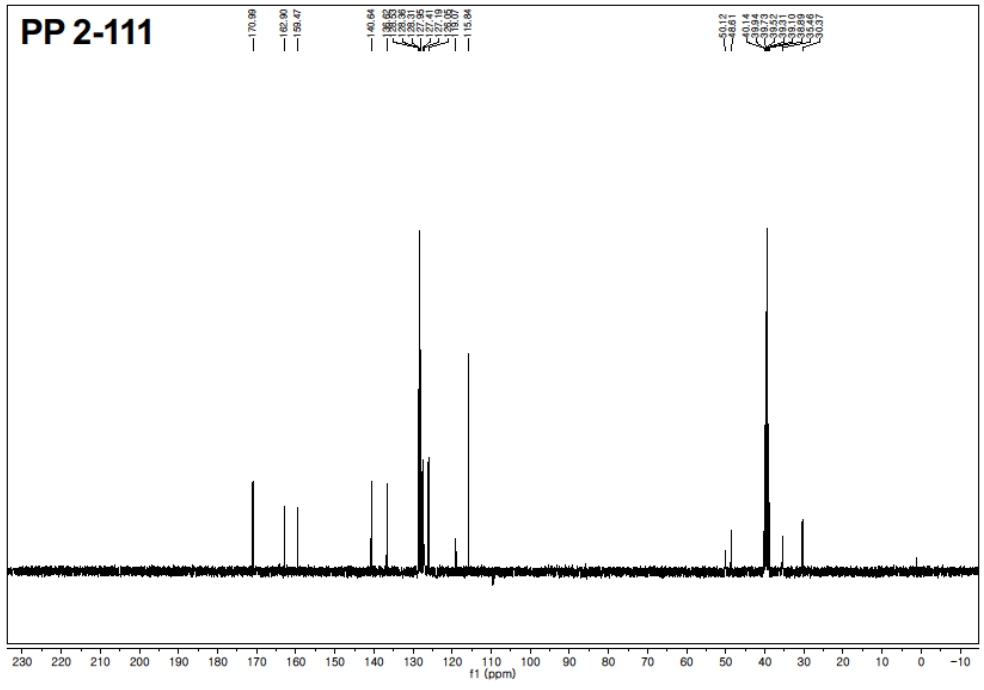
PP 2-111
f1 (ppm)

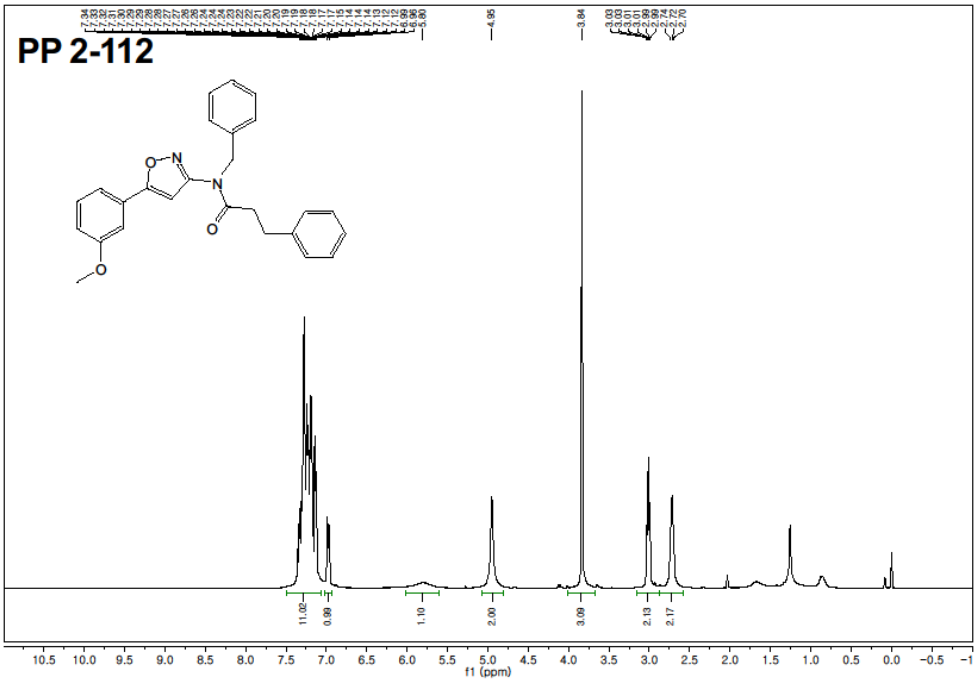
PP 2-112
O
N
N
O
O
11.02
0.89
1.10
2.00
3.09
2.13
2.17
f1 (ppm)

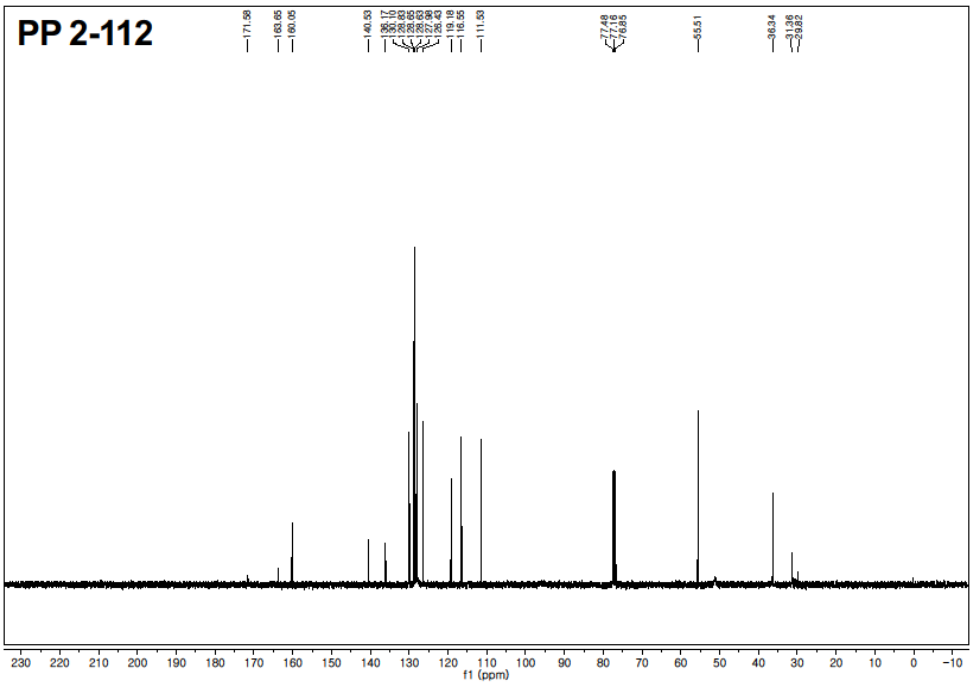
PP 2-112
f1 (ppm)

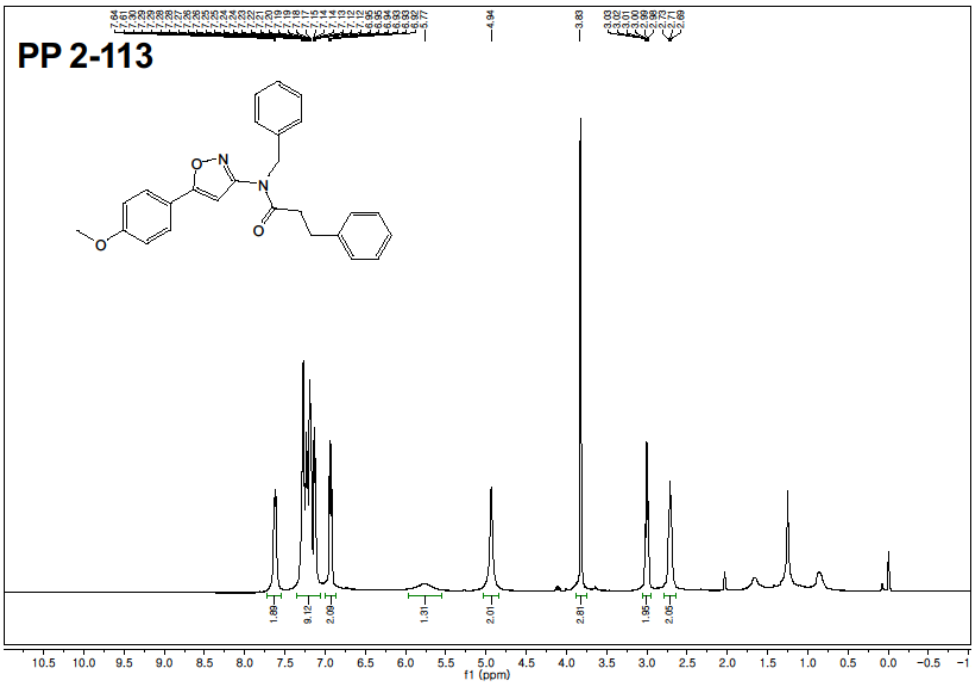
PP 2-113
f1 (ppm)

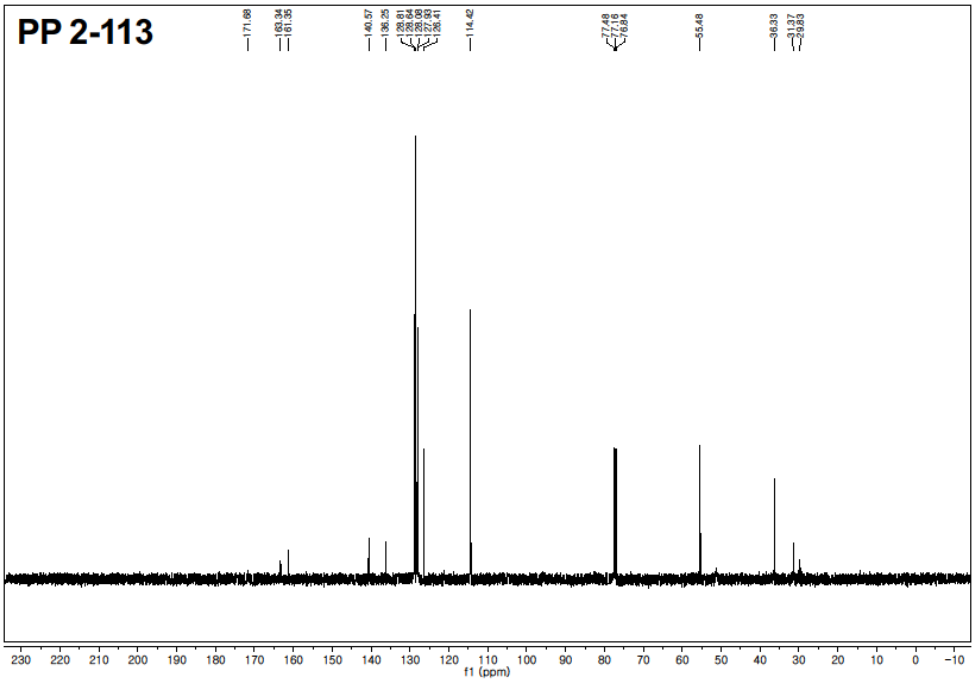
PP 2-113
f1 (ppm)

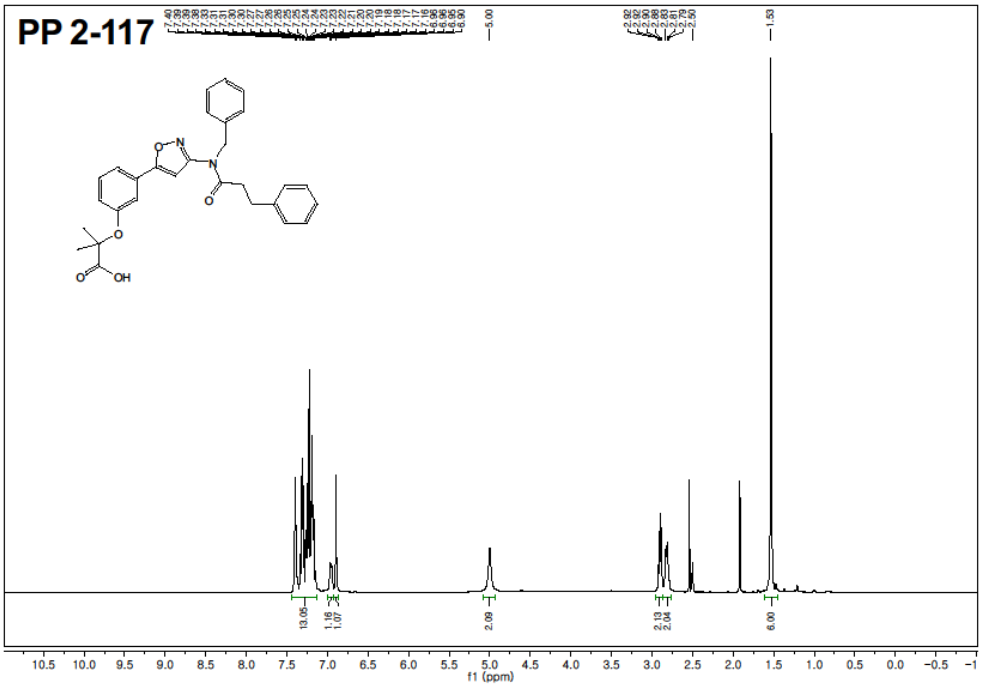
PP 2-117
f1 (ppm)

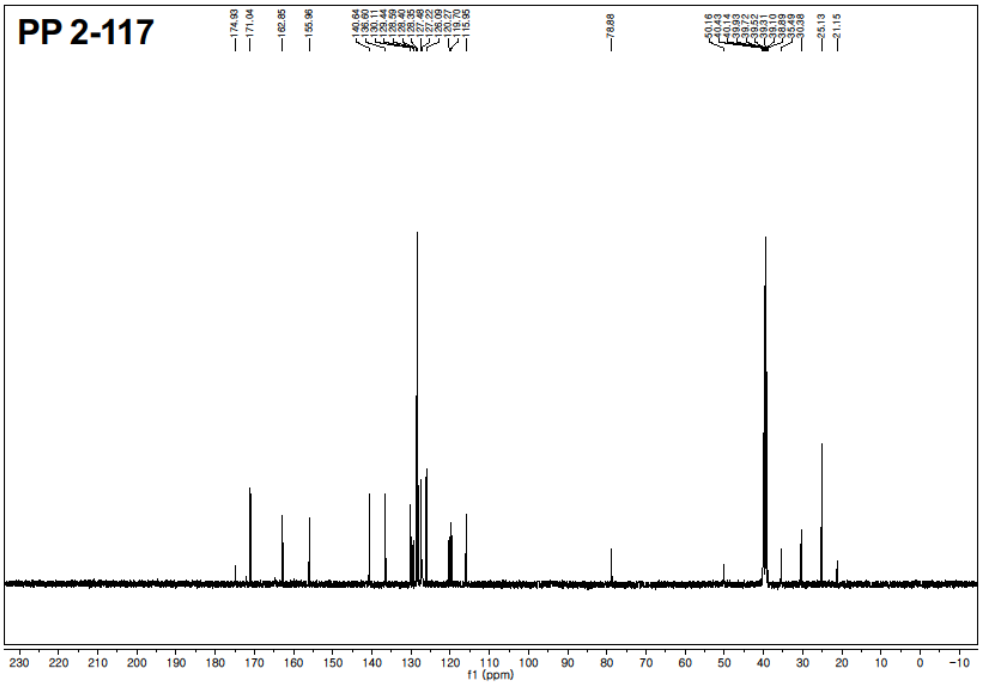
PP 2-117
f1 (ppm)

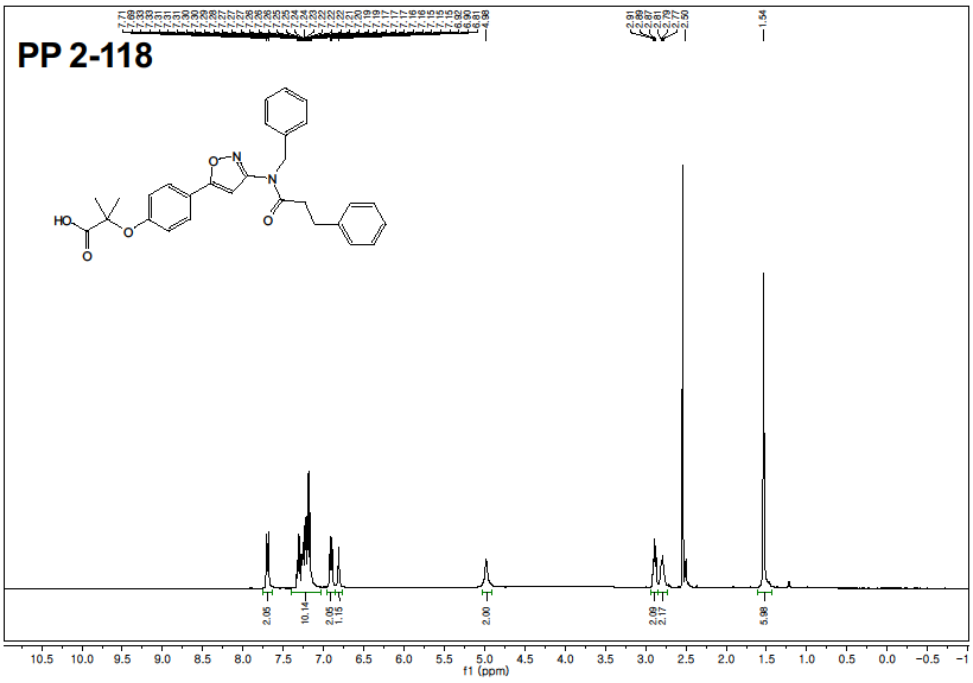
PP 2-118
HO
O
O
O
N
N
O
f1 (ppm)

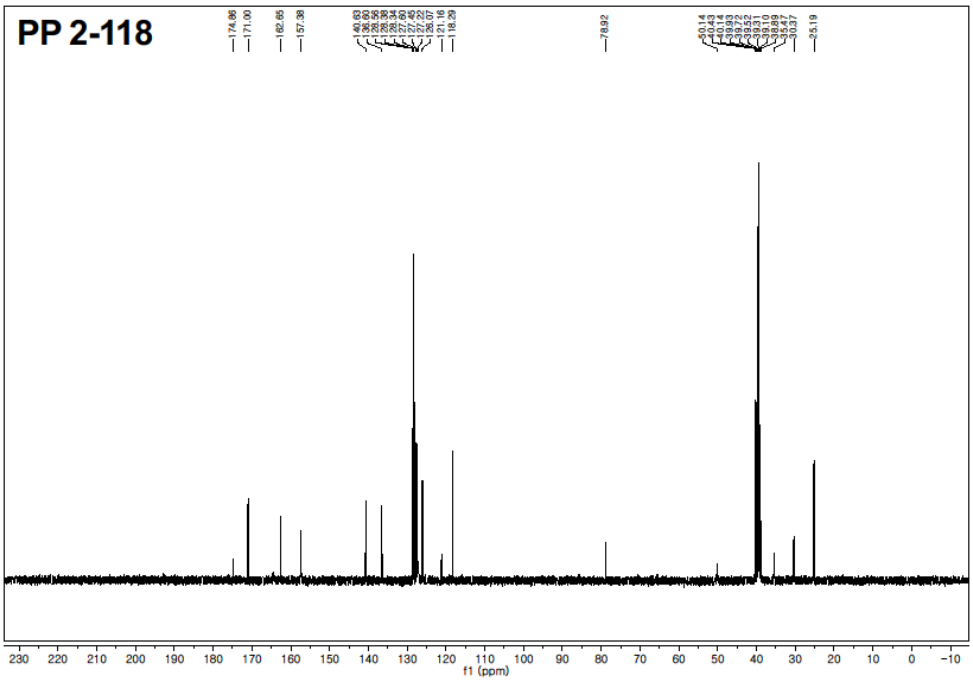
PP 2-118
f1 (ppm)

Chapter 2

The Library Construction of Small Molecule Autophagy Modulators

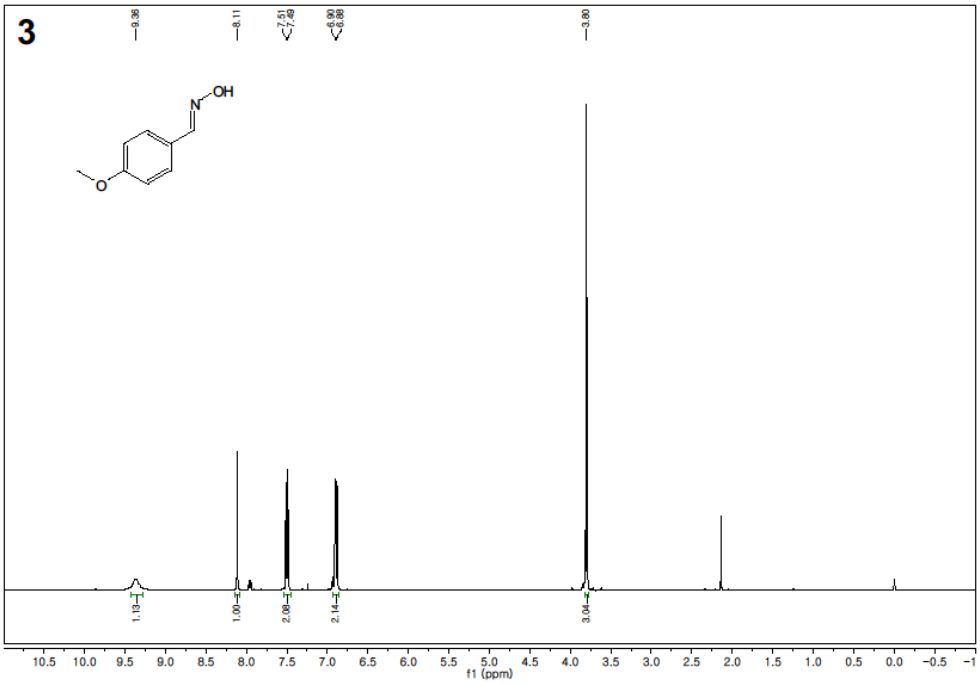
3
9.35
8.11
7.51
7.49
6.90
6.88
3.80
OH
N
O
1.13
1.00
2.08
2.14
3.04
10.5 10.0 9.5 9.0 8.5 8.0 7.5 7.0 6.5 6.0 5.5 5.0 4.5 4.0 3.5 3.0 2.5 2.0 1.5 1.0 0.5 0.0 −0.5 −1
f1 (ppm)

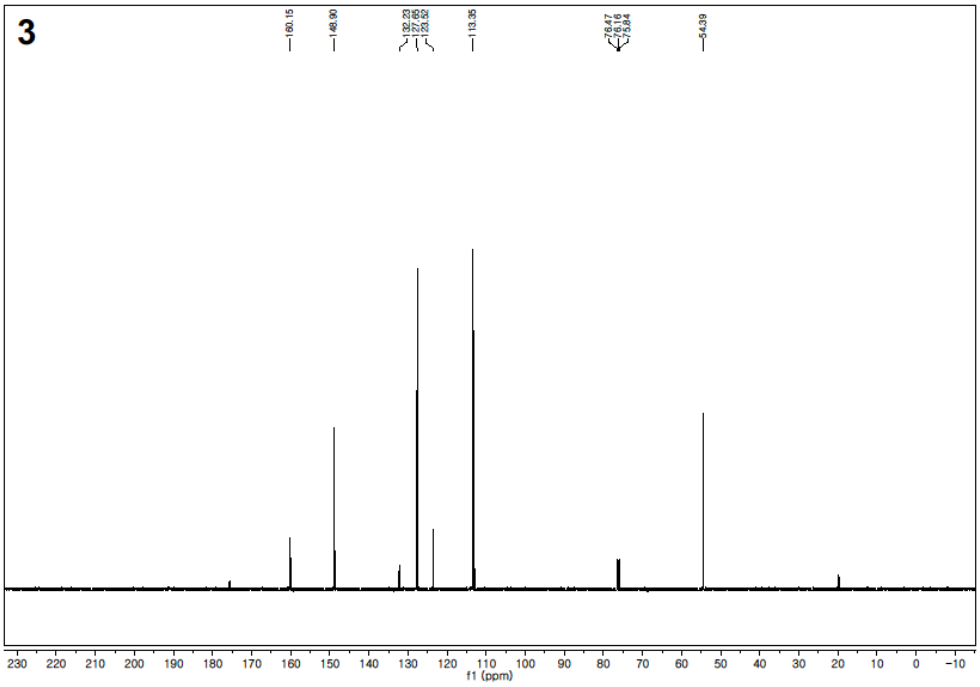
3
160.15
148.90
132.23
127.65
127.32
123.32
113.35
78.47
78.16
75.84
54.39
230 220 210 200 190 180 170 160 150 140 130 120 110 100 90 80 70 60 50 40 30 20 10 0 −10
f1 (ppm)

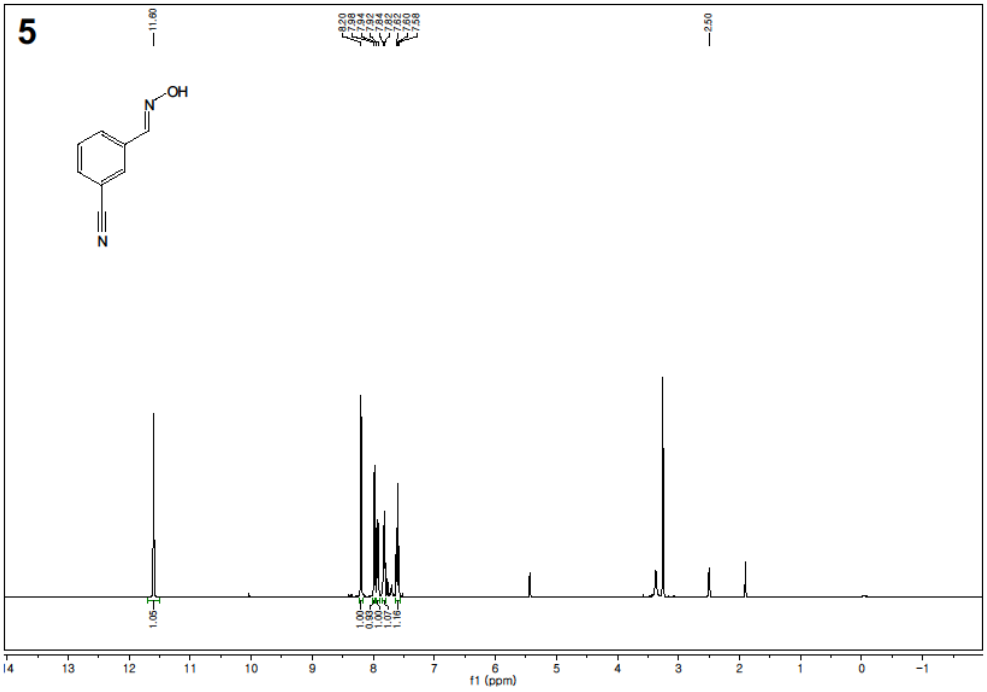
5
11.60
8.20
7.99
7.94
7.84
7.82
7.62
7.60
7.58
2.50
OH
N
N
1.05
0.00
0.85
1.00
1.07
1.16
f1 (ppm)

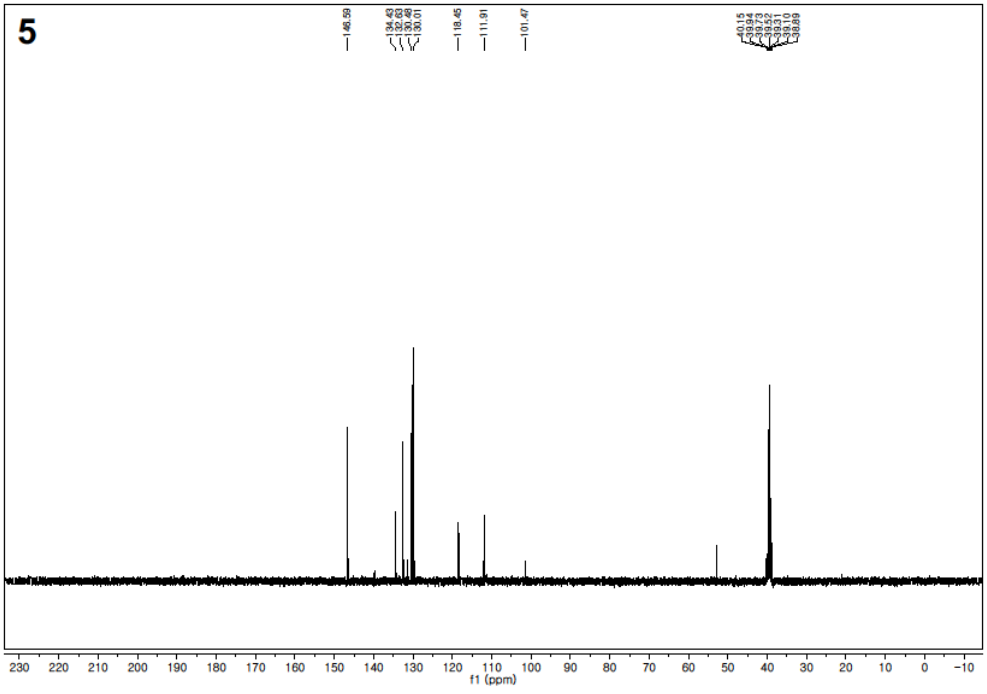
5
146.59
134.43
132.68
130.49
130.01
118.45
111.91
101.47
40.15
39.94
39.73
39.52
39.31
39.10
38.89
f1 (ppm)

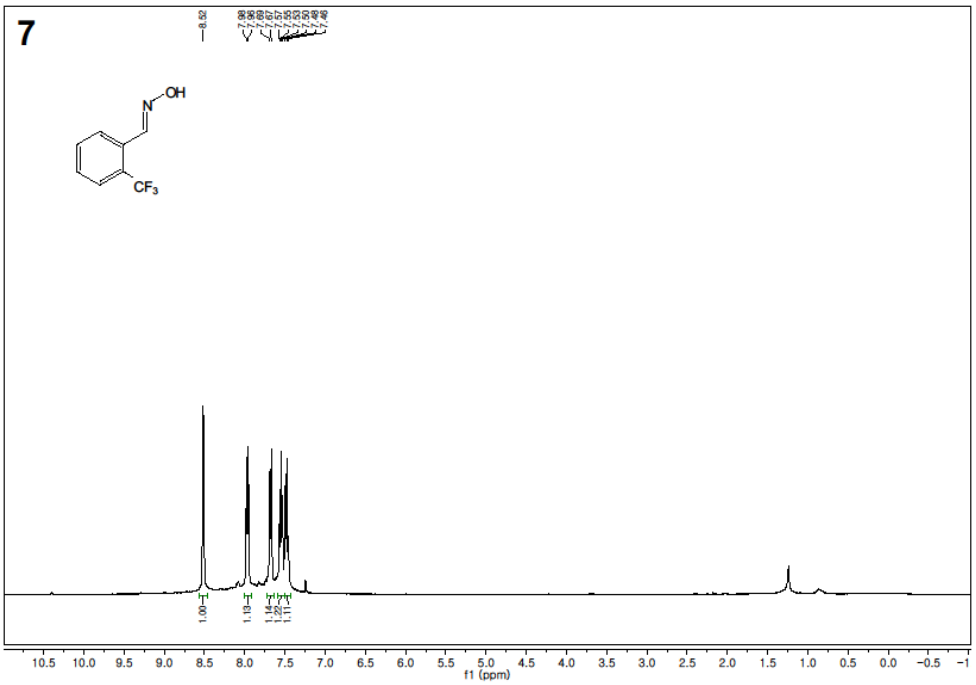
7
8.52
N
OH
CF3
1.00
1.13
1.14
1.22
1.11
10.5 10.0 9.5 9.0 8.5 8.0 7.5 7.0 6.5 6.0 5.5 5.0 4.5 4.0 3.5 3.0 2.5 2.0 1.5 1.0 0.5 0.0 −0.5 −1
f1 (ppm)

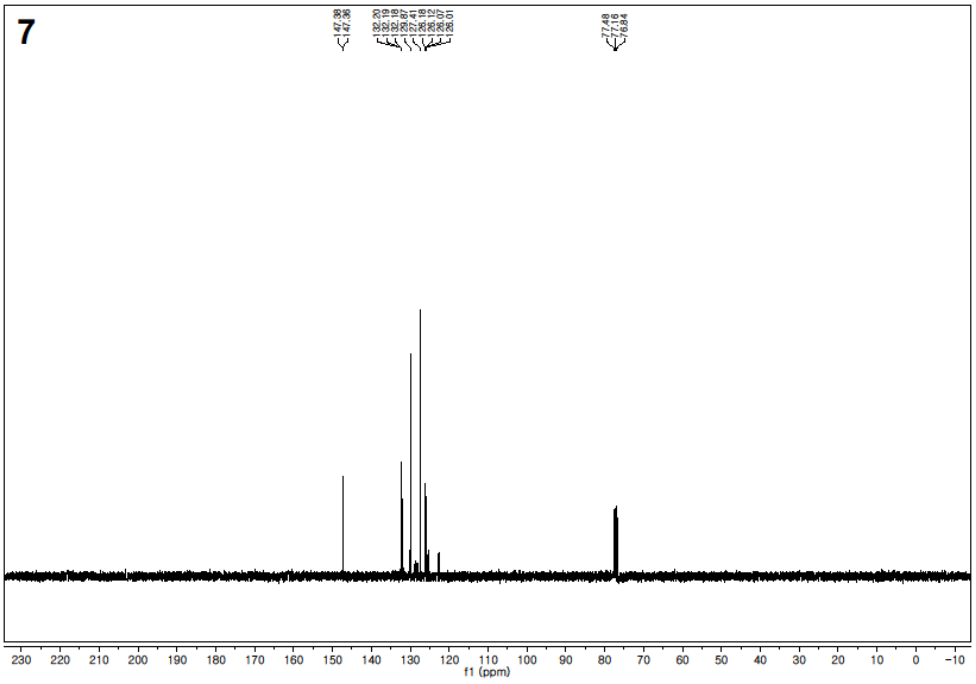
7
147.39
147.36
132.20
132.19
129.97
129.67
127.49
126.12
126.07
123.01
77.48
77.16
76.84
230 220 210 200 190 180 170 160 150 140 130 120 110 100 90 80 70 60 50 40 30 20 10 0 −10
f1 (ppm)

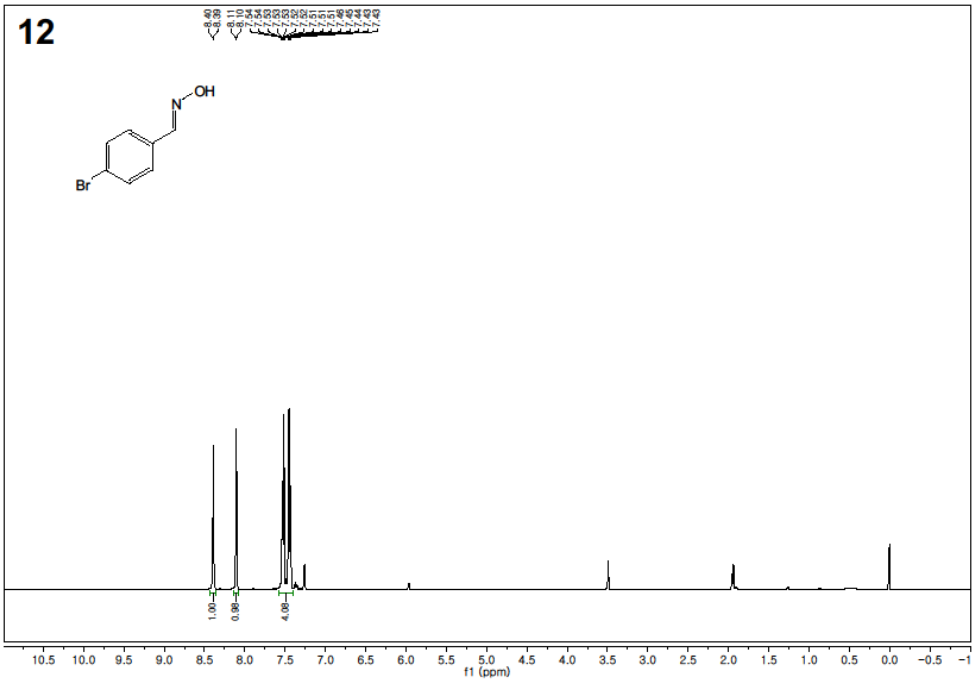
12
N
OH
Br
1.00
0.98
4.08
f1 (ppm)

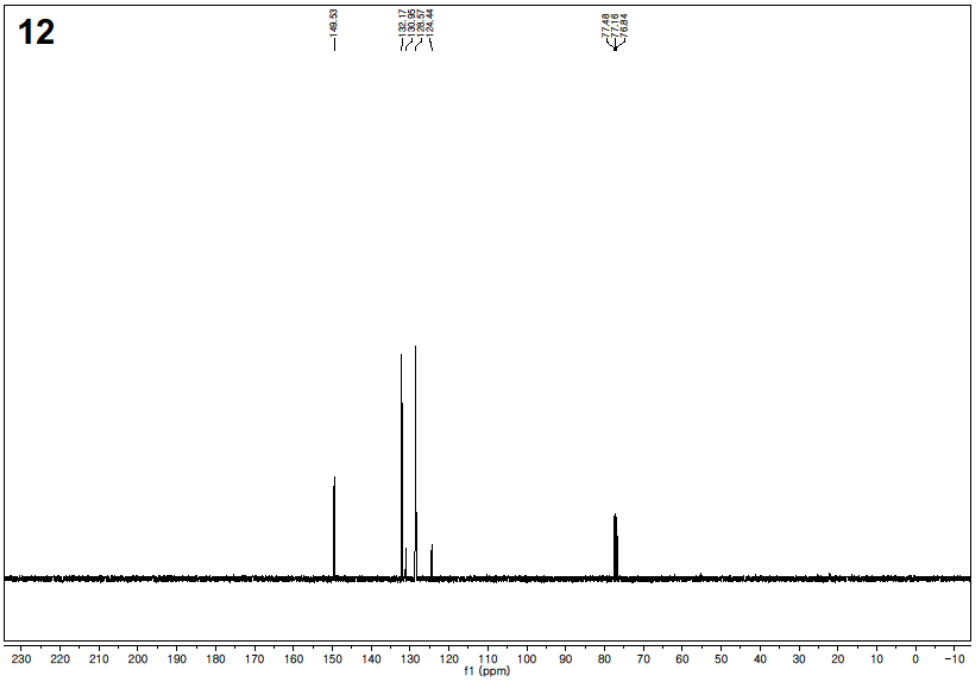
12
149.53
132.17
130.85
128.97
124.44
77.48
77.16
76.84
f1 (ppm)

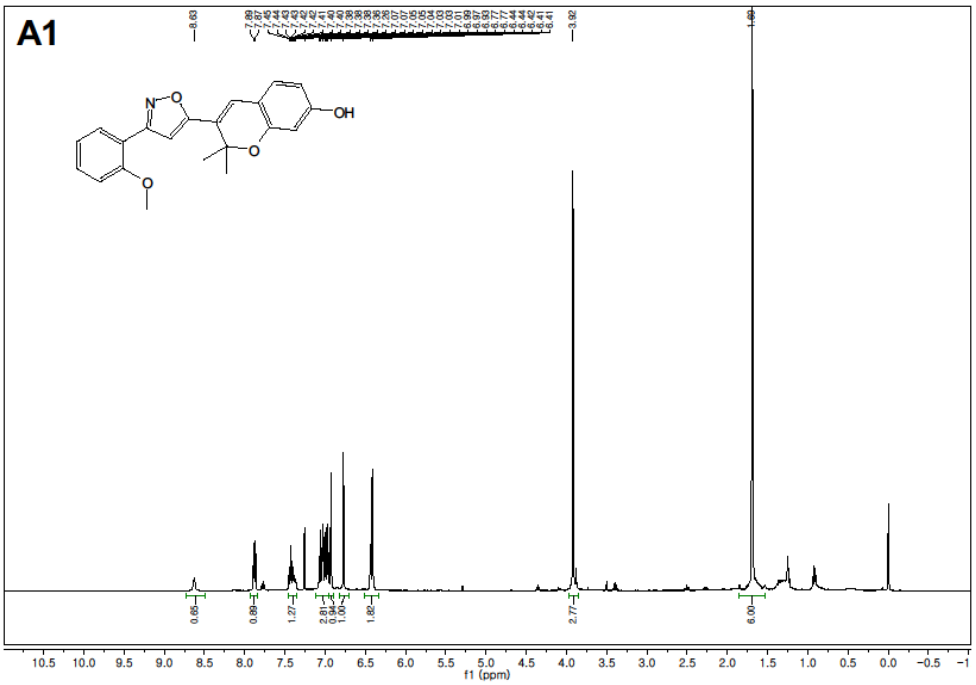
A1
OH
O
N
O
O
8.63
7.89
7.87
7.45
7.44
7.43
7.42
7.41
7.40
7.39
7.38
7.36
7.35
7.07
7.05
7.04
7.03
7.01
6.99
6.97
6.93
6.77
6.45
6.44
6.42
6.41
3.92
1.69
0.65
0.89
1.27
2.81
0.94
1.00
1.82
2.77
6.00
10.5 10.0 9.5 9.0 8.5 8.0 7.5 7.0 6.5 6.0 5.5 5.0 4.5 4.0 3.5 3.0 2.5 2.0 1.5 1.0 0.5 0.0 −0.5 −1
f1 (ppm)

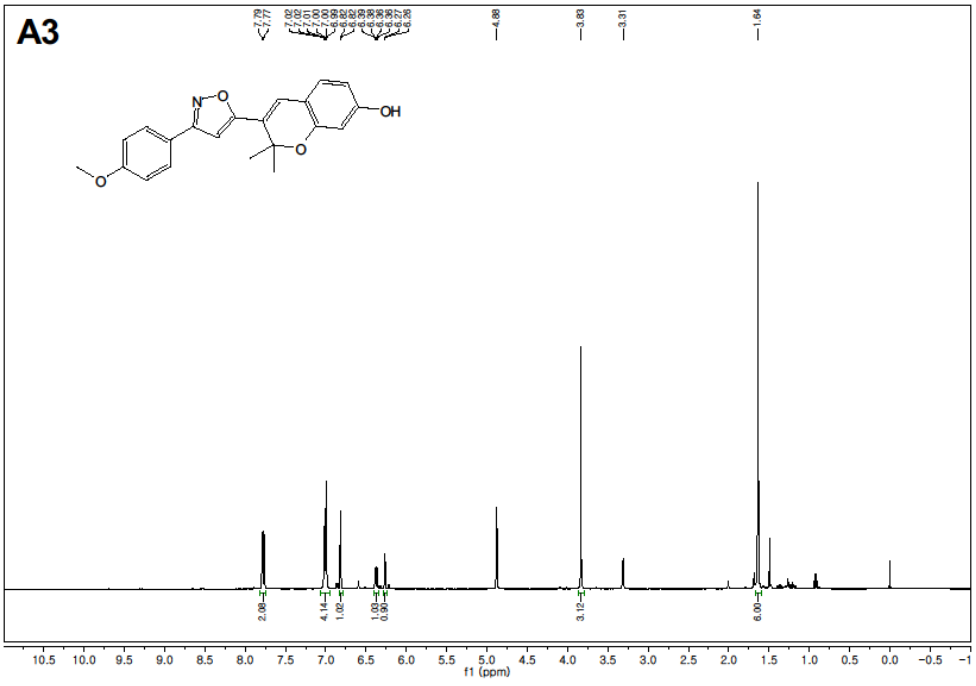
A3
OH
O
N
O
O
7.79
7.77
7.02
7.00
7.01
7.00
6.99
6.82
6.82
6.39
6.38
6.38
6.37
6.37
6.36
4.88
3.83
3.31
1.64
2.08
4.14
1.02
1.03
0.90
3.12
6.00
10.5 10.0 9.5 9.0 8.5 8.0 7.5 7.0 6.5 6.0 5.5 5.0 4.5 4.0 3.5 3.0 2.5 2.0 1.5 1.0 0.5 0.0 −0.5 −1
f1 (ppm)

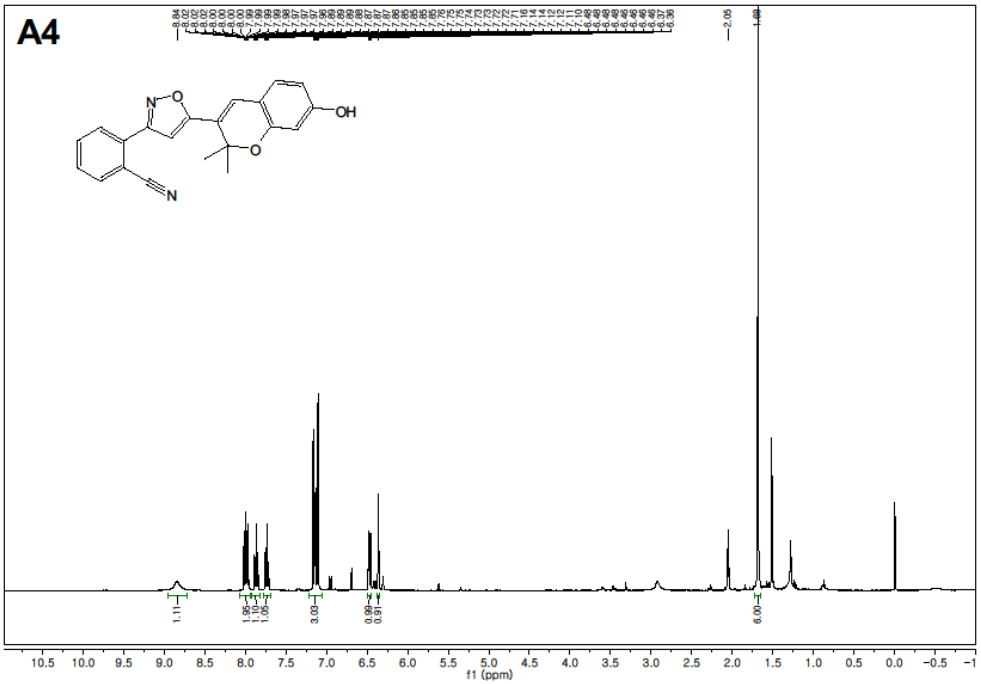
A4
OH
N
O
N
f1 (ppm)

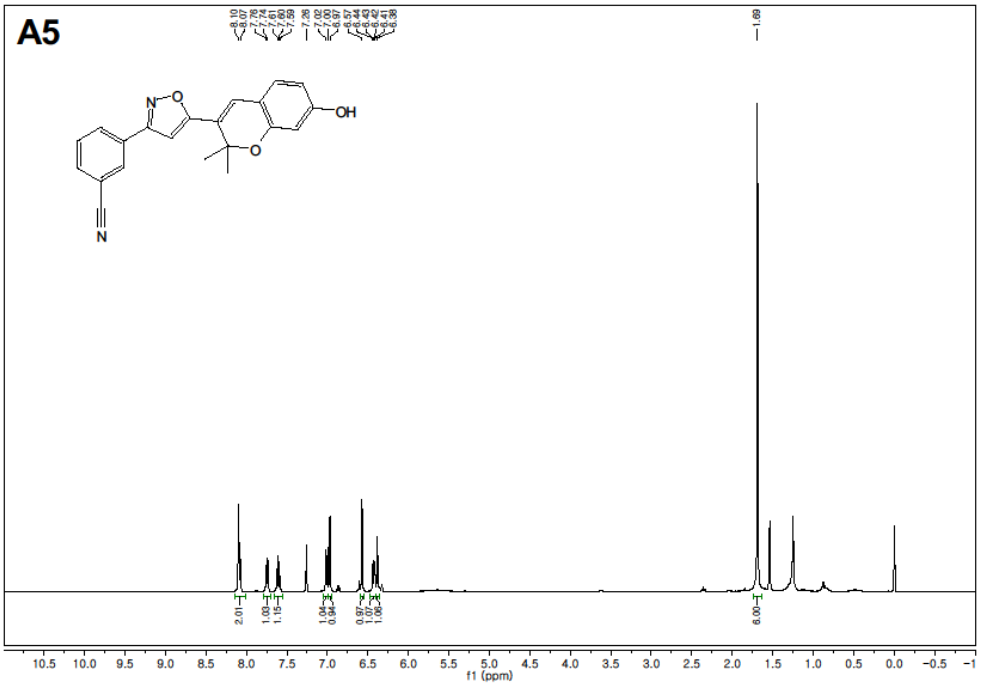
A5
OH
N
O
N
f1 (ppm)

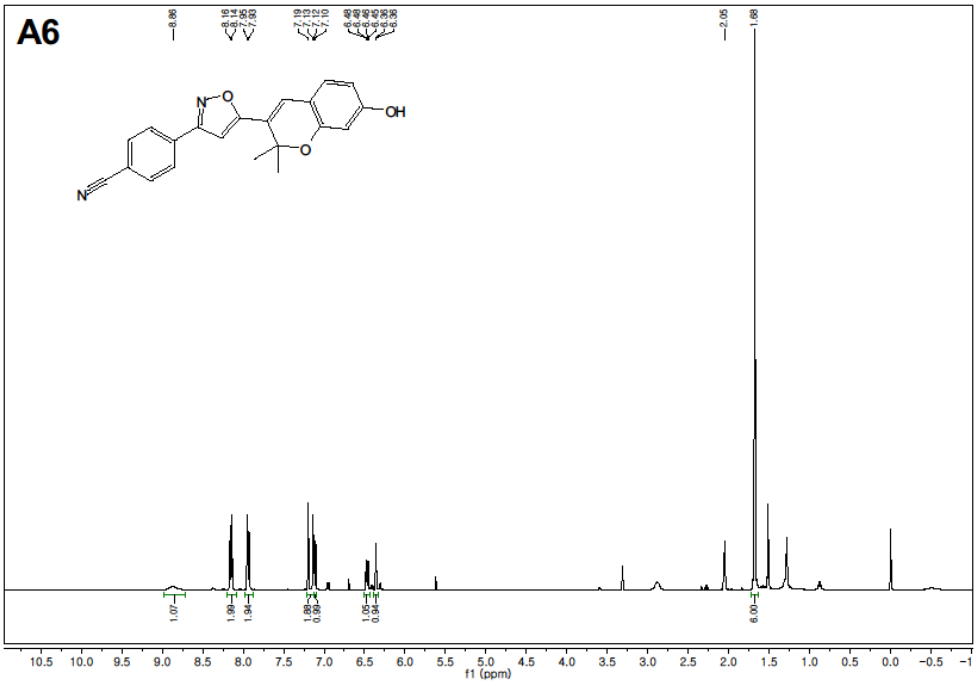
A6
N
O
OH
O
N
f1 (ppm)

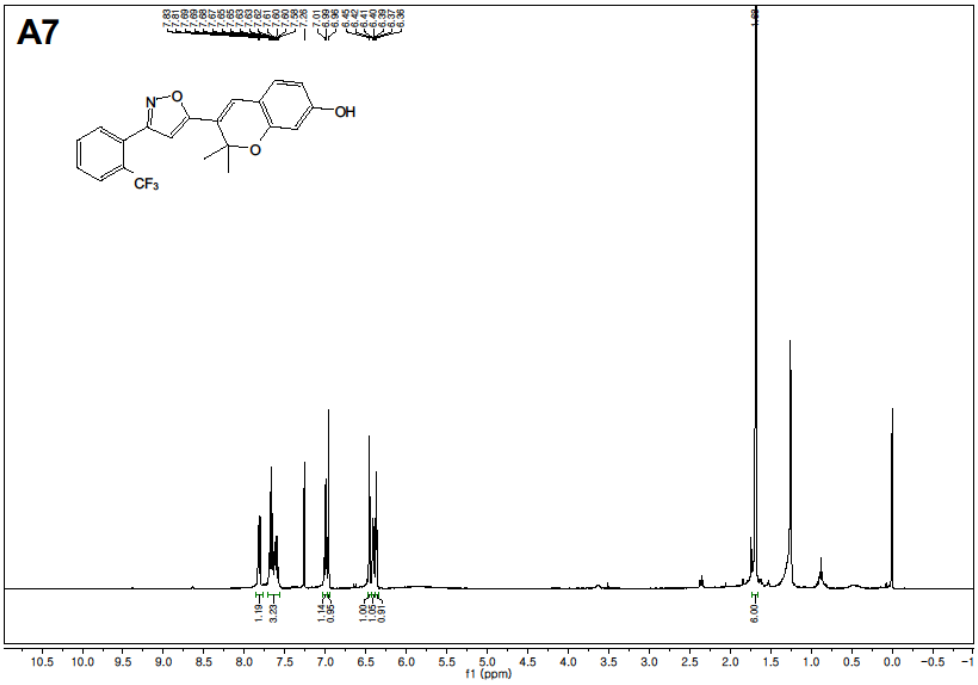
A7
N
O
OH
O
CF3
f1 (ppm)

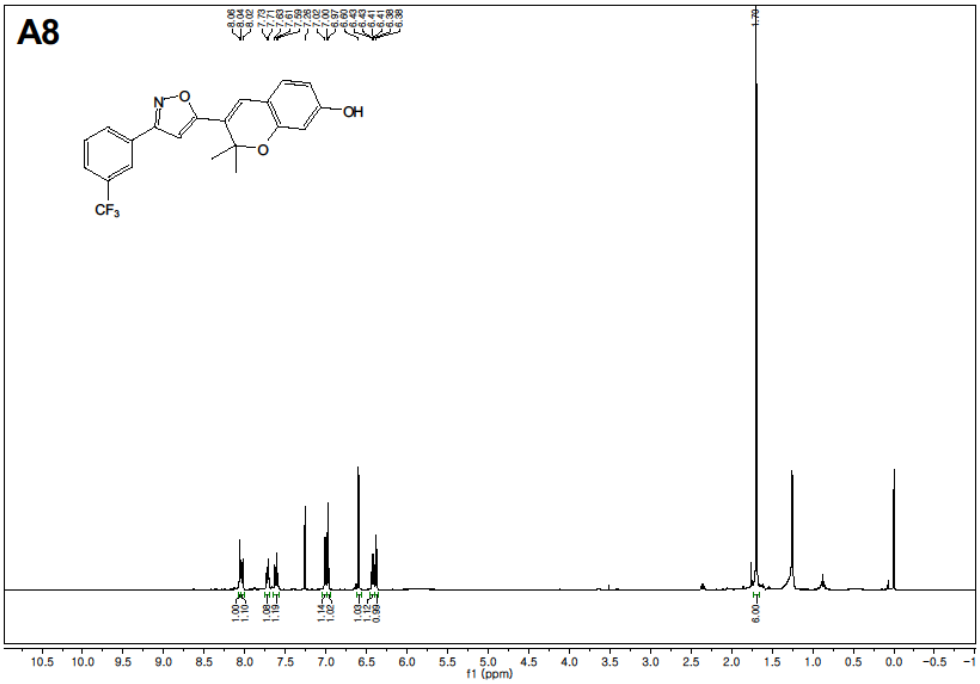
A8
OH
N
O
O
CF3
f1 (ppm)

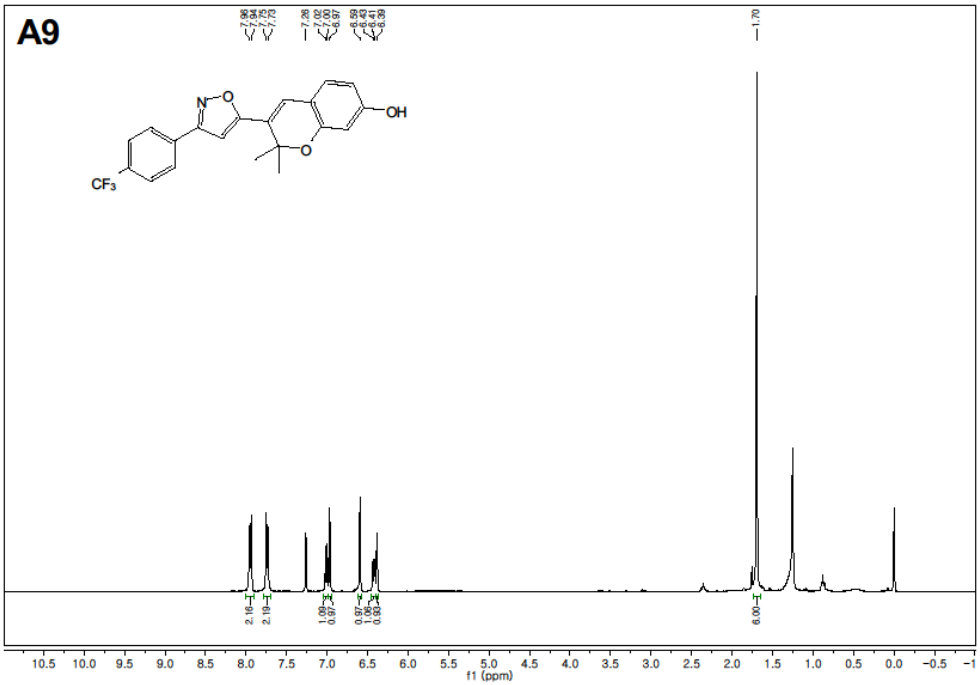
A9
OH
N
O
O
CF3
f1 (ppm)

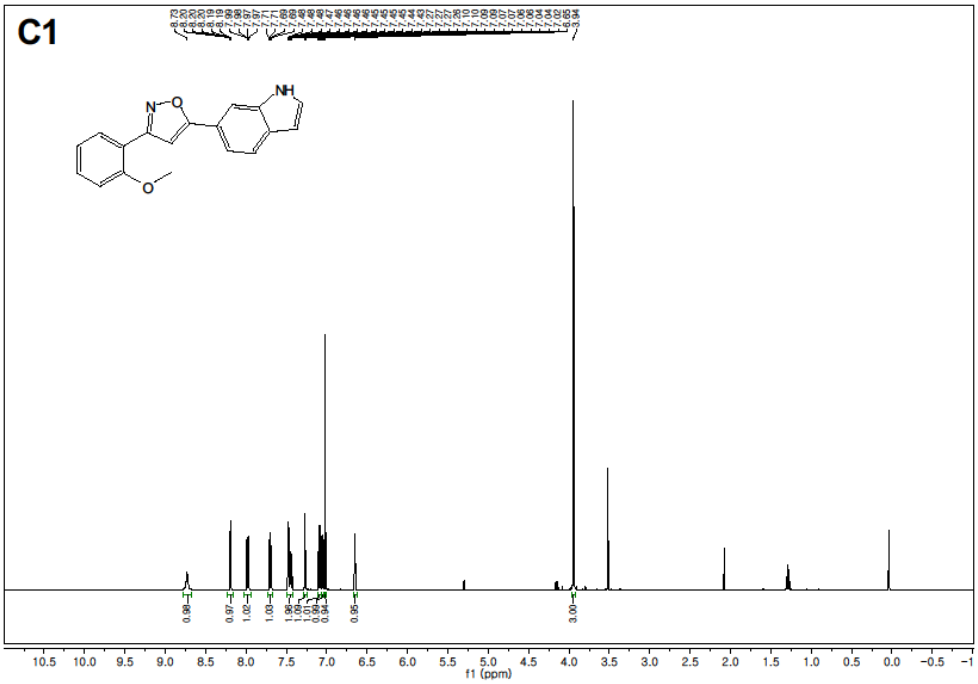
C1
NH
N
O
O
0.98
0.97
1.02
1.03
1.95
1.00
1.01
0.94
0.95
3.00
10.5 10.0 9.5 9.0 8.5 8.0 7.5 7.0 6.5 6.0 5.5 5.0 4.5 4.0 3.5 3.0 2.5 2.0 1.5 1.0 0.5 0.0 −0.5 −1
f1 (ppm)

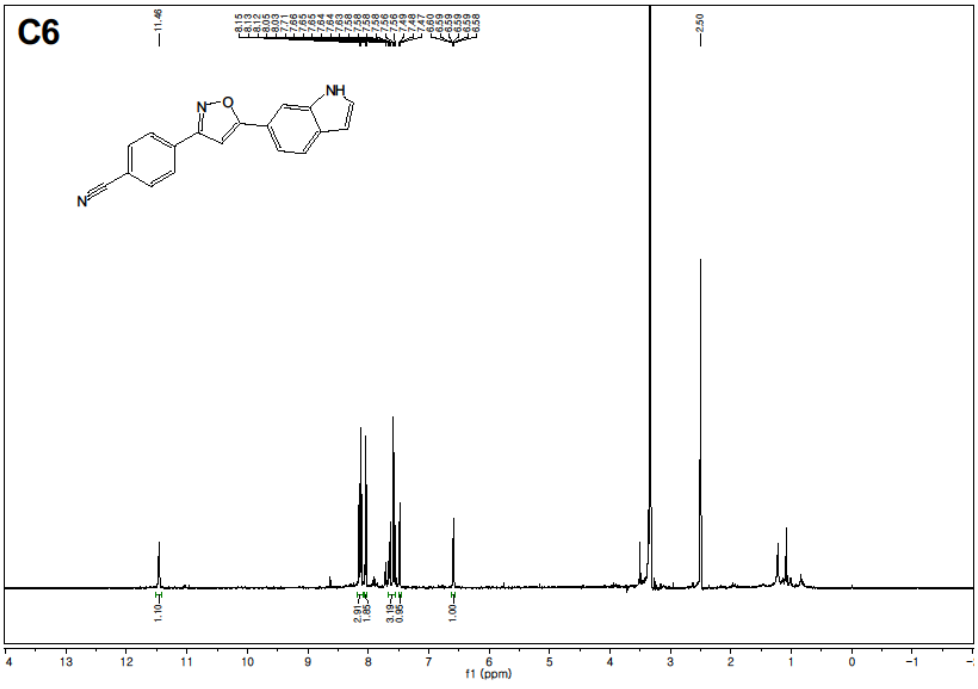
C6
11.46
2.50
NH
N
O
N
1.10
2.01
1.85
3.19
0.85
1.00
4 13 12 11 10 9 8 7 6 5 4 3 2 1 0 −1
f1 (ppm)

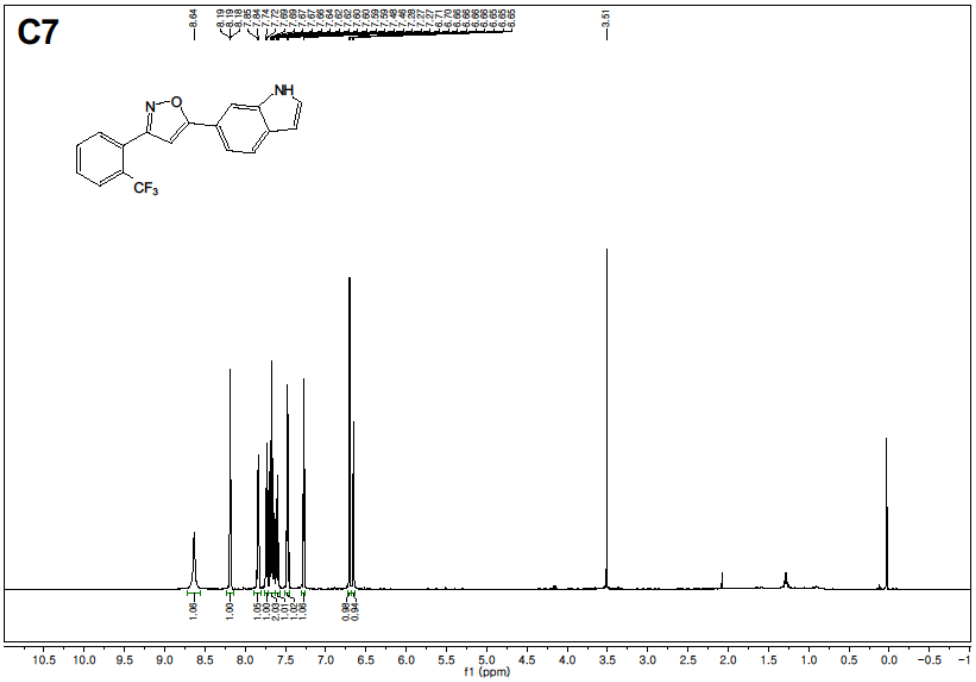
C7
NH
N
O
CF3
f1 (ppm)

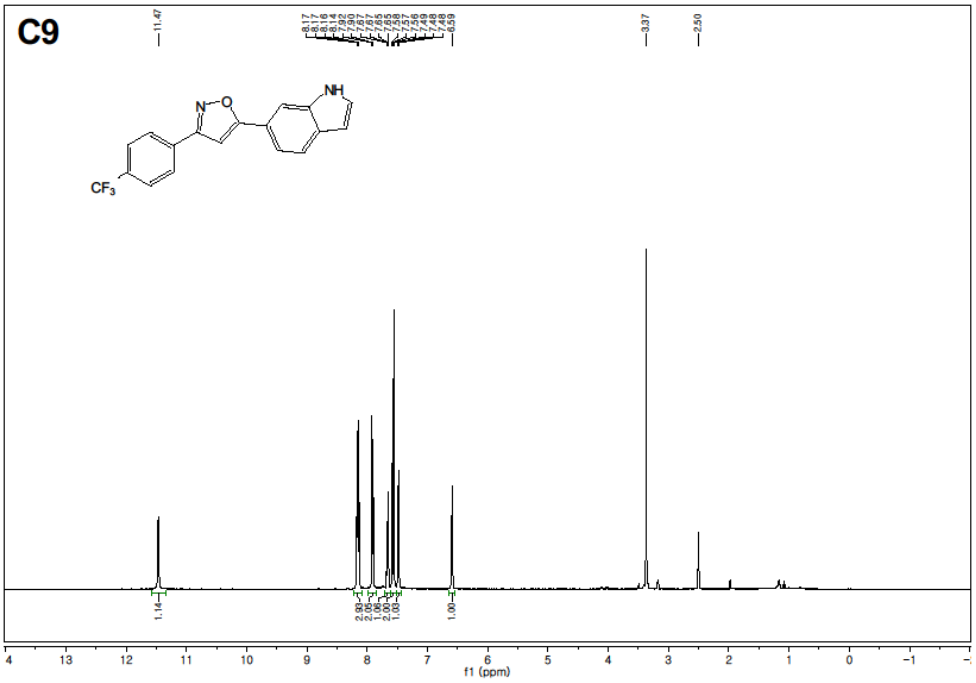
C9
NH
N
O
CF3
f1 (ppm)

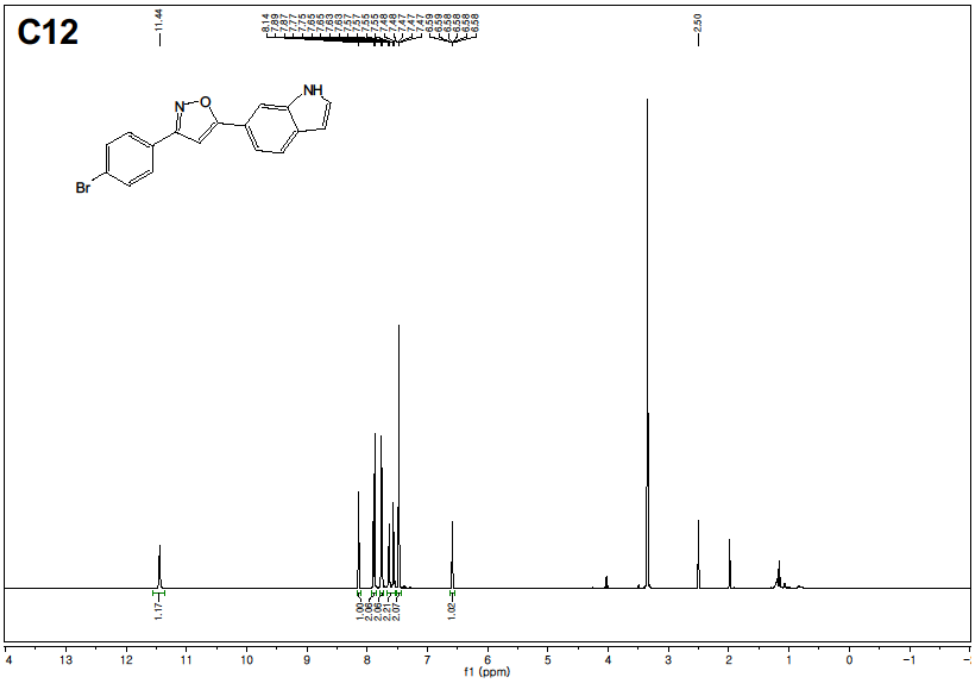
C12
11.44
8.14
7.89
7.87
7.77
7.75
7.65
7.63
7.57
7.55
7.48
7.47
6.59
6.58
6.58
6.58
2.50
NH
N
O
Br
1.17
1.00
2.06
2.21
2.07
1.02
f1 (ppm)

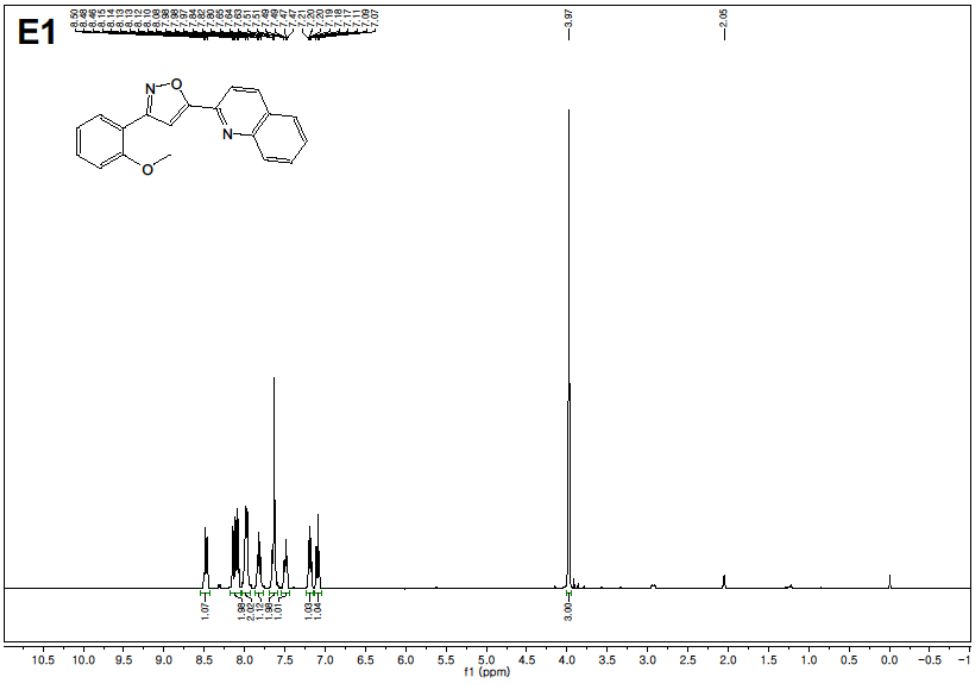
E1
8.50
8.49
8.46
8.45
8.14
8.13
8.12
8.10
8.09
7.98
7.97
7.95
7.84
7.83
7.65
7.64
7.63
7.51
7.49
7.48
7.47
7.21
7.20
7.19
7.17
7.11
7.09
7.07
3.97
2.05
N
O
N
O
1.07
1.96
2.00
1.13
1.06
1.01
1.00
1.04
3.00
f1 (ppm)

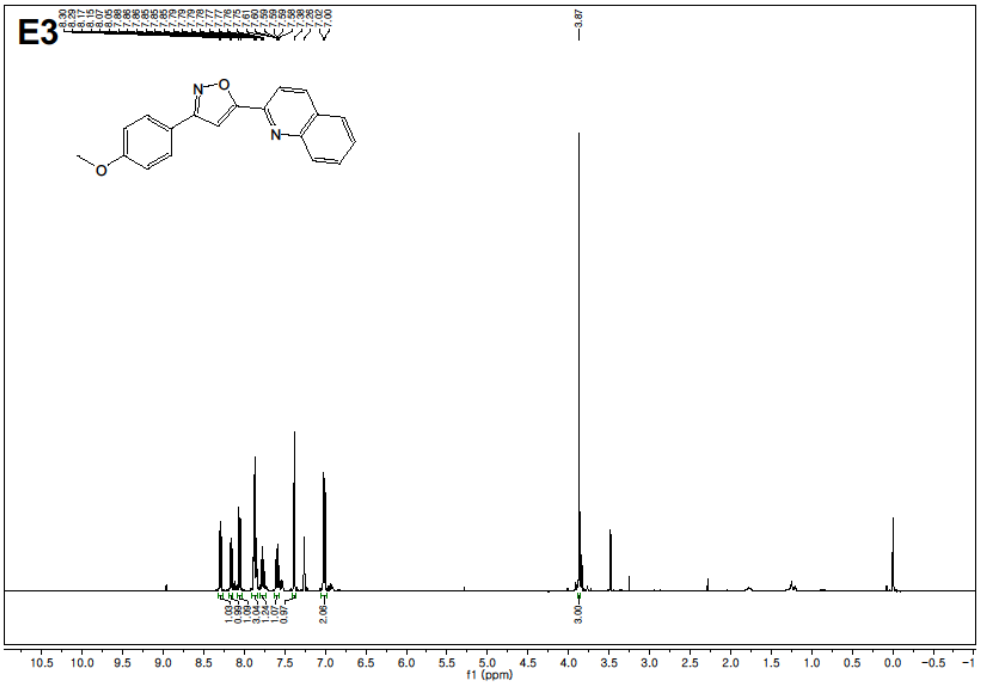
E3
3.87
f1 (ppm)

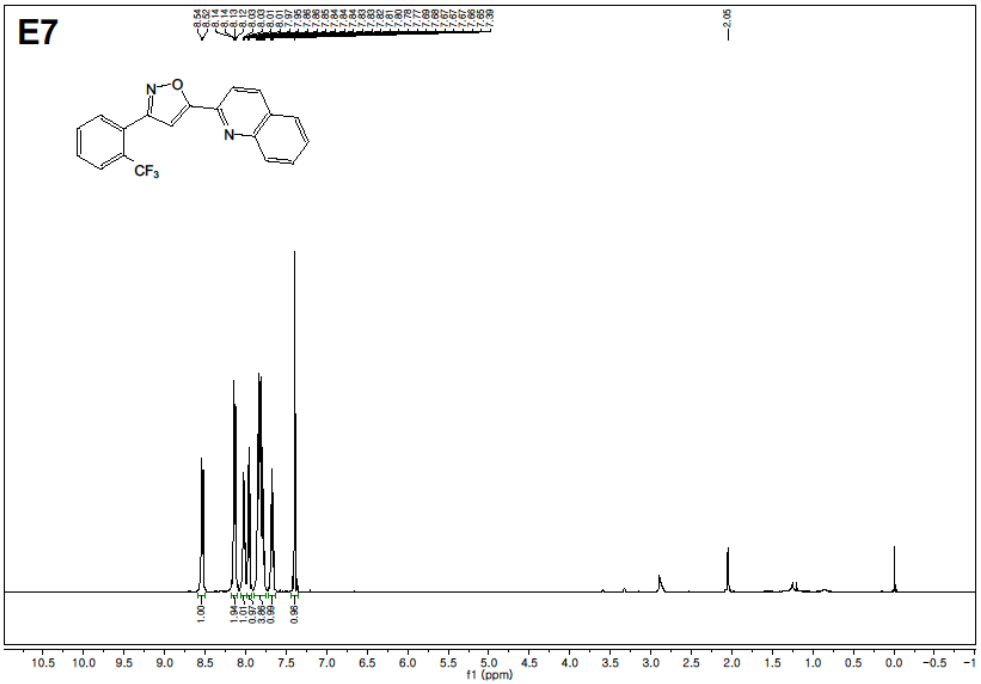
E7
2.05
f1 (ppm)

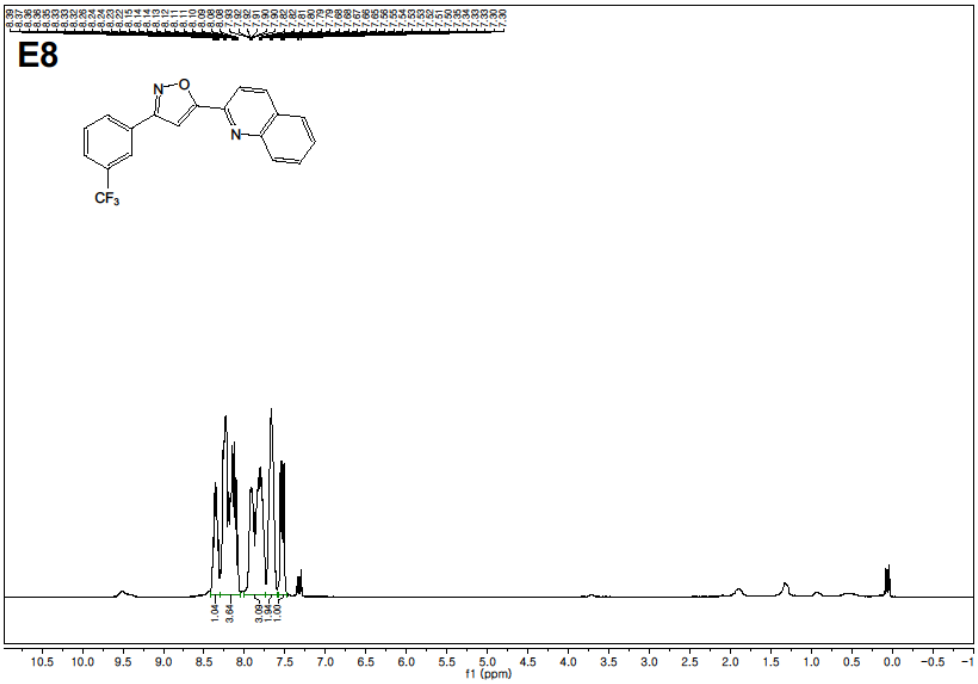
E8
N
O
N
CF3
1.04
3.84
3.09
1.04
1.00
10.5 10.0 9.5 9.0 8.5 8.0 7.5 7.0 6.5 6.0 5.5 5.0 4.5 4.0 3.5 3.0 2.5 2.0 1.5 1.0 0.5 0.0 −0.5 −1
f1 (ppm)

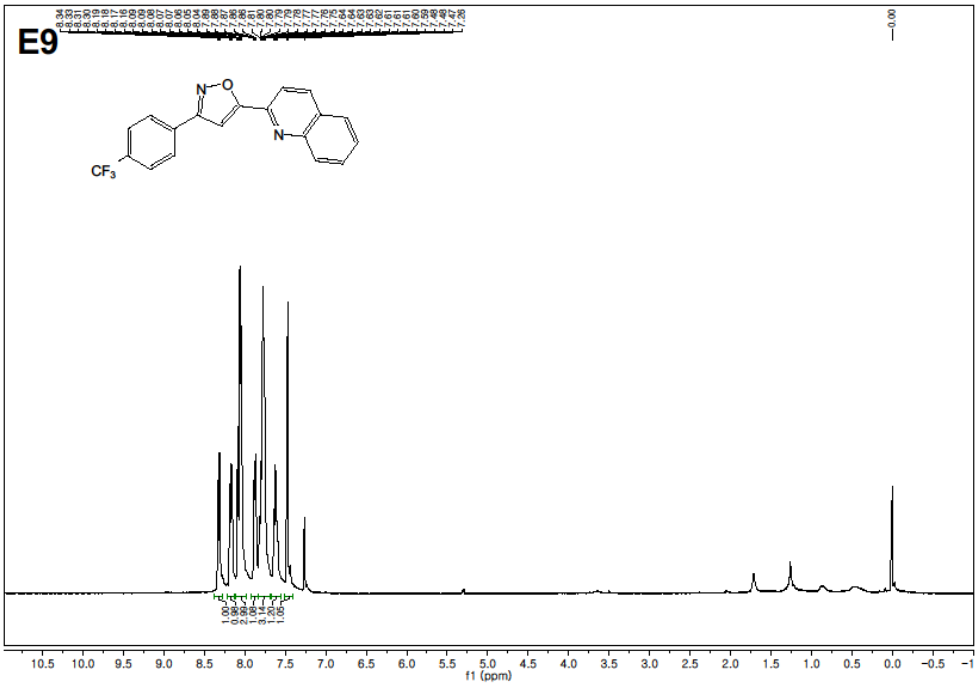
E9
0.00
N
O
N
CF3
1.00
0.99
2.08
3.14
1.04
1.05
10.5 10.0 9.5 9.0 8.5 8.0 7.5 7.0 6.5 6.0 5.5 5.0 4.5 4.0 3.5 3.0 2.5 2.0 1.5 1.0 0.5 0.0 −0.5 −1
f1 (ppm)

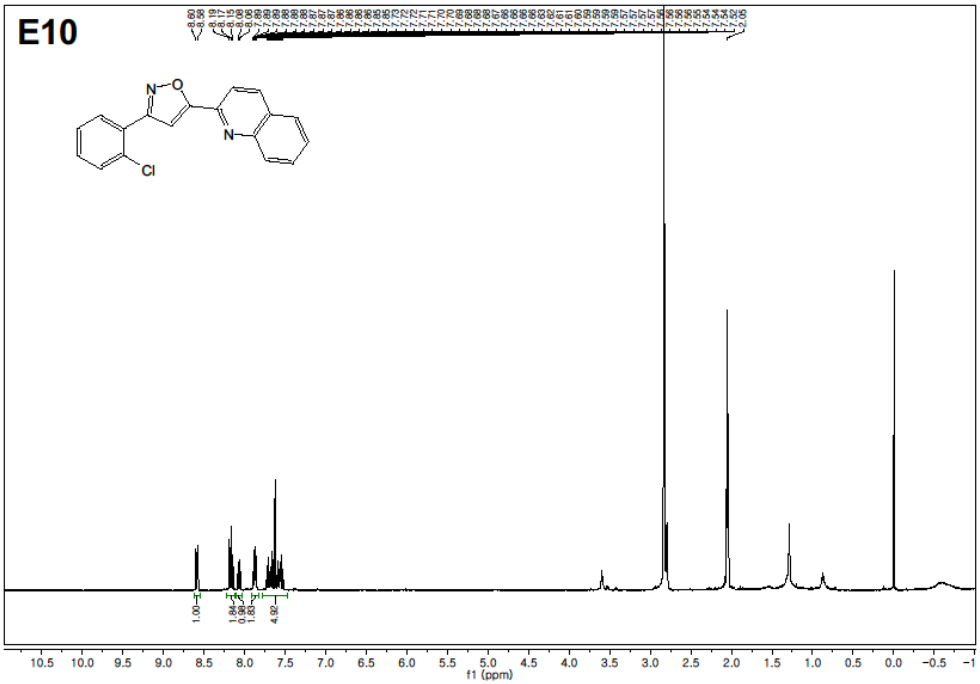
E10
N
O
N
Cl
1.00
1.84
0.88
1.83
4.92
10.5 10.0 9.5 9.0 8.5 8.0 7.5 7.0 6.5 6.0 5.5 5.0 4.5 4.0 3.5 3.0 2.5 2.0 1.5 1.0 0.5 0.0 −0.5 −1
f1 (ppm)

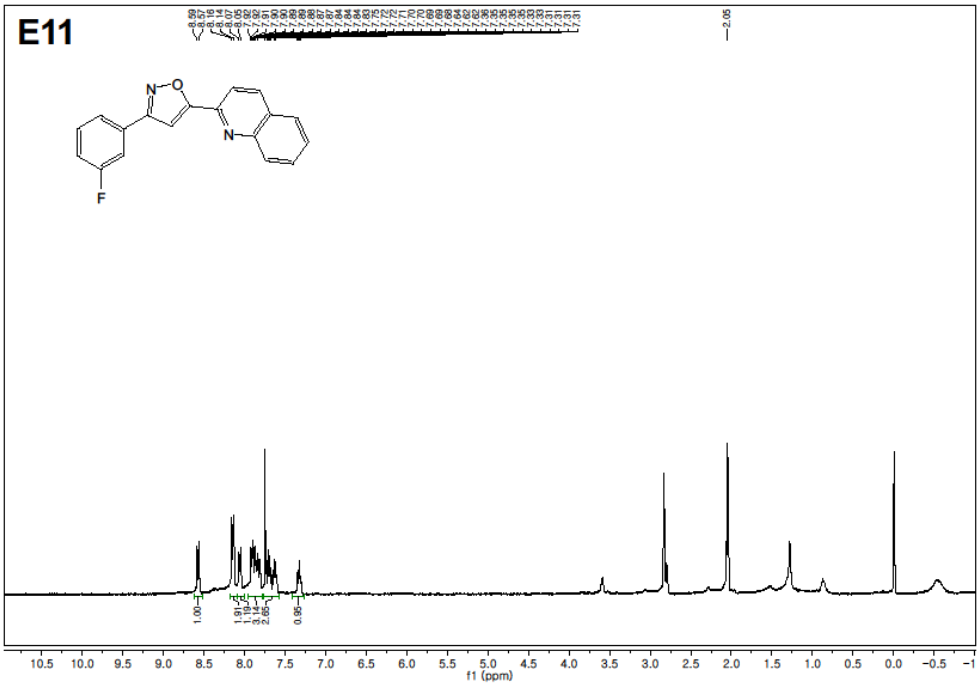
E11
2.05
N
O
N
F
1.00
1.91
1.19
1.14
2.65
0.95
10.5 10.0 9.5 9.0 8.5 8.0 7.5 7.0 6.5 6.0 5.5 5.0 4.5 4.0 3.5 3.0 2.5 2.0 1.5 1.0 0.5 0.0 −0.5 −1
f1 (ppm)